Examining the Limitations of $^{238}U/^{235}U$ in Marine Carbonates as a Paleoredox Proxy

by

Xinming Chen

A Thesis Presented in Partial Fulfillment
of the Requirements for the Degree
Doctor of Philosophy

Approved November 2018 by the
Graduate Supervisory Committee:

Ariel D. Anbar, Chair
Lynda B. Williams
Thomas Sharp
Richard L. Hervig
Stephen J. Romaniello

ARIZONA STATE UNIVERSITY

December 2018

ABSTRACT

Variations of $^{238}U/^{235}U$ in sedimentary carbonate rocks are being explored as a tool for reconstructing oceanic anoxia through time. However, the fidelity of this novel paleoredox proxy relies on characterization of uranium isotope geochemistry via laboratory experimental studies and field work in modern analog environmental settings. This dissertation systematically examines the fidelity of $^{238}U/^{235}U$ in sedimentary carbonate rocks as a paleoredox proxy focusing on the following issues: (1) U isotope fractionation during U incorporation into primary abiotic and biogenic calcium carbonates; (2) diagenetic effects on U isotope fractionation in modern shallow-water carbonate sediments; (3) the effects of anoxic depositional environments on $^{238}U/^{235}U$ in carbonate sediments.

Variable and positive shifts of $^{238}U/^{235}U$ were observed during U uptake by primary abiotic and biotic calcium carbonates, carbonate diagenesis, and anoxic deposition of carbonates. Previous $CaCO_3$ coprecipitation experiments demonstrated a small but measurable U isotope fractionation of ~0.10 ‰ during U(VI) incorporation into abiotic calcium carbonates, with ^{238}U preferentially incorporated into the precipitates (Chen et al., 2016). The magnitude of U isotope fractionation depended on aqueous U speciation, which is controlled by water chemistry, including pH, ionic strength, carbonate, and Ca^{2+} and Mg^{2+} concentrations. Based on this speciation-dependent isotope fractionation model, the estimated U isotope fractionation in abiotic calcium carbonates induced by secular changes in seawater chemistry through the Phanerozoic was predicted to be 0.11–0.23 ‰. A smaller and variable U isotope fractionation (0–0.09 ‰) was observed in primary biogenic calcium carbonates, which fractionated U isotopes in the same direction as abiotic calcium carbonates. Early diagenesis of modern shallow-water

carbonate sediments from the Bahamas shifted $\delta^{238}U$ values to be 0.27±0.14 ‰ (1 SD) higher than contemporaneous seawater. Also, carbonate sediments deposited under anoxic conditions in a redox-stratified lake—Fayetteville Green Lake, New York, USA— exhibited elevated $\delta^{238}U$ values by 0.16±0.12 ‰ (1 SD) relative to surface water carbonates with significant enrichments in U.

The significant U isotope fractionation observed in these studies suggests the need to correct for the U isotopic offset between carbonate sediments and coeval seawater when using $\delta^{238}U$ variations in ancient carbonate rocks to reconstruct changes in ocean anoxia. The U isotope fractionation in abiotic and biogenic primary carbonate precipitates, during carbonate diagenesis, and under anoxic depositional environments provide a preliminary guideline to calibrate $^{238}U/^{235}U$ in sedimentary carbonate rocks as a paleoredox proxy.

ACKNOWLEDGMENTS

Without the help of many people, this dissertation would not have been possible. First, I would like to appreciate my advisor, Dr. Ariel D. Anbar, for his encouragement, mentorship, support, and patience. I am really grateful for the great opportunity he offered me to study in School of Earth and Space Exploration, Arizona State University. His way of mentorship helps me to think critically and independently in scientific research. I am also greatly indebted to Dr. Stephen J. Romaniello for his hand-on-hand help in experiments, isotope measurements, and research. He is really nice and always ready to help.

I also appreciate the help and guidance of the committee members of my dissertation, and professors of graduate courses I have taken. In particular, I am grateful to my second project advisor, Dr. Lynda B. Williams for offering me the opportunity to conduct the very interesting experiments of killing bacteria and fungus using clay minerals. This project broadened my research scope and offered me the great opportunity to learn techniques of microbiological cultures. I appreciate Dr. Thomas Sharp and Richard Hevig for their insightful suggestions and comments about my research. I am indebted to Dr. Gorge Wolf for his amazing lectures in Physical Chemistry, and time and patience in paper discussion with me. With his help and mentorship, I have a solid physicochemical background in stable isotope fractionation theory.

Many thanks to Gwyneth Gordon, Wang Zheng, and Natalya Zolotova for their help. I appreciate Alyssa Sherry, Michael McCormick and undergraduate students from his lab for their help in the field work at Fayetteville Green Lake, New York, USA. I am grateful to Dr. Ian Hewson for providing me with anoxic sediment samples from Fayetteville Green Lake. I would like to thank all my friends and my family for supporting me all the way.

TABLE OF CONTENTS

Page

CHAPTER Page

CHAPTER Page

CHAPTER Page

LIST OF TABLES

Table Page

LIST OF FIGURES

Figure Page

CHAPTER 1

INTRODUCTION TO VARIATIONS OF $^{238}U/^{235}U$ IN SEDIMENTARY CARBONATES AS A PALEOREDOX PROXY

1.1 Metal Stable Isotopes as Paleoredox Proxies

The evolution of atmospheric oxygen on Earth has long fascinated geologists, ecologists, and evolutionary biologists because it is closely tied to biological evolution (e.g., Kasting and Siefert, 2002; Berner et al., 2007; Lyons et al., 2014; Thannickal, 2009; Fenchel and Finlay, 1994). It is generally accepted that oxygenic photosynthesis caused the rise of oxygen before the Great Oxidation Event (GOE, ~2.45 billion years ago) (e.g., Buick, 2008; Farquhar et al., 2011; Planavsky et al., 2014). The rise of animal life in the Late-Neoproterozic and Phanerozic, coincided with the oxygenation of the atmosphere and oceans, while the three major mass extinctions of the Phanerozoic—in the Later Devonian, Permian-Triassic, and Triassic-Jurassic—were associated with extended periods of oceanic anoxia (Canfield et al., 2007; Lenton et al., 2014; Berner et al., 2007; Reinhard et al., 2016; Mills et al., 2014). These intimate links strongly suggest that reconstruction of the oxygenation of the atmosphere and oceans through time is critical to the understanding of co-evolution of life and Earth.

To reconstruct the oxygenation of the atmosphere and oceans over geologic history, geochemists developed geochemical proxies, including variations in the stable isotopic ratios of light elements ($\delta^{13}C$, $\delta^{34}S$, $\Delta^{33}S$), in the abundances of redox-sensitive elements (Cu, V, Mn, Mo, Re, I, U, some rare earth elements), and in the isotopic ratios of some redox-sensitive elements ($\delta^{56}Fe$, $\delta^{53}Cr$, $\delta^{98}Mo$, $\delta^{82}Se$, $\varepsilon^{205}Tl$, $\delta^{238}U$) in sedimentary rocks such as organic-rich black shales, banded iron formations, phosphorite, and calcium carbonates (e.g., Pufahl and Hiatt, 2012;

Lyons et al., 2009; Anbar and Rouxel, 2007).

Carbon and sulfur isotopic ratios in sedimentary rocks have long been used to infer redox conditions of the atmosphere and oceans. It is generally accepted that the volcanogenic supply of C to Earth's surficial reservoirs (atmosphere, hydrosphere, and biosphere) is balanced by the burial of sedimentary carbonates and organic carbon, which have distinct C isotopic compositions by 20–30 ‰ at steady state (e.g., Schidlowski, 1988). Constrained by mass balance, variations of $\delta^{13}C$ in sedimentary carbonate rocks can provide a continuous record of overall burial rates of organic carbon, which causes oxygen to build up in the atmosphere (e.g., Brocker, 1970; Karhu and Holland, 1996; Kump and Arthur, 1999). Changes in $\delta^{13}C$ values of carbonates through time can, thus, provide a qualitative constraint on the rising and falling of oxygen in the atmosphere (e.g., Kump and Arthur, 1999).

Variations of S isotopic ratios ($\delta^{34}S$) in sulfates and pyrites can reflect changes in sulfate concentrations in seawater associated with the extent of oxidative weathering, while the mass-independent S isotope fractionation ($\Delta^{33}S$) has been used to constrain Archean atmospheric pO_2 to be $<10^{-5}$ of the present atmospheric level (e.g., Farquar et al., 2000; Kump, 2012).

The abundances of redox sensitive elements (Cu, V, Mn, Mo, Re, U) in organic-rich black shales or sedimentary carbonates can qualitatively reflect the extent of oceanic redox conditions of seawater. For example, U enrichment typically occurs under anoxic conditions, while Mo enrichment requires sulfidic conditions (Tribovillard et al., 2006; Algeo and Maynard, 2004). I/Ca ratios in calcium carbonates (e.g., foraminifera) decrease with shallow-water dissolved O_2 concentration in seawater (Lu et al., 2010; Glock et al., 2014). Variations in the abundance of Ce, one of the Rare Earth Elements (REEs), in sedimentary carbonate rocks has

also been explored as a proxy to qualitatively reconstruct local redox conditions (German and Elderfield, 1990).

With the advent of multi-collector inductively coupled plasma mass spectrometer (MC-ICP-MS), development of paleoredox proxies expanded to include metal isotopes systems such as $\delta^{56}Fe$, $\delta^{53}Cr$, $\delta^{98}Mo$, $\varepsilon^{205}Tl$ and $\delta^{238}U$, due to the ability of this new technique to resolve the relatively small isotope fractionation of these elements. The correlation between variations in these isotopic ratios and oceanic redox conditions results from the redox-driven changes in global oceanic isotopic budgets of these elements. Specifically, isotopic compositions of many redox-sensitive elements in seawater are controlled by the relative fractions of these elements removed by oxic vs. anoxic sedimentary sinks, and their isotope fractionation between these sinks and seawater, under a well-constrained isotopic composition of trace metal source to oceans (Anbar and Rouxel, 2007). The resultant isotopic mass balance in oceans can be described in a simple equation as follows:

$$\delta_{\text{seawater}} = \delta_{\text{source}} - f_{\text{anoxic}} \times \Delta_{\text{anoxic}} - (1 - f_{\text{anoxic}}) \times \Delta^{238}\text{U}_{\text{oxic}} \qquad \text{Eq. 1.1}$$

where $\delta_{seawater}$ and δ_{source} are isotopic compositions of trace metals in seawater and source, Δ_{anoxic} and Δ_{oxic} are isotope fractionation of redox-sensitive elements in anoxic and oxic sinks relative to seawater, and f_{anoxic} is the relative fraction of trace metals removed into anoxic sediments. Equation 1.1 would have the advantage of quantitatively estimating the changes in global redox conditions, if the residence time of trace metals were significantly longer than the oceanic mixing time.

When using isotopic ratios of redox-sensitive elements as paleoredox proxies, it is generally assumed that specific sedimentary rocks (e.g., black shales, Fe-Mn crust, calcium

carbonates) could record the isotopic ratios in coeval seawater with negligible isotope fractionation, or with a well-constrained isotope fractionation for which can be corrected. For example, Mo isotopes in black shales deposited under euxinic conditions, which facilitate quantitative Mo removal, are hypothesized to directly capture the Mo isotopic composition of seawater (e.g., Anbar and Rouxel, 2007; Duan et al., 2010). By comparing the δ^{98}Mo in these black shales to modern seawater, it is possible to quantitatively infer the redox conditions of oceans. Thallium isotopic composition in seawater is predominantly associated with manganese oxide burial over relatively short time periods, ~ million years (Owens et al., 2017). Tl isotopes in sediments deposited under euxinic conditions are hypothesized to directly record seawater ε^{205}Tl and therefore can be used as a proxy for changes in global manganese-oxide burial (Owens et al., 2017).

Attempts have also been made to apply U isotopic ratios ($^{238}U/^{235}U$) in black shales as a paleoredox proxy. However, the isotope fractionation between anoxic sediments and seawater for $^{238}U/^{235}U$ is variable and not well-constrained (Andersen et al., 2017). The constant isotope fractionation factors of Tl and U in ferromanganese crusts relative to seawater were used to reconstruct the redox conditions in oceans (Goto et al., 2014; Wang et al., 2016; Nielsen et al., 2009).

Instead of black shales, variations of $^{238}U/^{235}U$ in sedimentary carbonate rocks are being explored as a novel paleoredox proxy, assuming calcium carbonates directly record $^{238}U/^{235}U$ in seawater (Brennecka et al., 2011b; Azmy et al., 2015; Lau et al., 2016, 2017; Dahl et al., 2014, 2017; Jost et al., 2017; Zhang et al., 2018a, b; Clarkson et al., 2018; Elrick et al., 2018; Bartlett et al., 2018). $^{238}U/^{235}U$ in sedimentary carbonate rocks as a paleoredox proxy has several potential

advantages over other systems. First, the distribution of sedimentary carbonates rocks is more continuous both spatially and temporally, compared to the sporadic distributions of and black shales (irregularly distributed) (e.g., Pufahl and Hiatt, 2012). Specifically, sedimentary carbonate rocks accounted for >20 volume % of the total sedimentary rocks deposited after the early Proterozoic, and the oldest preserved carbonate rock was deposited at ~ 3.8 Ga (Ronov, 1964; Wilkinson and Walker, 1989; Shields and Veizer, 2002). Thus, the abundant sedimentary carbonate rock record could provide a complimentary, complete, and high-temporal resolution record of Earth's environmental conditions (e.g., anoxia) through the Phanerozoic and much of the Proterozoic (Morse and Mackenzie, 1990; Veizer et al., 1999; Prokoph et al., 2008; Vollstaedt et al., 2014). Second, U is readily incorporated into natural calcium carbonates at a concentration of 0.1–10 ppm, which can offer enough mass for U concentration and isotopic ratios measurements (e.g., Reeder et al., 2000; Romaniello et al., 2013).

However, this paleoredox proxy relies on the assumption that $^{238}U/^{235}U$ in sedimentary carbonate rocks directly capture U isotopic signals of coeval seawater. This dissertation focused on testing this assumption.

1.2 Uranium Isotopic Budget in Modern Oceans

Uranium (U) is a naturally occurring radioactive element which commonly exists as soluble U(VI) and insoluble U(IV) (e.g., Langmuir, 1978; McManus et al., 2005). In modern seawater, U mainly exists as Ca/Mg-UO_2-CO_3 complexes (Lee and Yun, 2013; Endrizzi and Rao, 2014; Endrizzi et al., 2016; Chen et al., 2016, 2017). The average concentration of U in modern seawater is ~13.9 nM with a residence time of ~500 kyr (Chen et al., 1986; Ku et al., 1977). Marine U predominantly comes from rivers (~90 %) during continental weathering with a

minor contribution from submarine groundwater discharge and dust (Dunk et al., 2002). Marine U sinks include metalliferous sediments (e.g., ferromanganese crust and nodules, 2 %), hydrothermal sediments (12 %), carbonate sediments (28 %), suboxic sediments (33 %), and anoxic sediments (25 %; Dunk et al., 2002; Noordmann et al., 2016). Diffusion of dissolved U into sediment pore-waters, and subsequent authigenic U reduction and precipitation in suboxic and anoxic sediments is the major process of U removal from seawater (e.g., Anderson, 1987; Barnes and Cochran, 1990, Klinkhammer and Palmer, 1991). The other marine U sinks remove U through adsorption to ferromanganese and/or coprecipitation with calcium carbonate precipitates (e.g., Andersen et al., 2017; Reeder et al., 2000; Russell et al., 2004).

U has two primordial isotopes ^{238}U ($t_{1/2}$≈4.5 Ga) and ^{235}U ($t_{1/2}$≈730 Ma), and one short-lived ^{234}U ($t_{1/2}$≈245,000 yr; Cheng et al., 2013; Jaffey et al., 1971). The natural abundances of ^{238}U, ^{235}U, and ^{234}U are 99.276, 0.718, and 0.004 %. Two U isotopic ratios are reported in this dissertation: $^{234}U/^{238}U$ and $^{238}U/^{235}U$, which are controlled by different geochemical processes. Due to alpha-recoil decay, ^{234}U is preferentially leached from damaged crystal lattice of minerals, leading to deviations of $^{234}U/^{238}U$ from secular equilibrium on Earth's surface, and significant enrichment of ^{234}U in rivers and seawater (e.g., Andersen et al., 2009; Ku, 1965; Thurber, 1962). Variations of $^{238}U/^{235}U$ in nature, however, are predominantly controlled by nuclear volume effects during U redox transformations, leading to the largest U isotope fractionation of ~ 1 ‰ (e.g., Basu et al., 2014; Stirling et al., 2015; Stylo et al., 2015; Wang et al., 2015a; Andersen et al., 2017). Smaller U isotope fractionations (0–0.2 ‰) were observed during U adsorption to Fe-Mn oxides, goethite, illite, and aquifer sediments, and coprecipitation with aragonite due to coordination changes of U in the aqueous solution and mineral surfaces

and equilibrium isotope fractionation among different U species (Weyer et al., 2008; Dang et al., 2016; Jemison et al., 2016; Brennecka et al., 2011a; Chen et al., 2016).

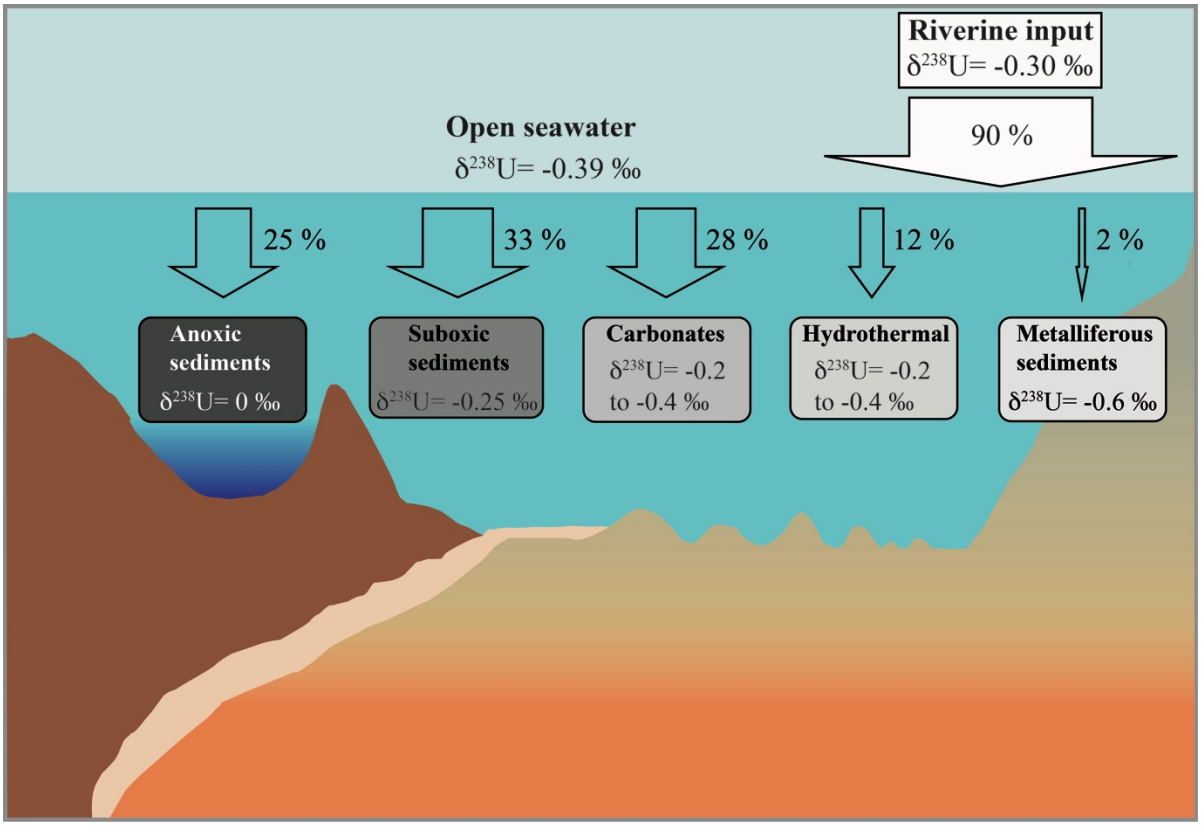

Figure 1.1. U isotopic budget in modern oceans (data from Noordmann et al., 2016; Andersen et al., 2017).

Variations of $^{238}U/^{235}U$ in seawater are predominantly driven by changes in oceanic redox conditions due to the significantly larger U isotope fractionation during removal by anoxic sediments relative to other U sinks (Figure 1.1). Marine U sinks fractionate U isotopes in opposite directions with variable magnitudes of isotope fractionation. The largest U isotope fractionation (0.6–1.0 ‰) is observed in modern anoxic sediments, which is preferentially enriched with ^{238}U due to U(VI) reduction to U(IV) (Stirling et al., 2007; Weyer et al., 2008; Brennecka et al., 2010; Montoya-Pino et al., 2010; Romaniello et al., 2012; Holmden et al., 2015; Andersen et al., 2017; Noormann et al., 2015, 2016; Rolison et al., 2018; Bura-Nkić et al.,

2018; Jemison et al., 2018). Carbonate sediments resulted in a small but significant U isotope fractionation of 0–0.3 ‰ with heavier U isotopes preferentially incorporated into calcium carbonate precipitates (Stirling et al., 2007; Weyer et al., 2008; Romaniello et al., 2013; Tissot et al., 2018). Hydrothermal sediments also fractionate U isotopes in the same direction as carbonate sediments with an isotope fractionation of 0–0.2 ‰ (Weyer et al., 2008; Tissot and Dauphas, 2015; Noormann et al., 2016; Andersen et al., 2017). In contrast, synthetic birnessite and marine Fe-Mn crust preferentially adsorbed light U isotopes, leading to an isotope fractionation of ~0.2 ‰ (Stirling et al., 2007; Weyer et al., 2008; Brennecka et al., 2011a; Dang et al., 2016; Jemison et al., 2016; Goto et al., 2014; Wang et al., 2016).

Because of the significant U isotope fractionation during U redox transformation, and notable authigenic enrichments of U in anoxic sediments due to U(VI) reductions, $\delta^{238}U$ in oceans is expected to change in response to variations in redox conditions due to U isotopic mass balance (e.g., Anderson, 1984; Barnes and Cochran, 1990; Klinkhammer and Palmer, 1991). For instance, if the oceans became more anoxic, more U would be reduced to insoluble U(IV), which is preferentially enriched in ^{238}U, leaving the remaining seawater $\delta^{238}U$ isotopically lighter, and vice versa. More specifically, the U isotopic mass balance in oceans can be described as:

$$\delta^{238}U_{seawater} = \delta^{238}U_{river} - f_{anoxic} \times \Delta^{238}U_{anoxic} - (1 - f_{anoxic}) \times \Delta^{238}U_{other} \quad \text{Eq. 1.2}$$

where $\delta^{238}U_{seawater}$ and $\delta^{238}U_{river}$ (–0.30 ‰) are the U isotopic compositions of seawater and the riverine input, respectively, and f_{anoxic} is the fraction of U removed into sediments underlying anoxic bottom waters (Andersen et al., 2016, 2017). $\Delta^{238}U_{anoxic}$ is the U isotope fractionation between anoxic sediments and seawater (0.6–1.0 ‰), and $\Delta^{238}U_{other}$ which includes carbonates, hydrothermal sediments, suboxic sediments, and metalliferous sediments is 0.03 ‰ (Brennecka

et al., 2011b; Tissot and Dauphas, 2015; Andersen et al., 2016, 2017; Jemison et al., 2018). If sedimentary rocks such as calcium carbonates could preserve $^{238}U/^{235}U$ signal of coeval seawater, variations of $^{238}U/^{235}U$ in this geologic record would be able to reconstruct the oceanic anoxia through time.

1.3 $^{238}U/^{235}U$ in Sedimentary Carbonates as a Paleoredox Proxy

Variations of $^{238}U/^{235}U$ in sedimentary carbonate rocks have been applied to infer redox conditions of oceans over the terminal Ediacaran Period, late Cambrian Steptoean positive carbonate isotope excursion (SPICE) event, Cambrian-Ordovician boundary, late Ordovician-early Silurian, end-Permian mass extinctions, end-Triassic extinction, and Oceanic Anoxic Event 2, (Brennecka et al., 2011b; Azmy et al., 2015; Lau et al., 2016, 2017; Dahl et al., 2014, 2017; Jost et al., 2017; Clarkson et al., 2018; Elrick et al., 2018; Bartlett et al., 2018). These studies assumed that $^{238}U/^{235}U$ in ancient carbonate rocks could directly record that of seawater.

To test this assumption, I conducted the first laboratory experiments of U isotope fractionation during coprecipitation of U(VI) with calcium carbonate during my master's thesis (Chen et al., 2016). These experiments demonstrated a small but significant U isotope fractionation of ~0–0.10 ‰ during U(VI) incorporation into aragonite at pH ~8.5, whereby ^{238}U is preferentially enriched in the carbonate precipitate. The magnitude of the U isotope fractionation in these abiotic calcium carbonate coprecipitation experiments depended on the aqueous U speciation, which was controlled by water chemistry, including pH, pCO_2, ionic strength, and Ca^{2+} and Mg^{2+} concentrations (e.g., Langmuir, 1978; Endrizzi et al., 2016). Previous studies have revealed secular variations in seawater chemistry over the Phanerozoic (e.g., Lowenstein et al., 2013). Consequently, these secular variations in seawater chemistry can

affect aqueous U speciation and U isotope fractionation during U(VI) incorporation into abiotic calcium carbonates over the Phanerozoic.

In contrast to abiotic calcium carbonate coprecipitation experiments, $\delta^{238}U$ in primary biogenic carbonates like corals has been found to be indistinguishable from modern seawater with $^{238}U/^{235}U$, at least to a measurement precision of ±0.10 ‰ (Stirling et al., 2007; Weyer et al., 2008). At this precision it was impossible to resolve the small U isotope fractionation of ~0.11 ‰ predicted by abiotic coprecipitation experiments (Chen et al., 2016), if such fractionation occurs during biogenic precipitation. Thus, it remained unclear whether primary biogenic carbonates fractionate U isotopes similarly to abiotic calcium carbonates.

In addition to the potential U isotope fractionation in primary abiotic and biogenic calcium carbonates, diagenesis might also alter the original $^{238}U/^{235}U$ in primary carbonates after deposition. This phenomenon is well-known for other geochemical proxies (e.g., $\delta^{13}C$, $\delta^{18}O$, $\delta^{11}B$; Swart, 2015; Stewart et al., 2015). Preliminary results in modern shallow-water carbonate sediments from the Bahamas showed a positive isotopic shift of 0.2–0.4 ‰ in $\delta^{238}U$ relative to primary biogenic carbonates and seawater during syndepositional diagenesis (Romaniello et al., 2013). Furthermore, Hood et al. (2016) also observed large variations in $\delta^{238}U$ values of various carbonate microfacies with different degrees of diagenetic alterations from the Cryogenian Balcanoona reef complex in South Australia. These studies strongly suggest that carbonate diagenesis could alter $\delta^{238}U$ values in sedimentary carbonate rocks.

Compared to the oxic depositional environments for modern carbonate sediments, anoxic depositional conditions might also affect $\delta^{238}U$ values in primary carbonates precipitated in the surface water. Because under anoxic conditions, authigenic U reduction below the sediment-

water interface significantly enriches U (e.g., Anderson et al., 1989). For example, anoxic sediments such as organic-rich black shales in modern oceans have an average U concentration of ~26 ppm, which is much higher than that in primary calcium carbonate precipitates (~ 1.5 ppm; e.g., Partin et al., 2013; Romaniello et al., 2013). As described in Section 1.2, U(VI) reduction to U(IV) causes the largest U isotope fractionation ($^{238}U/^{235}U$, ~1 ‰), compared to U(VI) adsorption to minerals and coprecipitation with calcium carbonates (0–0.2 ‰; e.g., Andersen et al., 2017). Consequently, carbonate sediments deposited under anoxic depositional environments would significantly enrich U and elevate $\delta^{238}U$ values relative to their primary calcium carbonate precipitates. Anoxic depositional environments might be extremely important for redox-stratified oceans in deep time such as the Proterozoic (Grotzinger and Knoll, 1995; Grotzinger and James, 2000; Gulin, 2000; Anbar and Knoll, 2002). Thus, it is important to investigate the effects of anoxic depositional conditions on variations of $\delta^{238}U$ in carbonate sediments.

To examine the limitations of $\delta^{238}U$ in sedimentary carbonate rocks as a paleoredox proxy, this dissertation explored: (1) U isotope fractionation between abiotic calcium carbonate precipitates and seawater induced by secular variations in seawater chemistry over the Phanerozoic (Chapter 2); (2) biological effects on U isotope fractionation in primary biogenic carbonates (Chapter 3); (3) diagenetic effects on U isotope fractionation in modern shallow-water carbonate sediments from the Bahamas (Chapter 4); (4) anoxic depositional conditions on $\delta^{238}U$ in carbonate sediments of the permanently redox-stratified Fayetteville Green Lake, New York, USA (Chapter 5).

1.4 U Isotope Fractionation in Abiotic Aragonite and Calcite

Because this dissertation extends from the results of my master's thesis—U isotope fractionation during U(VI) incorporation into inorganically precipitated aragonite and calcite—I summarize the results of my master's thesis in this section.

As a first step to examine the fidelity of $^{238}U/^{235}U$ in marine calcium carbonates as a paleoredox proxy, the experimental results of my master's thesis determined the U isotope fractionation during U incorporation into calcium carbonates by conducting abiotic aragonite and calcite coprecipitation experiments at pH ~7.5 and ~8.5 (Chen et al., 2016; Chen, 2016). Small but significant U isotope fractionations ($\Delta^{238}U_{abiotic}$=0.2–0.10 ‰; Figure 1.2) occurred in aragonite experiments at pH ~8.5, with ^{238}U preferentially incorporated into the carbonate precipitates. In contrast, no measurable isotope fractionation was observed in an aragonite experiment at pH ~7.5, or in calcite experiments at either pH.

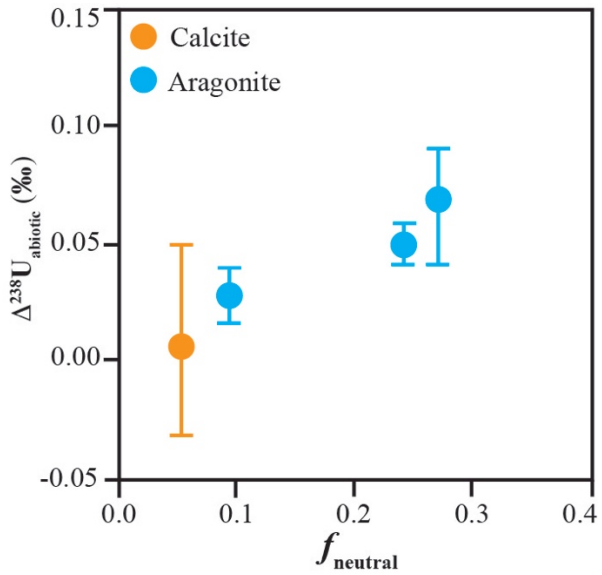

Figure 1.2. U isotope fractionation ($\Delta^{238}U_{abiotic}$) during U(VI) incorporation into aragonite and calcite at pH ~8.5 versus the fraction ($f_{neutral}$) of the neutrally charged U species—$Ca_2UO_2(CO_3)_3(aq)$. Blue and orange symbols represent aragonite and calcite experiments, respectively.

As part of this work, I proposed that equilibrium isotope fractionation between different aqueous U species coupled with preferential incorporation of some isotopically heavy U species into calcium carbonate could explain the U isotope fractionation observed in aragonite experiments. Specifically, this interpretation hypothesized that: (1) the negatively charged aqueous U species—$CaUO_2(CO_3)_3^{2-}$, $MgUO_2(CO_3)_3^{2-}$, and $UO_2(CO_3)_3^{4-}$ were preferentially incorporated into positively charged surface of aragonite at pH 8.5; (2) $\delta^{238}U$ of the neutrally charged $Ca_2UO_2(CO_3)_3(aq)$ has a lighter value relative to other charged U species in thermodynamic equilibrium. Under these hypotheses, the magnitude of the isotope fractionation in aragonite experiments should be expected to scale with the fraction of the neutrally charged U species—$Ca_2UO_2(CO_3)_3(aq)$—in the aqueous solution. This expectation was confirmed by aqueous U speciation modeling in aragonite experiments which fractionated U isotope.

These experimental findings suggest that variations of $^{238}U/^{235}U$ in ancient carbonates could also result from changes in the aqueous speciation of U(VI) in seawater without changes in oceanic redox conditions (Chen et al., 2016). Aqueous U(VI) speciation is controlled by pH, pCO_2, ionic strength, and Ca^{2+} and Mg^{2+} concentrations, all of which change over the Phanerozoic in oceans (Lowenstein et al., 2013; Ridgwell, 2005; Berner and Kothavala, 2001). The speciation-dependent isotope fractionation during U(VI) incorporation into abiotic calcium carbonates motivated the study of U isotope fractionation induced by aqueous U speciation due to secular changes in seawater chemistry over the Phanerozoic and its implications for $^{238}U/^{235}U$ in marine calcium carbonates as a paleoredox proxy (Chapter 2).

CHAPTER 2

URANIUM ISOTOPE FRACTIONATION INDUCED BY AQUEOUS SPECIATION: IMPLICATIONS FOR $^{238}U/^{235}U$ IN SEDIMENTARY CARBONATE ROCKS AS A PALEOREDOX PROXY

The work presented in this chapter has been published as: Chen X., Romaniello S. J., Anbar A. D. (2017) Uranium isotope fractionation induced by aqueous speciation: Implications for U isotopes in marine $CaCO_3$ as a paleoredox proxy. *Geochim. Cosmochim. Acta* **215**, 162–172.

Abstract

Natural variations of $^{238}U/^{235}U$ in marine $CaCO_3$ rocks are being explored as a novel paleoredox proxy to investigate oceanic anoxia events. Although it is generally assumed that U isotopes in $CaCO_3$ directly record $^{238}U/^{235}U$ of seawater, recently published laboratory experiments demonstrate slight U isotope fractionation during U(VI) incorporation into abiotic calcium carbonates. This fractionation is hypothesized to depend on aqueous U(VI) speciation, which is controlled by pH, ionic strength, pCO_2 and Mg^{2+} and Ca^{2+} concentrations. Secular variation in seawater chemistry could lead to changes in aqueous U(VI) speciation, and thus, may affect the extent of U isotope fractionation during U(VI) incorporation into $CaCO_3$. In this study, estimates of seawater composition over the Phanerozoic were combined with a model of aqueous U speciation and isotope fractionation to explore variations in the expected offset between the U isotope composition of seawater and primary marine $CaCO_3$ through time.

U isotope fractionation between U in primary marine $CaCO_3$ and seawater could have varied between 0.11 and 0.23 ‰ over the Phanerozoic due to secular variations in seawater chemistry. Such variations would significantly impact estimates of the extent of marine anoxia derived from the U isotope record. For example, at the Permo-Triassic boundary, this effect might imply that the estimated extent of anoxia is ~32 % more extreme than previously inferred. One significant limitation of the model in this study is that the existing experimental database covers only abiotic calcium carbonate precipitation, and does not include a possible range of biological effects which might enhance or suppress the range of isotopic fractionation calculated here. As biotic carbonates dominate the marine carbonate record, more work is required to assess controls on U isotopic fractionation into biotic marine carbonates.

2.1 Introduction

Marine paleoredox proxies based on non-traditional isotope systems of redox-sensitive metals such as Mo and U provide compelling insights into the timing, duration and extent of marine anoxia associated with biological radiations and extinctions (Siebert et al., 2004; Arnold et al., 2004; Wille et al., 2007, 2013; Montoya-Pino et al., 2010; Duan et al., 2010; Voegelin et al., 2010; Dahl et al., 2011; Kendall et al., 2011; Dickson and Cohen, 2012; Dickson et al., 2012; Herrmann et al., 2012; Czaja et al., 2012; Xu et al., 2012; Proemse et al., 2013; Kurzweil et al., 2015; Wen et al., 2015; Dickson et al., 2016; Brennecka et al., 2011b; Asael et al., 2013; Dahl et al., 2014; Kendall et al., 2013, 2015; Lau et al., 2016). Once confined mainly to relatively rare black shale lithologies, new advances such as the application of $^{238}U/^{235}U$ preserved in sedimentary carbonate rocks, facilitate the reconstruction of more complete, high resolution temporal records of ocean redox conditions which can be directly correlated to marine biostratigraphic records (Brennecka et al., 2011b; Lau et al., 2016; Elrick et al., 2016; Azmy et al., 2015).

The use of uranium (U) isotope variations preserved in carbonates offers several advantages as a marine paleoredox proxy. First, the residence time of U in seawater is relatively long (~500 kyr; Dunk et al., 2002) compared to the timescale of ocean mixing (~2 kyr; Jenkins, 2003). Because of this, the U isotopic composition of the open ocean is homogenous (within analytical uncertainties), and thus seawater from even a single locality may provide a globally-integrated measure of U marine geochemistry (Stirling et al., 2007; Weyer et al., 2008; Andersen et al., 2014, 2016; Tissot and Dauphas, 2015). Second, the widespread spatial and temporal distribution of marine carbonates enables relatively long, complete, and high-temporal resolution $^{238}U/^{235}U$ records, similar to those previously developed for $\delta^{13}C$, $\delta^{18}O$ and $^{87}Sr/^{86}Sr$ (Morse and

Mackenzie, 1990; Veizer et al., 1999; Prokoph et al., 2008; Vollstaedt et al., 2014). To better understand U isotopic signals recorded in sedimentary carbonates it is necessary to know if U isotopes fractionate during coprecipitation of U with primary calcium carbonates and, if so, to develop a mechanistic basis to correct for this effect.

It is commonly assumed that U in marine $CaCO_3$ directly records $^{238}U/^{235}U$ of seawater during U incorporation into $CaCO_3$ (Weyer et al., 2008; Brennecka et al., 2011b). As a first step toward testing this assumption experimentally, Chen et al. (2016) investigated U isotope fractionation during U(VI) incorporation into abiotic aragonite and calcite. They observed a small but measurable U isotope fractionation (as much as ~0.09 ‰) that was hypothesized to depend on aqueous U speciation, scaling with the fraction of the neutrally charged aqueous U(VI) species—$Ca_2UO_2(CO_3)_3(aq)$ (Chen et al., 2016). The extrapolated U isotope fractionation between U in abiotic $CaCO_3$ and modern seawater is 0.11±0.02 ‰. The importance of this effect in biotic $CaCO_3$ precipitation is not known. Higher precision measurements of $^{238}U/^{235}U$ (±0.03 ‰; Tissot and Dauphas, 2015; Andersen et al., 2014) in some modern and fossil coral samples were indistinguishable from modern seawater. However, $^{238}U/^{235}U$ measured in other biogenic primary carbonates such as red and green algae, and mollusks at ±0.10 ‰ precision (Stirling et al., 2007; Weyer et al., 2008; Romaniello et al., 2013) allows for the isotope effect observed in abiotic experiments (0.09 ‰).

Aqueous U(VI) speciation is controlled by pH, pCO_2, ionic strength, Ca^{2+} and Mg^{2+} concentrations (Dong and Brooks, 2006; Endrizzi and Rao, 2014), all of which have varied in seawater over geologic time (Lowenstein et al., 2013). Therefore, the magnitude of U isotope

fractionation between U in seawater and $CaCO_3$ may also vary with time. This possibility has not been considered before.

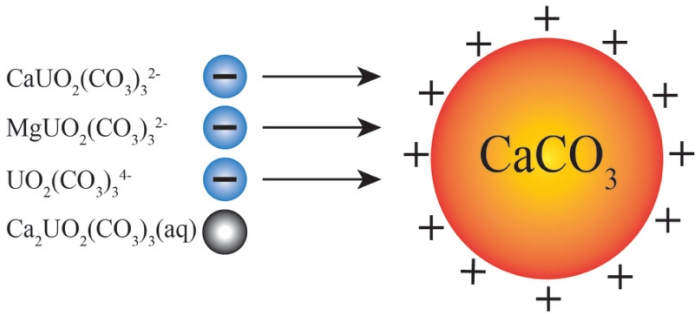

Figure 2.1. Schematic illustration of the hypothesis that negatively charged aqueous U(VI) species are preferentially incorporated into the positively charged $CaCO_3$ at pH=8.5.

Here, the aqueous U(VI) speciation over the Phanerozoic was calculated, and the speciation-dependent U isotope fractionation model (Chen et al., 2016) was used to explore how non-redox variations in Phanerozoic seawater chemistry may have impacted U isotope records in marine carbonates. As an illustrative example, this study applies these results to revisit estimates of ocean anoxia during the end-Permian mass extinction previously estimated from $^{238}U/^{235}U$ variations in carbonates deposited in late Permian and early Triassic oceans (Lau et al., 2016; Brennecka et al., 2011b).

2.2 Methods

To estimate the magnitude of isotope fractionation between U in marine $CaCO_3$ and seawater over the Phanerozoic, the aqueous U(VI) speciation was firsted calculated with published data of seawater chemistry using the software PHREEQC (Parkhurst and Appelo, 2004). Then the non-redox speciation-dependent U isotope fractionation model (Chen et al., 2016) was used to estimate the U isotope fractionation during U(VI) incorporation into $CaCO_3$. The sensitivity of U isotope fractionation to changes in seawater chemistry (pH, pCO_2, ionic

strength, Ca^{2+} and Mg^{2+} concentrations) was evaluated to determine the dominant factors that affect U isotope fractionation.

2.2.1 U Isotope Fractionation Factor and Aqueous U Speciation

Previous experimental study of aragonite and calcite coprecipitation with U(VI) showed that U isotope fractionation during U incorporation into $CaCO_3$ scaled with the fraction of U present as the neutral U species—$Ca_2UO_2(CO_3)_3(aq)$ (Chen et al., 2016). It was hypothesized that negatively charged U species with heavier U isotopic compositions were preferentially incorporated into calcium carbonate relative to the neutrally charged U species $Ca_2UO_2(CO_3)_3(aq)$, progressively enriching heavier U isotopes in the solid phase during calcium carbonate precipitation (Figure 2.1). The relationship between the U isotope fractionation (ε) and U speciation was derived as (details of the derivation is listed in Chen et al. (2016)):

$$\varepsilon = (\alpha - 1) = \Delta^{238}U_{2-1} \times \frac{f_{\text{neutral}}(f_1 - 1)}{f_{\text{neutral}} - 1} \qquad \text{Eq. 2.1}$$

where ε is the isotope fractionation factor between U in $CaCO_3$ and aqueous solution. The subscripts 1 and 2 refer to U in "Group 1" species [$Ca_2UO_2(CO_3)_3(aq)$, and $UO_2(CO_3)_3^{4-}$] and "Group 2" species [$CaUO_2(CO_3)_3^{2-}$ and $MgUO_2(CO_3)_3^{2-}$], differentiated on the basis of differences in the U chemical bonding environment. Specifically, all U(VI) species shared the same coordination number and bond length between U and axial oxygen ($U–O_{ax}$), except that the bond length between U and equatorial oxygen ($U–O_{eq}$) in "Group 1" species is longer than that in "Group 2" species (Docrat et al., 1999; Bernhard et al., 2001; Kerisit and Liu, 2010). Accordingly, $\Delta^{238}U_{2\text{-}1}=\delta^{238}U_2–\delta^{238}U_1$, which is the estimated difference in U isotopic composition between Group 2 and Group 1 (0.32±0.06 ‰; Chen et al., 2016). f_1 is the fraction

of U species in Group 1 and $f_{neutral}$ is the fraction of the neutral U species, $Ca_2UO_2(CO_3)_3(aq)$. Thus, equation 2.1 can be used to estimate the magnitude of U isotope fractionation between abiotic $CaCO_3$ and seawater with known water chemistry.

2.2.2 Geochemical Modeling of Aqueous U Speciation

The recent discovery of multiple ternary complexes of uranyl and carbonate with alkaline earth metals (Mg^{2+}, Ca^{2+}, Sr^{2+} and Ba^{2+}) has significantly impacted thermodynamic models of aqueous U speciation. Since the first report of aqueous $Ca_2UO_2(CO_3)_3(aq)$ by Bernhard et al. (1998), subsequent studies identified other important complexes of alkaline earth uranyl carbonates such as $CaUO_2(CO_3)_3^{2-}$, and $MgUO_2(CO_3)_3^{2-}$ (Klmykov and Choppin, 2000; Bernhard et al., 2001; Gipel et al., 2008; Lee and Yun, 2013). After considering these novel aqueous uranyl species, the dominant aqueous U species in seawater and natural alkaline groundwater are $Ca_2UO_2(CO_3)_3(aq)$, $CaUO_2(CO_3)_3^{2-}$, and $MgUO_2(CO_3)_3^{2-}$ (Lee and Yun, 2013; Endrizzi and Rao, 2014; Endrizzi et al., 2016), rather than $UO_2CO_3(aq)$, $UO_2(CO_3)_2^{2-}$ and $UO_2(CO_3)_3^{4-}$ previously reported (Langmuir, 1978). Thus, the three novel aqueous U species $Ca_2UO_2(CO_3)_3(aq)$, $CaUO_2(CO_3)_3^{2-}$, and $MgUO_2(CO_3)_3^{2-}$ were incorporated into the **sit.dat** database with the most recent U thermodynamic data (Grenthe et al., 1992; Guillaumont et al., 2003) for aqueous U speciation calculated by the software PHEEQC (Parkhurst and Appelo, 2004).

Although there are slight differences between the equilibrium constants determined by anion exchange resin and time-resolved laser fluorescence spectroscopy for the same complexes of alkaline earth uranyl carbonates (e.g., $CaUO_2(CO_3)_3^{2-}$), these differences are statistically identical within uncertainty (Dong and Brooks, 2006; Klmykov and Choppin, 2000; Bernhard et al., 2001; Gipel et al., 2008; Lee and Yun, 2013; Endrizzi and Rao, 2014). In this study, the

equilibrium constants reported by Dong and Brooks (2006) have been adopted to maintain consistency with previously reported results (Chen et al., 2016). Using these parameters, the fraction of neutral $Ca_2UO_2(CO_3)_3(aq)$ in modern seawater is predicted to be 44 %, which is slightly lower than that calculated in previous work (54 %) using equilibrium constants from Endrizzi and Rao (2014). If the uncertainty in the equilibrium constants of the Mg/Ca-UO_2-CO_3 complexes can cause an error of ±10 % in the fraction of the neutral $Ca_2UO_2(CO_3)_3(aq)$, the resulting uncertainty in U isotope fractionation induced by aqueous U speciation during U(VI) incorporation into $CaCO_3$ will be ~0.02 ‰ (Figure 8 in Chen et al., 2016). This uncertainty is relatively small compared to variations imposed by secular changes in seawater chemistry as discussed below.

2.2.3 Seawater Chemistry and Atmospheric CO_2 Over the Phanerozoic

Changes in seawater chemistry and atmospheric CO_2 over the Phanerozoic were compiled from the literature. These include: variations in the major ion composition of seawater (Mg^{2+}, Ca^{2+}, Na^+, K^+ and Cl^-) inferred from analyses of fluid inclusions in marine halites (Horita et al., 2002; Lowenstein et al., 2003, 2005; Timofeeff et al., 2006); variations in HCO_3^- concentration derived from silicate weathering (Gibbs et al., 1999; Ridgwell, 2005); variations in atmospheric CO_2 concentrations reconstructed from CO_2 proxies such as stomata on leaf surfaces, $\delta^{13}C$ of phytoplankton, liverworts and paleosol carbonate, $\delta^{11}B$ and B/Ca in marine carbonates, and the presence of rare sodium carbonate mineral ($NaHCO_3$) nahcolite (Royer et al., 2004; Beerling et al., 1998; Seki et al., 2010; Fletcher et al., 2008; Schaller et al., 2011; Pearson et al., 2009; Tripati et al., 2009; Lowenstein and Demicco, 2006; Lowenstein et al., 2013; Royer,

2013) and from the long-term global carbon cycle model GEOCARB III (Berner and Kothavala, 2001). The pH of surface seawater was estimated from the atmospheric CO_2 concentration and the HCO_3^-concentration in seawater (Ridgwell, 2005).

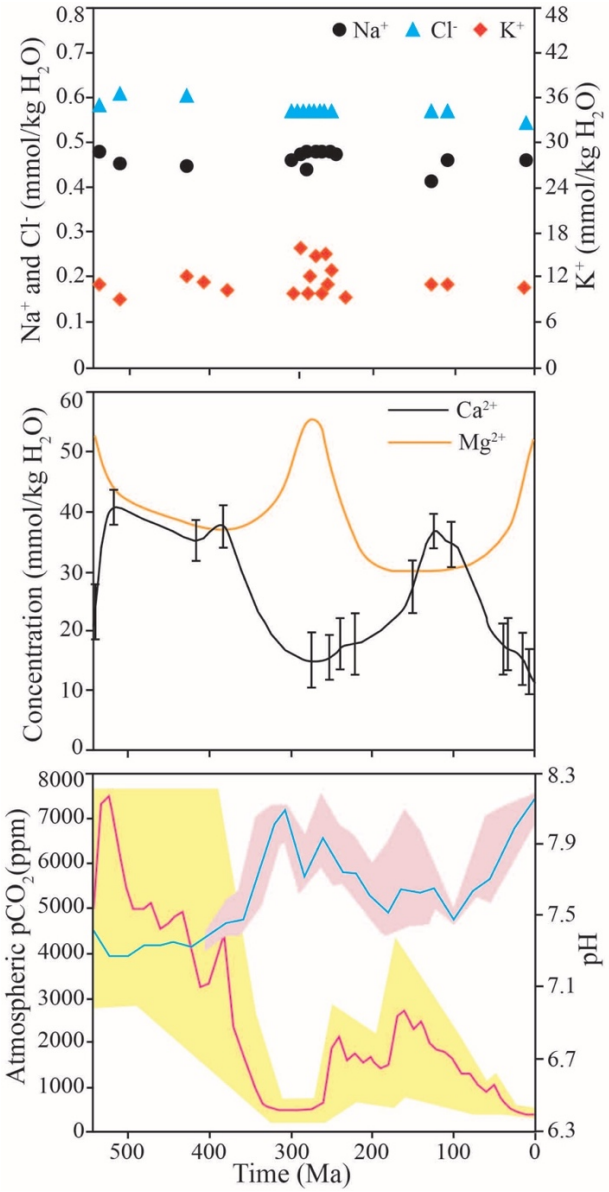

Figure 2.2. Secular variations in seawater chemistry over the Phanerozoic. The data of K^+, Na^+ and Cl^- and Mg^{2+} curve were from Hardie (1996), Hortia et al. (2002) and Lowenstein et al. (2005). The Ca^{2+} curve was modified from Lowenstein et al. (2003, 2005). The CO_2 concentration and pH were from Berner and Kothavala (2001), Royer et al. (2004) and Ridgwell (2005). The shadow zones in pH and pCO_2 panels are uncertainties.

2.3 Results

2.3.1 Seawater Chemistry and U Speciation over the Phanerozoic

As displayed in Figure 2.2a, the concentrations of Na^+, K^+ and Cl^- were relatively constant over the Phanerozoic, resulting in a narrow range of seawater ionic strength between 0.59 and 0.67 M. In contrast, the concentrations of Ca^{2+} and Mg^{2+} and seawater pH are suggested to have fluctuated significantly (Figure 2.2b and c) and thus are probably the most significant drivers for changes in seawater U speciation over the past 500 Ma.

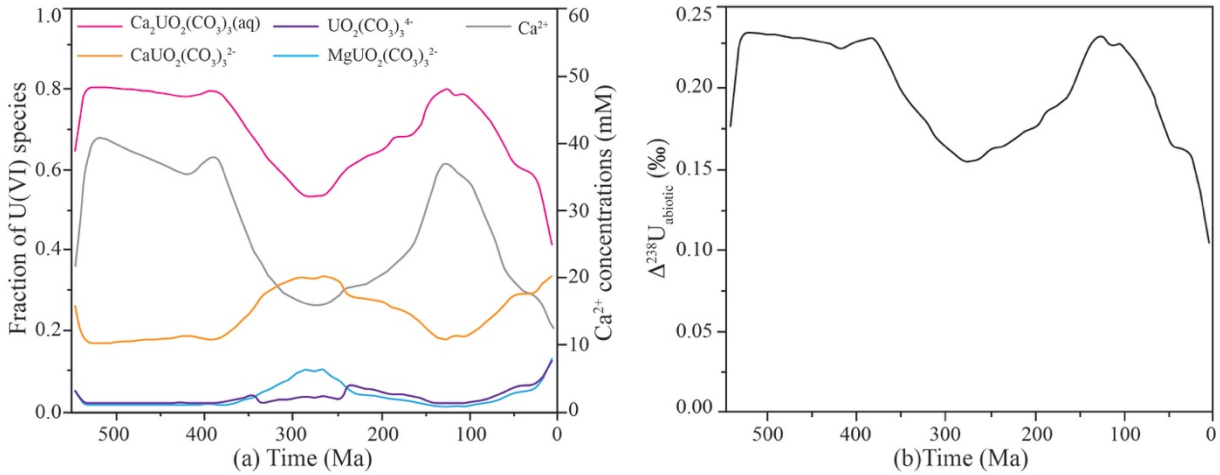

Figure 2.3. Aqueous U speciation in seawater over the Phanerozoic (a); the predicted α between U in primary $CaCO_3$ and seawater over the Phanerozoic (b). The dotted, dashed and dash-dotted lines are the fractions of aqueous $CaUO_2(CO_3)_3^{2-}$, $UO_2(CO_3)_3^{4-}$ and $MgUO_2(CO_3)_3^{2-}$. The black and gray solid lines are the fraction of dissolved $Ca_2UO_2(CO_3)_3(aq)$ and concentration of Ca^{2+}, respectively.

Figure 2.3a shows the predicted aqueous U speciation in seawater over the Phanerozoic. The neutral U species—$Ca_2UO_2(CO_3)_3(aq)$ is the predominant species during this entire time, accounting for 40–80 % of the total dissolved U(VI). Not surprisingly, the predicted fraction of $Ca_2UO_2(CO_3)_3(aq)$ covaries with the estimated seawater Ca^{2+} concentration.

2.3.2 U Isotope Fractionation into Marine $CaCO_3$ over the Phanerozoic

The model predicts that U isotope fractionation (denoted ε) between U in primary abiotic $CaCO_3$ and seawater over the Phanerozoic varied from 0.11 to 0.23 ‰ (Figure 2.3b), favoring heavy U isotopes in the solid phase. The U isotope fractionation scaled with the fraction of the neutral U species—$Ca_2UO_2(CO_3)_3(aq)$.

2.3.3 Sensitivity of the Isotopic Fractionation to Seawater Chemistry

The sensitivity of the U isotopic fractionation, ε, to variations in pH, pCO_2, Ca^{2+} and Mg^{2+} concentrations, and ionic strength was assessed to determine the relative importance of these factors to the magnitude of U isotope fractionation during incorporation to carbonates. Although variations in temperature can also change U speciation and U isotope fractionation, they are not considered here because the temperature-dependence of the equilibrium constants governing U speciation are not well known, and theoretical extrapolation from known values is beyond the scope of this study.

The variations of ε in response to pH, pCO_2, Ca^{2+} and Mg^{2+} concentrations, and ionic strength can be divided into two groups. As pH, pCO_2, Mg^{2+} concentration and ionic strength increase, ε decreases due to the decrease in the fraction of the neutrally-charged $Ca_2UO_2(CO_3)_3(aq)$. In contrast, when Ca^{2+} concentration increases, ε increases dramatically because of the significant elevation in the fraction of $Ca_2UO_2(CO_3)_3(aq)$ (Figure 2.4, 2.5, 2.6, and 2.7).

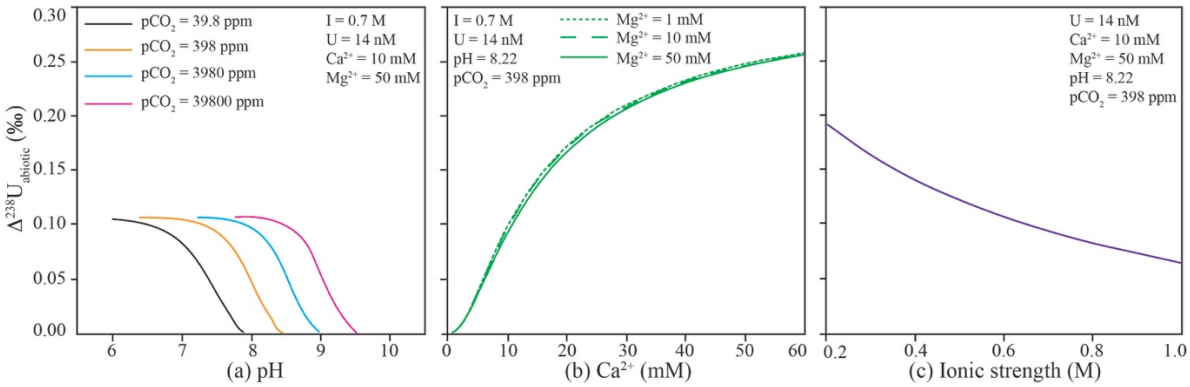

Figure 2.4. The sensitivity of U isotope fractionation ε to (a) pH and pCO_2, (b) Mg^{2+} and Ca^{2+} concentrations, and (c) ionic strength.

As seen in Figure 2.4, ε is relatively insensitive to pH, pCO_2, Mg^{2+} concentration and ionic strength. The maximum variations in ε is 0.1 ‰ even if pH changes by ~2 units, or if pCO_2 varies by an order of magnitude (Figure 2.4a). Interestingly, ε stays almost constant when Mg^{2+} concentration increases from 1 to 50 mM (Figure 2.4b). The U isotope fractionation ε decreases almost linearly at a rate of 0.16 ‰ per unit of ionic strength (Figure 2.4c). The fractionation ε is particularly sensitive to the variations in Ca^{2+} concentration. Relative to other factors, Ca^{2+} concentration can cause the largest variations in ε which increases from 0.00 to 0.25 ‰ in response to the elevation in Ca^{2+} (from 0 to 60 mM, Figure 2.4b).

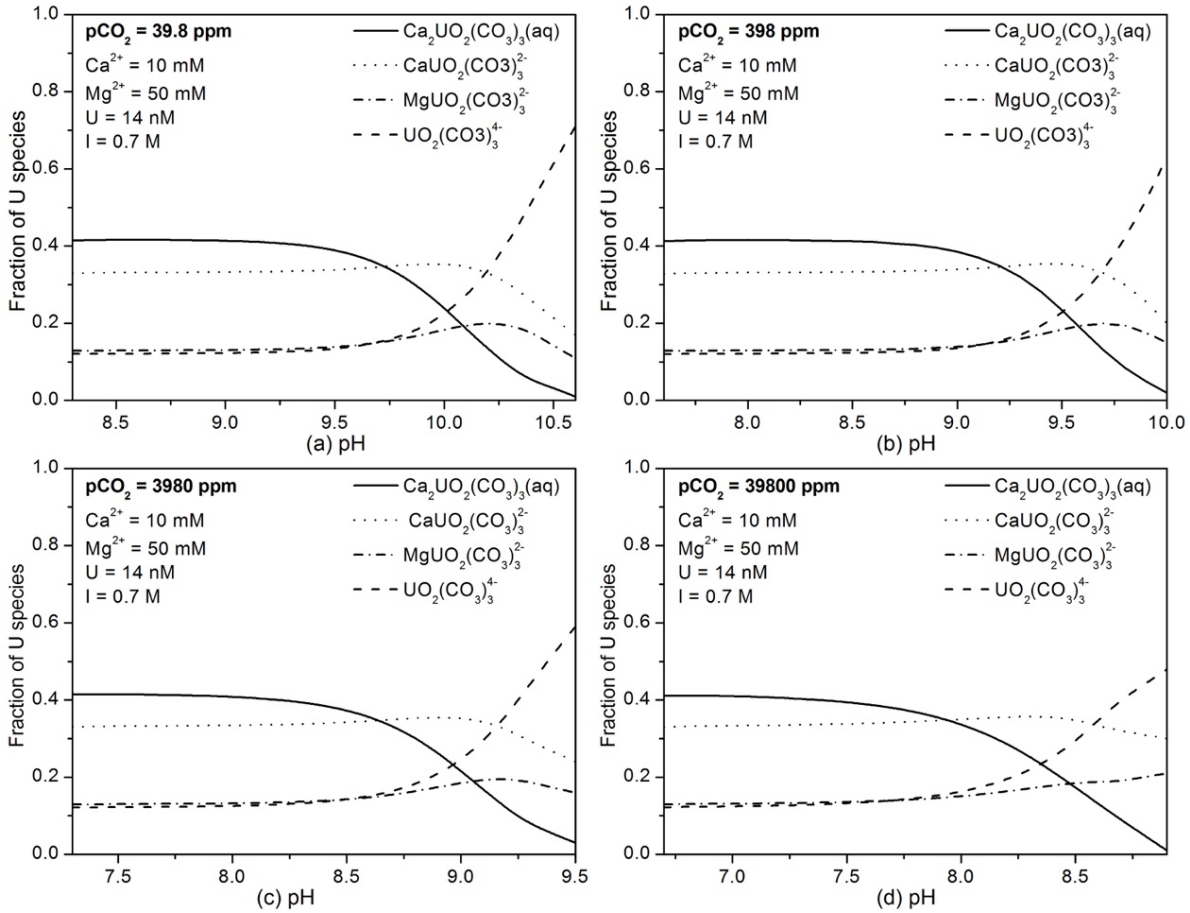

Figure 2.5. Aqueous U(VI) speciation vs. pH at constant pCO_2 with ionic strength of 0.7 M, $[Ca^{2+}]$=10 mM, $[Mg^{2+}]$=50 mM and [U(VI)]=14 nM. (a) pCO_2=39.8 ppm; (b) pCO_2=398 ppm; (c) pCO_2=3980 ppm; (d) pCO_2=39800 ppm.

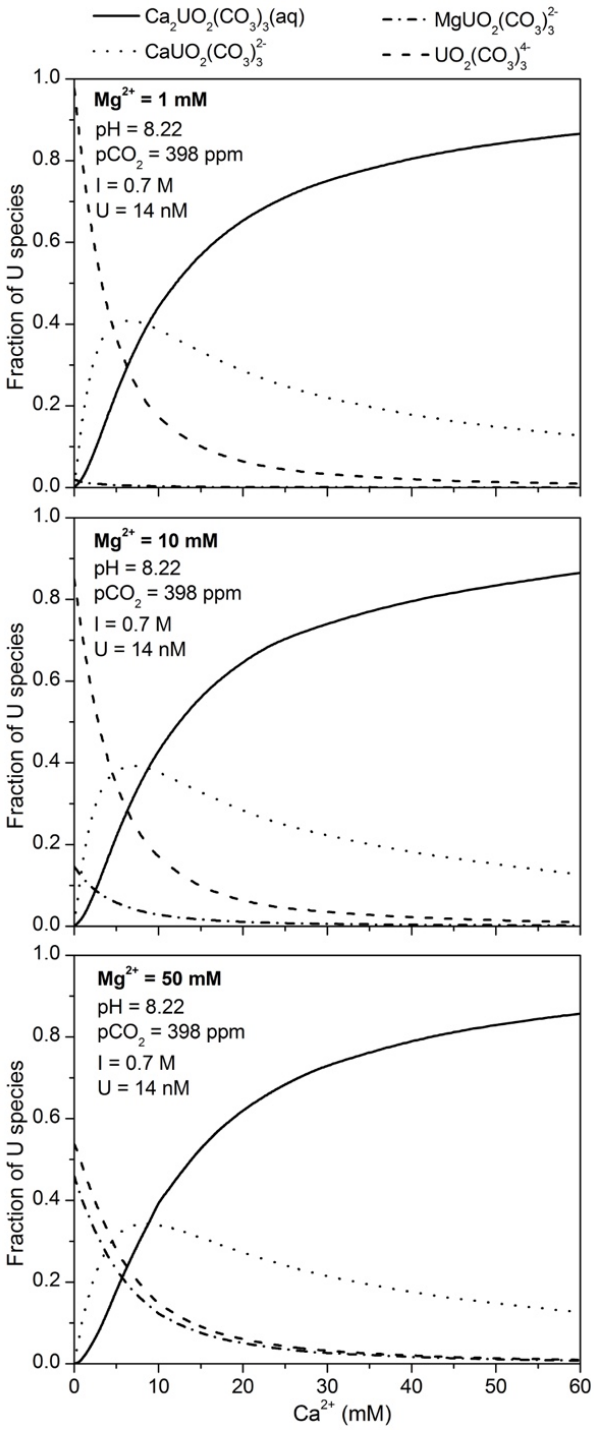

Figure 2.6. Aqueous U(VI) speciation vs. Ca^{2+} concentration at constant Mg^{2+} concentration with ionic strength of 0.7 M, pH=8.22, [U(VI)]=14 nM and pCO_2=398 ppm.

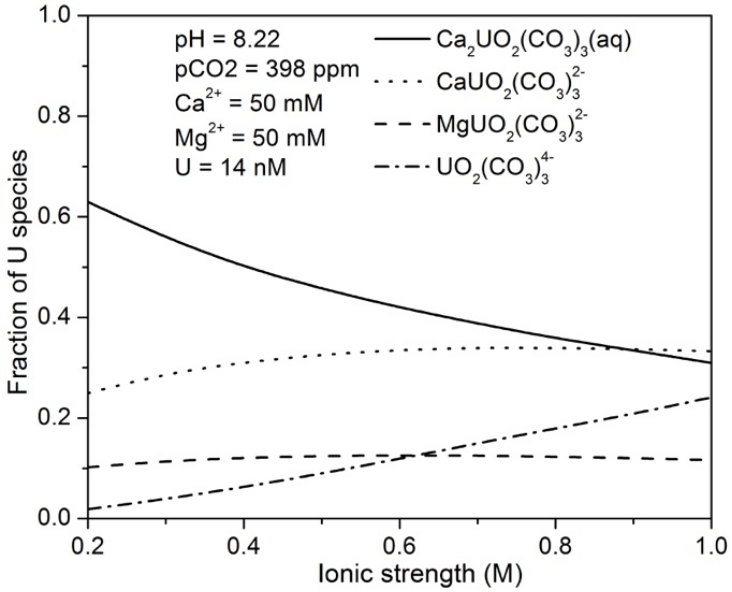

Figure 2.7. Aqueous U(VI) speciation vs. ionic strength with[Ca^{2+}]=10 mM, [Mg^{2+}]=50 mM, [U(VI)]=14 nM, pCO_2=39.8 ppm and pH=8.22.

In view of these sensitivities, uncertainties in the reconstructions of pH, pCO_2, Mg^{2+} concentration and ionic strength are not important to this study. However, uncertainty in the paleo-seawater Ca^{2+} concentration (typically ±5 mM; Lowenstein et al., 2003) is important. For example, if Ca^{2+} concentration is 10 mM, the typical uncertainty from inferred Ca^{2+} will cause a corresponding uncertainty of ±0.05 ‰, which is about 50 % of the estimated isotopic offset between U in $CaCO_3$ and modern seawater (0.11 ‰).

2.4 Discussion

2.4.1 Effects of U Isotopic Offset on Estimation of Oceanic Anoxia

The estimated isotopic offset between U in primary abiotic $CaCO_3$ and seawater over the Phanerozoic should not be overlooked when using U isotopes in carbonates to infer the extent of oceanic anoxia. First, the magnitude of U isotope fractionation during incorporation into calcium

carbonates (0.11–0.23 ‰) is comparable to all the other U sinks (0–0.25 ‰) in oceans except the anoxic/euxinic U sinks (~0.6 ‰; Tissot and Dauphas, 2015). Calcium carbonates scavenge 14–32 % of the total U from seawater (Dunk et al., 2002). As a result, $CaCO_3$ can shift U isotopic composition of seawater to be more negative by about 0.01–0.07 ‰, which is equivalent to the isotopic shift generated by increasing anoxic/euxinic U sinks by 3–12 %.

Second, the preferentially incorporation of heavier U isotopes into $CaCO_3$ observed in experiments (Chen et al., 2016) suggests that the actual $\delta^{238}U$ in seawater is lighter than that measured in natural carbonate samples. Compared to total expected range of redox-driven shifts in $\delta^{238}U$ (~0.8 ‰), the magnitude of isotopic offset between U in $CaCO_3$ and seawater over the Phanerozoic (0.11–0.23 ‰) can significantly impact reconstruction of seawater $\delta^{238}U$ from carbonate samples. This directly impacts the estimated extent of oceanic anoxia calculated from such records (details are discussed in the sections below).

2.4.2 Implications for U Isotopes in Biogenic Carbonates

Because most Phanerozoic calcium carbonate rocks are biogenic, it is important to consider the relevance of U isotope fractionation in abiotic experiments—which are the basis of this model—to biogenic carbonates. As in abiotic experiments, aqueous U speciation undoubtedly affects the uptake of U by biogenic carbonates. The best evidence comes from bulk measurements of U/Ca in corals and foraminiferal calcite, which show strong dependence on CO_3^{2-} concentration outside these calcifying organisms (Russell et al., 2004; Keul et al., 2013; Inoue et al., 2011; Raddatz et al., 2014).

Unfortunately, the chemical conditions at the calcification sites in these organisms are not well enough understood for quantitative modeling of U speciation. For example, *in situ*

measurement of pH using microelectrodes and indirect inference from B isotopes demonstrate that pH is generally elevated by as much as ~1 pH unit in the calcifying sites as compared to ambient external seawater (Nooijer et al., 2009; Trotter et al., 2011; Rollion-Bard and Erez, 2010; Tanaka et al., 2015; Georgiou et al., 2015; Martin et al., 2016). This might suggest a smaller U isotope effect. However, Ca^{2+} and CO_3^{2-} concentrations are likely higher at the calcifying sites because Ca-ATPase ion transporters exchanged $2H^+$ for Ca^{2+} to elevate the pH (McConnaughey et al., 1997; Zoccola et al., 2004; Al-Horani et al., 2003; Cohen and McConnaughey, 2003). The higher Ca^{2+} might lead to a larger U isotope effect, but there is not enough data on the Ca^{2+} concentration to estimate the magnitude of this effect. Other factors such as ionic strength and kinetic isotope effects during U transport to the calcifying sites may be important and are poorly constrained.

Therefore, while it is likely that secular variations in U speciation leads to secular variations in isotopic fractionation for biogenic as well as abiotic carbonates, yet there is no sufficient information to predict the magnitude of this effect during biogenic calcium carbonate precipitation. However, the potential consequences for paleoredox reconstructions can be explored under the assumption that the effects are similar, though future experimental work is needed to test the validity of this assumption.

2.4.3 Implications for $^{238}U/^{235}U$ in Carbonates as a Paleoredox Proxy

Changes in the chemical speciation of U in seawater could drive small but significant variations in U isotope fractionation during incorporation into marine carbonates, and this could have a significant impact on marine paleoredox reconstructions. For example, recent studies have demonstrated that Permo-Triassic carbonates record a 0.40 ‰ decrease in marine $\delta^{238}U$

coinciding with the Late Permian Mass Extinction (LPME), which suggests that the fraction of U incorporated in the anoxic marine U sink increased from ~10 % to 70–90 % of total inputs (Brennecka et al., 2011b; Lau et al., 2016; Elrick et al. 2017). To reconstruct seawater $\delta^{238}U$, Brennecka at al. (2011b) and Lau et al. (2016) assumed that the fractionation between seawater and carbonates was close to zero ($\Delta^{238}U_{carb}$=0 ‰), while Elrick et al. (2017) assumed a much larger diagenetic offset ($\Delta^{238}U_{carb}$=0.5 ‰). One challenge faced by all these studies is how to best explain the unusually heavy $\delta^{238}U$ values recorded in the latest Permian carbonates prior to the mass extinction event. This study demonstrates that by accounting for variations in seawater U speciation, the speciation-dependent isotope fractionation can readily explain these observations and provide a revised estimate for the magnitude of ocean anoxia during the LMPE.

As in previous studies, a two-component isotopic mass balance model was used to assess the extent of ocean anoxia. Assuming steady state, the marine U isotopic budget can be calculated as:

$$\delta^{238}U_{seawater} = \delta^{238}U_{river} - f_{anoxic} \times \Delta^{238}U_{anoxic} - (1 - f_{anoxic}) \times \Delta^{238}U_{other} \quad \text{Eq. 2.2}$$

where $\delta^{238}U_{seawater}$ and $\delta^{238}U_{river}$ (–0.30±0.05 ‰; Andersen et al., 2016) are the U isotopic compositions of seawater and the riverine input, respectively, and f_{anoxic} is the fraction of U removed into sediments underlying anoxic bottom waters. Following previous authors, if the fractionation between U in anoxic sediments and seawater ($\Delta^{238}U_{anoxic}$) is +0.60 ‰, and that the fractionation between U in remaining sinks and seawater ($\Delta^{238}U_{other}$ which includes metalliferous sediments, suboxic sediments, hydrothermal sediments, and carbonates) is +0.03 ‰ (Brennecka et al., 2011b; Tissot and Dauphas, 2015; Andersen et al., 2016).

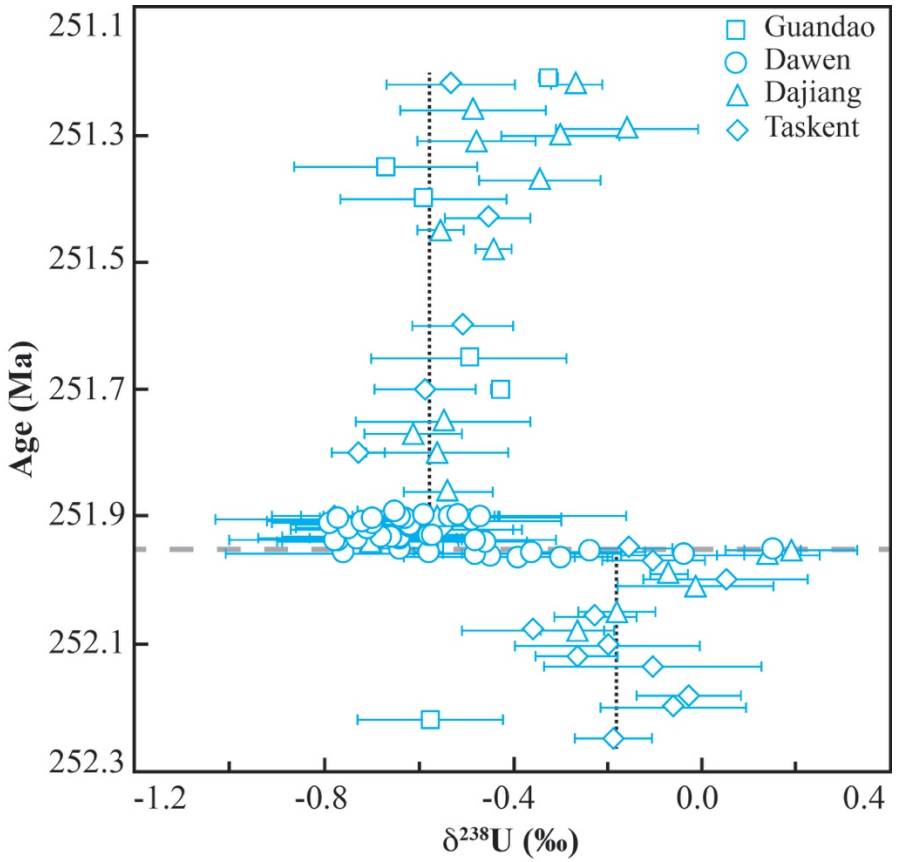

Figure 2.8. U isotopic compositions over the end-Permian mass extinction from four different carbonate sections: Dajiang (triangles), Dawen (circles), Guandao (rectangles) and Taskent (diamonds). These data points were from Brennecka et al. (2011b) and Lau et al. (2016). The horizontal dashed line is the late Permian Mass Extinction (LPME). The vertical dashed lines below and above LPME are the average U isotopic compositions before (–0.22 ‰) and after LPME (–0.58 ‰).

Using the high-resolution data from Brennecka et al. (2011b) and Lau et al. (2016), the estimated average $\delta^{238}U$ values measured in carbonates before and after the end-Permian extinction horizon are –0.18 ‰ and –0.58 ‰, respectively (Figure 2.8). The range of $\delta^{238}U$ values in Late Permian carbonates (–0.22 to 0.0 ‰) are significantly heavier than modern seawater (–0.39 ‰, Tissot and Dauphas, 2015). These values are potentially difficult to explain in a conventional U isotope mass balance model as they require nearly 100 % removal to oxic sinks and even exceed the model parameter space in some cases (Figure 2.9c). While

syndepositional diagenetic enrichment with isotopically heavy U(IV) offers one possible explanation from these heavy values (Romaniello et al., 2013), the paleo-reconstruction of seawater U speciation suggests that late-Permian carbonates probably precipitated with an isotopic offset of about +0.18 ‰ induced by aqueous U speciation during U(VI) incorporation into $CaCO_3$ (Fig 3b). After applying this correction, late Permian $\delta^{238}U_{seawater}$ was estimated to be between –0.40 ‰ and –0.18 ‰, similar to or slightly heavier than modern seawater. Based on this estimate, equation 2.2 was used to calculate that f_{anoxic} less than ~16 % prior to the extinction horizon (Figure 2.9c).

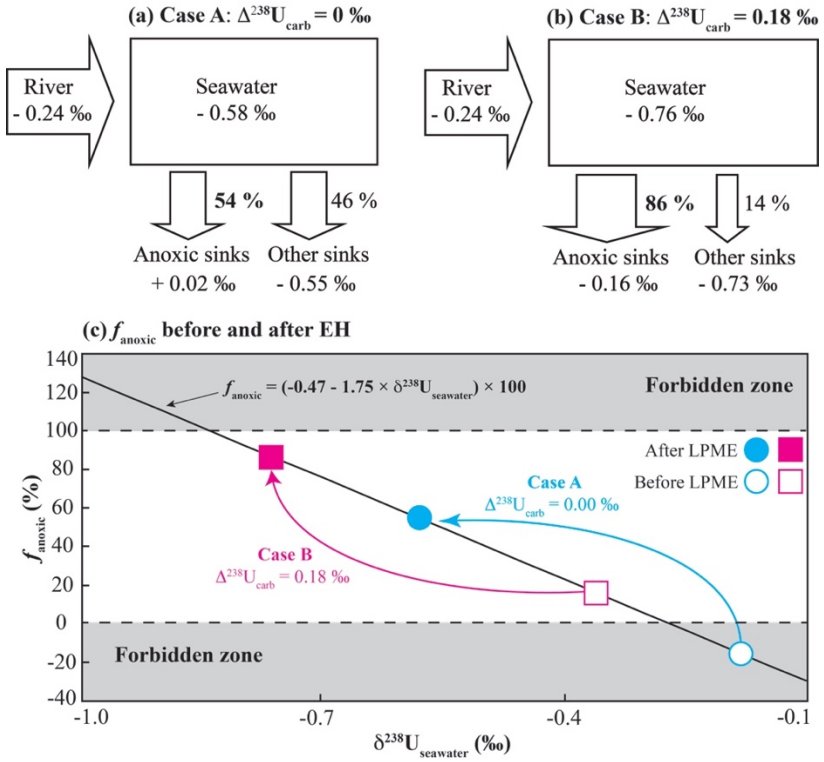

Figure 2.9. Calculated fractions of anoxic U sinks (f_{anoxic}) for the late Permian Mass Extinction (LPME) under two scenarios: $\Delta^{238}U_{carb}$=0 ‰ (a) and $\Delta^{238}U_{carb}$=0.18 ‰ (b), using equation 2.2. $\Delta^{238}U_{carb}$ is the U isotope fractionation between U in $CaCO_3$ and seawater. The $\delta^{238}U$ values in carbonates of the end-Permian mass extinction event were compiled from Brennecka et al. (2011b) and Lau et al. (2016). Calculated fraction of anoxic U sinks before and after LPME as a function of $\delta^{238}U_{seawater}$ for $\Delta^{238}U_{carb}$=0 ‰ and 0.18 ‰ (c). The forbidden zones indicate the values of f_{anoxic}>100 % or f_{anoxic}<0 %.

Applying the same correction to carbonates after the extinction event, which have an average $\delta^{238}U$ of –0.58 ‰, the $\delta^{238}U$ of early Triassic seawater was estimated to be –0.76 ‰. Using equation 2.2, f_{anoxic} was predicted to be 54 % in the absence of any correction vs. 86 % assuming $\Delta^{238}U_{carb}$=0.18 ‰ (Figure 2.9b). Clearly, there is a significant increase in f_{anoxic} when the U isotope fractionation during U coprecipitation with $CaCO_3$ is considered. Ocean acidification and increased seawater [Ca^{2+}], which have both been suggested for the LPME (Payne et al. 2010, Clarkson et al., 2015) would both result in an even larger value of $\Delta^{238}U_{carb,}$ and thus further increased estimates of LPME anoxia. Correcting for $\Delta^{238}U_{carb}$ results in more estimates suggesting more extreme anoxia, in an absolute sense, at the LPME and thus might help explain why the LPME was the largest mass extinction in the Earth history (Stanley, 2007). While it is cautioned that these calculations are subject to the uncertainties discussed above, they highlight the importance of understanding the effects of changes in U(VI) speciation on U isotope fractionation in carbonates, and should motivate future work to constrain the magnitude of this fractionation in biogenic systems through experimental studies and higher precision measurements in natural samples than have been conducted so far.

2.5 Conclusions

This study predicted that aqueous U(VI) speciation likely varied significantly in response to the secular variations in seawater chemistry over the Phanerozoic, especially due to large changes in seawater Ca^{2+} concentration. The modeling and sensitivity tests demonstrate that the U isotope fractionation, ε, between U in abiotic $CaCO_3$ and aqueous solution should be sensitive to these changes and result in an isotopic offset of 0.11 to 0.23 ‰ between U in abiotic $CaCO_3$

and seawater over this period. One important conclusion of this modeling that although the modern day isotopic offset between U in carbonates and seawater is relatively small (0.11 ‰), this value was probably larger over most of the Phanerozoic, with the Cenozoic and Holocene conditions representing a recent anomaly (Figure 2.3b).

U isotope fractionation induced by aqueous U speciation during U(VI) incorporation into $CaCO_3$ can significantly affect estimates of the extent of marine anoxia using U isotopes in marine $CaCO_3$, provided that the U isotope effect observed in abiotic $CaCO_3$ coprecipitation experiments is relevant to that in biogenic carbonates. For example, this offset potentially helps to explain high $\delta^{238}U$ values found in late Permian carbonates, and results in a significantly larger anoxic U sink at the LMPE. Because consideration of this effect can significantly impact U-based paleoredox estimates, it is important to consider this isotopic offset during future work. Future work is needed to refine these estimates and consider how changes in seawater chemistry might interact with possible biological effects to impact records of $\delta^{238}U$ in biogenic $CaCO_3$.

CHAPTER 3

BIOLOGICAL EFFECTS ON URANIUM ISOTOPE FRACTIONATION ($^{238}U/^{235}U$) IN PRIMARY BIOGENIC CARBONATES

The work presented in this chapter has been published as: Chen X., Romaniello S. J., Herrmann A. D., Samankassou E. and Anbar A. D. (2018) Biological effects on uranium isotope fractionation ($^{238}U/^{235}U$) in primary biogenic carbonates. *Geochim. Cosmochim. Acta* **240,** 1–10.

Abstract

Determining whether U isotopes are fractionated during incorporation into biogenic carbonates could help to refine the application of $^{238}U/^{235}U$ in $CaCO_3$ as a robust paleoredox proxy. Recent laboratory experiments have demonstrated that heavy uranium (U) isotopes were preferentially incorporated into abiotic aragonite, with an isotope fractionation of ~0.10 ‰ ($^{238}U/^{235}U$). In contrast, no detectable U isotope fractionation has been observed in most natural primary biogenic carbonates, but the typical measurement precision of these studies was ±0.10 ‰ and so could not resolve a fractionation of the magnitude observed in the laboratory.

To resolve this issue, a high precision $^{238}U/^{235}U$ method (±0.02 ‰, 2SD) has been developed, and utilized to investigate $^{238}U/^{235}U$ in primary biogenic carbonates including scleractinian corals, calcareous green and red algae, echinoderms, and mollusks, as well as ooids from the Bahamas, Gulf of California, and French Polynesia.

These results reveal that many primary biogenic carbonates indeed fractionate U isotopes during U incorporation, and that this fractionation is in the same direction as observed in abiotic $CaCO_3$ coprecipitation experiments. However, the magnitude of isotope fractionation in biogenic carbonates is often smaller than that predicted by abiotic $CaCO_3$ coprecipitation experiments (0.00–0.09 ‰ vs. 0.11±0.02 ‰), suggesting that one or more processes suppress U isotope fractionation during U incorporation into biogenic carbonates. It is proposed that closed-system behavior due to the isolation of the local calcification sites from ambient seawater, and/or kinetic/disequilibrium isotope fractionation caused by carbonate growth kinetics, explains this observation. These results indicate that U isotope fractionation between biogenic carbonates and seawater might help to constrain U partition coefficients, carbonate growth rates, or seawater chemistry during coprecipitation.

3.1 Introduction

Because of the relatively long residence time of uranium (U) in the oceans (~500 kyr; Dunk et al., 2002), the wide spatial-temporal distribution of sedimentary carbonate rocks in geologic record (Shields and Veizer, 2002; Mackenzie and Morse, 1992), and the fractionation of U isotopes during removal into anoxic sedimentary environments, the measurement of variations of $^{238}U/^{235}U$ in marine carbonates is finding application as a promising proxy to reconstruct global redox conditions of oceans through time (Brennecka et al., 2011b; Lau et al., 2016, 2017; Elrick et al., 2017; Dahl et al., 2014, 2017; Jost et al., 2017; Song et al., 2017; Bartlett et al., 2018; Zhang et al., 2018a, b; Clarkson et al., 2018). Early efforts to develop this proxy assumed that marine carbonates directly record seawater $^{238}U/^{235}U$ (e.g., Brennecka et al., 2011b). However, there is a risk that abiotic and/or biological processes fractionate U isotopes during incorporation into biogenic precipitates as is observed for other isotopes systems (e.g., $\delta^{53}Cr$ and $\delta^{11}B$; Wang et al., 2016; Henehan et al., 2016). If there were U isotope fractionation in these processes, $^{238}U/^{235}U$ in sedimentary carbonates would fail to faithfully record that of seawater, and significantly affect the reconstruction of paleoredox conditions. For example, an isotope fraction of 0.10 ‰ for $^{238}U/^{235}U$ during U incorporation into calcium carbonates corresponds to an offset of 18 % in the inferred extent of oceanic anoxia (Chen et al., 2017). Thus, it is essential to examine the U isotope fractionation during U incorporation into biogenic carbonates.

To address this issue, several previous studies examined $^{238}U/^{235}U$ variations in biogenic carbonates including corals, calcareous green and red algae, and mollusks and found that $^{238}U/^{235}U$ ratios were statistically indistinguishable from modern seawater at a typical measurement precision of ±0.10 ‰ (2SD; Stirling et al., 2007; Weyer et al., 2008; Romaniello et

al., 2013). A few higher precision measurements of fossil coral samples reached a similar conclusion at precision of approximately ±0.03 ‰ (2SD; Andersen et al., 2010). However, abiotic $CaCO_3$ coprecipitation experiments demonstrated measurable U isotope fractionation (~0.10 ‰) during U incorporation into carbonates at pH ~8.5, with heavier U isotopes preferentially enriched in precipitates (Chen et al., 2016). Based on these experiments, Chen et al. (2017) predicted that the isotope fractionation between modern seawater and abiotic carbonates should be ~0.11±0.02 ‰. However, this estimate is inconsistent with available evidence that suggests no apparent fractionation in biogenic carbonates. This inconsistency suggests that either the current the precision of U isotope measurement have not been able to resolve the U isotope fractionation in biogenic carbonates, or that biogenic carbonates display so called 'vital effects' which cause U to fractionate differently when partitioning into biogenic and abiogenic carbonates. Clarifying this issue has important implications for both understanding the mechanisms of U incorporation into biogenic carbonates and improving the U isotope paleoredox proxy. To this end, a new method for high precision measurement of $^{238}U/^{235}U$ was developed and applied to measure $^{238}U/^{235}U$ in a variety of primary biogenic carbonates.

3.2 Samples

A variety of primary biogenic carbonates samples including several species of scleractinian corals, calcareous green and red algae, mollusks and echinoderms were measured (Table 3.1). Specimens were mainly collected from the pertidal and subtidal zones of the Exumas region of the Bahamas at the Little Darby Research Station and were previously described by Romaniello et al. (2013). Individual hand samples were collected from the sediment surface.

When necessary, multiple specimens from the same sample location were pooled to provide sufficient U for high precision U isotope analyses. Ooid sands, which cover hundreds of square kilometers on the Bahamas platform (Harris, 2010), were sieved to purify ooids from the remaining detritus. Two additional coral samples from French Polynesia (Pretet et al., 2013) and one mollusk specimen from the Gulf of California are also included. All these biogenic carbonate precipitates are aragonite, except the red algae (high-magnesium calcite) and echinoderms (calcite, Romaniello et al., 2013).

Table 3.1. Sample information, U concentration, $\delta^{234}U$, and $\delta^{238}U$ for modern carbonate samples.

				Romaniello et al. (2013)			This study			
Samples	**Species**	**Locations**	**Carbonate mineralogy**	**$\delta^{238}U$ ‰**	**2 SE ‰**	**N**	**U ppm**	**$\delta^{238}U$ ‰**	**2 SE ‰**	**N**
Coral	*Diploria strigose*	Bahamas	Aragonite	–0.39	0.08	3	2.56	–0.37	0.01	16
Coral	*Siderastrea radians*	Bahamas	Aragonite	–0.37	0.08	3	2.6	–0.37	0.01	8
Coral	*Porites divaricata*	Bahamas	Aragonite	–0.37	0.09	3	2.61	–0.37	0.02	8
Coral	*Porites asteroides*	Bahamas	Aragonite	–0.37	0.09	3	2.86	–0.37	0.02	8
Coral	*Porites spirobranchus*	French Polynesia	Aragonite	–	–	–	2.32	–0.38	0.02	8
Coral	*Porites spirobranchus*	French Polynesia	Aragonite	–	–	–	2.11	–0.37	0.02	8
Mollusks	*Tellina listeri* (dead)	Bahamas	Aragonite	–0.38	0.08	3	0.06	–0.40	0.02	3
Mollusks	*Modiolus capax* (dead)	Gulf of California	Aragonite	–	–	–	0.06	–0.31	0.02	3
Green algae	*Acetabularia crenulata* (head, live)	Bahamas	Aragonite	–0.36	0.06	3	0.58	–0.33	0.02	3
Green algae	*Acetabularia crenulate* (stalk, live)	Bahamas	Aragonite	–0.34	0.09	3	1.05	–0.36	0.02	4
Green algae	*Rhipocephalus phoenix* (stalk, live)	Bahamas	Aragonite	–0.41	0.06	3	2.22	–0.34	0.01	8
Green algae	*Rhipocephalus phoenix* (leaves, live)	Bahamas	Aragonite	–0.42	0.09	3	1.65	–0.37	0.01	5
Green algae	*Halimeda incrassate* (whole, live)	Bahamas	Aragonite	–	–	–	1.25	–0.36	0.02	6
Green algae	*Penicillus capitatus* (head, live)	Bahamas	Aragonite	-0.43	0.07	3	1.95	–0.34	0.02	7
Green algae	*Penicillus capitatus* (stalk, live)	Bahamas	Aragonite	–0.25	0.06	3	1.33	–0.38	0.01	5
Red algae	*Neogoniolithon strictum* (live)	Bahamas	High-Mg calcite	–0.44	0.06	3	0.68	–0.35	0.02	7
Echinoderm	*Clypeaster subdepressus* (dead)	Bahamas	Calcite[1]	–	–	–	0.26	–0.30	0.02	4
Ooids	–	Bahamas	Aragonite	–0.27	0.07	3	2.85	–0.24	0.02	7
Seawater	–	Bahamas	–	–	–	–	0.003	–0.39	0.02	3

Note: [1]Gilbert and Wilt (2011). N represents the number of measurements for each sample on the MC-ICP-MS. $\delta^{238}U$ is the average value of multiple measurements.

3.3 High Precision $^{238}U/^{235}U$ Measurement

U isotopic ratios ($^{238}U/^{235}U$ and $^{234}U/^{238}U$) were measured on a multiple collector inductively coupled plasma mass spectrometer (MC-ICP-MS) using the ^{233}U-^{236}U double-spike method (Weyer et al., 2008; Chen et al., 2016). To increase the precision of the measurement of $^{238}U/^{235}U$ compared to prior studies, sample solutions were measured at a concentration of 200 ppb as compared to the more typical 50 ppb. To this end, the mass spectrometer was configured with 10^{10} Ω and 10^{12} Ω resistors on particular Faraday collectors, as described below. Some modifications of the sample preparation and U purification procedures necessitated by these larger sample sizes were also described below.

3.3.1 Sample Preparation

Primary biogenic carbonate precipitates were cleaned using Milli-Q water (18.2 MΩ) and dried at 105 °C for 48 hours. Dried samples were powdered in a ball mill equipped with trace-metal-clean silicon carbide mortars. To acquire the bulk U concentration and isotopic compositions of these biogenic carbonate samples, chunks of ~15 g of corals and red algae, and the whole mollusks, green algae, and echinoderms were powdered for chemical analysis.

Carbonate samples (0.5–10 g) were dissolved in excess 1M HNO_3 (all the reagents used are trace-metal grade) overnight and centrifuged at a rate of 4500 rpm to remove any insoluble material. A 50 μL aliquot of clear supernatant was used for analysis of major cations and trace metal concentrations on a Thermo iCAP Q ICP-MS at ASU. Samples were spiked with a ^{233}U-^{236}U double-spike (IRMM-3636) at a 0.0363 spike:sample molar ratio (Verbruggen et al., 2008; Chen et al., 2016). The spiked samples were then dried down completely and digested with

concentrated HNO_3 + 30% H_2O_2 repeatedly to remove any residual organic matter. The digested samples were finally dissolved in 3M HNO_3 in preparation for column chemistry. To avoid high concentrations of Ca^{2+} and SO_4^{2-}, which spontaneously nucleate and precipitate as $CaSO_4$ on the UTEVA resin, the Ca concentration was kept under 20 mg/ml in the loading acid.

3.3.2 U Purification

A slightly modified purification protocol was used to accommodate the larger sample sizes required for high-precision analyses. Briefly, after rinsing the polypropylene columns with 18.2 MΩ-cm deionized water, ~1 ml UTEVA resin (Eichrom Technologies, LLC) was loaded into 10mL chromatography columns (Bio-Rad Laboratories, Inc.). The resin was cleaned with 4×2.5 ml 0.05 M HCl to remove any trace U introduced during the loading step. Following this, the resin was washed with 3×1 ml 3 M HNO_3 to convert it to the nitrate form. Samples were loaded onto the columns in ~50 ml of 3 M HNO_3. To completely remove all the matrix ions except U and Th, an extended elution consisting of ~15 ml of 3 M HNO_3 (loaded in 1+2+3+4+5 mL aliquots) was used to rinse the resin. The remaining steps used to elute Th and U were identical to those reported in Chen et al. (2016). This UTEVA column protocol was repeated a second time to further purify U in order to ensure high-precision isotopic analyses. Following column chemistry, the U-containing eluent was dried down and digested with concentrated HNO_3 + 30% H_2O_2 several times to remove trace organic contamination from the resin.

3.3.3 U Isotope Analysis

In order to obtain higher analytical precision, the U concentration and beam intensity used during analysis were increased, while accommodating the high dynamic range of $^{238}U/^{235}U$ ratios by using a 10^{10} Ω resistor on the Faraday collector assigned to ^{238}U and three 10^{12} Ω resistors on the collector for ^{233}U, ^{235}U, and ^{236}U. ^{234}U was measured using a 10^{11} Ω resistor. Analyses at a series of increasing U concentrations (50, 100, 200, and 400 ppb) were tested, which were all introduced using a 50 μL min^{-1} PFA nebulizer and Apex-Q desolvation system (Elemental Scientific, Inc) and a combination of "Jet" sample cone and normal "H" skimmer cone (Thermo Fisher Scientific, Inc.). Under these conditions, signal intensity increased linearly with concentration, and measurement voltages for ^{235}U and ^{238}U were about 0.88 V and 120 V, respectively, when using a 200 ppb U solution. Each measurement consisted of a 110 s uptake time, 50 cycles (8.4 s per cycle), and a 210 s washout time. Samples analyses were bracketed by analyses of identically double-spiked CRM145a standard every 2 analyses in order to account for any non-ideal behavior of the double-spike correction due to peak tailing and deviation from a pure exponential law mass bias in the ICP-MS interface as previously reported (Chen et al., 2016).

U isotopic composition is reported in δ notation relative to the standard CRM-145a using the following equation:

$$\delta^{238}U = \left[\frac{\left({}^{238}U/{}_{235}U \right)_{sample}}{\left({}^{238}U/{}_{235}U \right)_{CRM-145a}} - 1 \right] \times 1000 \qquad \text{Eq. 3.1}$$

where the subscripts 'sample' and 'CRM-145a' stand for sample and the U reference standard CRM-145a. To obtain lower uncertainty in $\delta^{238}U$, each carbonate sample was measured ~8 times

following U purification. The uncertainty of the U isotopic compositions in samples was reported as two standard error of the mean (2 SE). For these high precision measurements, this study prefers to report the standard error of the mean rather than the more commonly used standard deviation in order to recognize the additional precision obtained through repeated analyses of samples solutions following column chemistry.

3.4 Results

3.4.1 Precision and Accuracy of $\delta^{238}U$ Analysis

The precision obtained for both $\delta^{238}U$ and $\delta^{234}U$ increase with U concentration (Figure 3.1). The observed improvement in measurement precision is consistent with errors predicted from the combined consideration of counting errors, thermal noise, and electronic noise in the amplifier circuits (John and Adkins, 2010).

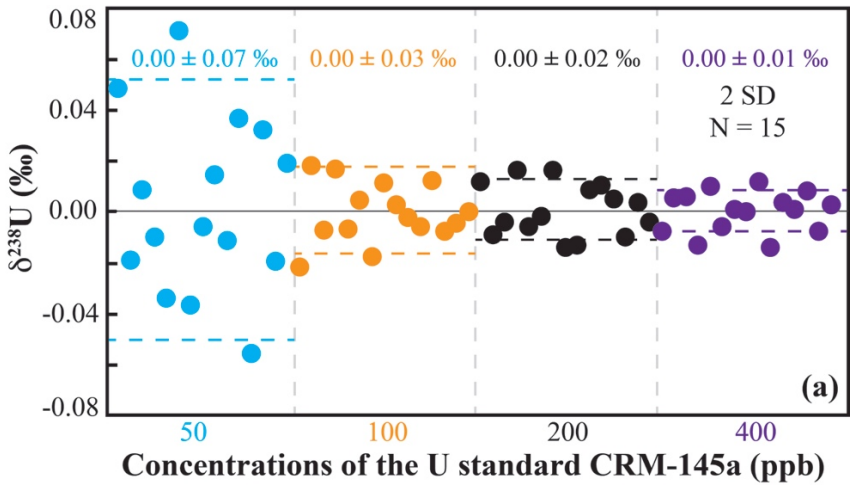

Figure 3.1. $\delta^{238}U$ of CRM-145a measured at U concentrations of 50, 100, 200 and 400 ppb. The horizontal solid line represents the overall average values of $\delta^{238}U$. The horizontal dashed lines represent theoretically predicted 2 SD uncertainty for $\delta^{238}U$ based on counting errors, thermal noise, and electronic noise in the amplifiers (e.g., John and Adkins, 2010).

Considering the sample size required for U isotopic measurement and significant improvement of the measurement precision for $\delta^{238}U$ at higher U concentrations, natural carbonate samples was measured at a U concentration of 200 ppb, which allows ~8 analyses of typical 1 g carbonate sample containing ~1.6 g of U. The typical precision achieved for $\delta^{238}U$ measurements in natural carbonate samples (±0.03–0.05 ‰, 2 SD) is slightly worse than achieved for the pure CRM-145a reference standard (±0.02 ‰). Subsequent method development suggests that this might have been due to small amounts of Na which is often leached from the UTEVA resin during sample purification.

The blank from the U purification procedure was about 0.09±0.05 ng (2 SD, N=6, see Table A.3), which was negligible compared to the amount of U used in each sample (>600 ng). Six aliquots of the pure CRM-145a were processed through the UTEVA column chemistry together with natural biogenic carbonate samples and acquired an average $\delta^{238}U$ value of 0.00±0.03 ‰ (2 SD, N=6, see Table A.3), which was the same as the direct measurement of pure CRM-145a (0.00±0.03 ‰).

3.4.2 U Concentration in Primary Biogenic Carbonates

U concentration varies significantly among different types of primary biogenic carbonates, in the descending order of scleractinian corals (2.11–2.86 ppm), calcareous red and green algae (0.58–2.22 ppm), echinoderm (0.26 ppm) and mollusks (0.06 ppm, Table 3.1 and Figure 3.2b). The ooids in this study had a U concentration of 2.85 ppm.

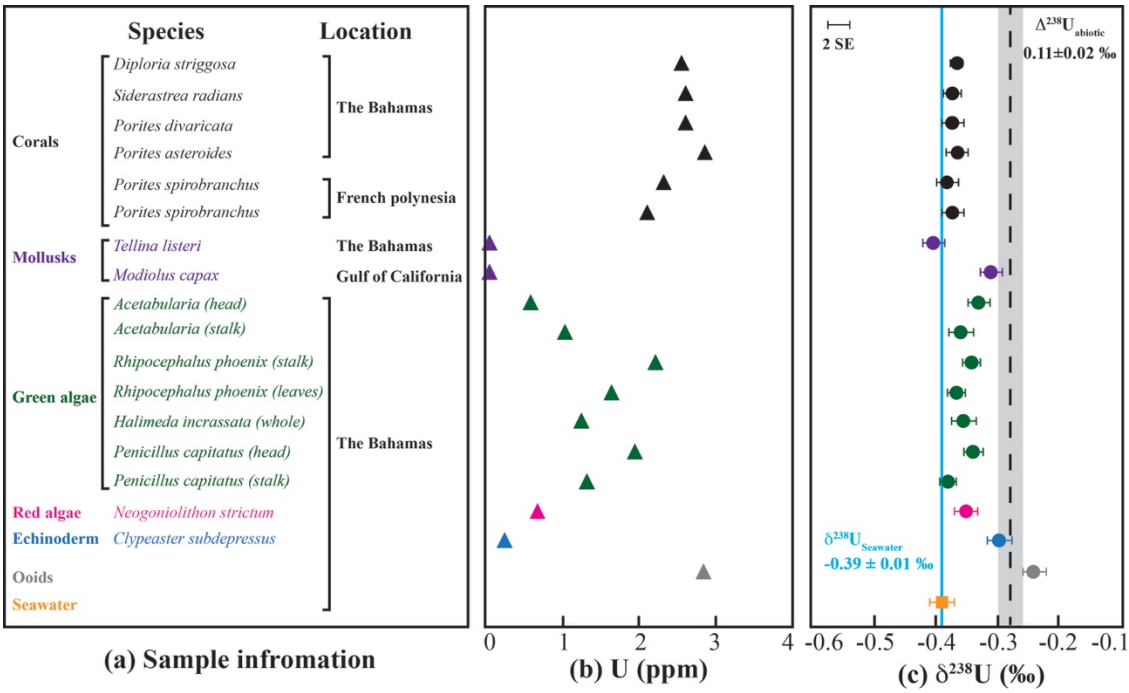

Figure 3.2. Sample information (a), U concentration (b), and $\delta^{238}U$ (c) in modern carbonates. The blue solid lines in panels (c) represents $\delta^{238}U$ in modern seawater (Tissot and Dauphas, 2015; this study). The gray band in panel (c) stands for the predicted range of $\delta^{238}U$ in abiotic carbonates in equilibrium with modern seawater ($\Delta^{238}U_{abiotic}$=0.11±0.02 ‰; Chen et al., 2016).

3.4.3 $\delta^{238}U$ in Carbonates

In contrast with previous measurements, the new high precision measurements of $\delta^{238}U$ demonstrate that many primary biogenic carbonates show small, but clearly resolved, isotope fractionation from seawater. Compared to the average $\delta^{238}U$ of modern seawater, –0.39±0.01 ‰ (Tissot and Dauphas, 2015; this study), samples in this study display fractionation over a range of 0.00–0.09 ‰, with the carbonate phase enriched in ^{238}U (Figure 3.2c). Corals, algae, and all primary biogenic carbonates display $\delta^{238}U$ significantly heavier than seawater (Student's t-test, $p < 0.05$, Table A.1 and A.2). $\delta^{238}U$ in scleractinian corals from the Bahamas and French Polynesia are the same with an average value of –0.37±0.01 ‰ (2 SE, number of coral samples, N=6). In

contrast, $\delta^{238}U$ values in mollusks are most likely species-dependent. Although *Tellina listeri* and *Modiolus capax* shared the same U concentration (0.06 ppm), $\delta^{238}U$ in the latter (–0.31±0.02 ‰, 2 SE) is heavier than the former (–0.40±0.02 ‰, 2 SE). Similarly, green and red algae fractionate U isotopes by about 0.01–0.06 ‰. The echinoderm sand dollar specimen (*Clypeaster subdepressus*) displayed the largest isotopic offset, ~0.09 ‰. $\delta^{238}U$ of the ooids is 0.15 ‰ heavier than modern seawater.

3.5 Discussion

3.5.1 U Isotope Fractionation in Primary Biogenic Carbonates

High-precision measurements of $^{238}U/^{235}U$ variations in biogenic carbonates reveal a range of U isotope fractionation in these samples with values typically 0.00–0.09 ‰ heavier than coeval seawater. To interpret the observed range of variation for U isotopes recorded in biogenic carbonates, two hypotheses were proposed: (1) equilibrium isotope fractionation occurs at calcification sites with varying degrees of restriction from seawater; or (2) kinetic/disequilibrium isotope fractionation is caused by rapid $CaCO_3$ precipitation at calcification sites. These hypotheses are discussed in more detail below.

3.5.1.1 Semi-restricted equilibrium isotope fractionation model

One possible explanation for the variation in isotopic fractionation observed between different biogenic carbonates is that the intrinsic equilibrium fractionation of U isotopes in primary biogenic carbonates is similar to that observed in abiotic $CaCO_3$ coprecipitation experiments, but that the magnitude of the isotope fractionation depends on the extent of the isolation of the local calcification sites from ambient seawater (Figure 3.3; Chen et al., 2016).

Previous abiotic $CaCO_3$ coprecipitation experiments demonstrated an equilibrium isotope fractionation of 0.00–0.10 ‰. This fractionation was interpreted to be dependent on the aqueous speciation of U, which in turn depends on Ca^{2+} and Mg^{2+} concentrations, alkalinity, pCO_2, pH and ionic strength (Chen et al., 2016). Based on this work, the U isotope fractionation during coprecipitation of U with abiotic calcite and aragonite in modern seawater was predicted to be 0.11±0.02 ‰ (Chen et al., 2017). If the calcification sites of primary biogenic carbonates are fully open to exchange with seawater and coprecipitation took place at isotopic equilibrium, an isotope fractionation of 0.11±0.02 ‰ would be expected (Chen et al., 2016, 2017). On the other hand, increasing restriction of calcification sites should lead to more closed system behavior which reduces the apparent isotope fractionation factor due to mass balance. In the end-member case, where calcification sites are completely isolated from the ambient seawater, almost quantitative U removal from the calcifying fluid will result in no isotope fractionation from seawater.

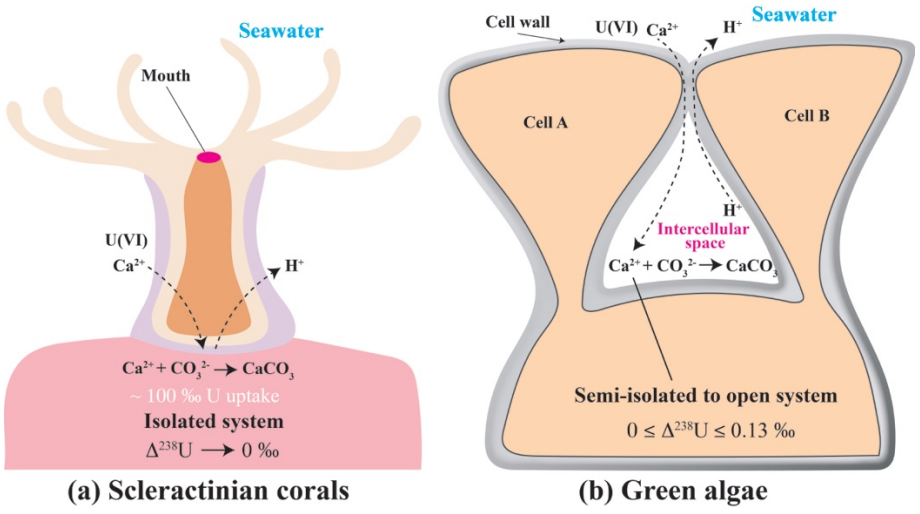

Figure 3.3. Schematic illustration of U uptake and isotope fractionation in (a) scleractinian corals and (b) green algae (modified from Galloway et al., 2007; Adey and Loveland, 2007).

Here, a Rayleigh fractionation model was applied to examine the U isotope fractionation in scleractinian corals and calcareous green algae. Experimental studies demonstrated direct and rapid transport of the surrounding seawater to the coral calcification sites, which are mostly isolated from ambient seawater (Figure 3.3a; Gagnon et al., 2007, 2012; Tambutté et al., 2012). Elevation of pH by ~1 unit at the local calcification sites leads to rapid precipitation of $CaCO_3$, leading to almost 100 % incorporation of U into carbonates (Al-Horani et al., 2003; Gaetani et al., 2011). This agrees with the observation that the $^{238}U/^{235}U$ of corals is very close to that of the ambient seawater in this study.

The variable U isotope fractionation in green algae might result from variable isolation of the calcification sites during different growth stages of the organism. $CaCO_3$ precipitates in the intercellular spaces of green algae (Figure 3.3b; Adey and Loveland, 2007). At the early growth stage of green algae cells, the intercellular spaces are open to seawater, resulting in an open-system Rayleigh isotope fractionation similar to abiotic $CaCO_3$ precipitates in seawater (0.11±0.02 ‰; Chen et al., 2017). However, as the walls of the adjacent cells grow together, the intercellular space becomes increasingly isolated from ambient seawater (Figure 3.3b; Adey and Loveland, 2007). Once completely isolated, U inside the intercellular spaces will be 100 % incorporated into carbonate precipitates in green algae, directly recording $^{238}U/^{235}U$ of the ambient seawater. Incorporation of U into green algae cells at different growth stages can therefore explain variable U isotope fractionation in these species, and even variable isotope fractionation between different parts of the same individual (e.g., stalk and head). Similar to green algae, calcification process occurs in the intercellular spaces in red algae (Krumbein, 1979), suggesting that the semi-restrict equilibrium isotope fractionation model could also interpret the U isotope fractionation observed in red algae.

Although the specific mechanisms of U incorporation into mollusks and echinoderms are not well understood, Ca uptake by these organisms suggests that U isotope fractionation might be governed by U transport processes within mollusks and echinoderms in addition to the extent of isolation of the calcification site from ambient seawater. For example, experiments using ^{45}Ca radiotracer demonstrated that mollusks adsorb dissolved Ca^{2+} from ambient seawater via the epithelial cells of the gill, inner mantle, and digestive canal. Ca is then delivered by the body fluids to the extrapallial space, which is isolated from ambient seawater, for calcification (Jodrey, 1953). If U were incorporated into mollusks in the same way as Ca, U isotope fractionation in the shells of mollusks would be controlled by U transport processes and the extent of the isolation of the calcification site. Similar to mollusks, the formation of skeletons of echinoderms is also a biologically controlled intracellular biomineralization process (Nakano et al., 1963; Gorzelak et al., 2011). Thus, variations in $d^{238}U$ of the shells of mollusks and echinoderms likely result from the biologically controlled U transport processes and the isolation of the calcification site from ambient seawater.

3.5.1.2 Kinetic/Disequilibrium Isotope Fractionation Model

An alternative explanation for the variation in U isotope fractionation observed between different primary biogenic carbonates is that U isotopic fractionation is controlled by differences in kinetic/disequilibrium isotopic effects resulting from differences in the $CaCO_3$ precipitation rates. The U isotope fractionation ($\Delta^{238}U_{biogenic}$) between primary biogenic carbonates (except one mollusk sample) and seawater appears to decrease with the U partition coefficients (K_d) in $CaCO_3$ (Figure 3.4a). The U partition coefficient K_d is defined as:

$$K_d = \frac{\left({}^{[U]}/_{[Ca]}\right)_{CaCO_3}}{\left({}^{[U]}/_{[Ca]}\right)_{aqueous}} \qquad \text{Eq. 3.2}$$

where $([U]/[Ca])_{CaCO3}$ and $([U]/[Ca])_{aqueous}$ are the molar concentration ratios of U to Ca in the bulk $CaCO_3$ and the aqueous solution, respectively (Curti, 1999).

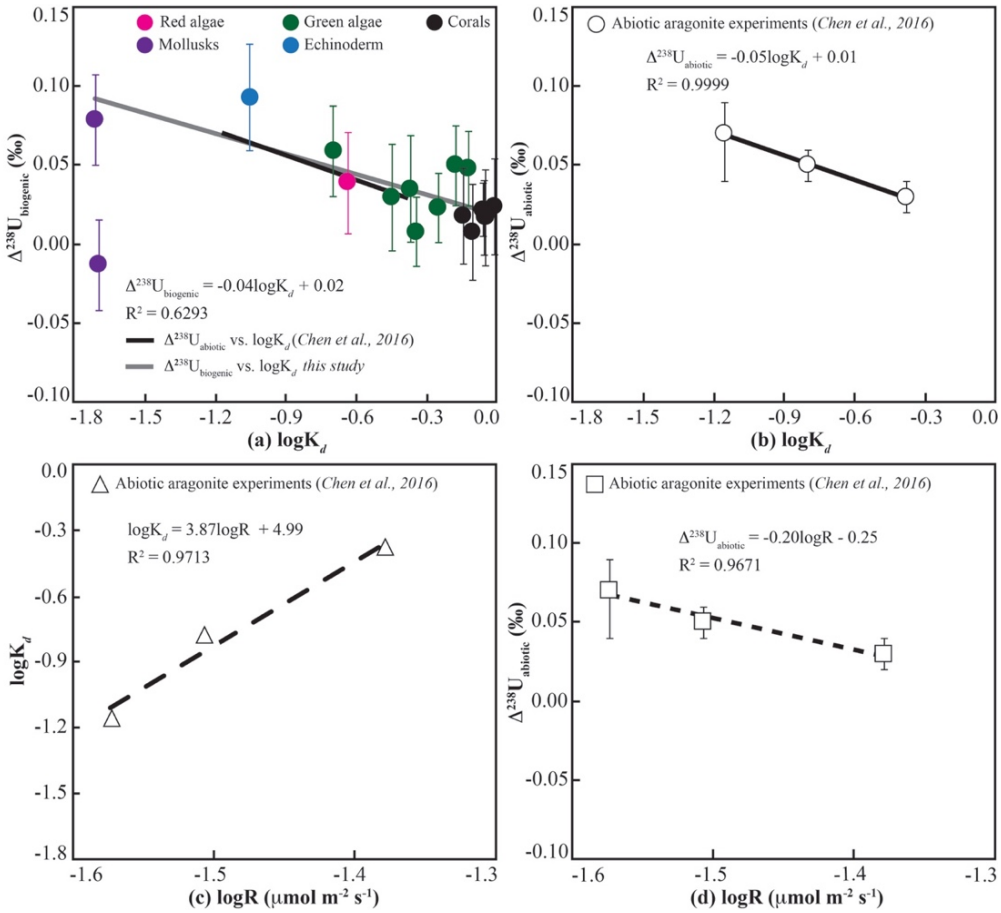

Figure 3.4. U isotope fractionation during U incorporation into (a) primary biogenic carbonates ($\Delta^{238}U_{biogenic}$; this study, 2 SE) and (b) abiotic aragonite ($\Delta^{238}U_{abiotic}$; Chen et al., 2016) versus U partition coefficient $logK_d$ (Figure A.1) (c) U partition coefficient $logK_d$ in abiotic aragonite versus growth rate logR. (d) $\Delta^{238}U_{abiotic}$ versus abiotic aragonite growth rate logR (Figure A.1). The black solid lines in (a) and (b) represent the linear regression of $\Delta^{238}U_{abiotic}$ over $logK_d$ observed in abiotic aragonite coprecipitation experiments (Chen et al., 2016). The gray solid line in (a) is the linear regression of $\Delta^{238}U_{biogenic}$ vs. $logK_d$, excluding one mollusk sample ($d^{238}U$=–0.40 ‰). The black dashed lines in (c) and (d) are the linear regressions of $logK_d$ and $\Delta^{238}U_{abiotic}$ over logR.

U isotope fractionation in laboratory-synthesized abiotic aragonite also showed a decreasing U isotope fractionation with increasing partition coefficient of U, suggesting that biogenic carbonates might fractionate U isotopes in the same way as abiotic aragonite (Figure 3.4b and Table 3.2; Chen et al., 2016). In abiotic aragonite coprecipitation experiments, K_d of U increased with aragonite growth rate (Figure 3.4c; Gabitov et al., 2008; Chen et al., 2016), resulting in an overall trend toward smaller U isotope fractionation with increasing precipitation rate (Figure 3.4d). One possible explanation for this pattern is that at high precipitation rates, U is less selectively incorporated into the rapidly growing carbonate lattice, while at slower precipitation rates, incorporation of various aqueous U species is more selective leading to the preferential incorporation of one or more isotopically heavy U species.

Table 3.2. Summary of U partition coefficients, carbonate growth rates and U isotope fractionation in abiotic aragonite coprecipitation experiments.

Aragonite experiments	$f_{neutral}$	K_d	logK_d	R mmol.m^{-2}s^{-1}	logR mmol.m^{-2}s^{-1}	$\Delta^{238}U_{abiotic}$ ‰
A1	0.27	0.07	–1.15	0.0267	–1.57	0.07+0.02/–0.03
A1*	0.24	0.17	–0.77	0.0311	–1.51	0.05+0.01/–0.01
A3	0.13	0.42	–0.38	0.0418	–1.38	0.03+0.01/–0.01

Note: $f_{neutral}$ is the fraction of the neutral U species $Ca_2UO_2(CO_3)_3(aq)$. R is the aragonite growth rate (Figure A.1). All these data were from previous abiotic aragonite coprecipitation experiments (Chen et al., 2016).

Likewise, differences in biogenic carbonate precipitation rates might also lead to variations in $\Delta^{238}U_{biogenic}$. The $CaCO_3$ precipitation rate of corals typically ranges from 2.5 to 6.9 mol m^{-2} s^{-1}, which is much faster than that observed for the green and red algae (0.001–0.74 mol m^{-2} s^{-1}; Gattuso et al., 1993, 1996; Ohde and van Woesik, 1999; Bates et al., 2001; Wray, 1977; Ortegón-Azna et al., 2017). Although areal calcification rates are unavailable for mollusks and

echinoderms, the close correlation between the apparent K_d and U isotope fractionation in biogenic carbonates suggest that a similar process might explain the range of observed values.

So far, no dedicated biotic experiments designed to test the effect of varying carbonate precipitation rate on U isotope fractionation during U coprecipitation with calcite or aragonite, but observations above suggest that such work might be warranted.

3.5.2 U Isotope Fractionation in Ooids

The U isotope fractionation observed in ooids is uniquely significant because the formation of these precipitates most closely resembles the processes occurring in abiotic aragonite coprecipitation experiments (Chen et al., 2016). While the formation of ooids is microbially meditated through prenucleation of amorphous calcium carbonate that transforms into aragonite in the ambient seawater (Daiz et al., 2014, 2015, 2017), this process most likely is continuous and in direct contact with ambient seawater. Radiocarbon ages for the innermost and outermost cortices of Bahamian ooids suggest that formation probably occurs episodically over a period of hundreds to thousands of years (Duguid et al., 2010). The magnitude of U isotope fractionation ($\Delta^{238}U$) in the ooid samples (0.15±0.02 ‰) is close to the U isotope fractionation predicted for the abiotic coprecipitation of U with $CaCO_3$ in modern seawater (0.11±0.02 ‰, Chen et al., 2016, 2017), which provides empirical support for the speciation-controlled isotopic fractionation model of Chen et al. (2016), although a kinetic origin for the observed isotope fractionation as discussed above can not be definitely ruled out.

3.5.3 Implications for U Incorporation into Biogenic Carbonates

The magnitude of U isotopic fractionation during U coprecipitation into biogenic carbonates might provide novel constraints on the processes controlling U/Ca partitioning in various biogenic carbonates. The U/Ca ratio in biogenic carbonates such as corals has been suggested as a proxy for reconstructing paleoclimate conditions because of its strong correlations with seawater temperature, pH, or CO_3^{2-} concentration (Min et al., 1995; Felis et al., 2009; Inoue et al., 2011; Shen and Dunbar, 1995; Arimid et al., 2011; Anagnostou et al., 2011). However, the exact factors which predominantly control U/Ca ratios in biogenic carbonates remain a matter of debate.

The negative correlation between U isotope fractionation and both the U distribution coefficient and carbonate growth rate might provide clues to answer this question. Uranium isotopes likely provide a unique probe of aqueous U speciation at the calcification site, which reflects a complex interplay between pH and CO_3^{2-} concentrations in the calcifying fluids as well as factors like restriction of the calcification site from seawater and the local calcification rate (e. g., Edrizzi and Rao, 2014; Keul et al., 2013; DeCarlo et al., 2015). For example, the elevations in pH, Ca^{2+}, and CO_3^{2-} concentrations at the calcification sites of corals significantly increased the supersaturation of aragonite, to 6 times that of seawater and changed aqueous U speciation (Al-Horani et al., 2003; Chen et al., 2016). Similarly, calcareous green algae also have isolated calcification sites between two cells that increased $CaCO_3$ supersaturation (Adey and Loveland, 2007; Wizemann et al., 2014; Borowitzka, 1982). These isolated calcification sites significantly increased the carbonate growth rate and elevated the partition coefficient of U in biogenic carbonates (Gabitov et al., 2008; Chen et al., 2016). Although understanding of how these processes impact U isotope fractionation is admittedly in its infancy, future work combining

studies of partition coefficients and U isotope fractionation during U coprecipitation in biogenic carbonates might offer better constraints than have been available from U/Ca ratios alone.

3.6 Conclusions

High precision measurements of $\delta^{238}U$ demonstrate small but resolvable U isotope fractionation (0.00–0.09 ‰) during U incorporation into primary biogenic carbonates. The magnitude of U isotope fractionation in these biogenic carbonates is similar to or smaller than previously reported abiotic aragonite coprecipitation experiments. Variations of $\delta^{238}U$ in different primary biogenic carbonates likely depend on either the extent of the isolation of the calcification sites from ambient seawater or calcium carbonate growth rates. In addition, U isotope fractionation during coprecipitation may eventually prove to be useful probe of aqueous U speciation in seawater and/or local calcifying fluids.

CHAPTER 4

DIAGENETIC EFFECTS ON URANIUM ISOTOPE FRACTIONATION IN CARBONATE SEDIMENTS FROM THE BAHAMAS

The work presented in this chapter has been published as: Chen X., Romaniello S. J., Herrmann A. D., Hardisty D., Gill B. C. and Anbar A. D. (2018) Diagenetic effects on uranium isotope fractionation in carbonate sediments from the Bahamas. *Geochim. Cosmochim. Acta* **237**, 294–311.

Abstract

Uranium isotope variations ($\delta^{238}U$) recorded in sedimentary carbonate rocks are a promising new proxy for the extent of oceanic anoxia through geological time. However, the effects of diagenetic alteration on the U isotopic composition in carbonate sediments, which are crucial to understand the accurate reconstruction of marine $\delta^{238}U$, are currently poorly constrained. This study examines the effects of the aragonite-to-calcite transition in the Pleistocene Key Largo Limestone of South Florida, and assess the effects of vadose meteoric, phreatic meteoric, and phreatic marine diagenesis on U isotope fractionation in carbonate sediments from the Bahamas Transect, including the well-studied Clino, Unda, and ODP Site 1006 drill cores.

The results of this study suggest that early diagenetic processes in Bahamas carbonate sediments fractionate U isotopes by an average of 0.27±0.14 ‰ (1 SD) heavier than contemporaneous seawater. Downcore variations of $\delta^{238}U$ in slope and basin sediments display little, if any, correlation with U concentration and common geochemical indicators of diagenesis

($\delta^{13}C$, $\delta^{18}O$, Mn/Sr, Mg/Ca, Sr/Ca), enrichments of redox-sensitive elements, or rare earth elements anomalies. Two possible mechanisms are proposed to interpret the positive change in the $\delta^{238}U$ during carbonate diagenesis: authigenic enrichment of isotopically positive U(IV) in carbonates and preferential incorporation of isotopically positive aqueous U(VI) species into carbonates. These processes likely operate during early (syndepositional) diagenesis on the banktop. Further diagenesis during deeper burial is limited by the low solubility of U(IV) under reducing pore water conditions.

The early diagenetic behavior of U isotopes in Bahamas carbonate sediments is likely broadly representative of carbonate diagenesis in the geological past. This study suggests that the mean diagenetic offset determined in this study be applied when reconstructing seawater $\delta^{238}U$ from ancient carbonates. Furthermore, early diagenesis induces significant statistical variability in sediment $\delta^{238}U$ values, pointing to the need for large, high resolution data sets in order to average out stochastic variations in individual bulk sediment samples.

4.1 Introduction

The development of new paleoredox proxies which can be applied to sedimentary carbonates offers significant advantages over more traditional proxies established for black shales (e.g., Algeo and Maynard, 2004; Algeo and Rowe, 2011; Pufahl and Hiatt, 2012). Whereas black shale deposition is often confined to relatively rare marginal basins leading to a spatially—and temporally intermittent record, the ubiquitous and often—continuous deposition of sedimentary carbonate rocks along passive continental margins offers the potential for long, continuous records of past ocean redox conditions. Such records would directly complement the well-established Phanerozoic records of carbonate $\delta^{13}C$ and $\delta^{18}O$, and $^{87}Sr/^{86}Sr$ and therefore provide important insights into the links between tectonics, climate, nutrient cycling, and atmospheric and ocean redox conditions (Morse and Mackenzie, 1990; Shields and Veizer, 2002; Jacobsen and Kaufman, 1999; Veizer et al., 1999).

Among a range of prospective carbonate paleoredox proxies, which includes redox sensitive elements (Huang et al., 2009; Chun et al., 2010), I/Ca (Lu et al., 2010; Zhou et al., 2014, 2015), and $\delta^{53}Cr$ (Frei et al., 2011, 2013; D'Arcy et al., 2017; Holmden et al., 2016; Wang et al., 2016; Gilleaudeau et al., 2016), uranium isotopes ($\delta^{238}U$) are uniquely capable of integrating global average paleoredox conditions. The $\delta^{238}U$ value of seawater changes due to isotope fractionation between oxidized U(VI) and reduced U(IV), which results in the preferential removal of ^{238}U to sediments under anoxic conditions, leaving residual seawater ^{238}U-depleted (Weyer et al., 2008; Basu et al., 2014; Wang et al., 2015; Stirling et al., 2015; Stylo et al., 2015; Andersen et al., 2017). Because of the long residence time of U in seawater (~400 kya), the $\delta^{238}U$ of the open ocean is uniform, and thus $\delta^{238}U$ of seawater—and potentially

of carbonates that precipitate from it—offers a globally averaged record of ocean redox conditions (Dunk et al., 2002; Tissot and Dauphas, 2015; Romaniello et al., 2013). This technique has already seen growing application to ancient carbonate sediments including the late Cambrian SPICE event and the Permo-Triassic and End-Triassic mass extinction events (Brennecka et al., 2011b; Dahl et al., 2014; Lau et al., 2016, 2017; Elrick et al., 2016; Jost et al., 2017; Azmy et al., 2015).

A significant challenge in applying the $\delta^{238}U$ proxy to carbonates is understanding the potential impact of syndepositional and post-depositional diagenesis in these permeable sediments. The potential impact of carbonate diagenesis on a wide range of geochemical proxies is well-known (e.g., $\delta^{13}C$, $\delta^{18}O$, I/Ca, $\delta^{11}B$; Swart, 2015; Stewart et al., 2015; Hardisty et al., 2017). $\delta^{238}U$ is no exception. Although modern primary biogenic carbonates record $\delta^{238}U$ values close to seawater, Romaniello et al. (2013) found that $\delta^{238}U$ in modern banktop carbonate sediments from the Bahamas are 0.2–0.4 ‰ more positive than seawater, due to reductive authigenic enrichments of U from sulfide-rich pore water. Similarly, Hood et al. (2016) found large variations of $\delta^{238}U$ in samples of different carbonate microfacies with varying degrees of diagenetic alteration from the Cryogenian Balcanoona reef complex in South Australia.

The goal of this project was to systematically explore the impact of early diagenesis on bulk-sediment $\delta^{238}U$ values in well-characterized modern settings. Because the $\delta^{238}U$ of seawater has been almost constant over the Cenozoic, the initial $\delta^{238}U$ value of these sediments can be assumed to be close to modern seawater (Wang et al., 2016; Romaniello et al., 2013; Chen et al., 2016). During early diagenesis, carbonate dissolution and recrystallization typically results in mineralogy transformations, loss of the endogenous U and incorporation of the exogenous U into

the secondary carbonate precipitates, and changes in pore water chemistry (e.g., Ca^{2+}, Mg^{2+}, and CO_3^{2-} concentrations). Pervasive recrystallization of metastable aragonite and replacement by calcite is one of the most important early diagenetic transitions, especially given that the partition coefficients for U into calcite are much lower than those for aragonite, resulting in the preferential loss of U from recrystallized sediments (Reeder et al., 2000, 2001; Chen et al., 2016).

In order to explore U isotope fractionation during the reaction of aragonite to calcite during meteoric diagenesis, this work measured $\delta^{238}U$ along a transect of an *Orbicella annularis* (previously named as *Montastrea annularis*) coral head from the Pleistocene Key Largo Limestone, South Florida (Gill et al., 2008). Additional alteration of carbonate sediments occurs in a number of settings, including further meteoritic diagenesis due to changes in sea level and exposure of sediments to freshwater, and phreatic marine diagenesis. These more aggressive diagenetic regimes can result in extensive recrystallization of carbonates, including replacement of sedimentary fabrics and dolomitization of sediments, as well as potential exchange of U with exogenous diagenetic fluids. To examine the effect of these different diagenetic processes, $\delta^{238}U$ variations in the extremely well-characterized Bahamas carbonate transect were measured, including samples from the Unda, Clino and Site 1006 (ODP, Leg 166) drill cores. Fluid-rock interaction modeling was used to set the observations in this study into a theoretical context, and combine these empirical and theoretical results to draw broader conclusions about how to identify and correct for the most likely patterns of $\delta^{238}U$ diagenetic alteration in ancient sediments.

4.2 Samples

4.2.1 Key Largo Limestone Samples

The *Orbicella annularis* coral head KL1 from the Pleistocene Key Largo Limestone, provides a simple case study of U isotope fractionation during aragonite-to-calcite alteration resulting from meteoric diagenesis (Gill et al., 2008). The corals which now form the Key Largo Limestone grew on the Florida platform during Marine Isotope Stage 5e (MIS 5, Eemian interglacial period, 119–124 ka), when sea-level was 6–9 meters higher than present (Broecker and Thurber, 1965; Hoffmeister and Multer, 1968). Due to falling sea level, these coral skeletons were continuously exposed to meteoric fluids for the past ~100 ky (Martin et al., 1986). The primary carbonate mineralogy of the coral skeleton was exclusively aragonite, which has been partially altered to calcite (Wunder, 1974; Martin et al., 1986; Gill et al., 2008). The coral head KL1 (Figure 4.1) shows a sharp, cm-scale aragonite-to-calcite transition without any apparent textural gradient (Gill et al., 2008). Previous measurements of I/Ca ratio, which is sensitive to the reduction of iodate (IO_3^-) to iodide (I^-) occurring under nitrate-reducing redox conditions, suggests that recrystallization that occurred under primarily oxidizing conditions is expected to preclude reduction of U(VI) to U(IV) (Hardisty et al., 2017). Uranium concentrations and isotopic compositions were measured at six points drilled along a transect that crosses aragonite-to-calcite transition and includes three aragonite samples and three calcite samples (Figure 4.1).

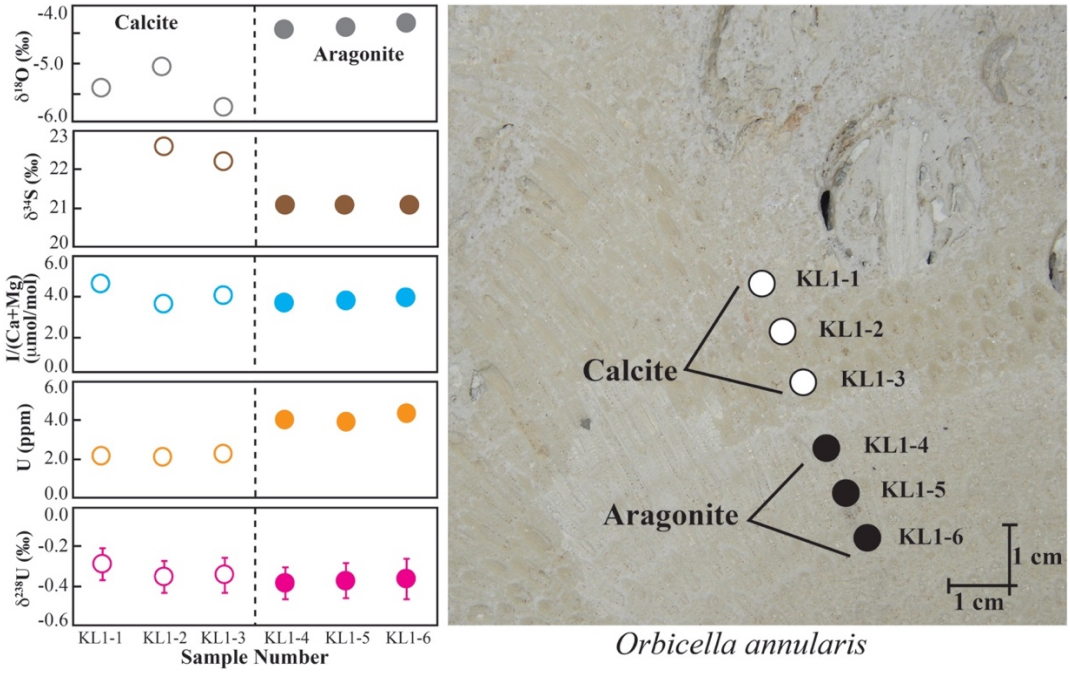

Figure 4.1. $\delta^{18}O$, $\delta^{34}S_{CAS}$, I/(Ca+Mg), U concentration and $\delta^{238}U$ along the aragonite-to-calcite transition of an *Orbicella annularis* coral head from the Pleistocene Key Largo Limestone. The $\delta^{18}O$ and $\delta^{34}S_{CAS}$, and I/(Ca+Mg) data are from Gill et al. (2008), and Hardisty et al. (2017). The dashed line is the aragonite to calcite transformation boundary.

4.2.2 Bahamas Carbonate Sediment Samples

Carbonate sediments from the western Bahamas platform are among the best-studied modern examples of carbonate diagenesis, and have been the subject of two different scientific drilling campaigns. Two shallow water cores, Unda and Clino, were drilled by the Bahamas Drilling Project (BDP) in order to explore patterns of sediment deposition and diagenesis along the margins of carbonate platforms (Figure 4.2; Ginsburg, 2001; Eberli et al., 1997; Kenter et al., 2001; Melim et al., 1995). The cores were complemented by a series of deeper-water cores collected during ODP Leg 166 Bahamas Drilling Transect, which extended the record of post-depositional carbonate diagenesis to sediments that have predominantly underwent phreatic marine diagenesis (Eberli et al., 1997). Samples from Unda, Clino, and the most distal core from

Site 1006 (ODP, Leg 166) were selected to explore diagenesis along modern slope-basin carbonate transect. Increasing the value of comparative paleo geochemical studies, other paleoredox and diagenetic indicators $\delta^{13}C$, $\delta^{18}O$, I/(Ca+Mg), Ce/Ce*, and mineralogical data are available from these exact same samples from Hardisty et al., (2017) and previous works have measured $\delta^{11}B$ and $\delta^{24}Mg$ and $\delta^{44}Ca$ from similar depths of these same cores (Stewart et al., 2015; Higgins et al., 2018; Liu et al., 2015).

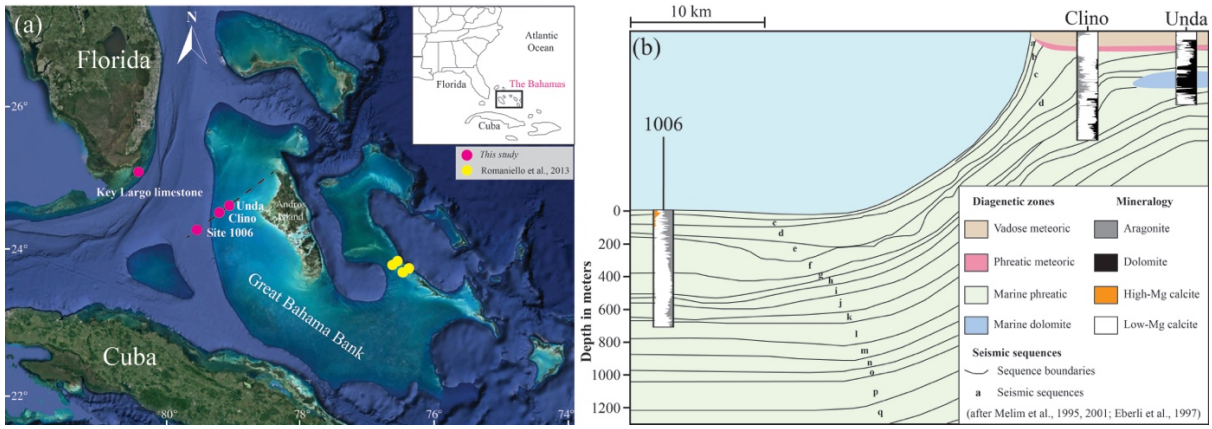

Figure 4.2. Site map of the Bahamas transect showing sites Clino and Unda, and Site 1006 (after Eberli et al., 1997; Melim et al., 1995, 2001), and the *Orbicella annularis* coral head KL1 from Key Largo Limestone, Florida (pink symbols). The locatios of the core-top samples from Romaniello et al. (2013) were displayed as yellow symbols.

Unda consists of three intervals of shallow-water platform sands and reefal deposits that occur at 8.6–108.1 m, 292.8–354.7 m, and 443–453.5 m (Eberli et al., 1997). These intervals alternate with deeper shelf deposits of silt and fine-sand. Clino also has three intervals: (1) shallow-water platform (21.6–98.45 m) with seven units each of which is capped by a subaerial exposure horizon; (2) reefal deposits (98.45–197.44 m); (3) slope sediments predominated by monotonous intervals of skeletal and non-skeletal grains of silt to fine sand size (197.44–677.27 m; Eberli et al., 1997; Melim et al., 2001). Carbonates in the distal core Site 1006 is a mixture of pelagic and bank-top derived carbonates containing small amounts of siliciclastic clays (Frank and Bernet, 2000; Malone, 2000).

Because of Pleistocene sea level fluctuations (up to ~120 m; Fairbanks, 1989), the upper sections of shallow-water carbonates in the Unda and Clino drill cores underwent significant vadose meteoric diagenesis, characterized by significant negative changes in the $\delta^{13}C$ and $\delta^{18}O$ extending from 0–80 m in Unda and 0–105 m in Clino (Melim et al., 2004). Below this upper interval, an interval of covariance in $\delta^{13}C$ and $\delta^{18}O$ extends from 80–120 m in Unda and 105–

145 m in Clino, with phreatic marine diagenesis dominating in the lower section of these two cores. While the zone of covariance has been previously interpreted as resulting from alteration in the mixing zone (Melim et al., 2004), recent work has concluded the zone of covariance arises within the meteoric phreatic zone (Swart and Oehlert, 2018). In contrast to Clino and Unda, Site 1006 is situated ~ 658 m below the modern sea level and has not been exposed to meteoric fluids, thus has only experienced marine diagenesis (Swart, 2000; Henderson, 2002). The lowest sea level has been since the Miocene is about ~120 m lower than present day (Swart and Oehlert, 2017).

The original aragonite-rich sediments in Bahamas carbonates from Clino and Unda have been altered to varying degrees by diagenetic processes. Carbonate mineralogy in the upper portion of Clino (0–150 m) has been transformed from aragonite to mostly low-Mg calcite (LMC), while deeper sediments consist of a mixture of aragonite, LMC, and minor amounts of dolomite. In contrast, while the upper portion of Unda core (0–60 m) is primarily LMC, deeper sediments are nearly completely dolomitized (Eberli et al., 1997; Melim et al., 1995, 2001, 2002; Swart et al., 2001). Sediments at the deeper water Site 1006 consist primarily of a mixture of aragonite and LMC. Calcite cements (micrite, isopachous spar, and dogtooth spar) are common throughout Unda and Clino, but only accounting for 5 % of the total carbonates (Eberli et al., 1997). The top 30 m of Site 1006 is unlithified (Frank and Bernet, 2000; Malone, 2000).

From the three drill cores, a total of 96 samples were selected from the three diagenetic intervals showing different degrees of carbonate mineralogy alteration and distinctive pore water chemistry. Samples from Site 1006 correspond to samples previously analyzed for their initial $^{234}U/^{238}U$ ratios by Henderson (2002). This site has been previously described by several workers (Eberli et al., 1997; Melim et al., 1995).

4.3 Methods

4.3.1 U Concentration and Isotopic Ratios Measurements

$\delta^{238}U$ was measured using multi-collector inductively-coupled plasma mass spectrometry (MC-ICP-MS) at Arizona State University (ASU). Carbonate sample powders (0.5–1.2 g) were dissolved in 50 mL 1 M HNO_3 overnight and then centrifuged at 4500 rpm to remove insoluble residues. A 50 μL aliquot of clear supernatant was extracted for subsequent major cations and trace metal concentration analysis on a Thermo iCAP Q ICP-MS at ASU. Aliquots containing 250–500 ng of U were taken from each sample and spiked with a ^{233}U-^{236}U double-spike (IRMM-3636) at a U_{spike}:U_{sample} molar ratio of 0.0363 (Verbruggen et al., 2008; Chen et al., 2016). The spiked samples were then dried down completely and brought up in 3 M HNO_3 for U purification.

Purification of U was performed using the Eichrom UTEVA resin procedure (Chen et al., 2016). Purified samples were measured at a concentration of ~50 ppb in 0.32 M HNO_3 on a Thermo Scientific Neptune MC-ICP-MS equipped with an ESI Apex desolvating nebulizer at ASU. The signals of ^{233}U, ^{235}U, ^{236}U and ^{238}U were collected with Faraday cups connected to 10^{12} Ω, 10^{12} Ω, 10^{12} Ω, and 10^{11} Ω resistors, respectively. The typical signal for the isotope ^{238}U from a 50 ppb U solution was ~30 V. The U isotope data are reported in standard δ notation relative to the CRM-145a isotopic standard:

$$\delta^{238}U = \left[\frac{\left({}^{238}U/{}_{235}U \right)_{sample}}{\left({}^{238}U/{}_{235}U \right)_{CRM-145a}} - 1 \right] \times 1000 \qquad \text{Eq. 4.1}$$

At least 3 replicate measurements were obtained for each sample solution. The U isotopic composition precision is presented as twice the standard deviation (2 SD), calculated using the standard deviation of either of the sample or standards, whichever was larger. The reproducibility of replicate measurements of $\delta^{238}U$ for CRM-145a was 0.08 ‰ (2 SD, N=134). The accuracy of the U isotope measurement was checked by analyzing the standard CRM-129a. The average value of $\delta^{238}U$ for CRM-129a was –1.70±0.08 ‰ (2 SD, N=23), in agreement with previous work (Wang et al., 2015; Chen et al., 2016).

Uranium isotope measurements were corrected for detrital uranium using measured aluminum (Al) concentrations and normalization to the Post-Archean Australia Shale (PAAS, Tribovillard et al., 2006). The fraction of U from detrital components was calculated as $f_{detrital} = (U/Al)_{PAAS}/(U/Al)_{sample}$. The corrected $\delta^{238}U$ was then calculated as:

$$\delta^{238}U = \frac{\delta^{238}U_{sample} - f_{detrital} \times \delta^{238}U_{detrital}}{1 - f_{detrital}} \quad \text{Eq. 4.2}$$

where $\delta^{238}U_{sample}$ and $\delta^{238}U_{detrital}$ (–0.29 ‰; Tissot and Dauphas, 2015) are the values of the sample and detrital components, respectively. The magnitude of this detrital correction was small (<0.015 ‰), reflecting the low detrital content of Bahamian carbonates.

4.3.2 Fluid-rock Interaction Modeling

To better understand the processes controlling diagenetic modification of $\delta^{238}U$ in carbonates, the well-established open-system fluid-rock interaction model was applied to simulate evolution of trace element abundances (Mn, Sr, and U) and isotopic compositions ($\delta^{13}C$, $\delta^{18}O$ and $\delta^{238}U$) during diagenetic alteration of primary carbonates (Banner and Hanson, 1990; Jacobsen and Kaufman, 1999). The utility of such modeling for understanding diagenetic

controls on $\delta^{238}U$ was recently demonstrated by Lau et al. (2017). This approach was tailored for diagenesis in Bahamian sediments.

For the open-system fluid-rock interaction model, the concentration of element *i* in the rock is calculated using the equation (Jacobsen and Kaufman, 1999):

$$C_i^r = D_i + \left(C_i^{r0} - D_i C_i^{f0}\right)\exp\left(\frac{N}{D_i}\right) \quad \text{Eq. 4.3}$$

where D_i ($=C_i^r/C_i^f$), the effective fluid-rock distribution coefficient, is defined as the ratio of the concentration of the element i in the rock (C_i^r) to the fluid (C_i^f); C_i^{r0} and C_i^{f0} are the initial concentrations of the element in the fluid and rock, respectively; and N is the weight ratio of fluid to rock.

The isotopic compositions for element i in the rock (δ_i^r) is calculated by the equation:

$$\delta_i^r = \frac{\left(\frac{C_i^{r0}}{C_i^{f0}}\right)\delta_i^{r0} + D_i\left[\exp\left(\frac{N}{D_i}\right) - 1\right]\left[\Delta_i + \delta_i^{f0}\right]}{\left\{\left(\frac{C_i^{r0}}{C_i^{f0}}\right) + D_i\left[\exp\left(\frac{N}{D_i}\right) - 1\right]\right\}} \quad \text{Eq. 4.4}$$

where δ_i^{r0} and δ_i^{f0} are initial isotopic compositions of element i in the rock and fluid; Δ_i (= 1000× ($\alpha_{r\text{-}f}$ –1)) is the isotope fractionation between the rock and fluid.

The effective distribution coefficients (D_i) and isotope fractionation factor ($\alpha_{r\text{-}f}$) between the rock and the fluid are derived from experimental studies or from natural carbonates (See Table B.3). The initial elemental concentration (C_i^{r0}) and isotopic compositions (δ_i^{r0}) are from direct measurements of primary Bahamian carbonates (Romaniello et al., 2013; Swart et al., 2009). The initial elemental concentrations (Ca, Mn and Sr) and isotopic compositions of the fluids ($\delta^{13}C$ and $\delta^{18}O$) come from measurements of the pore fluids of the Bahamas carbonate platform (Swart et al., 2000, 2009; Romaniello et al., 2013; Hu and Burdige, 2007; Bowen and

Revenaugh, 2003). U concentration in the meteoric and marine fluids is assumed to be the same. Dissolved U concentrations under oxic and anoxic conditions are 3 and 0.5 ppb, similar to open seawater and Bahamian pore water (Chen et al., 1986; Henderson et al., 1999). The initial $\delta^{238}U$ in the meteoric and marine fluids are –0.30 and –0.39 ‰. Under oxic conditions, the U isotope fractionation factor (α) between the rock and diagenetic fluids were estimated according to Chen et al. (2016). Under anoxic conditions, α is assigned as the typical value (1.0 ‰) during U(VI) reduction to U(IV) in natural environments (Andersen et al., 2017).

4.4 Results

4.4.1 U Concentration and $\delta^{238}U$ During Aragonite-to-calcite transition

Concentration and isotopic data for the KL1 coral head samples are provided in Figure 4.1 and Table 4.1. Previous work showed that concentrations of trace elements and anions (Sr, Na, SO_4^{2-}) and oxygen isotopic composition ($\delta^{18}O$) dropped abruptly across the aragonite-to-calcite transition in the KL1, although the sulfur isotopic composition of carbonate-associated sulfate (CAS) increases only slightly (~1 ‰, Gill et al., 2008). U concentrations show a similar depletion, decreasing about 50 % from ~4 ppm in the primary coral aragonite to ~2 ppm in the recrystallized calcite. Despite this, the $\delta^{238}U$ remained nearly invariant (aragonite: –0.37±0.02 ‰ vs. calcite: –0.33±0.07 ‰, 2 SD, *p*-value of Student's t-test is 0.39).

Table 4.1. $\delta^{13}C$, $\delta^{18}O$, $\delta^{34}S_{CAS}$, I/(Ca+Mg), U concentration and $\delta^{238}U$ across the aragonite-to-calcite transect in the coral heal KL1.

Sample Number	$\delta^{13}C$ ‰	$\delta^{18}O$ ‰	$\delta^{34}S_{CAS}$ ‰	I/(Ca+Mg) µmol/mol	U ppm	$\delta^{238}U$ ‰	2 SD ‰
KL1-1	–2.20	–5.41	22.60	4.55	2.15	–0.29	±0.08
KL1-2	–1.20	–5.05	22.20	3.53	2.07	–0.35	±0.08
KL1-3	–4.40	–5.74	–	4.00	2.27	–0.35	±0.09
KL1-4	–1.60	–4.42	21.10	3.59	4.03	–0.38	±0.08
KL1-5	–1.50	–4.39	21.10	3.73	3.9	–0.37	±0.09
KL1-6	–1.40	–4.32	21.10	3.88	4.33	–0.36	±0.10

4.4.2 U Concentration and $\delta^{238}U$ in Drill Cores Clino, Unda and Site 1006

Concentration and isotopic data for the Bahamas Transect samples are provided in Figure 4.3 and Table B.1. Samples recovered from Clino, Unda, and Site 1006 have experienced a range of diagenetic conditions which are reflected in the mineralogy, and the $\delta^{13}C$ and $\delta^{18}O$ of these sediments (Fig 3, Melim et al., 2004). The U concentrations in carbonate sediments from cores Clino, Unda and Site 1006 are typically between 2–5 ppm, with occasional values up to ~10 ppm (Figure 4.3). These U concentrations are generally consistent with those found in banktop shallow-water carbonate sediments from the Bahamas (Chung and Swart, 1990; Romaniello et al., 2013), and previously reported measurements of U concentrations in other ODP Leg 166 samples (Henderson, 2002).

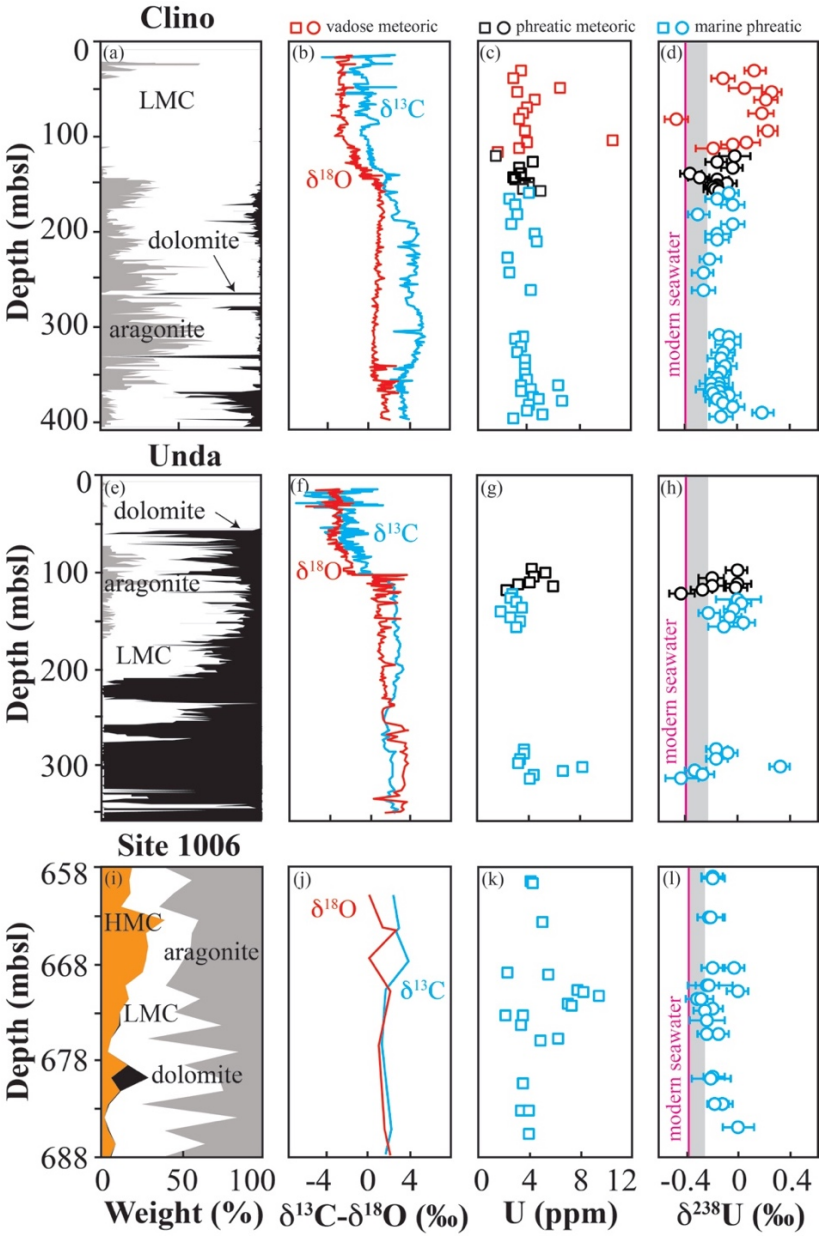

Figure 4.3. Carbonate mineralogy, carbon and oxygen isotopes, U concentration, and $\delta^{238}U$ in the Clino, Unda and Site 1006 drill cores. The depth on y-axis is in meters below sea level (mbsl). The water depth of Site 1006 is 657.9 m below the sea level. The mineralogy, and $\delta^{13}C$ and $\delta^{18}O$ have been taken from Melim et al. (1995). The gray bands in the right most panels represent the estimated range of U isotope fractionation expected to result from aqueous speciation of U(VI) in the diagenetic fluids, assuming these fluids start with a seawater isotope composition (Chen et al., 2016). The red, black, and blue symbols represent vadose meteoric, phreatic meteoric, and phreatic marine diagenesis.

The $\delta^{238}U$ values of Clino, Unda, and Site 1006 samples range from –0.47 to +0.26 ‰ with a mean of –0.12±0.14 ‰. Despite significant variability, nearly all samples are more positive than modern seawater (–0.39 ‰; Tissot and Dauphas, 2015). The data between zones of vadose meteoric, phreatic meteoric, and phreatic marine diagenesis were divided, as identified by Melim et al. (2000, 2004) in Clino, Unda and Site 1006 (Figure 4.4). Samples in the meteoric vadose zone of the Clino core (0-100 mbsl) are characterized by $\delta^{238}U$ typically greater than 0 ‰ (mean 0.03±0.22 ‰, 1 SD) and are systematically higher in $\delta^{238}U$ than samples exposed to phreatic meteoric and marine diagenesis (–0.17±0.12 ‰ and –0.14±0.11 ‰, respectively, 1 SD).

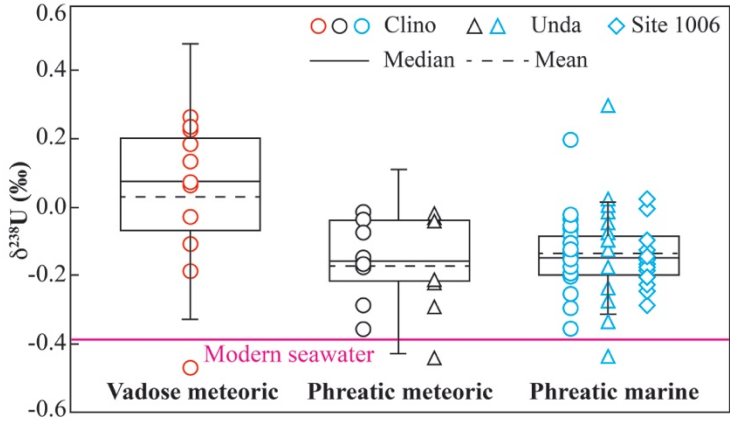

Figure 4.4. Boxplot of $\delta^{238}U$ under different types of carbonate diagenesis. Whiskers denote the minimum and maximum of data with 1.5 times the interquartile range from the median. The circles, triangles and diamonds represent $\delta^{238}U$ in cores Clino, Unda, and Site 1006, respectively. Red, black, and blue symbols stand for vadose meteoric, phreatic meteoric, and phreatic marine diagenesis.

An additional 20 factors which might explain the distribution of U concentrations and $\delta^{238}U$ in these sediments were examined, including mineralogy, traditional diagenetic proxies such as Mg/Ca, Mn/Sr, and Sr/Ca ratios, concentrations of detrital (Al, Th) and redox sensitive elements (Fe, V, Mo, Re, U) and Ce, and Eu rare earth elements (REE) anomalies. Surprisingly,

little correlation between these proxies and the concentrations of U or $\delta^{238}U$ was found (Figure B.1).

4.5 Discussion

4.5.1 Patterns of U Isotope Fractionation During Carbonate Diagenesis

Early diagenesis of Bahamas carbonate samples leads to an increase in both the mean and standard deviation of $\delta^{238}U$ in bulk sediments. For example, samples from Unda, Clino, and Site 1006 all displayed elevated $\delta^{238}U$ values compared to that of seawater and primary carbonate precipitates such as corals, mollusks, and calcareous green and red algae from the Bahamas Bank (Figure 4.5, Table B.2). Sediment data have a 1 SD=0.14 ‰ compared to a 1 SD=0.06 ‰ for primary precipitates.

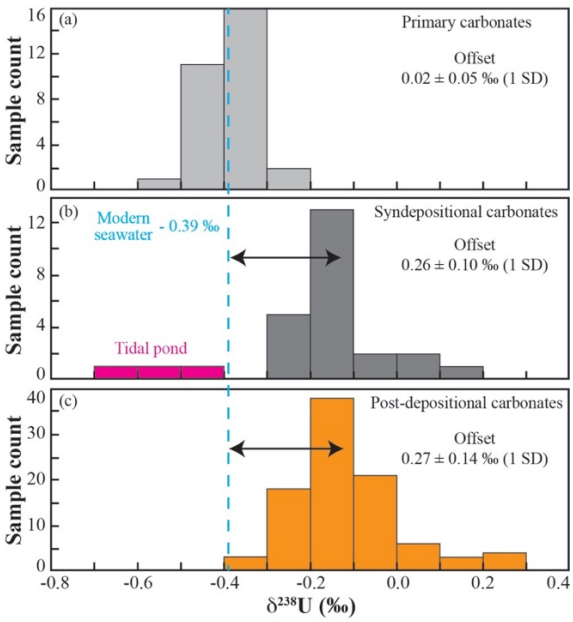

Figure 4.5. Histograms of $\delta^{238}U$ in primary (light gray) and syndepositional (dark gray) reported by Romaniello et al. (2013) and post-depositional carbonates (orange, drill cores of Unda, Clino, and Site 1006 in *this work*). The dashed blue line represents the $\delta^{238}U$ value of modern seawater (–0.39 ‰). The arrows represent the average U isotopic offset between carbonates and seawater.

The overall distributions (mean and standard deviation) of $\delta^{238}U$ in drill core samples (Unda, Clino and Site 1006) and shallow banktop sediment cores were quite similar, particularly if a small number of tidal pond samples (N=3) with low $\delta^{238}U$ are excluded (Figure 4.5, Table B.2). Although it does not significantly change the interpretation, excluding these tidal pond samples is reasonable because their $\delta^{234}U$ values are characteristic of Eemian age carbonate sediments and were mostly likely deposited in a freshwater or evaporative pond well above sea level as a result of weathering that occurred during the last glacial cycle (Romaniello et al., 2013). The similarity between unconsolidated banktop and drill core samples were interpreted to indicate that diagenesis of $\delta^{238}U$ in these carbonates is primarily syndepositional—occurring within ~25 cm of the sediment-water interface on the banktop—and that this signal is subsequently transported to the slope regions by downslope transport of sediments by tides and storms (Kenter et al., 2001; Neuman and Land, 1975). Banktop sediments have spatially variable U concentrations and $\delta^{238}U$ which depend on local sources of organic matter input such as green algae and sea grass beds (Romaniello et al., 2013). The admixture of heterogeneous banktop sediments during downslope transport may at least partially explain the distribution of U concentrations and $\delta^{238}U$ in slope sediments.

The influence of early diagenesis on $\delta^{238}U$ is supported by results from Henderson (2002) who demonstrated that many Site 1006 samples displayed closed-system behavior of $^{230}Th/^{234}U$ activity ratios (Figure 4.6a). This study has reanalyzed these same sediment horizons for their $\delta^{238}U$ (Figure 4.6b). Samples which display closed-system evolution of $^{230}Th/^{234}U$ show a narrow range of $\delta^{238}U$ typical of other downcore samples measured in this study. Because late addition of U or Th would lead to open-system behavior of $^{230}Th/^{234}U$, the diagenetic processes which

impacted $\delta^{238}U$ in these samples must have occurred before significant ingrowth of ^{230}Th. This supports the hypothesis that diagenesis of $\delta^{238}U$ is a rapid process occurring during early burial, rather than a later on-going process. This interpretation is consistent with recent measurement of the calcium and magnesium isotopic composition of nearby Bahamas sediments along the same slope-to-margin transect which provide evidence that diagenetic mineralogical transformations occurred largely in exchange with seawater (Higgins et al., 2018).

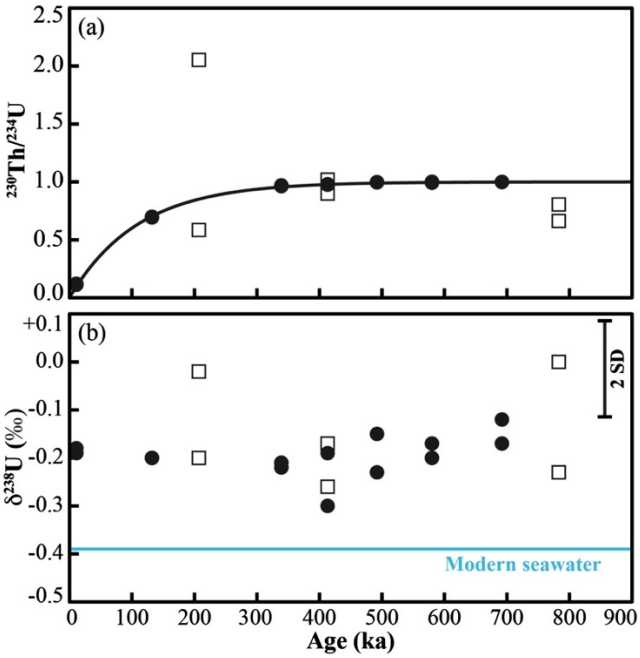

Figure 4.6. (a) $^{230}Th/^{234}U$ for Site 1006 samples with independent age control (Henderson, 2002). The curve is the expected $^{230}Th/^{234}U$ for closed system samples of that age. Filled circles (which contain overlapping data points) have $^{230}Th/^{234}U$ within 3 % of the expected closed-system value. Open squares represent $^{230}Th/^{234}U$ more than 3 % from the expected values that are not considered as a closed system. (b) $\delta^{238}U$ values for the same samples. Filled circles are the samples with expected $^{230}Th/^{234}U$ above, and open squares are those with $^{230}Th/^{234}U$ values indicative of open-system resetting. The horizontal blue line represents $\delta^{238}U$ in modern seawater. The typical uncertainty in $\delta^{238}U$ is ±0.10 ‰ (2 SD).

4.5.2 Mechanisms of Syndepositional $\delta^{238}U$ Diagenesis

Based on recent experimental and field observations, early diagenetic alteration of $\delta^{238}U$ in carbonate sediments is the product of speciation effects involving only U(VI) with a small isotopic fractionation as well as redox-related effects involving reduction of U(VI) to U(IV) with an associated large isotopic fractionation (Figure 4.7a). In comparison to better-established carbonate seawater proxies, such as $\delta^{18}O$ and $^{87}Sr/^{86}Sr$, the diagenesis of $\delta^{238}U$ depends not only on the water chemistry (pH, CO_3^{2-}, Ca^{2+} and Mg^{2+} concentrations) of the fluid flowing through the sediments, but also the pore water redox conditions which control both the mobility of U in pore fluids and the isotope fractionation during the precipitation of carbonate. These factors are discussed in turn below.

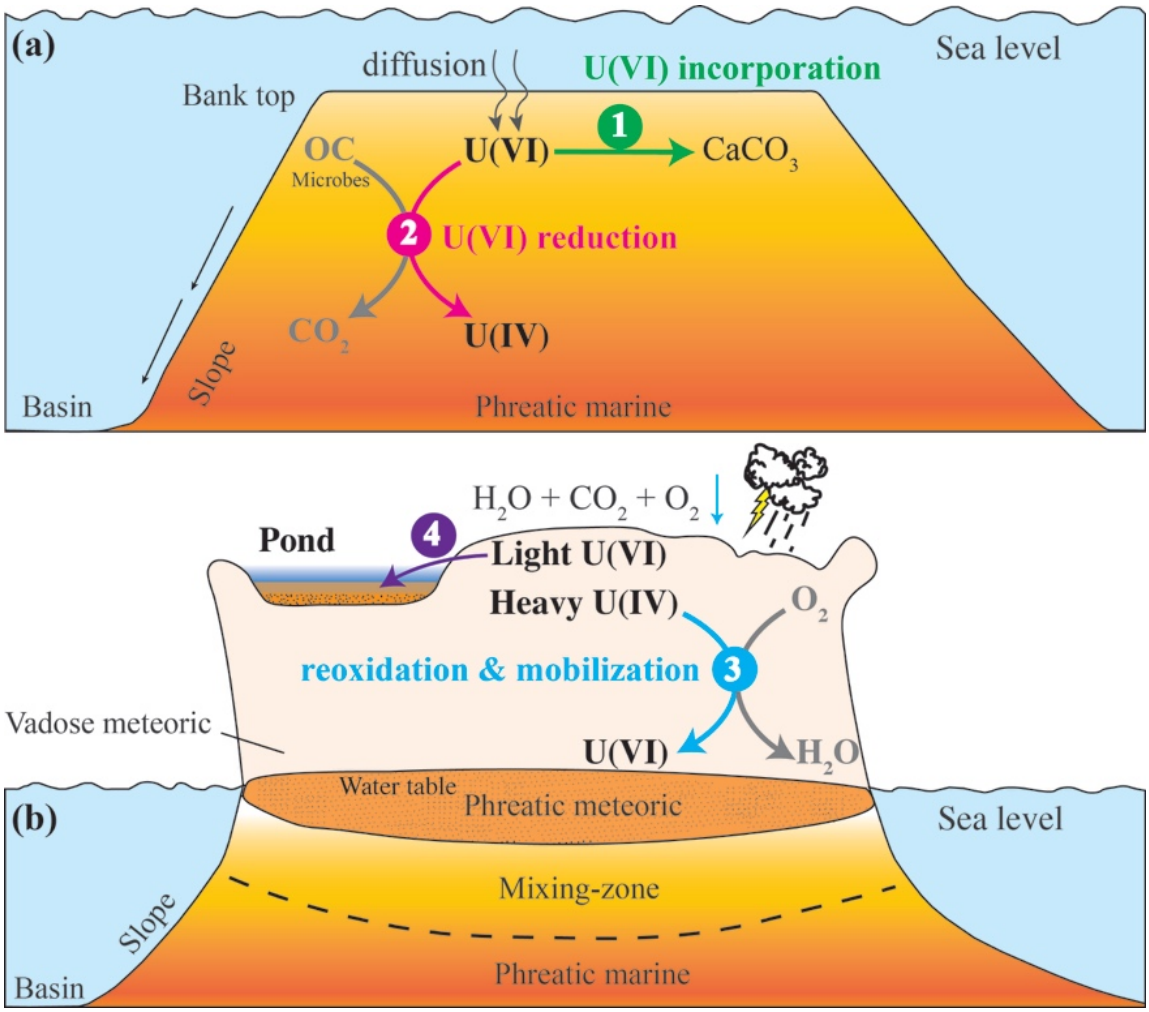

Figure 4.7. Schematic illustration of U isotope fractionation mechanisms during carbonate diagenesis at sea level high stand (a) and low stand (b) in the isolated carbonate platform of the Bahamas. The four fractionation mechanisms are: (1) equilibrium isotope fractionation during U(VI) incorporation into carbonates; (2) reductive authigenic U(IV) enrichment coupled with organic carbon oxidation; (3) U(IV) reoxidation by oxygen from meteoric fluids and mobilization to carbonates in the successive layer; (4) mobilization of the residual lighter $\delta^{238}U$ in the top layer carbonates into ponds after meteoric diagenesis. OC in (a) represents organic carbon.

4.5.2.1 U Isotope Fractionation During Carbonate Recrystallization

During early diagenesis, carbonate dissolution and recrystallization is an important process that allows potential exchange of elements in the carbonate crystal lattice with those of surrounding pore fluids (Swart, 2015). This process is particularly important for metastable

aragonite precipitates, which eventually undergo conversion to thermodynamically stable calcite, resulting in the rejection of a significant fraction of lattice-bound trace elements such as Sr and U due to their lower partition coefficients into calcite compared to aragonite (Curti, 1999; Swart, 2015; Reeder et al., 2000, 2001).

While modern biogenic primary carbonate precipitates incorporate U with little if any fractionation of U isotopes from seawater, inorganically-precipitated aragonite and calcite exhibit a small but detectable U isotope fractionation (~0.09 ‰) with ^{238}U preferentially partitioned into the solid phase (Chen et al., 2016). Chen et al. (2016) proposed that this fractionation depends on aqueous U(VI) speciation, especially the abundance of the neutrally charged $Ca_2UO_2(CO_3)_3(aq)$. Aqueous U(VI) speciation is controlled by pH, ionic strength, alkalinity, and Ca^{2+} and Mg^{2+} concentrations (Dong and Brooks, 2006; Endrizzi and Rao, 2014). Chen et al. (2017) explored the sensitivity of these parameters, and demonstrated that the Ca^{2+} concentration of natural waters likely plays the most important role in determining the magnitude of U isotope fractionation during U(VI) coprecipitation with calcium carbonates, with higher Ca^{2+} concentrations leading to larger U isotope fractionation. Based on these conclusions, it would be reasonable to expect the recrystallization of biogenic aragonite in low-Ca meteoric water to result in a negligible U isotope fractionation while reprecipitation in marine pore water would be associated with an isotope fractionation of ~0.12 ‰ (Chen et al., 2016, 2017).

Consistent with this expectation, transformation of aragonite to calcite did not significantly alter $\delta^{238}U$ in the primary aragonite of the coral head KL1, despite significant reduction in U concentration from 4 to 2 ppm. The preservation of I/(Ca+Mg) and the sulfur isotopic composition of carbonate-associated sulfate ($\delta^{34}S_{CAS}$) across the mineralogical transition

suggests that meteoric diagenesis occurs under predominantly oxic conditions without significant sulfate reduction, and thus rules out more extensive U isotope fractionation associated with U(VI) reduction (Figure 4.1, Gill et al., 2008; Hardisty et al., 2017). In this case, carbonate recrystallization occurred in oxic meteoric water with an extremely small contribution of exogenous U from rainwater (e.g., <0.04 ppb in rainwater of Japan; Muramatsu et al., 1994), any U isotope fractionation observed would be wholly due to transformation of the carbonate mineralogy. Although the meteoric fluid was unable to be measured directly, the equilibrium Ca^{2+} concentration in equilibrium with typical rain water at 250–500 ppm CO_2 can be calculated, is 1 to 2 mM. Under these low-Ca^{2+} conditions, an isotope fractionation of <0.02 ‰ would be predicted during U coprecipitation (Chen et al., 2016, 2017). Thus, this case study suggests that, by itself, carbonate recrystallization in meteoritic waters is unlikely to significantly fractionate U isotopes (although secondary oxidation of U(IV) and/or reduction of U(VI) may induce fractionation during meteoritic diagenesis as discussed in Section 5.2.3).

In contrast to meteoric diagenesis, recrystallization of biogenic carbonates and the eventual conversion of biogenic aragonite and HMC to LMC in seawater and marine pore fluids is predicted to be associated with a larger isotope fractionation. To estimate the U isotope fractionation during U(VI) incorporation into altered carbonates, the experimental results were extrapolated using the pore water chemistry data from cores Clino, Unda and Site 1006 (Chen et al., 2016, 2017; Swart et al., 2001). The chemical composition of the pore fluids in the upper 20 m of Site 1006 is similar to modern seawater, and results in a predicted fractionation of ~0.12 ‰ (Eberli et al., 1997). For the Clino and Unda cores, only the Ca^{2+} concentration of pore fluids is available, but these concentrations are higher than seawater (up to 19 mM; Swart et al., 2001). Using this data, the aqueous U(VI) speciation in pore fluids of Clino and Unda can lead to a

maximum U isotope fractionation of ~0.17 ‰ relative to modern seawater (Figure 4.3). The range of the isotope fractionations predicted between seawater and carbonates for each core are shown as the gray band in Figure 4.3. All three cores demonstrate a clear correspondence between the maximum modeled offset with the minimum observed $\delta^{238}U$ values, strongly supporting the suggestion that carbonate recrystallization and the aqueous U speciation of pore waters plays an important role in controlling the minimum offset between $\delta^{238}U$ in seawater and early diagenetic carbonate sediments. Over the range of Phanerozoic seawater conditions, this speciation-dependent fractionation probably ranged from 0.11 to 0.23 ‰ and thus the Bahamian sediments measured here are probably typical of well-preserved Phanerozoic carbonates sediments in general (Chen et al., 2017).

4.5.2.2 Authigenic Enrichment of Isotopically Heavy U(IV) in Carbonates

A second important mechanism of early diagenesis in carbonate sediments is the authigenic enrichment of U(IV) from the reduction of U(VI) diffusing into anoxic and sulfidic sediment pore water (Figure 4.7a). In many areas of the Bahamas, green algae and sea grass meadows provide significant amounts of organic carbon to sediments, resulting in anoxic and sulfide-rich sediment pore water with H_2S concentrations ranging from 100–1200 μM producing favorable conditions for U(VI) reduction (Romaniello et al., 2013). Uranium concentrations in sediments are consistent with this authigenic enrichment model. Banktop sediments in the Bahamas display downcore increases in sediment U concentrations over the upper 30 cm of deposition and both the banktop and slope sediments in the Bahamas are characterized by average U concentrations (~4.1 ppm) which are higher than the primary carbonate precipitates (e.g., corals, red and green algae, and mollusks, ~ 1.5 ppm, Romaniello et al., 2013). During the

reduction of U(VI) to U(IV), ^{238}U is preferentially enriched in the reduced U(IV) product with an isotope fractionation of ~1 ‰ (Bopp et al., 2009; Wang et al., 2015; Basu et al., 2014; Stirling et al., 2015; Stylo et al., 2015). Therefore, it is argued that in addition to recrystallization effects which probably impact nearly all Bahamas sediments, reduction of U(VI) to U(IV) results in additional sporadic enrichment of U concentrations and $\delta^{238}U$ as observed in Figure 4.3. This U(IV) could be present in sediments either as dispersed $UO_2(s)$ or as U(IV) substituting for Ca in the carbonate lattice (Sturchio et al., 1998; Pingitore et al., 2002).

4.5.2.3 Redox Control of U Geochemistry During Burial and Meteoritic Diagenesis

One key difference between the diagenesis of U in carbonate sediments and the behavior of better-studied carbonate isotope proxies such as $\delta^{13}C$, $\delta^{18}O$, and $^{87}Sr/^{86}Sr$ is that the solubility and mobility of U is strongly controlled by pore water redox chemistry. Under reducing pore water conditions, reduction of U(VI) to insoluble U(IV) essentially renders U immobile. This likely explains why no evidence of diagenetic alteration following deeper sediment burial (e.g., during dolomitization) is found in this study, which suggests that it is the result of closure of the U isotope system due to the low solubility of U(IV) in anoxic pore water. Low concentrations of U in anoxic pore fluids, as observed by Henderson et al. (1999), require significantly more fluid flow to substantially change the U isotope composition of bulk sediments, even as other elements such as Ca, Mg, and Sr are readily exchanged.

In contrast, under oxic conditions, U(VI) is highly soluble, particularly when complexed by Ca^{2+} and CO_3^{2-} ions. Under this scenario, U can be readily mobilized into and out of sediments, and thus oxic conditions increase the potential for diagenetic alteration of U in carbonates. Furthermore, reduction of U(VI) to U(IV) at oxic-anoxic transitions may result in

significant enrichment of $\delta^{238}U$ similar to that observed in roll-front deposits (Bopp et al., 2009; Brown et al., 2016). Conversely, reoxidation of isotopically positive U(IV), such as might occur as sediments are exposed during sea level lowstands, could lower $\delta^{238}U$ in upper horizons while providing a source of high $\delta^{238}U$ fluids that could influence lower horizons (Figure 4.7b).

This remobilization of isotopically positive U(IV) from sediments exposed to meteoric waters during sea level lowstands most likely explains why the meteoric vadose zone of the Clino core (0–90 mbsl) display more positive $\delta^{238}U$ values. This is consistent with dolomitized tidal pond sediments displaying the Eemian ^{234}U ages reported by Romaniello et al. (2013). The tidal ponds sediments were interpreted as the rare preservation of the isotopically negative $\delta^{238}U$ complement and mobilized positive $\delta^{238}U$ source following partial reduction and reoxidization of sediment U(IV) during sediment deposition, exposure, and weathering (Figure 4.7b). If this hypothesis is correct, then low $\delta^{18}O$ and $\delta^{13}C$ (derived from the oxidation of sediment organic matter), and high $\delta^{238}U$ (derived from the oxidation of sediment U(IV)) may be a common fingerprint of sea level lowstands and vadose meteoric diagenesis, at least under oxidizing Phanerozoic atmospheric conditions (Melim et al., 2001; Oehlert and Swart, 2014; Knauth and Kennedy, 2009).

4.5.2.4 Implications of Diagenesis for the Correlation Between $\delta^{238}U$ and U Concentrations in Carbonates

Given that each of the above diagenetic mechanisms would naturally lead to a correlation between $\delta^{238}U$ and U concentrations, one of the most difficult challenges for understanding U isotope fractionation during diagenesis is why virtually no correlation was observed between these parameters (Figure B. 1). To understand why this might be the case, it is important to

consider the different mechanisms controlling $\delta^{238}U$ and U concentration in carbonate sediments during diagenesis.

The U isotope fractionation during reductive authigenic enrichment of U(IV) is probably the most significant control on the $\delta^{238}U$ in sediments, because the fractionation during U(VI) reduction (~1 ‰) is much larger than fractionation controlled by aqueous speciation of U(VI) (0–0.17 ‰; Chen et al., 2016; Andersen et al., 2017). Naturally, as U(IV) is added to sediments, the total U concentration of the sediments must also increase. However, assuming the bulk sediment consists of U(VI) and U(IV) which are fractionated from modern seawater by 0.1 and 1.0 ‰ respectively (Chen et al., 2016; Andersen et al., 2017), reaching an average sediment $\delta^{238}U_{Total}$ of –0.12 ‰ only requires a 18 % increase of total sediment U as U(IV).

Unlike the $\delta^{238}U$, authigenic U(IV) is not the dominant factor controlling U concentration in carbonates. During U(VI) incorporation into primary $CaCO_3$, U concentration in the solid phase is controlled by dissolved U and CO_3^{2-} concentrations, pH, $CaCO_3$ growth rate, carbonate mineralogy, and biogenic effects (Meece and Benninger, 1993; Reeder et al., 2000; Russell et al., 2004; Gabitov et al., 2008; Inoue et al., 2011; Raddatz et al., 2014; DeCarlo et al., 2015; Chen et al., 2016). These factors can result in 2 to 5-fold variation in the U concentration of the primary $CaCO_3$ (Gabitov et al., 2008; Reeder et al., 2000). Romaniello et al. (2013) reported a nearly 50-fold range in the U concentration of primary biogenic Bahamian carbonates ranging from mollusks (~0.05 ppm U) to corals and ooids (2.5–3.5 ppm U). Because the reductive authigenic enrichment U(IV) need only account for a small proportion of total sediment U, the correlation expected between U concentration and isotopes is likely masked by the significant variability of initial U concentrations in primary precipitates.

4.5.3 Developing a Theoretical Framework for $^{238}U/^{235}U$ During Diagenesis

In order to more systematically explore the evolution of various geochemical indicators of diagenesis alongside changes in the $\delta^{238}U$, an open system fluid-rock interaction model was applied for diagenesis of U and several possible diagenetic tracers including $\delta^{13}C$ and $\delta^{18}O$, and Sr and Mn concentrations (Banner and Hanson, 1990; Jacobsen and Kaufman, 1999). Considering the various types of diagenesis identified and discussed above, models to simulate carbonate diagenesis in meteoritic and marine fluids. For each fluid were constructed. The behavior of U under oxic and anoxic conditions was also considered.

Meteoric and marine diagenesis were simulated assuming these fluids have distinct chemical compositions (Romaniello et al., 2013; Hu and Burdige, 2007; Swart et al., 2009; Bowen and Revenaugh, 2003; Chen et al., 1986; Land, 1985; LeGrande and Schmidt, 2006; Andersen et al., 2016; Henderson et al., 1999). Meteoric and marine fluids mainly differ in salinity, Ca concentration (2.5 vs. 10 mM Ca), $\delta^{13}C_{VPDB}$ (–1.2 vs. +2 ‰), $\delta^{18}O_{VPDB}$ (–34.2 vs. –29.3 ‰), and $\delta^{238}U$ (–0.30 vs. –0.39 ‰). To simulate the behavior of U under oxidizing conditions, seawater simulations considered relatively high U concentrations in seawater with a moderate distribution coefficient based on U(VI) coprecipitation experiments (Meece and Benninger, 1993; Reeder et al., 2000; Gabitov et al., 2008; Chen et al., 2016). In contrast, for the anoxic seawater case, a low U concentration (0.5 ppb; Henderson et al., 1999) and 1000-fold higher distribution coefficient were invoked, considering the tendency for U to be rapidly scavenged from solution as U(IV) (Sturchio et al., 1999). Meteoric U models were conducted similarly. Further details of the parameters used in this model are discussed in the Text B.3 in APPENDIX B.

4.5.3.1 Sequence of Diagenetic Transformations

Results of fluid-rock interaction modeling, shown in Figure 4.8, provide a theoretical basis for examining the sequence of diagenetic transformations which occur as carbonate rocks experience increasing amounts of fluid interaction, expressed by the fluid/rock mass ratio (N). In agreement with previous results, the models in this study predict that $\delta^{18}O$ is altered rapidly at very low fluid/rock ratios (N=0.1–10), followed by Sr (N=10–1000), then $\delta^{13}C$ and Mn (N=10^3–10^5) and demonstrate similar direction and magnitude of alteration when compared to the observed diagenetic parameters summarized in Table 4.2 (Eberli et al., 1997; Melim et al., 1995, 2001). When compared to these better studied markers, U concentrations and $\delta^{238}U$ experience alteration at fluid rock ratios intermediate between those of Sr and $\delta^{18}O$, depending on pore water redox conditions. Under oxic conditions, high concentrations of pore water U and a moderate distribution coefficient leads to more rapid diagenetic modification of U at fluid/rock ratios of N=10–1000. Under more reducing conditions where U(IV) is the dominant species, lower U concentrations in pore water means that much larger fluid/rock ratios are required for diagenetic alteration (N=10^3–10^5), though the magnitude of isotopic fractionation is potentially much larger at high fluid/rock ratios. These results are similar to patterns modeled by Lau et al. (2017).

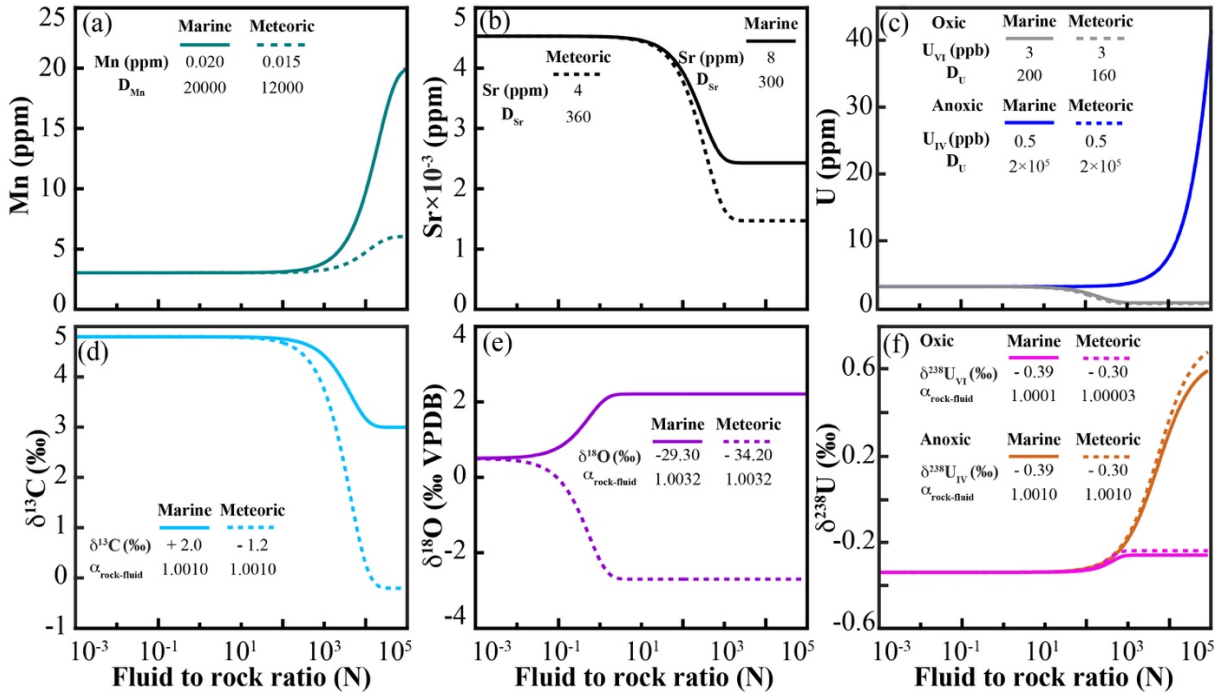

Figure 4.8. Evolution of Sr, U and Mn concentrations (a), and $\delta^{13}C$, $\delta^{18}O$ and $\delta^{238}U$ (b) in carbonates vs. varying fluid to rock ratio during primary carbonates interaction with meteoric and marine fluids in an open system. Primary carbonates initial compositions: Sr=4500 ppm, U=3 ppm, Mn=3 ppm, $\delta^{13}C$=+4.8 ‰, $\delta^{18}O$=+0.5 ‰, and $\delta^{238}U$=–0.37 ‰. The initial compositions of marine and meteoric fluids are displayed in the figure. D_i (i=Sr, U, and Mn) is the concentration ratio of element i in the rock to the fluid. $\alpha_{rock\text{-}fluid}$ is the isotope fractionation factor between the rock and fluid. For U concentration and $\delta^{238}U$, incorporation of U(VI) and U(IV) into $CaCO_3$ under oxic and anoxic conditions were simulated, respectively.

Table 4.2. Mean values of trace element concentrations and isotopic compositions in vadose meteoric, phreatic meteoric, and phreatic marine carbonates from the Bahamas.

Diagenesis types	Mn ppm	Sr ppm	U ppm	$\delta^{13}C$ ‰	$\delta^{18}O$ ‰	$\delta^{238}U$ ‰	N
Vadose meteoric	4 ± 2	1653 ± 1119	4 ± 2	-0.13 ± 0.96	–2.76 ± 0.39	0.03 ± 0.21	11
Phreatic meteoric	9 ± 3	1329 ± 318	4 ± 1	0.95 ± 0.86	–0.77 ± 1.34	–0.17 ± 0.12	17
Phreatic marine	20 ± 20	2582 ± 2694	4 ± 1	3.26 ± 1.21	1.24 ± 1.08	–0.14 ± 0.11	68

Note: N is the number of samples for vadose meteoric, phreatic meteoric and phreatic marine diagenesis.

4.5.3.2 Cross-correlations of U Concentration and $\delta^{238}U$ with Diagenetic Parameters

Studies of $\delta^{238}U$ in ancient sedimentary carbonates often assume that diagenetic transformations of U will be accompanied by strong correlations between $\delta^{238}U$ and various diagenetic parameters such as $\delta^{18}O$, $\delta^{13}C$, Mn/Sr, and U concentration (Brennecka et al., 2011b; Lau et al., 2016, 2017; Jost et al., 2017). However, no simple linear correlations between $\delta^{238}U$ and these diagenetic parameters were deteced in Bahamas slope sediments (Figure B. 1). Diagenetic modeling results in Figure 4.9 demonstrate why such strong correlations might not be expected. Cross-plots of diagenetic indicators result in strongly curvilinear (hyperbolic) trends, and these trends vary between oxidizing and reducing, as well as marine and meteoric conditions. Because the sensitivities of different proxies to diagenesis often vary by more than an order of magnitude, the trajectory of many diagenetic processes on cross-plots results in movement along only a single parameter axis (and therefore these parameters will show no correlation). Moreover, sediments that experience combinations of different diagenetic processes, or exist as a linear combination of two different sediment phases (e.g., calcite and aragonite) are likely to display complex patterns of evolution. These results point to the need for caution when interpreting diagenetic cross-plots, and suggest that previous attempts to rule out diagenetic alteration of $\delta^{238}U$ of based on such plots might have been overly optimistic. Further work is needed to identify more robust indicators of $\delta^{238}U$ diagenesis in carbonate sediments. Recent work by Hood et. al. (2016) suggests that integrated sedimentology and in situ analyses may provide clearer evidence of diagenetic influence, though more work on more recent sediments with known seawater $\delta^{238}U$ is needed to fully evaluate this approach.

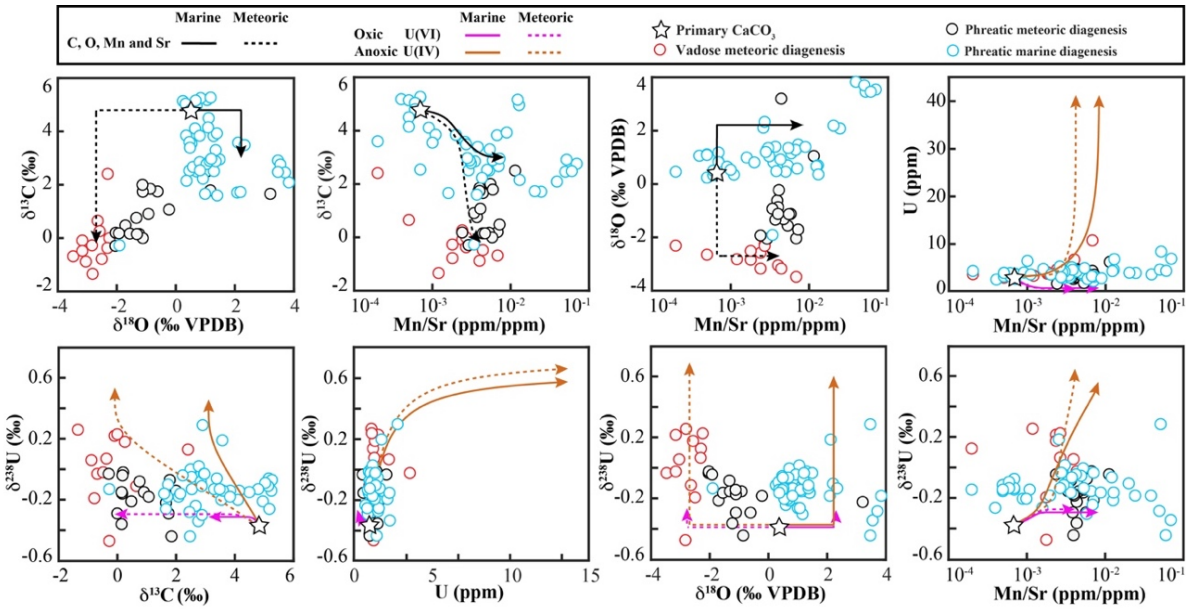

Figure 4.9. Comparison of the simulated evolution of geochemical indicators ($\delta^{13}C$, $\delta^{18}O$, $\delta^{238}U$, Mn/Sr and U concentrations) during diagenesis by marine (solid lines) and meteoric fluids (dashed lines) versus these indicators measured in the carbonate sediments which have experienced vadose meteoric (red circles), phreatic meteoric (black circles) and phreatic marine diagenesis (blue circles) in drill cores Clino, Unda and Site 1006. The arrows in the figure indicate the evolution direction of different geochemical indicators in primary carbonates during diagenesis.

4.5.4 Implications of Diagenesis for U Isotope Paleoredox Proxy

The results in this study demonstrate that early carbonate diagenesis alters the U isotopic signal ($^{238}U/^{235}U$) in primary carbonates by making the $\delta^{238}U$ more positive by 0.27±0.14 ‰, (1 SD). If not corrected, this effect could lead to estimates of seawater $\delta^{238}U$ which are too high, suggesting more oxidizing marine conditions. To assess how the correction would affect the estimation of oceanic anoxia, the steady state U isotopic mass balance model was used as follows:

$$\delta^{238}U_{seawater} = \delta^{238}U_{river} - f_{anoxic} \times \Delta^{238}U_{anoxic} - (1 - f_{anoxic}) \times \Delta^{238}U_{other} \quad \text{Eq. 4.5}$$

where $\Delta^{238}U_{anoxic}$ (+0.6 ‰) is the U isotopic fractionation between U in anoxic sediments and seawater, and $\Delta^{238}U_{other}$ (+0.03 ‰) is the fractionation between U in the remaining sinks and seawater (Tissot and Dauphas, 2015; Andersen et al., 2016). $\delta^{238}U_{river}$ (–0.34 ‰; Andersen et al., 2016) is the U isotopic composition of river, and f_{anoxic} is the fraction of U removed by anoxic sediments.

Estimation of f_{anoxic} using the high-resolution data with large negative excursions of $\delta^{238}U$ from multiple sections of Sturtian and Permian-Triassic was taken as an example (Jost et al., 2017; Brennecka et al., 2011b; Lau et al., 2016; Zhang et al., 2018a, b). The estimated extent of oceanic anoxia (f_{anoxic}) is more extreme when the correction to U isotopic offset induced by carbonate diagenesis was applied (Table 4.3). All the corrected f_{anoxic} of end-Permian suggest less than 100 % of U removal by anoxic sediments except the Sturtian anoxic event which has f_{anoxic} (=1.05) slightly larger than 1. According to equation 4.5, f_{anoxic} could also be influenced by the variability of $\Delta^{238}U_{anoxic}$ (0.6–1.2 ‰; Andersen et al., 2014, 2017). For example, if $\Delta^{238}U_{anoxic}$=0.7 ‰, the corrected f_{anoxic} would yield a reasonable value of 0.84 over the anoxic event of the Sturtian (660–640 Ma; Lau et al., 2017). Because of the large difference in the estimated the extent of oceanic anoxia before and after corrections to the U isotopic offset during carbonate diagenesis, this study suggests that future studies of U isotopes in carbonates as a paleoredox proxy should apply a correction based on the early diagenetic shift identified.

Table 4.3. Estimation of the oceanic anoxia over Sturtian and end-Permian with and without correction to the U isotopic offset induced by carbonate diagenesis.

Time	Sections	$\delta^{238}U_{anoxic}$ (‰)		f_{anoxic}		References
		original	corrected	original	corrected	
Sturtian	Mongolia	–0.70	–0.97	0.58	1.05	Lau et al., 2017
end-Permian	Dawen, China	–0.65	–0.92	0.49	0.96	Brennecka et al., 2011b
end-Permian	Dajiang, China Guandao, China Taskent, Turkey	–0.62	–0.89	0.44	0.91	Lau et al., 2016
end-Permian	Kamura, Japan Zal, Iran	–0.57	–0.84	0.35	0.82	Zhang et al., 2018a, b
end-Triassic	Val Adrara, Italy Italcementi, Italy	–0.58	–0.85	0.37	0.84	Jost et al., 2017

Note: $\delta^{238}U_{anoxic}$ and f_{anoxic} are the U isotopic composition of carbonates and the fraction of U removal by anoxic sinks over the anoxic event.

The second, subtler effect of sedimentary diagenesis is the apparent increase in the spread of $\delta^{238}U$ values, as expressed by the larger standard deviation of sedimentary carbonates (±0.14‰, 1 SD) compared to primary carbonate precipitates (±0.05‰, 1 SD). The stochastic spread of $\delta^{238}U$ values observed in Bahamas drill core samples shows little if any correlation with a variety of diagenetic parameters and, as a result, determining an accurate mean value for sediment $\delta^{238}U$ requires averaging data from several successive sediment samples, for example, using running mean or locally-weighted regression scatter plot smoothing (LOWESS) fit approach. There is also a serious risk that if only a limited number of samples are measured over a stratigraphic interval, then a small number of statistical outliers could easily appear as a secular shift in $\delta^{238}U$ when they are in fact diagenetic scatter.

Based on the spread of values observed in this study, the minimum number of samples needed to both accurately determine the mean $\delta^{238}U$ of paleo-seawater and to robustly identify secular shifts in seawater $\delta^{238}U$ was evaluated. Determining paleo-seawater $\delta^{238}U$ from carbonates to within 0.10 ‰ (2 SD, similar to typical measurement precision) requires the mean of at least eight discrete sediment samples. This finding emphasizes the need for large, high-

resolution stratigraphic data sets to define trends in the mean sediment $\delta^{238}U$. To reach this conclusion, a 2-group, equal-variance Student's t-test was used to evaluate the minimum number of samples that would be required to robustly detect secular shifts in sediment $\delta^{238}U$ of varying magnitudes ($\alpha<0.05$, two-tail). These results are presented in Table 4.4. As an example, detection of a mean 0.15 ‰ secular shift in $\delta^{238}U$ in a sample set with twenty total samples requires that at least six of the samples define the isotopic excursion. Excursions defined by fewer samples cannot be confidently distinguished from statistical fluctuations in the background $\delta^{238}U$ value. These tests provide important constraints on the number of samples and sampling resolution required for robust interpretation of $\delta^{238}U$ trends in an individual sediment profile. Of course, measurements revealing similar patterns of secular variation between multiple, widely-spaced sections, can be used to build further confidence in the identification of $\delta^{238}U$ excursions (e.g., Zhang et al., 2018a). However, contemporaneous sediments may not always be available, instead requiring careful statistical treatment of data from just a single locality.

Table 4.4. Number of samples required to define a statistically significant secular shift in $\delta^{238}U$ based on the magnitude of the shift and total number of the samples in the data set, assuming a diagenetic scatter of 0.14‰ (1 SD).

Total number of samples	Secular shift in $\delta^{238}U$ (‰)					
	0.05	0.1	0.15	0.2	0.3	0.5
5	Not detectable at $\alpha < 0.05$					1
10					2	1
20			6	3	2	1
30			5	3	1	1
50		10	4	3	1	1

4.6 Conclusions

The well-characterized Key Largo and Bahamas Transect carbonates provide important constraints on the relative importance of different diagenetic factors controlling $\delta^{238}U$ in bulk carbonate sediments. Analysis of these recent carbonate sediments, where the $\delta^{238}U$ of coeval seawater can be reasonably inferred, provides a critical test of the ability to reconstruct the $\delta^{238}U$ of paleoseawater from more ancient carbonates. This study has several main conclusions which are summarized below:

- Bulk carbonate sediments on the Bahamas platform margin and slope record higher $\delta^{238}U$ than modern seawater. The isotopic compositions of individual core samples are stochastically-distributed and have an average isotopic offset of 0.27±0.14 ‰ (1 SD) heavier than modern seawater. This study suggests that studies of $\delta^{238}U$ in ancient carbonates should be corrected for this offset.
- A comparison of banktop versus slope sediments in the Bahamas shows a nearly identical distribution of $\delta^{238}U$ values. The simplest explanation for this observation is that $\delta^{238}U$ is altered primarily through syndepositional diagenesis occurring in shallow banktop sediments, and that this signal is then transferred to deeper water sediments by down-slope transport of carbonate sediments with little further modification. This study found no evidence of diagenetic alteration following deeper sediment burial (e.g., during dolomitization), which suggests that it is the result of closure of the U isotope system due to the low solubility of U(IV) in anoxic pore water.
- While meteoric recrystallization of aragonite to calcite alone does not appear to induce significant fractionation of $\delta^{238}U$, shallow Bahamas sediments which show carbon and

oxygen isotopic evidence for meteoric alteration display significantly heavier $\delta^{238}U$ values than samples that did not experience meteoric diagenesis. Due to the solubility of U(VI), samples which have experienced meteoritic alteration in the relatively oxidizing vadose zone may exhibit open-system behavior leading to more extreme diagenetic effects. Studies of ancient sedimentary carbonates should carefully screen for meteoric diagenesis occurring at the time of deposition or during later exposure in outcrop, as either of these processes could potentially lead to open system behavior of U isotopes and alteration of the original carbonate $\delta^{238}U$.

- Syndepositional diagenesis affecting $\delta^{238}U$ in carbonates likely results from a combination of two processes. First, nearly all samples display a nearly uniform minimum isotopic offset from seawater which is consistent with the fractionation predicted by Chen et al. (2016) for precipitation of abiotic carbonates from seawater. This suggests that recrystallization of biogenic carbonate fragments and/or deposition of early cements results in $\delta^{238}U$ consistent with values predicted by abiotic models. In addition, many carbonate sediments experience further reductive authigenic U enrichment from anoxic pore water, resulting in the preferential incorporation of ^{238}U in disseminated U(IV) mineral species and possible incorporation into the carbonate mineral lattice. These high $\delta^{238}U$ sediments are transported downslope and mixed into slope sediments resulting in the stochastic range of $\delta^{238}U$ values observed in slope sediments.
- The fluid-rock interaction model predicts that bulk carbonate $\delta^{238}U$ should be less susceptible to diagenetic alteration than $\delta^{13}C$ and $\delta^{18}O$, or $^{87}Sr/^{86}Sr$. However, these models also predict strongly hyperbolic trends on cross-plots of diagenetic indicators, which could easily mask evidence of diagenesis in ancient sediments. With the exception of $\delta^{13}C$ and $\delta^{18}O$ values

suggesting meteoric alteration, this study found no other obvious correlations between variation in $\delta^{238}U$ values in Bahamas sediments and a wide variety of common sedimentary diagenetic indicators including Mg/Ca ratios, U and Sr concentrations, Mn/Sr ratios, and redox-sensitive trace metal concentrations.

- The stochastic variation of $\delta^{238}U$ in Bahamas sediment cores suggests the need for caution when interpreting evidence for seawater $\delta^{238}U$ excursions in ancient sediments. $\delta^{238}U$ excursions defined by a single or small number of samples may represent only statistical fluctuation in the diagenetic offset from seawater. Robust identification of seawater $\delta^{238}U$ excursions in ancient sediments requires that a sufficient number of sediment analyses are available to determine statistically significant shifts $\delta^{238}U$ in the face of diagenetically-induced noise.

CHAPTER 5

$^{238}U/^{235}U$ IN ANOXIC CARBONATE SEDIMENTS OF THE MEROMICTIC FAYETTEVILLE GREEN LAKE, NEW YORK, USA: IMPLICATIONS FOR URANIUM ISOTOPES IN SEDIMENTARY CARBONATES AS A PALEOREDOX PROXY

The work presented in this chapter is in preparation to submit to Geochimica et Cosmochimica Acta: Chen X., Romaniello S. J., McCormick M., Sherry A., Havig J. R. Zheng W. and Anbar A. D. $^{238}U/^{235}U$ in anoxic carbonate sediments of the meromictic Fayetteville Green Lake, New York: Implications for uranium isotopes in sedimentary carbonates as a paleoredox proxy.

Abstract

Variations of the uranium isotope ratio ($^{238}U/^{235}U$) in sedimentary carbonate rocks are being applied as a novel paleoredox proxy to reconstruct oceanic anoxia through time. Most of these applications assume that this proxy has good fidelity when carbonate sediments deposit under anoxic conditions in redox-stratified oceans. However, this assumption has not been tested in modern analog environments. This is the first such test.

To better understand the effect of anoxic deposition conditions on $^{238}U/^{235}U$ in carbonate sediments, I investigated U isotopic systematics in a permanently redox-stratified lake—Fayetteville Green Lake (FGL), New York, USA—where carbonates deposit under anoxic conditions. Dissolved U concentrations (from 10 to 3 nM) and $\delta^{238}U$ (–0.50 to –0.96 ‰) were

significantly depleted across the chemocline of the water column. Parallel with the depletion in dissolved U concentration and $\delta^{238}U$, $\delta^{238}U$ values of the authigenic U in sinking particles increased with depth from –0.44 to –0.16 ‰. $\delta^{238}U$ in anoxic carbonate sediments was higher than in the surface water of FGL by ~0.2 ‰. The overall U isotopic mass balance in FGL reveals that FGL is an open system, where surface inlet (31 %) and groundwater (69 %) are U sources, and surface outlet (95.3 %) and sediments (4.7 %) are U sinks. $\delta^{238}U$ values in the surface inlet, groundwater, and surface outlet were indistinguishable at ~ –0.55 ‰ while $\delta^{238}U$ in the anoxic carbonate sediments was –0.35 ‰.

The depletion in dissolved U concentration and $\delta^{238}U$ below the chemocline of FGL resulted from U reduction in the anoxic water column and below the sediment-water interface. The progressive increase of $\delta^{238}U$ in the authigenic U in sinking particles below the chemocline of FGL suggests reduction of dissolved U(VI) in the water column to U(IV). The authigenic U flux in sinking particles only accounted for ~7.7 % of the total authigenic U flux in the anoxic sediments, suggesting that U reduction below the sediment-water interface was the predominant factor drawing down dissolved U concentration and $\delta^{238}U$ below the chemocline of FGL. The finding that U reduction occurs in the anoxic water column and below the sediment-water interface of FGL is different from previous studies that claimed U reduction only occurred below the sediment-water interface in FGL and other modern anoxic basins such as the Black Sea (Anderson, 1984; Anderson et al., 1989a).

The significantly higher $\delta^{238}U$ in the anoxic carbonate sediments (–0.35±0.12 ‰, 1 SD) compared to the shallow water carbonates (–0.51 ‰) in FGL indicates that carbonates deposited under anoxic conditions have elevated $\delta^{238}U$ due to authigenic U reduction. Thus, the U isotopic

offset induced by anoxic depositional conditions should be corrected when applying $\delta^{238}U$ as a paleoredox proxy.

5.1 Introduction

The reconstruction of the past oxygenation of the Earth's atmosphere and ocean is crucial to understanding the evolution of life on Earth (e.g., Kasting, 1993; Canfield, 2005; Meyer and Kump, 2008; Lyons et al., 2014). Geochemical signatures preserved in ancient sedimentary rocks offer a means of tracking the timing and nature of Earth's environmental oxygenation (e.g., Pufahl and Hiatt, 2012). The relative abundance of the redox-sensitive element uranium (U) in organic-rich black shales, for example, has been suggested to qualitatively reflect the evolution of oxygen in Earth's atmosphere and ocean through time (e.g., Partin et al., 2013; Lyons et al., 2014). However, this type of paleoredox proxy cannot be used to quantify the global extent of redox conditions through time for two reasons. First, authigenic enrichments of U in anoxic sediments are strongly affected by local depositional conditions such as primary productivity, and sedimentation and mass accumulation rates (Anderson et al., 1989a; McManus et al., 2005; Partin et al., 2013; Andersen et al., 2014; Hinojosa et al., 2016). Second, black shales are only sporadically distributed on Earth over geologic history (e.g., Condie et al., 2001; Le Heron et al., 2009; Tourtelot, 1979).

Compared to the U abundance in black shales, variations of $^{238}U/^{235}U$ in sedimentary carbonate rocks are a promising paleoredox proxy to constrain or even quantify global redox conditions via oceanic U isotopic budget through time. There are several reasons to support this argument described in detail below.

First, variations of $^{238}U/^{235}U$ in seawater are predominantly driven by changes in redox conditions of the oceans. Seawater U is mainly removed into anoxic sediments (~56 % of the total marine U removal from seawater) via diffusion of dissolved U(VI) into sediments and subsequent precipitation as insoluble U(IV), accompanied by a significant U isotope fractionation ($\Delta^{238}U_{other}$) of ~0.6 ‰ relative to seawater (Anderson et al., 1989a, b; Barnes and Cochran, 1990; Klinkhammer and Palmer, 1991; Weyer et al., 2008; Tissot and Dauphas, 2015; Andersen et al., 2016, 2017; Romaniello et al., 2009; Rolison et al., 2017; Holmden et al., 2015; Noordman et al., 2015; Bura-Nakić et al., 2018). Other marine U sinks including ferromanganese crusts, hydrothermal sediments, and carbonate sediments, exhibit much smaller U isotope fractionation (Brennecka et al., 2011a; Jemison et al., 2017; Dang et al., 2017; Noordmann et al., 2016; Chen et al., 2016, 2017, 2018a, b; Romaniello et al., 2013). The average value of U isotope fractionation in the other U sinks ($\Delta^{238}U_{other}$) is ~0.03 ‰ (e.g., Tissot and Dauphas, 2015). The U isotopic budget in modern oceans is therefore described as:

$$\delta^{238}U_{seawater} = \delta^{238}U_{river} - f_{anoxic} \times \Delta^{238}U_{anoxic} - (1 - f_{anoxic}) \times \Delta^{238}U_{other} \quad \text{Eq. 5.1}$$

where $\delta^{238}U_{seawater}$ and $\delta^{238}U_{river}$ (–0.30 ‰) are U isotopic compositions of seawater and rivers, respectively, and f_{anoxic} is the relative fraction of U removal by anoxic sediments (e.g., Andersen et al., 2016). According to equation 5.1, variations of $\delta^{238}U_{seawater}$ could be used to quantitatively estimate changes in oceanic redox conditions.

Second, because the residence time of U in modern seawater (500 kyr) is much longer than the global oceanic mixing time of ~2 kyr, the U concentration and $^{238}U/^{235}U$ ratio of open ocean seawater is well-mixed and homogenous (Dunk et al., 2002; Jenkins, 2003; Stirling et al., 2007; Weyer et al., 2008; Tissot and Dauphas, 2015; Andersen et al., 2016; Chen et al., 2018a).

Thus, $^{238}U/^{235}U$ at any individual locality may represent the global seawater value and reflect global redox conditions.

Third, the wide temporal and spatial distribution of sedimentary carbonate rocks on Earth could provide a more continuous, high-resolution record of redox conditions of the oceans through time (e.g., Shields and Veizer, 2002; Ronov, 1964; Wilkinson and Walker, 1989). For these reasons, variations of $^{238}U/^{235}U$ in sedimentary carbonates rocks have been extensively applied to infer global redox conditions of ancient oceans (Brennecka et al., 2011b; Lau et al., 2016, 2017; Elrick et al., 2017; Zhang et al., 2018a, b; Dahl et al., 2014, 2017; Amzy et al., 201; Jost et al., 2017; Clarkson et al., 2018; Bartlett et al., 2018).

Yet, the quantification of the extent of oceanic anoxia using equation 5.1 relies heavily on the fidelity with which sedimentary carbonate rocks record $^{238}U/^{235}U$ in coeval seawater. The ability of sedimentary carbonate rocks to capture and record $^{238}U/^{235}U$ of seawater has been examined in primary abiotic and biogenic calcium carbonates, as well as in diagenetically altered modern shallow-water carbonate sediments from the Bahamas (Romaniello et al., 2013; Chen et al., 2016, 2017, 2018a, b; Tissot et al., 2018). An isotope fractionation of 0–0.3 ‰ was observed for these modern carbonates, which precipitated and deposited under oxic conditions with a minor U enrichment (from 1.5 to 4 ppm) during diagenesis (Chen et al., 2016, 2017, 2018a, b; Tissot et al., 2018). However, in the redox-stratified oceans of deep time like the Proterozoic Eon, calcium carbonates might have precipitated in the shallow surface water but deposited under the anoxic conditions typical of deeper waters (Grotzinger and Knoll, 1995; Grotzinger and James, 2000; Gulin, 2000; Anbar and Knoll, 2002). Under anoxic conditions, significant authigenic U enrichment (~26 ppm) and isotope fractionation (~0.4 ‰) have been observed in modern anoxic sediments such as black shales due to reductive accumulation of U below the

sediment-water interface (e.g., Dunk et al., 2002; Partin et al., 2013; Anderson et al., 1989; Noordmann et al., 2016; Andersen et al., 2017). Under this scenario, U concentrations and $^{238}U/^{235}U$ in these anoxic carbonate sediments would be predominantly controlled by authigenic U reduction, which progressively enriches ^{238}U in U(IV) in the sediments (e.g., Andersen et al., 2017). The isotopic offset between anoxic carbonate sediments and surface water carbonates could strongly impact the inferred extent of oceanic anoxia, in a manner similar to the consequences of diagenetic effects on $^{238}U/^{235}U$ in modern shallow-water carbonate sediments (Chen et al., 2018b). It is, therefore, important to investigate variations of $^{238}U/^{235}U$ in carbonate sediments deposited under anoxic conditions.

Fayetteville Green Lake (FGL), New York is an excellent modern analogue in which to investigate U isotopic systematics of carbonate sediments deposited under anoxic conditions. First, it is a permanently redox-stratified lake with a relatively low sulfate concentration of 9.5–15.6 mM, similar to Phanerozoic (250–550 Ma) and Proterozoic (2.1–2.3 Ga) oceans (Eggleton, 1956; Brunskill and Lumlam, 1969; Zerkel et al., 2010; Havig et al., 2015; Algeo et al., 2015; Planavsky et al., 2012). Second, large quantities of calcite precipitate in the surface water due to the photosynthetic activity of cyanobacterial picoplankton (often as so-called “whiting events”). These calcite precipitates sink past the chemocline and are deposited under anoxic conditions (Thompson et a., 1997). These carbonates account for 70–90 weight % of the total mass of anoxic sediments (Brunskill, 1969; Herndon et al., 2018; Havig et al., 2017). This combination of unique water column chemistry and sediment geochemistry, combined with relatively easy access, make FGL a promising modern analogue for carbonate-hosted proxies in ancient redox-stratified oceans.

5.2 Study Site and Sampling

5.2.1 Study Site

Fayetteville Green Lake (FGL) is a freshwater meromictic lake that lies in the Green Lake State Park, New York, USA (Fig. 1). FGL is a small (0.258 km^2) and deep (52.5 m) lake with an average slope of 18°42′ (Brunskill and Ludlam, 1969). It is recharged by surface water from Round Lake and groundwater (> 50 %), and discharges through a surface outlet into the Pools Brook (Brunskill and Ludlam, 1969; Takahashi et al., 1968). Saline groundwater discharges into FGL at about 18 m, maintaining the permanent density stratification and elevated sulfate concentration in the water column of this lake (Brunskill, 1969; Takahashi et al., 1968). The density stratification results in three layers: (1) mixolimnion (0–15 m) with well-oxygenated mixed water mass; (2) chemocline (15–21 m) with significant decrease in dissolved O_2 and oxidation-reduction potential (ORP); (3) monolimnion (21 - 52.5 m) with stagnant anoxic water mass and H_2S up to ~ 2 mM (Brunskill and Ludlam, 1969; Eggleton, 1956; Havig et al., 2015; Torgersen et al., 1981). In the mixolimnion layer, summer-time blooms of cyanobacteria lead to high rates of primary productivity which draw down surface water pCO_2. The cyanobacteria themselves provide carbonate nucleation sites, inducing calcite precipitation in the open water column and leading to the extensive accumulation of benthic bioherm carbonates along the shoreline of the lake (Thompson et al., 1997; Thompson and Ferris, 1990; Wilhelm and Hweson, 2012). The FGL chemocline is inhabited by a dense population of anoxygenic photosynthetic bacteria including both green and purple sulfur bacteria (Culver and Brunskill, 1969; Thompson et al., 1990; Zerkel et al., 2010). Biological

sulfate reduction coupled with organic matter degradation by sulfate reducing organisms below the chemocline generates high concentration of H_2S (Havig et al., 2017).

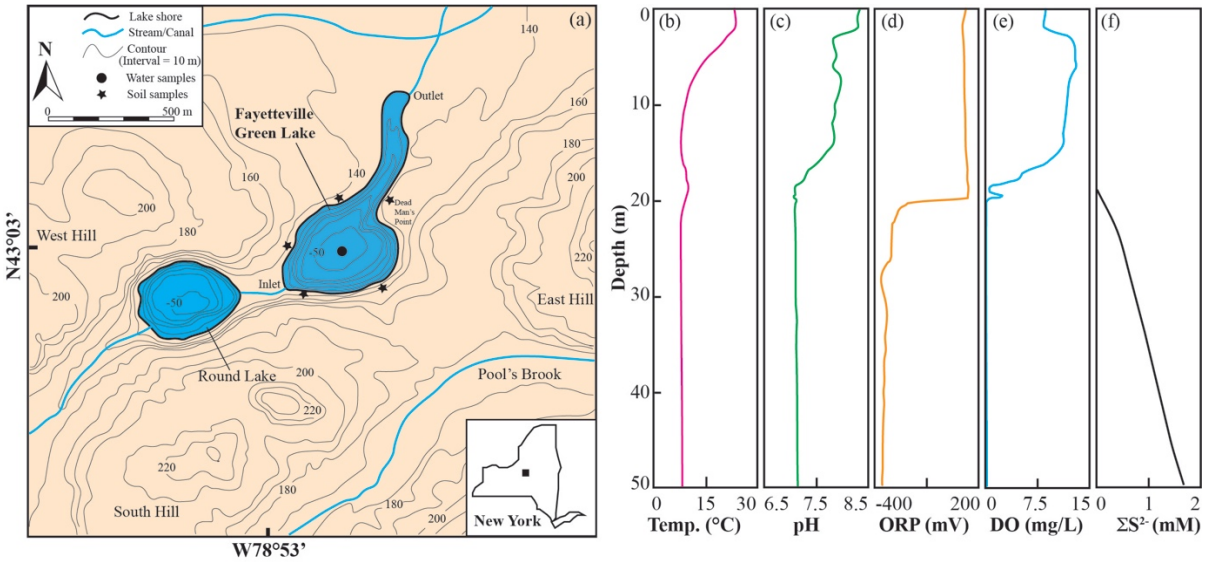

Figure 5.1. Site map (a) and physicochemical properties (b, c, d, e, and f) of Fayetteville Green Lake (FGL), New York, USA, modified from Hilfinger et al. (2001) and Havig et al. (2015). The circle in the center of FGL is the sampling point of water samples and anoxic sediments. Stars around FGL are locations of soil samples. The physicochemical properties data were from Havig et al. (2015).

5.2.2 Sampling

5.2.2.1 Water Samples

Water samples were collected across the chemocline of the water column at the deepest point (~52.5 m) of FGL with high depth-resolution in July 2015 using the apparatus developed by McCormick et al. (2014). Trace-metal-clean syringes (60 mL in volume) were sealed with closed glass pipette tips and the plungers drawn and pinned backed to create a vacuum. The syringes were deployed every 2 meters along a tube suspended vertically in the water column (except between 16 and 24 m depth, where syringes were set every 0.5 meter). The glass pipette tips were broken with a messenger (a short metal rod), allowing the syringes to fill. This method

provides precise, synoptic sampling of the entire water column. Water samples were held at ~4 °C and transported to Hamilton College (Clinton, NY) within 2 hours, where they were filtered through 0.22 μm membranes and acidified to pH < 2 with trace metal grade nitric acid. Water samples from the surface inlet and outlet of FGL were also collected.

5.2.2.2 Sinking Particles in the Water Column

Sediment traps were deployed in the water column at four different depths above (13.5 m) and below (21.5, 27.5 and 45.5 m) the chemocline to capture $^{238}U/^{235}U$ in the sinking particles. Traps were deployed from July 12–21, 2017. At each depth, four trace-metal clean pit-style traps (3.5 inches in diameter) were fixed on a PVC cross frame. Traps were spaced along a single mooring line anchored at the lake bottom and held taught by a submerged subsurface buoy (to minimize wave action).

Before deployment, each sediment trap was filled with water pumped from its target depth. Plastic mesh on the top of each trap was used to avoid collection of large pieces of plant detritus and limit disturbance by fish and other large detritivores. Upon collection, each trap was tightly sealed and transported to Hamilton College. Water was carefully siphoned from each trap and particulate matter was separated from the water via centrifugation at 5000 rpm in 50 ml trace-metal clean tubes. Particulate matter was subsequently frozen prior to analysis.

5.2.2.3 Anoxic Carbonate Sediments

A 40-cm sediment core was collected using a gravity corer on Dec 12th, 2012 by Brown (2015). The sediment core was kept between 0 and 4 °C. The sediment core was pushed up through the core tube and sectioned into 0.5 to 1 cm thick cross-sections. These core slices were stored in 50 ml tubes at –80 °C.

5.2.2.4 Bedrock and Soils

Samples of local bedrock and soil were collected to better constrain the U budget in FGL. Four soil samples (0–5 cm, 100 g each) were collected in acid cleaned plastic bags around FGL (depicted as stars in Figure 5.1). Bedrock, including the red Vernon shale, green Vernon shale (Hamilton college), and dolomite around FGL were also sampled (100 g each).

5.3 Chemical Analysis

5.3.1 Elemental Concentration Analysis

The concentrations of trace metals and major cations in all the samples were determined using the iCAP Q inductively coupled plasma mass spectrometry (ICP-MS) at Arizona State University (ASU). Prior to analysis, soil and rock samples were dried 50 °C for 24 h and then powdered using a silicon nitride ball mill. Sediment powders (~100 mg each) were ashed overnight at 650 °C to remove organic matter. The ashed soil and rock powders were quantitatively transferred into 22 ml Savillex beakers and digested with a mixture of conc. HF/HNO_3 (3:1), aqua regia, and conc. HNO_3 + 30 % H_2O_2 until a completely clear solution was obtained.

Anoxic carbonate sediment samples were dissolved in 3 M HNO_3 to dissolve the calcium carbonate and centrifuged at 4500 rpm to separate the insoluble solid. The dissolved fraction was digested using conc. HNO_3 + 30 % H_2O_2 while the insoluble fraction was digested following the procedure for soil and bedrock samples described above (Chen et al., 2018b). After digestion, the soluble and insoluble fractions of each sample ran through UTEVA column chemistry separately for elemental concentration and U isotopic ratio measurements. The digested samples were

diluted in 0.32 HNO_3 for concentration analysis. The measurement precision for trace elements was generally ± 5 % by ICP-MS.

The sinking particles from the sediment traps were freeze-dried (Millrock BT-48 freeze dryer) and weighed to obtain the net dry masses of the samples to calculate the flux of particles in the water column at different depths. The dried samples were digested using aqua regia, and conc. HNO_3 + 30 % H_2O_2 for elemental concentration analyses.

5.3.2 Total Organic Carbon Measurement of Sediment Trap Samples

Sample preparation procedure for total organic content (TOC) analysis followed Stüeken et al. (2015). Sediment trap samples were dried 4 ml glass vials at 60 °C to constant weight. Then, sufficient amount of 1 M HCl was added into the glass vials to completely dissolve the inorganic carbonates from the samples. These acidified samples were then dried at 60 °C to constant weight. The residual solids were ground to a homogeneous powder and transferred into 2 ml glass vials for storage in a desiccator. About 0.6–15 mg sinking particles from each sediment trap was used for TOC analysis.

Carbon concentrations in sinking particles were measured by continuous flow isotope ratio mass spectrometry (CF-IRMS) in the W. M. Keck Foundation Laboratory for Environmental Biogeochemistry, ASU. Three replicates of each sample were measured to determine an average TOC concentration (wt %). The TOC content was estimated using the equation:

$$\mathrm{TOC} = \mathrm{M_C} \times \frac{\mathrm{M_{acid}}}{\mathrm{M_{IRMS}}} \times \frac{1}{\mathrm{M_{particles}}} \times 100\ \% \qquad \text{Eq. 5.2}$$

where M_C is the total mass of carbon measured on IRMS, M_{IRMS} is the mass of decarbonated sample introduced into IRMS. $M_{particles}$ and M_{acid} are the dry weights of sinking particles before and after decarbonation.

5.3.3 U Isotopic Ratio Measurements

U isotopic compositions were measured using the ^{233}U-^{236}U double-spike method by multiple collector (MC) ICP-MS (Chen et al., 2016) at ASU. Prior to U purification, each digested sample was well-mixed with double-spike U solution (IRMM-3636) to achieve a spike:sample molar ratio of 0.0363 (Verbruggen et al., 2008; Chen et al., 2016). The double-spiked is used to correct for any isotope fractionation that might occur during the U purification process and sample analysis.

The protocol of U purification followed Chen et al. (2016). After rinsing the polypropylene columns (BioRad#7311550) with 10 ml 18.2 MΩ-cm deionized water, a volume of 1 ml UTEVA resin (Eichrom Technologies, LLC) was loaded on each column. The resin was then conditioned by passing through 2.5 ml 0.05 M HCl four times to remove impurities, and 0.8 ml 3 M HNO_3 three times to convert the resin to nitric form. Then the double-spiked U sample (dissolved in 3 M HNO_3) was loaded on the column and rinsed with 3 M HNO_3 (2 + 2 + 2 + 3 +3 ml) to remove all matrix ions except U and Th. The resin was then converted to chloride form by passing through 10 M HCl (3 × 1 ml) through the column. Thorium was removed by a mixture of 5 M HCl and 0.05 M oxalic acid (3 × 1 ml). Then, the oxalic acid was removed by rinsing 5 M HCl (3 × 1 ml). The adsorbed U on the resin was eluted using 0.05 M HCl (1 + 1 + 1 + 2 + 2 ml). The U cuts were dried down and then heated with a mixture of 2 ml concentrated HNO_3 and 0.2

ml 30 % H_2O_2 to remove any organic residue eluted from the UTEVA resin. This process was repeated twice to ensure sample purity.

After UTEVA column chemistry, U samples dissolved in 0.32 M HNO_3 were measured MC-ICP-MS at a U concentration of ~ 50 ppb. Ion beams of ^{233}U, ^{235}U, ^{236}U, and ^{238}U were collected with Faraday cups connected to 10^{12} Ω, 10^{12} Ω, 10^{12} Ω, and 10^{11} Ω resistors, respectively. The typical voltage for ^{238}U at a U concentration of 50 ppb was ~ 30 V. Uranium isotopic compositions are reported in δ notation relative to the reference standard CRM-145a as follows:

$$\delta^{238}U = \left[\frac{\left({}^{238}U/_{235}U \right)_{sample}}{\left({}^{238}U/_{235}U \right)_{CRM-145a}} - 1 \right] \times 1000 \qquad \text{Eq. 5.3}$$

$$\delta^{234}U = \left[\frac{\left({}^{234}U/_{238}U \right)_{sample}}{\left({}^{234}U/_{238}U \right)_{sec.eq.}} - 1 \right] \times 1000 \qquad \text{Eq. 5.4}$$

where sec. eq. stands for secular equilibrium (Andersen et al., 2008). To report the measured $\delta^{234}U$ vs. secular equilibrium, a $\delta^{234}U$ value of –36.92 ‰ was assumed for CRM-145a when compared to the secular equilibrium standard (Harwell uraninite, Andersen et al., 2008).

After UTEVA column chemistry, each sample was typically analyzed in triplicate, provided that adequate U was available. The precision of the U isotope measurement in this study was reported as twice the standard deviation (2 SD) of the reference standard CRM-145a or the 2 SD of triplicate analyses of the samples, whichever was larger. The standard CRM-145a was analyzed before and after every two samples to correct for small amounts of instrument drift.

The reproducibility of multiple runs of $\delta^{238}U$ and $\delta^{234}U$ for the standard CRM-145a were within ± 0.10 ‰ and ± 6 ‰, respectively (2 SD, N = 45). The accuracy of U isotope measurement was confirmed by multiple analyses of the secondary standard CRM-129a, which gave a value of –1.70 ± 0.08 ‰ (N = 8, 2 SD), indistinguishable from independent measurements by other laboratories (Wang et al., 2015; Amzy et al., 2015; Lau et al., 2016; Shiel et al., 2016). My measured value of CRM-129a is lighter than $\delta^{238}U$ of one separate aliquot of CRM-129a measured at Stanford University (–1.52 ± 0.13 ‰) and the certified value of CRM-129a by New Brunswick Laboratory (–0.90 ± 0.53 ‰). This suggests that one or more batches of CRM-129a may be heterogeneous.

The blank from the UTEVA column chemistry purification step was about 0.02 ± 0.02 ng (2 SD, N = 6), which was negligible relative to the >100 ng U sample. Four aliquots of the reference standard CRM-145a were purified together with natural samples of FGL. The average value of $\delta^{238}U$ for these aliquots of CRM-145a was 0.00 ± 0.03 ‰, which was identical to the direct measurement of pure CRM-145a (0.00 ± 0.03 ‰).

5.4 Results

5.4.1 FGL U Sources

5.4.1.1 Surface Inlet and Outlet

U concentrations in the surface outlet and surface water were similar (~9.4 nM) and slighter higher than the inlet (7.6 nM, Figure 5.2). $\delta^{234}U$ values in the outlet and surface were close (~677 ‰), but much lower than the inlet (767 ‰). In contrast, $\delta^{238}U$ values for the surface inlet (–0.55 ‰), outlet (–0.57 ‰), and surface water (–0.55 ‰) were indistinguishable.

5.4.1.2 Bedrocks and Soils

U concentrations in bedrock samples of FGL ranged from 0.26–1.29 ppm, significantly lower than that in soils (~2.5 ppm). $\delta^{234}U$ values in the soil and bedrock were consistently low, ranging from –50 to –200 ‰, and significantly lighter than the surface water (680 ‰). The $\delta^{238}U$ values of soils (–0.48 to –0.30 ‰) and bedrock samples (–0.38 to –0.24 ‰) were close to average continental crust values (–0.30 ± 0.04 ‰; Andersen et al., 2016) but slightly higher than that of the surface water in FGL (–0.55 ‰).

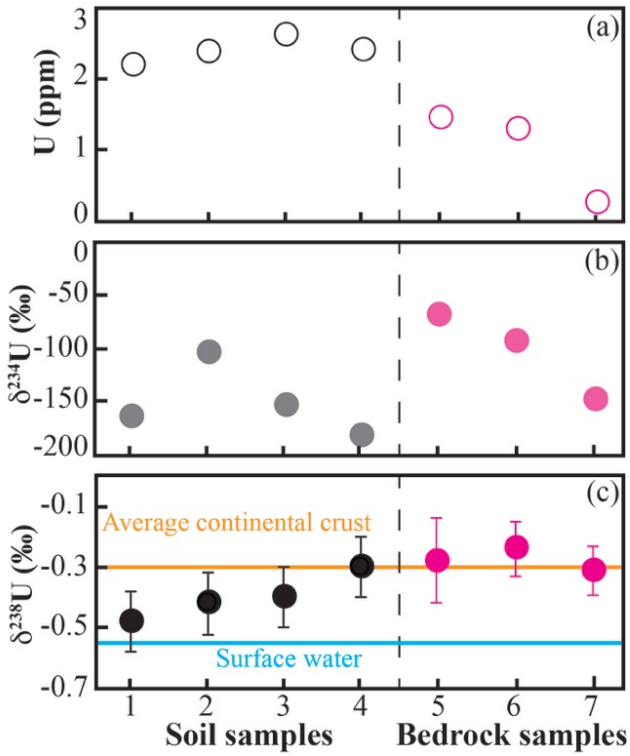

Figure 5.2. U concentrations (a), $\delta^{234}U$ (b) and $\delta^{238}U$ (c) in soils and bedrock samples around FGL. The blue and orange horizontal lines represents $\delta^{238}U$ of the surface water in FGL and average continental crust (–0.30 ‰; Andersen et al., 2016).

5.4.2 FGL Water Column

5.4.2.1 Major Cations and Anions

Concentrations of major cations (Na^+, Mg^{2+}, and Ca^{2+}; this study) and anions (Cl^- and SO_4^{2}; Havig et al., 2015) showed subtle or little continuous increase above and below the chemocline, but significant elevation across the chemocline (Figure 5.3). The sharp increase in the conservative elements (Na^+, Mg^{2+}, Ca^{2+}, SO_4^{2-}, and Cl^-) is consistent with previous studies of significant saline groundwater recharge at ~18 m and dissolution of calcite and halite below 18 m in the water column (Thompson et al., 1990).

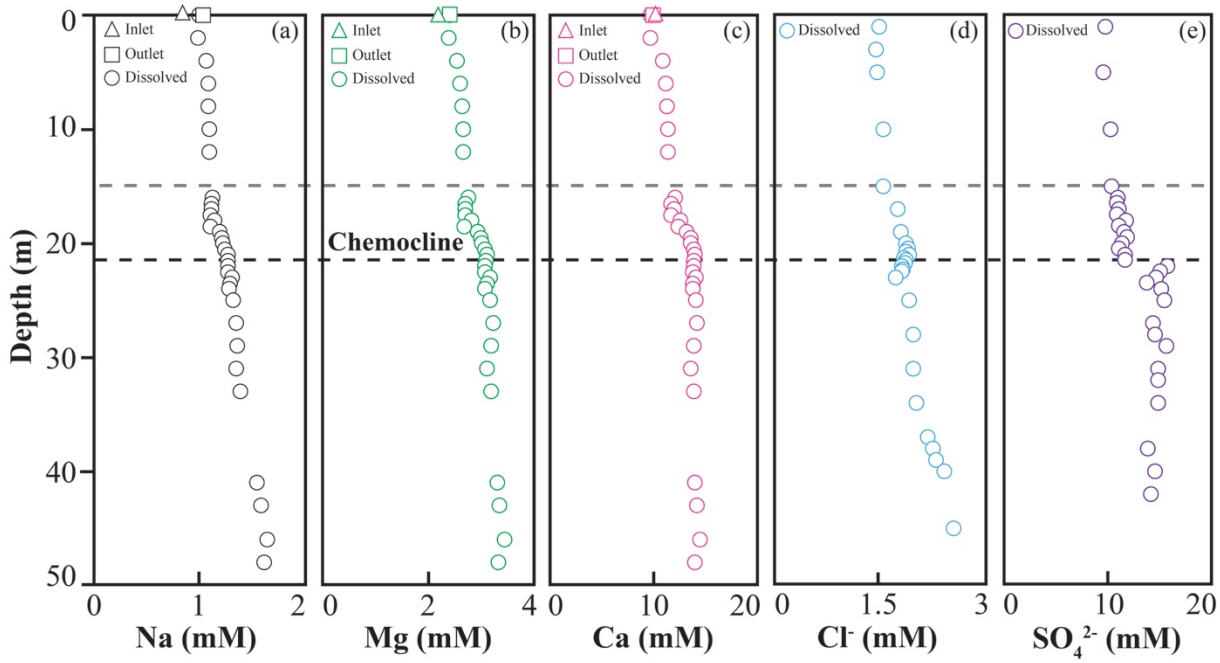

Figure 5.3. Major cations (Na^+, Mg^{2+}, and Ca^{2+}, *this study*) and anions (Cl^- and SO_4^{2-}, Havig et al., 2015) in the water column (blue circles), inlet (open circles), and outlet (gray circles) of FGL. The gray band is the chemocline.

5.4.2.2 Dissolved Redox-sensitive Elements

Concentrations of redox-sensitive elements (Mn, Fe, Mo and U) follow the typical trend across the chemocline in the water column of FGL. Above the chemocline (0 - 15 m), Mn, Fe, and Mo were nearly uniform at 10, 10, and 16 nM, respectively (Figure 5.4). In contrast, U increased continuously from 9 nM to 12 nM.

Across the chemocline (15 - 21 m), however, concentrations of these elements varied in three different ways: (1) Mn and Fe increased continuously to their maximum values (20.1 μM and 4.6 nM) at the lower boundary; (2) Mo dropped drastically to a very low concentration (1.3 nM); (3) U stayed almost constant.

Below the chemocline, Fe, and Mn decreased abruptly with in the first 2 m, and became invariant at 4.0 and 0.1 μM deeper in the anoxic water column. U followed the same trend but with a slow, continuous drop throughout this layer to 3.5 nM. After a rapid drop, Mo concentrations remained invariant around 1 nM throughout the monoliminion.

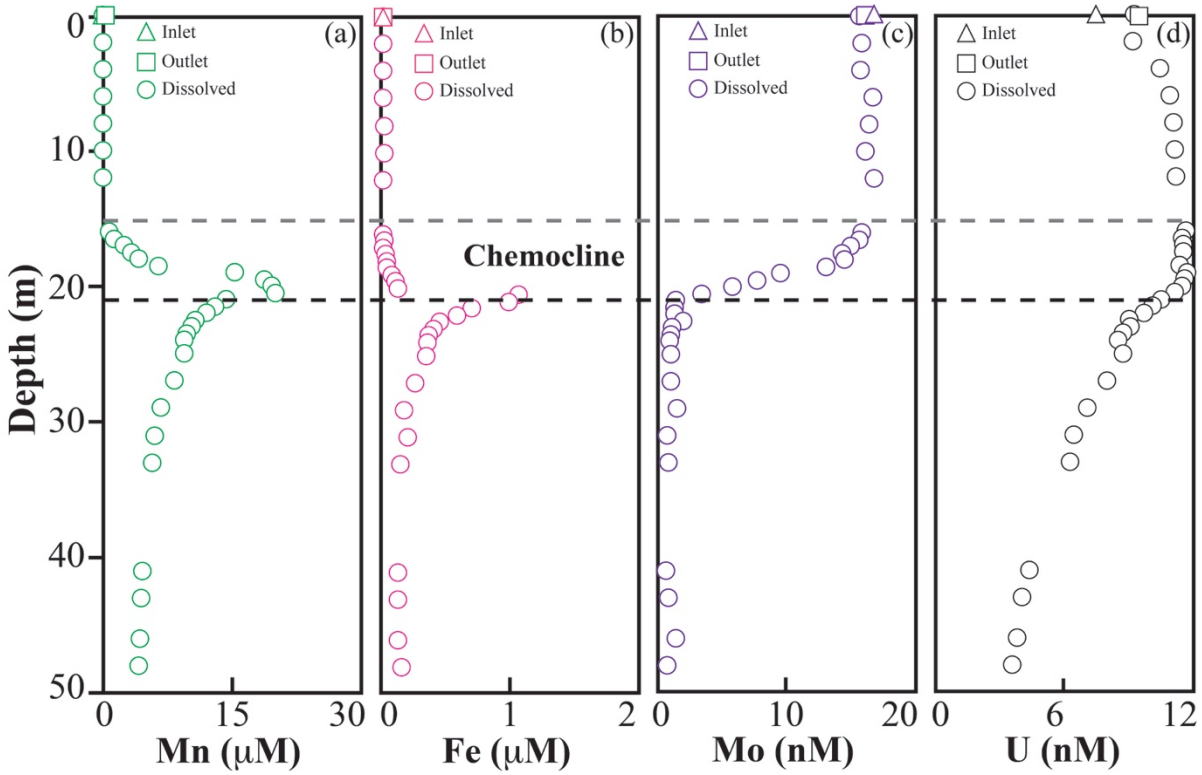

Figure 5.4. Concentrations of Mn, Fe, Mo and U in the water column (blue circles), inlet (open circles), and outlet (gray circles) of FGL. The gray band is the chemocline.

5.4.2.3 U Concentration and Isotopic Compositions in the Water Column

Dissolved $\delta^{238}U$ in the water column decreased significantly below the chemocline, following the same trend as dissolved U concentration (Figure 5.5). $\delta^{238}U$ was invariant at –0.52 ‰ above the chemocline, and progressively decreased to –0.96 ‰ throughout the water column. $\delta^{234}U$ increased from 680 ‰ in the upper 15 m to 718 ‰ below the chemocline.

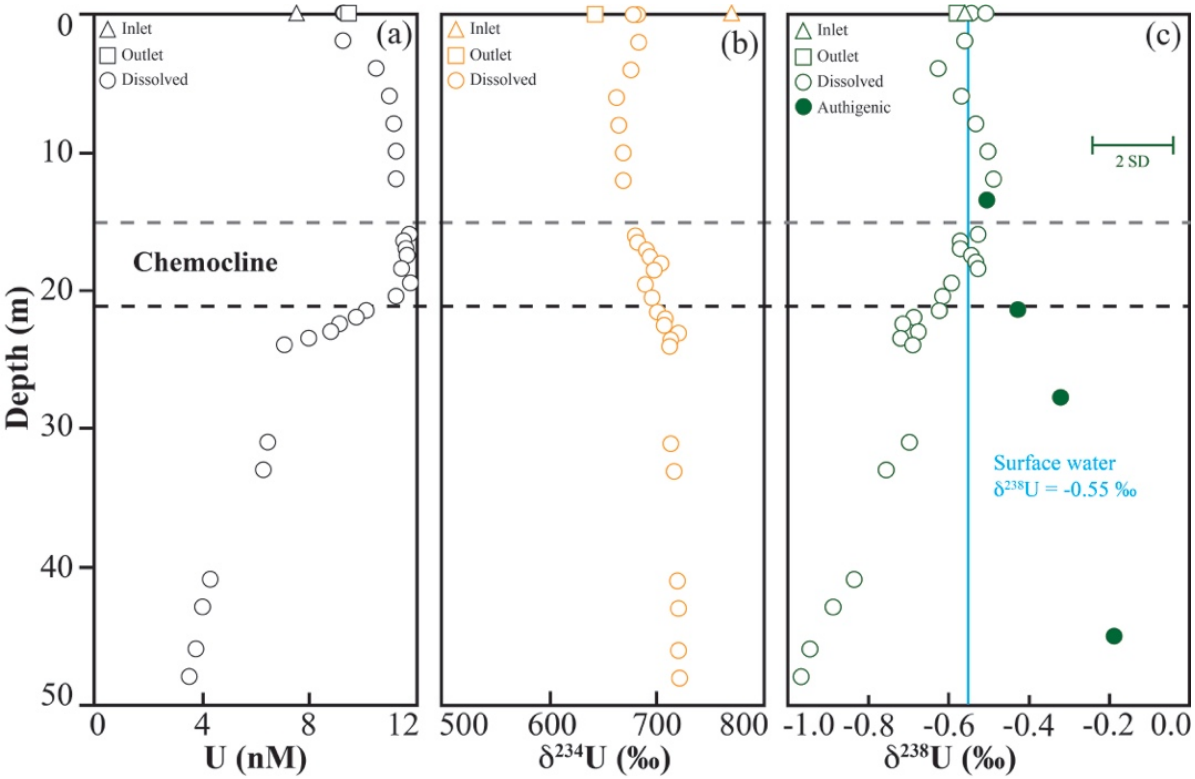

Figure 5.5. Dissolved U concentration (a), $\delta^{234}U$ (b), and $\delta^{238}U$ in the water column, inlet (triangles), outlet (rectangles) of FGL. 'Authigenic' in panel c represents the particulate authigenic $\delta^{238}U$ in the sediment traps of FGL.

5.4.3 Sinking Particles

The daily total mass flux of the sinking particles at different depths of FGL in July, 2017 was 1.96–2.57 g m^{-2} day^{-1} (see Table C.3). The daily total mass flux of sinking particles in FGL increased significantly from 13.5 to 21.5 m but decreased below the chemocline. Because ~90 % of the total sedimentation in FGL occurs from June through October each year, the estimated

average annual total mass flux from my sediment trap data ranged from 331 to 434 g m^{-2} yr^{-1} (Table 1), close to previous the previous study (~300 g m^{-2} yr^{-1}; Brunskill, 1969). The estimated annual TOC flux covaried with the total annual total mass flux below the chemocline of FGL, decreasing from 23 to 10 g m^{-2} yr^{-1}.

Table 5.1. Summary of U concentration and $\delta^{238}U$, and annual total mass, TOC, and authigenic U fluxes in sediment traps.

Depth	Annual total mass flux	Annual TOC flux	Annual authigenic U flux	U	f_{auth}	$f_{detrital}$	f_{carb}	$\delta^{238}U$	$\delta^{238}U_{auth}$
m	g m^{-2} yr^{-1}	g m^{-2} yr^{-1}	μmol m^{-2} yr^{-1}	ppm	%	%	%	‰	‰
13.5	336	–	0.42	0.59	50	15	35	–0.48	–0.51
21.5	434	23	0.58	0.58	54	15	31	–0.45	–0.44
27.5	362	10	0.53	0.63	55	15	30	–0.37	–0.30
45.5	331	11	0.45	0.56	56	16	28	–0.28	–0.16

Note: TOC is the organic carbon content. f_{auth}, $f_{detrital}$ and f_{carb} are authigenic, detrital and carbonate fractions of U.

Bulk U concentrations in sinking particles were almost invariant at ~0.6 ppm through the water column (Table 5.1) while bulk $\delta^{238}U$ appeared to slightly increase from –0.48 to –0.28 ‰ below the chemocline. These bulk data were used to calculate authigenic U concentration and isotopic compositions, assuming that the bulk sinking particles consists of detritus, carbonate, and authigenic fractions (Andersen et al., 2014). The detrital fraction ($f_{detrital}$) of U was estimated by normalization of U/Al to the average shale (Tribovillard et al., 2006; Wedepohl, 1971, 1991) using the equation:

$$f_{\text{detrital}} = \frac{\left({}^{\text{U}}/_{\text{Al}}\right)_{\text{AS}}}{\left({}^{\text{U}}/_{\text{Al}}\right)_{\text{sample}}} \qquad \text{Eq. 5.5}$$

where the subscript 'AS' represent average shale. $(U/Al)_{AS}$ (3.37×10^{-5}) is close to the average values of U/Al in the three bedrock samples of FGL (3.48×10^{-5}). The carbonate fraction of U (f_{carb}) was calculated using the equation:

$$f_{\mathrm{carb}} = \frac{\left({}^{\mathrm{U}}/_{\mathrm{Ca}}\right)_{\mathrm{calcite}}}{\left({}^{\mathrm{U}}/_{\mathrm{Ca}}\right)_{\mathrm{sample}}} \quad \text{Eq. 5.6}$$

where $(U/Ca)_{calcite}$ (0.65×10^{-6}) is the U to Ca ratio in calcite formed at the surface water of FGL (see Text C.1). As a result, authigenic U concentration (U_{auth}) and isotopic composition ($\delta^{238}U_{auth}$) are calculated as:

$$\mathrm{U_{auth}} = \mathrm{U_{sample}} \times (1 - f_{\mathrm{detrital}} - f_{\mathrm{carb}}) \quad \text{Eq. 5.7}$$

$$\delta^{238}\mathrm{U_{auth}} = \frac{\delta^{238}\mathrm{U_{sample}} - f_{\mathrm{detrital}} \times \delta^{238}\mathrm{U_{detrial}} - f_{\mathrm{carb}} \times \delta^{238}\mathrm{U_{calcite}}}{1 - f_{\mathrm{detrital}} - f_{\mathrm{carb}}} \quad \text{Eq. 5.8}$$

where $\delta^{238}U_{detrital}$ is –0.30 ‰ (Bedrock samples in this study), and $\delta^{238}U_{calcite}$ is –0.51 ‰ (Table C.2).

After corrections for the U from detrital and carbonate fractions, authigenic U concentration accounts for ~50 % of the total U in all the sinking particles. The authigenic U flux in sinking particles increased from 0.42 to 0.58 μmol m^{-2} yr^{-1} within 13.5–21.5 m and then decreased to 0.45 μmol m^{-2} yr^{-1} below this depth, covarying with total mass and TOC fluxes. In contrast, the particulate $\delta^{238}U_{auth}$ increased with depth from –0.51 to –0.16 ‰ below the chemocline.

5.4.4 Anoxic Carbonate Sediments

U concentrations, U/Al ratios and $\delta^{234}U$ in the bulk anoxic carbonate sediments remained relatively invariant above 18.5 cm, but increased below 18.5 cm (Table 5.2, Figure 5.6). Bulk U concentration was about 2 ppm above 18.5 cm, and then increased up to 5 ppm below this depth. Bulk U/Al ratio stayed around 3 above 18.5 cm and elevated continuously to ~11. Bulk $\delta^{234}U$ seems to co-vary with bulk U/Al ratio, increasing from 600 to 720 ‰. In contrast, bulk $\delta^{238}U$ in almost all these anoxic carbonate sediment samples was invariant with an average value of –0.34 ± 0.14 ‰ (2 SD, N = 11). A significantly lighter value of –0.64 ‰ was measured at 22.5 cm.

Table 5.2. Summary of bulk and authigenic U concentrations and $\delta^{238}U$ in anoxic sediments.

Sample	Depth	U	$\delta^{234}U$	$\delta^{238}U$	U/Al	f_{auth}	$f_{detrital}$	f_{carb}	U_{auth}	$\delta^{238}U_{auth}$
	cm	Ppm	‰	‰	ppm/wt%	%	%	%	ppm	‰
LS01	0.25	1.75	571	–0.32	3.0	79	11	9	1.39	–0.30
LS03	2.25	1.83	579	–0.38	3.2	81	11	8	1.49	–0.37
LS05	4.25	1.91	637	–0.30	4.7	83	7	10	1.58	–0.27
LS07	6.25	1.69	529	–0.43	3.0	79	10	11	1.33	–0.43
LS09	8.25	2.74	591	–0.31	7.6	89	4	7	2.43	–0.29
LS11	10.5	2.25	521	–0.23	2.9	80	11	8	1.81	–0.19
LS13	14.5	2.11	495	–0.32	3.2	80	10	9	1.69	–0.30
LS15	18.5	2.03	539	–0.38	2.5	77	14	9	1.57	–0.37
LS17	22.5	3.22	640	–0.64	4.4	87	8	6	2.79	–0.68
LS19	26.5	1.92	680	–0.43	7.3	86	5	9	1.66	–0.43
LS21	32	4.66	683	–0.33	11.0	95	0	4	4.45	–0.32
LS23	40	2.61	705	–0.28	10.6	92	0	7	2.41	–0.26

Note: f_{auth}, $f_{detrital}$ and f_{carb} are authigenic, detrital and carbonate fractions of U.

Similar to the analysis of sinking particles described above, the contribution of U from detrital and carbonate fractions can be corrected to calculate the value of authigenic $\delta^{238}U$ in anoxic carbonate sediments in FGL (Table 5.2, Figure 5.6). Authigenic U accounts for about 77–93 % of the bulk U in anoxic carbonate sediments of FGL. Above 18.5 cm, U from both detrital and carbonate fractions was about 10 % of the bulk U. Below this depth, the detrital U fraction

decreased significantly to 0.3 %, while the carbonate U fraction decreased to about 4 %. Because of low U contributions from the detrital and carbonate fractions, $\delta^{238}U$ values in the bulk sediments and the authigenic fraction were statistically indistinguishable.

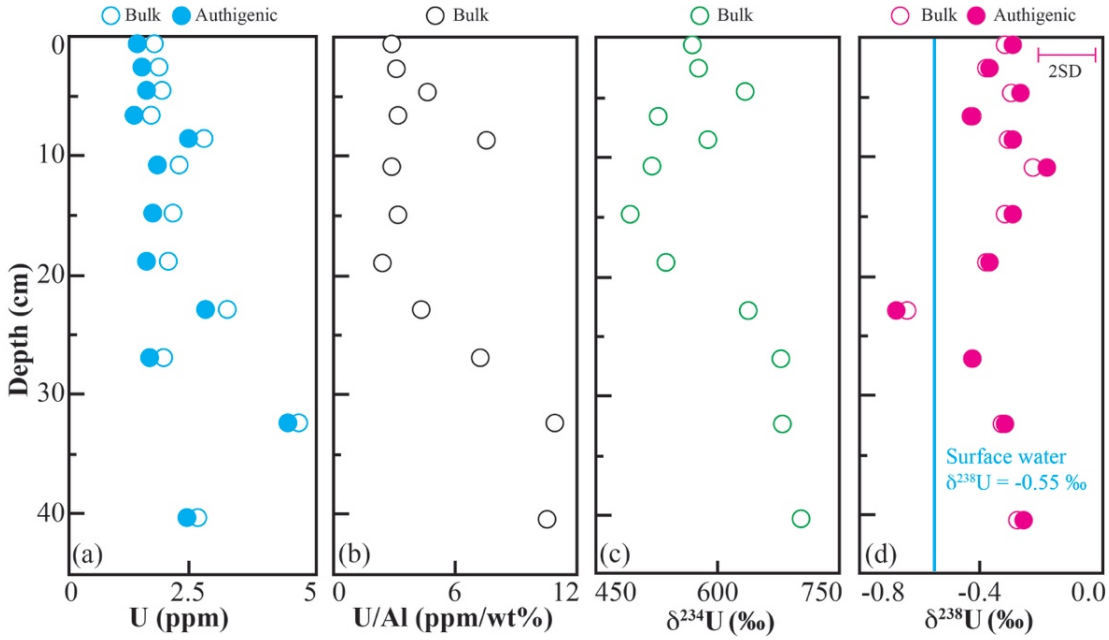

Figure 5.6. Depth profile of U concentration (a), U/Al (b), $\delta^{234}U$ (c), and $\delta^{238}U$ (d) in anoxic sediments of FGL. Open and close symbols represent bulk and authigenic values, respectively. The vertical blue line in panel (d) is the $\delta^{238}U$ value of surface water in FGL.

5.5 Discussion

To elucidate the U isotopic systematics in FGL, the U isotopic mass balance to characterize the U sources and sinks in the whole lake was first performed. Applying U isotopic mass balance, the fluxes of authigenic U in sinking particles and in anoxic carbonate sediments were estimated to evaluate their roles in drawing down the dissolved U concentration and affecting $\delta^{238}U$ in the anoxic water column. Then, the effects of anoxic depositional

environments on $\delta^{238}U$ in carbonate sediments and their implications for $\delta^{238}U$ in anoxic carbonate sediments as a paleoredox proxy were assessed.

5.5.1 U Isotopic Mass Balance in FGL

To determine the overall U isotope mass balance for FGL, the water mass balance developed by Brunskill et al. (1968) and Takahashi et al. (1968) was adopted. FGL is recharged by surface inlet (IN) from the Round Lake, precipitation (P), and groundwater (GW), and discharges via surface outlet (OUT) and evaporation (E) (Thompson et al., 1990; Torgersen et al., 1981). The water mass balance for FGL can be described as:

$$Q_{IN} + Q_P + Q_{GW} = Q_{OUT} + Q_E \quad \text{Eq. 5.9}$$

where Q_i is the water flux from i (Table 5.3; Brunskill et al., 1968; Takahashi et al., 1968).

Table 5.3. Summary of water and U isotopic mass balance in FGL.

	Inputs			**Outputs**		
	Inlet	Precipitation	Groundwater	Outlet	Evaporation	Sediments
Q (10^6 m^3 yr^{-1})	0.85	0.23	1.11	2.07	0.12	–
U (nM)	7.60	0.17	12.84	9.58	0	–
F (mol yr^{-1})	6.46	0.04	14.25	19.83	0	0.92
$\delta^{238}U$ (‰)	–0.55	–0.30	–0.57	–0.57	–	–0.34

Note: water fluxes, U concentrations, and $\delta^{238}U$ in all inputs and outputs were measured except the groundwater.

As for U mass balance, there are three U sources from surface inlet, precipitation and groundwater, and two U sinks into surface outlet and sediments (S) in FGL. Consequently, the U mass balance in FGL is written as:

$$F_I + F_P + F_G = F_O + F_{S1} + F_{S2} \quad \text{Eq. 5.10}$$

where F_i ($=Q_i \times U_i$) and U_i are the dissolved U flux and concentration from each term i (Table 3). The water fluxes and U concentrations from all these U sources and sinks were measured except

the groundwater. U concentrations in the surface inlet (7.6 nM) and outlet (9.58 nM) were measured on July 2015. U concentration in precipitation is assumed to be ~0.17 nM (e.g., Muramatsu et al., 1994). F_{S1} and F_{S2} represent U fluxes removed into sediments above and below the chemocline.

Above the chemocline (21 m), U is conservative under oxic conditions (e.g., Langmuir, 1978). Thus, all sedimentary U is assumed to come from the sinking particles in the water column. The U flux (F_{S1}) into sediments above the chemocline is estimated using the equation:

$$F_{S1} = R_{SP} \times U_{SP} \times (A_0 - A) \quad \text{Eq. 5.11}$$

where R_{SP} (=336 g m^{-2} yr^{-1}) and U_{SP} (=0.59 ppm) are sedimentation rate and U concentration in sinking particles above 21 m, and A_0 (= 0.26 $\times 10^6$ m^2) and A (0.15 $\times 10^6$ m^2) are surface areas of FGL at 0 and 21 m. In this study, sediment trap data at 13.5 m was used to represent sedimentation rate and U concentration in sinking particles above the chemocline. Placing these parameters into Eq. 11, U flux into sediments above the chemical is estimated to be 0.09 mol yr^{-1}.

Below the chemocline, significant authigenic U accumulation occurs below the sediment-water-interface with minor contributions from sinking particles (e.g., Anderson et al., 1989). Thus, U flux (F_{S2}) into sediments below the chemocline is estimated using the equation:

$$F_{S2} = MAR \times U_{SD2} \times A \quad \text{Eq. 5.12}$$

where MAR and U_{S2} are mass accumulation rate of sediment in units of g m^{-2} yr^{-1} and U concentration (~ 2 ppm) in the anoxic sediment in FGL. MAR can be estimated using the equation:

$$MAR = LSR \times \rho \quad \text{Eq. 5.13}$$

where ρ and LSR are the dry density of sediments (= 1.00 g ml^{-1}) and the sedimentation rate of sediments (0.7 mm/year; Hilfinger IV et al., 2001). Placing these values into equations 5.12 and 5.13, F_{S2} and MAR are 0.88 mol yr^{-1} and 700 g m^{-2} yr^{-1}, respectively.

With U fluxes in sediments above and below the chemocline, the U flux (F_G) and concentration (U_G) in groundwater are estimated as:

$$F_G = F_O + F_S - F_I - F_P \quad \text{Eq. 5.14}$$

$$U_G = \frac{F_G}{Q_G} \quad \text{Eq. 5.15}$$

The U isotopic mass balance in FGL can be described as:

$$F_I\delta^{238}U_I + F_P\delta^{238}U_P + F_G\delta^{238}U_G = F_O\delta^{238}U_O + F_{S1}\delta^{238}U_{S1} + F_{S2}\delta^{238}U_{S2} \quad \text{Eq. 5.16}$$

where $\delta^{238}U_i$ is U isotopic composition in term i. $\delta^{238}U_{S1}$ (= –0.48 ‰) and $\delta^{238}U_{S2}$ (= –0.35 ‰) are U isotopic compositions in sediments above and below the chemocline of FGL. Thus, the U isotopic composition in groundwater is calculated as:

$$\delta^{238}U_G = \frac{F_O\delta^{238}U_O + F_{S1}\delta^{238}U_{S1} + F_{S2}\delta^{238}U_{S2} - F_I\delta^{238}U_I - F_P\delta^{238}U_P}{F_G} \quad \text{Eq. 5.17}$$

Combining Eq. 9, 14, 15, and 17, the inferred water flux, U concentration, and $\delta^{238}U$ in groundwater were 1.11×10^6 m^3 yr^{-1}, 12.84 nM, and –0.57 ‰.

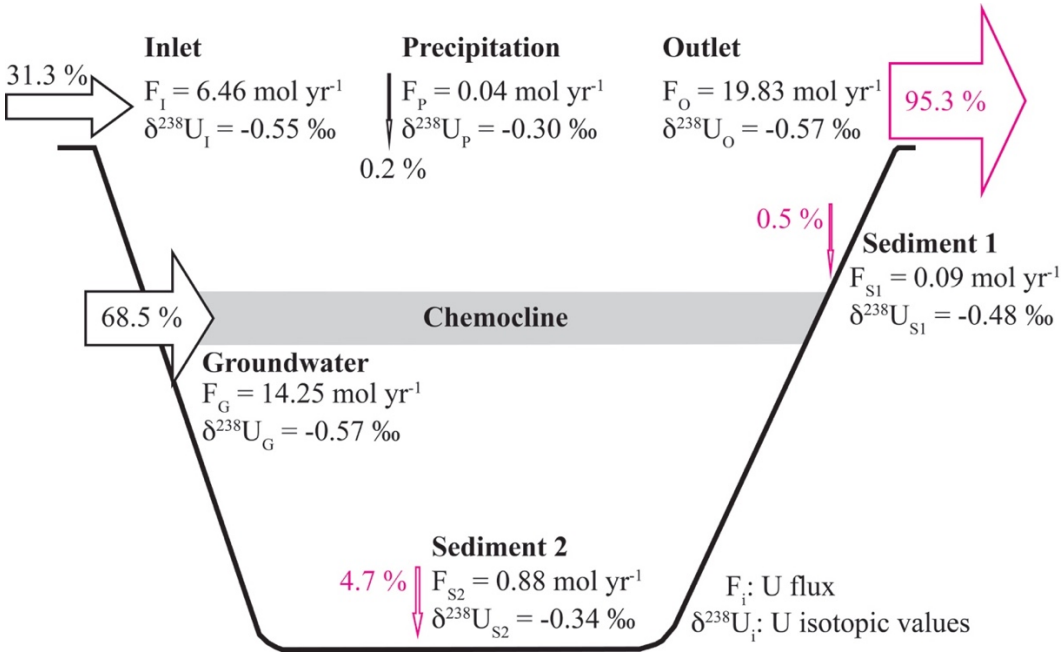

Figure 5.7. Water and U isotopic mass balance in FGL. The gray horizontal band represents the chemocline. The widths of the arrows are proportional to the U fluxes. The black and red arrows represent inputs and outputs of U in FGL, respectively.

The U isotopic mass balance in FGL reveals that groundwater contributes about 69 % of U to the total U source into FGL with a $\delta^{238}U$ value similar to the surface inlet (–0.55 ‰) and outlet (–0.57 ‰). Most of the U in FGL discharges through the surface outlet (95.3 %) with only minor fractions removed by sediments above (0.5 %) and below (4.2 %) the chemocline.

5.5.2 U Isotope Fractionation in the Water Column

5.5.2.1 Particulate U

Previous studies of U geochemistry in Fayetteville Green Lake and modern anoxic basins such as the Black Sea concluded that there was negligible removal of U to authigenic particles via reduction of U(VI) to U(IV) in the anoxic water column (Anderson et al., 1982; Anderson, 1984; Anderson et al., 1989a; Barnes and Cochran, 1990; Klinkhammer and Palmer, 1991). This conclusion was based on the invariant particulate authigenic U fluxes throughout redox-stratified

water column (e.g., Anderson, 1984; Anderson et al., 1989a). In contrast, sediment trap data from FGL suggest U(VI) to U(IV) in the anoxic water column (Table 5.1).

The combination of increasing particulate $\delta^{238}U_{auth}$ (from –0.44 to –0.16 ‰) and decreasing particulate authigenic U fluxes below the chemocline of FGL result from the combined effects of authigenic reduction of U(VI) to U(IV), and remineralization of particulate organic matter (POM) in the anoxic water column (Figure 5.8). Only U(VI) reduction and calcium carbonate coprecipitation processes have been demonstrated to be able to preferentially enrich ^{238}U in the reaction products (e.g., Stylo et al., 2015; Brown et al., 2018; Chen et al., 2016, 2018a). But the anoxic water column of FGL is undersaturated with respect to calcite (Brunskill, 1969; Takahashi et al. 1968; Havig et al., 2015). Consequently, the elevation in particulate $\delta^{238}U_{auth}$ in FGL is attributed to authigenic U reduction in the anoxic water column.

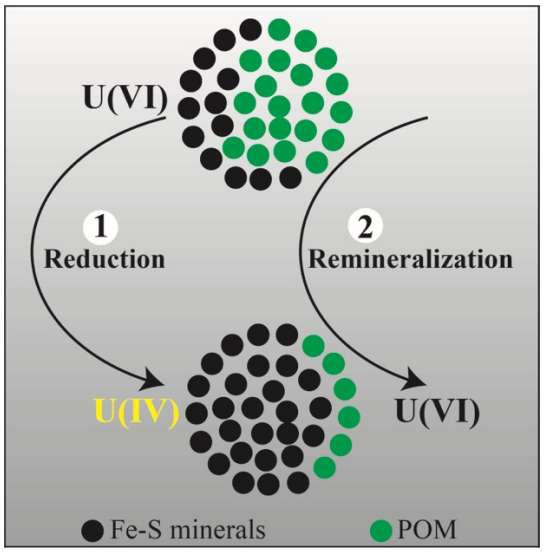

Figure 5.8. A conceptual model of variations in particulate U_{auth} fluxes and $\delta^{238}U_{auth}$ due to U reduction and remineralization of particulate organic matter (POM) in the anoxic water column. As particles settle down in the anoxic water column, the sinking particles will be richer in pyrite and poorer POM. As these processes happen, more U(IV) ends up in the sinking particles with pyrite while U(VI) is released from the POM which is being remineralized.

The formation of syngenetic iron sulfide minerals such as pyrite and the presence of sulfate-reducing bacteria in the anoxic water column of FGL suggest that authigenic abiotic and biotic U reduction on the sinking particles are possible (Suit and Wilkin, 1990; Zerkel et al., 2010; Havig et al., 2018; Thompson et al., 1990). Experimental studies demonstrated that U reduction by FeS and sulfate-reducing bacteria preferentially accumulated heavy U isotopes in the reducing insoluble product U(IV), with an isotope fractionation of up to ~1.0 ‰ (Brown et al., 2018; Basu et al., 2014; Stirling et al., 2015; Sytlo et al., 2015). As a result, authigenic U reduction can easily shift $\delta^{238}U$ values of authigenic U in sinking particles from –0.44 to –0.16 ‰. But these reduction processes should also increase the authigenic U concentration in sinking particles, inconsistent with the decreasing authigenic U flux observed in the anoxic water column

of FGL. This inconsistency suggests that some geochemical process must release particulate U back into the water column.

Potentially, the process responsible for the release of particulate U to the water column is remineralization of POM. The significant decrease in the particulate organic carbon (POC) concentration from 8 to <1 mg/L (Fulton et al., 2018), and TOC flux (from 23 to 10 g m^{-2} yr^{-1}, this study) in the anoxic water column of FGL suggest strong remineralization of POM. It has been demonstrated that U abundances show a good positive correlation with total organic carbon (TOC) in anoxic sedimentary rocks, in recent sediments and sinking particles in oceans (e.g., Choumiline et al., 2017; Tribovillard et al., 2006). Similarly, my sediment trap data showed covariation of the authigenic U flux with the TOC flux in the sinking particles. Thus, remineralization of POM could release the U associated with organic matter back into the anoxic water column in FGL, decreasing particulate U_{auth} in sinking particles.

5.5.2.2 Dissolved U

The depletion in dissolved U concentration and $\delta^{238}U$ below the chemocline in FGL result from U reduction in the anoxic water column and anoxic carbonate sediments. As discussed above, the more positive particulate $\delta^{238}U_{auth}$ values (–0.44 to –0.16 ‰) below the chemocline suggest that ^{238}U is preferentially removed from the water column, contributing to the depletions in $\delta^{238}U$ values of dissolved U in the anoxic water column. However, sinking particles below the chemocline might release part of the U associated with POM back into the anoxic water column.

Another important process that typically draws down dissolved U concentration and $\delta^{238}U$ in modern anoxic basins is authigenic reduction of U below the sediment-water interface under anoxic conditions (Romaniello et al., 2012; Andersen et al., 2014; Holmden et al., 2015; Noordman et al., 2015; Rolison et al., 2017; Bura-Nakić et al., 2018). The diffusion of dissolved U(VI) from the overlying water column into the anoxic sediments and subsequent reduction to insoluble U(IV), which preferentially enriches ^{238}U in sediments, could effectively reduce the dissolved U concentration and $\delta^{238}U$ below the chemocline (Anderson, 1984; Anderson et al., 1989a, b; Barnes and Cochran, 1990; Klinkhammer and Palmer, 1991). Therefore, the significant enrichment of U in authigenic anoxic sediments (enrichment factors 4–21), and the more positive values of $\delta^{238}U_{auth}$ in the anoxic sediment (–0.30 ‰) vs. the surface water (–0.55 ‰) of FGL are consistent with observed water profile of dissolved U concentration and $\delta^{238}U$ in the anoxic water column.

To quantitatively assess the contributions of those two authigenic U reduction processes to the water profile of dissolved U concentration and $\delta^{238}U$ below the chemocline, the annual authigenic U flux in the sinking particles of the deepest sediment trap (45.5 m) was compared with that in the anoxic carbonate sediments. The annual particulate authigenic U flux (S_{PA}) at 45.5 m is calculated as:

$$S_{PA} = \frac{AF \times U_{auth}}{M_U} \qquad \text{Eq. 5.18}$$

where AF is the annual total mass flux (331 g m^{-2} yr^{-1}, Table 5.1) of sinking particles, U_{auth} is the authigenic U concentration in the bulk sinking partiles (0.32 ppm), and M_U is the molecular weight of U (238.029 g mol^{-1}). Substituting these values into equation 5.18, AF_{PA} at 45.5 m is 0.45 μmol m^{-2} yr^{-1}.

The annual authigenic U flux (AF_{anox}) in the anoxic carbonate sediments is estimated using the equation:

$$AF_{anox} = \frac{MAR \times U_{anox-auth}}{M_U} \quad \text{Eq. 5.19}$$

where MAR is the annual mass accumulation rate of sediments (700 g m^{-2} yr^{-1}, see Supplement material), and $U_{anox\text{-}auth}$ (~2 ppm) is the authigenic U concentration in anoxic carbonate sediments. Substituting these parameters into equation 5.19, AF_{anox} is 5.88 μmol m^{-2} yr^{-1}. Thus, sinking particles in FGL contributes about 7.7 % of U to the anoxic carbonate sediments, which predominantly control the shape of the water profile of dissolved U concentration and $\delta^{238}U$ below the chemocline as observed in other modern anoxic basins such as the Black Sea (Noordmann et al., 2015; Holmden et al., 2015; Bura-Nakic et al., 2017; Rolison et al., 2017).

However, the fraction of particulate authigenic U to anoxic sediments is significantly larger than in the Black Sea (<1 %) but smaller than Saanich Inlet (~45 %; Anderson et al., 1982; Anderson et al., 1989a, b). The variations in the fractions of particulate authigenic U to anoxic sediments of these anoxic basins/lake might result from their differences in TOC fluxes below the chemocline. Specifically, the TOC fluxes in the anoxic water column of the Black Sea (10–30 mg m^{-2} day^{-1}), FGL (60–135 mg m^{-2} day^{-1}, this study), and Saanich Inlet (93–222 mg m^{-2} day^{-1}) increased (Andersen et al., 1989a, b). Because of the strong positive correlation of U abundance with TOC, it would be expected that the elevation in TOC flux would increase the contribution of particulate U to anoxic sediments.

5.5.3 $\delta^{238}U$ in Anoxic Carbonates and Its Implications for Use as a Paleoredox Proxy

The high content (70–90 weight %) of calcium carbonate in anoxic sediments of the meromictic FGL offers an excellent modern analogue to study the effects of anoxic depositional environments on $\delta^{238}U$ in carbonate sediments. To calculate U isotopic composition in anoxic carbonate sediments ($\delta^{238}U_{anox\text{-}carb}$), the U contributed by the detrital fraction is exclude using the equation:

$$\delta^{238}U_{anox-carb} = \frac{\delta^{238}U_{sample} - f_{detrital} \times \delta^{238}U_{detrial}}{1 - f_{detrital}} \quad \text{Eq. 5.20}$$

According to equation 5.20, $\delta^{238}U$ in anoxic carbonate sediments of FGL was displayed in Figure 5.9. Compared to the U concentration in surface water carbonates (~0.26 ppm) in FGL, anoxic carbonate sediments were significantly enriched in U by 1.33–4.45 ppm due to authigenic U reduction in the water column and anoxic sediments. Consistent with significant authigenic accumulation of isotopically heavy U(IV), $\delta^{238}U_{anox\text{-}carb}$ values in anoxic carbonate sediments of FGL were more positive than the surface water (–0.55 ‰) by about 0.20±0.12 ‰ (1 SD). The relatively small U isotope offset (~0.2 ‰) between anoxic carbonate sediments and surface water in FGL results from diffusion of dissolved U(VI) in the overlying water column with significantly lighter $\delta^{238}U$ (–0.96 ‰) than the surface water (–0.55 ‰) into pore waters of anoxic sediments for subsequent U reduction and precipitation.

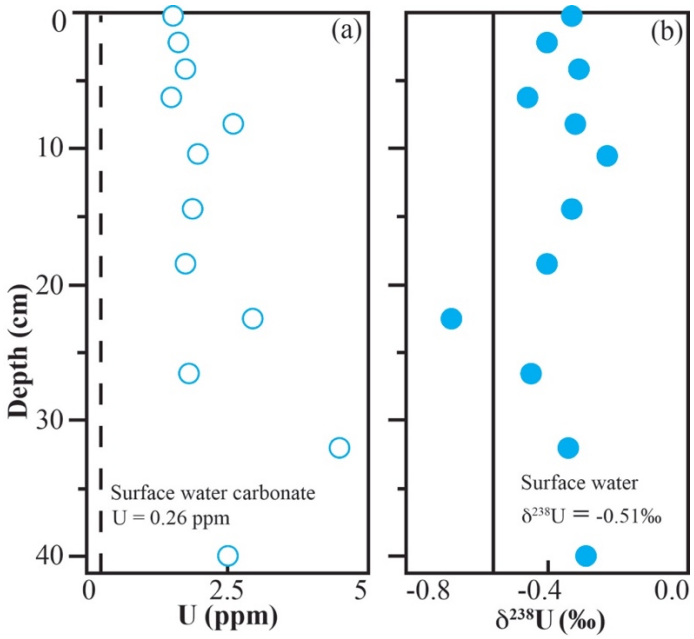

Figure 5.9. U concentration (a) and $\delta^{238}U$ (b) in surface water carbonates (dashed and solid lines) and anoxic carbonate sediments (circles) in FGL.

The U isotope fractionation in carbonate sediments due to anoxic depositional conditions (0.20±0.12 ‰, 1 SD) in the redox-stratified lake of FGL is slightly smaller than that induced by diagenesis (0.27±0.14 ‰, 1 SD) in modern shallow-water carbonate sediments of the Bahamas (*p*-value of Mann-Whitney test is 0.04; Chen et al., 2018b; Tissot et al., 2018). Similar to the U isotope fractionation induced by carbonate diagenesis in modern carbonate sediments, the significant enrichment of U (Figure 5.9a) and higher $\delta^{238}U$ values (Figure 5.9b) in anoxic carbonate sediments relative to surface water carbonates in FGL would also affect the inferred extent of oceanic anoxia (Chen et al., 2018b). The $\delta^{238}U$ data of the oceanic anoxia over the late Permian Mass Extinction (LPME) event was taken as an example to estimate the offset in the inferred oceanic anoxia using the U isotopic mass balance (equation 5.1) with and without correction to the U isotope fractionation observed between anoxic carbonate sediments and surface water carbonates (~0.16 ‰) in FGL.

Compiling all the published $\delta^{238}U$ data over the LPME, an average $\delta^{238}U$ value of –0.56 ‰ was obtained for seven carbonates sections of different localities over the world (Brennecka et al., 2011a; Lau et al., 2016; Elrick et al., 2017; Zhang et al., 2018a, b). According to equation 5.1, the fraction of U by anoxic sediments is estimated by

$$f_{\text{anoxic}} = \frac{(\delta^{238}\text{U}_{\text{river}} - \delta^{238}\text{U}_{\text{seawater}}) - \Delta^{238}\text{U}_{\text{other}}}{\Delta^{238}\text{U}_{\text{anoxic}} - \Delta^{238}\text{U}_{\text{other}}} \qquad \text{Eq. 5.21}$$

where $\delta^{238}U_{river}$ (= –0.30 ‰), $\Delta^{238}U_{anoxic}$ (= 0.60 ‰) and $\Delta^{238}U_{other}$ (= 0.03 ‰) were defined in previous studies (e.g., Andersen et al., 2016). If anoxic carbonate sediments accurately reflect $\delta^{238}U$ values in surface water carbonates, the estimated f_{anoxic} would be 0.40. However, if a U isotope fractionation (0.20 ‰) between anoxic carbonate sediments and surface water carbonates similar to that observed in FGL is considered, the predicted f_{anoxic} would be 0.75. The dramatic increase in the extent of oceanic anoxia suggests that the isotopic offset between anoxic carbonate sediments and surface water carbonates should be considered for further application of $\delta^{238}U$ in anoxic carbonate sediments to reconstruct redox conditions of redox-stratified ancient oceans.

5.6 Conclusions

U isotope geochemistry in FGL is predominantly controlled by U(VI) reduction below the sediment-water interface, consistent with other modern anoxic basins. This study examined variations of $^{238}U/^{235}U$ in both dissolved and particulate U across the chemocline, quantitatively assessed the contributions of authigenic U reduction in the water column and anoxic carbonate sediments, and evaluated the effect of anoxic deposition conditions on $^{238}U/^{235}U$ values in carbonate sediments. The main conclusions are summarized as follows:

- U isotopic mass balance showed that U predominantly came from groundwater (69 %) and surface inlet (31 %), and was removed by the surface outlet (95.3 %) and sediments (4.7 %). $\delta^{238}U$ values in all these U sources and sinks were indistinguishable within the $^{238}U/^{235}U$ measurement uncertainty of ~ –0.55 ‰, with the exception of the anoxic sediments (–0.35 ‰).
- Particulate $\delta^{238}U_{auth}$ in sediment trap samples demonstrated authigenic U reduction in the anoxic water column of FGL, in disagreement with the previous studies finding that authigenic U reduction below the sediment-water interface was the only process of U removal in FGL and anoxic basins. The authigenic U reduction in the anoxic water column accounted for 7.7 % of the total authigenic U in anoxic sediments. Consequently, authigenic U reduction in the water column and below the sediment-water interface drew down the dissolved U concentration and $\delta^{238}U$ below the chemocline of FGL.
- The progressive increase in particulate $\delta^{238}U_{auth}$ coupled with a decrease in particulate authigenic U flux below the chemocline is best explained as resulting from two processes operating in parallel: authigenic U reduction in the water column and remineralization of POM. The authigenic U reduction would elevate particulate authigenic $\delta^{238}U$ and the U flux, while remineralization of POM would release U associated with organic matter, reducing the particulate U flux below the chemocline.
- Carbonates deposited under anoxic conditions would also cause an isotopic offset of 0.20±0.12 ‰ (1 SD) relative to surface water in FGL. The isotopic offset due to anoxic depositional conditions should be corrected for future applications of $\delta^{238}U$ in anoxic carbonate sediments as a paleoredox proxy.

CHAPTER 6

SUMMARIES, CONCLUSIONS, AND FUTURE DIRECTIONS

6.1 Summaries and Conclusions

This dissertation provides a comprehensive understanding on the variations of $\delta^{238}U$ in synthetic and natural calcium carbonate precipitates, and guidelines to calibrate $\delta^{238}U$ in ancient carbonates as a paleoredox proxy to reconstruct oceanic anoxia through time. I systematically examined the fidelity of $^{238}U/^{235}U$ in sedimentary carbonate rocks as a paleoredox proxy in three ways: (1) variations of $\delta^{238}U$ in primary abiotic and biogenic carbonates; (2) diagenetic effects on alterations of $\delta^{238}U$ in primary carbonates; (3) U isotopic systematics in a redox-stratified lake and its effect on $\delta^{238}U$ in organic-rich anoxic carbonates.

Chapter 2 explored the effects of the secular variations in seawater chemistry on the U isotope fractionation in primary abiotic calcium carbonates over the Phanerozoic. The former was based on the experimental results that U isotope fractionation during U(VI) incorporation into abiotic calcium carbonates depends on aqueous U speciation (Chen et al., 2016). The speciation-dependent U isotope fractionation model predicted an isotope fractionation of 0.10–0.23 ‰ between primary abiotic carbonates and seawater due to secular variations in seawater chemistry (pH, pCO_2, alkalinity, ionic strength, and Ca^{2+} and Mg^{2+} concentrations) over the Phanerozoic. The U isotopic offset during U incorporation into calcium carbonates could significantly affect estimation of the extent of marine anoxia.

Chapter 3 investigated whether primary biogenic carbonate fractionate U isotopes in the same way as abiotic calcium carbonate. I developed a high-precision $^{238}U/^{235}U$ method (±0.02

‰, 2SD) to determine $\delta^{238}U$ in primary biogenic carbonates including scleractinian corals, calcareous green and red algae, echinoderms, and mollusks from the Bahamas, Gulf of California, and French Polynesia. Primary biogenic carbonates fractionate U isotopes in the same direction as abiotic calcium carbonates, but with a variable and smaller U isotope fractionation (0.00–0.09 ‰) than that predicted by abiotic calcium carbonate coprecipitation experiments (~0.10 ‰; Chen et al., 2016, 2017). I proposed two conceptual models to interpret the variable U isotope fractionation in primary biogenic carbonates. One is the semi-restricted equilibrium isotope fractionation model, which hypothesizes that U isotope fractionation during U uptake by primary biogenic carbonates is similar to abiotic calcium carbonates, but the magnitude of the U isotope fractionation in primary biogenic carbonates depends on the extent of the isolation of the calcification sites from ambient seawater. For example, the rapid calcium carbonate precipitation rate at the local calcification sites, which is isolated from ambient seawater, in corals would result in almost 100 % incorporation of U into coral skeleton, and thus, similar $\delta^{238}U$ values in corals and seawater. This is consistent with the observed results (Chen et al., 2018a). Another model assumes that U isotope fractionation in primary biogenic carbonates is controlled by differences in kinetic/disequilibrium isotopic effects resulting from differences in calcium carbonate growth rates. Specifically, U isotope fractionation in primary biogenic carbonates appeared to decrease with the carbonate precipitate growth rates. The possible interpretation for this observation is that at slower carbonate growth rates, aqueous U species is more selectively incorporated into carbonate lattice resulting in the preferential incorporation of isotopically heavy U species, while at higher carbonate growth rates, U is less selectively incorporated into $CaCO_3$. The small but significant U isotope fractionation in primary biogenic calcium carbonates

is also important for $\delta^{238}U$ in marine carbonates as a paleoredox proxy. For example, an isotope fractionation of 0.10 ‰ between calcium carbonates and seawater corresponds to an offset of 18 % in the inferred extent of oceanic anoxia (Chen et al., 2017). Thus, this U isotopic offset should be corrected for applications of $\delta^{238}U$ in well-preserved primary calcium carbonates to reconstruct oceanic anoxia.

Chapter 4 examined the effects of carbonate diagenesis on U isotope fractionation in modern shallow-water carbonate sediments on the Bahamas platform margin and slope. These carbonate sediments showed an average U isotopic offset ($^{238}U/^{235}U$) of 0.27±0.14 ‰ (1 SD) relative to modern seawater. The banktop and slope sediments shared an identical distribution of $\delta^{238}U$ values, suggesting that $\delta^{238}U$ is altered primarily through syndepositional diagenesis in shallow banktop sediments, which is then transported to deeper water sediments with little alterations of $\delta^{238}U$ after subsequent sediment burial. Meteoric vadose diagenesis caused significantly larger U isotope fractionation than meteoric phreatic and phreatic marine diagenesis. The more extreme diagenetic effects during meteoric vadose diagenesis might result from the open-system behavior of U(VI) in oxic vadose zone. This finding suggests that ancient sedimentary carbonates should be thoroughly scrutinized for meteoric diagenesis.

The carbonate diagenesis affecting the variations of $\delta^{238}U$ values in carbonate sediments of the Bahamas likely results from two processes: (1) aqueous U speciation-dependent isotope fractionation during abiotic calcium carbonate precipitation, leading to a uniform minimum positive shift in carbonate sediments during recrystallization of biogenic carbonate fragments and/or cementation (Chen et al., 2016, 2017); (2) authigenic U reduction in anoxic pore water, preferentially accumulating ^{238}U in carbonate sediments. Statistical analyses displayed no

correlations in $\delta^{238}U$ with common geochemical indicators ($\delta^{13}C$, $\delta^{18}O$, Mg/Ca ratios, U and Sr concentrations, Mn/Sr ratios, and redox-sensitive trace metal concentrations) for carbonate diagenesis. The stochastic variation of $\delta^{238}U$ in shallow-water carbonates sediment from the Bahamas suggests that high-resolution data profile of $\delta^{238}U$ in multiple synchronous sedimentary carbonate sections at different localities should be used to faithfully identify global shifts in marine $\delta^{238}U$ rather than the effects of diagenetically-induced noise.

Chapter 5 investigated the effects of anoxic depositional environments on $\delta^{238}U$ values in carbonate sediments of a permanently redox-stratified alkaline lake—Fayetteville Green Lake (FGL), New York, USA—where calcium carbonates precipitate in the oxic surface water but deposit under anoxic conditions. U concentration and isotopic compositions of various U sources and sinks, water column, and sinking particles were measured to perform U isotopic mass balance and characterize U isotope fractionation across the chemocline of FGL.

Dissolved U concentration (from 10 to 3 nM) and $\delta^{238}U$ (from –0.50 to –0.96 ‰) decreased significantly with depth in the anoxic water column of FGL. Parallel with these depletions, authigenic $\delta^{238}U$ in the sinking particles became progressively more postivie from –0.44 to –0.16 ‰. Authigenic $\delta^{238}U$ in the anoxic carbonate sediments was about 0.2 ‰ higher than the surface water of FGL. U isotopic mass balance showed that U in FGL was predominantly recharged by surface inlet (31 %) and groundwater (69 %), and removed by surface outlet (95 %) and sediments (5 %). $\delta^{238}U$ values in U sources and sinks were statistically indistinguishable at about –0.55 ‰ except the anoxic carbonate sediments (–0.35±0.12 ‰, 1 SD).

The increase of particulate authigenic $\delta^{238}U$ but decrease in particulate U flux with depth below the chemocline of FGL result from authigenic U reduction in the water column by Fe-S minerals (e.g., pyrite) and sulfate-reducing bacteria, and remineralization of particulate organic matter (POM). Authigenic U reduction would preferentially enrich ^{238}U and accumulate U, while remineralization of POM could release authigenic U associated with POM back into the water column. The smaller fraction of particulate authigenic U flux in the sinking particles (0.45 μmol m^{-2} yr^{-1}) relative to the anoxic carbonate sediments (5.88 μmol m^{-2} yr^{-1}) suggests that authigenic U reduction is the predominant factor that draw down dissolved U concentration and $\delta^{238}U$ in FGL.

The higher $\delta^{238}U$ values (–0.35±0.12 ‰, 1 SD) and U concentration (2–5 ppm) in anoxic carbonate sediments relative to the surface water carbonates (–0.51 ‰ and 0.26 ppm) demonstrated anoxic depositional environments could significantly enrich U and elevate $\delta^{238}U$ values, leading to significant offsets in the inferred oceanic anoxia as observed in carbonate diagenesis. Thus, future applications of $\delta^{238}U$ in carbonate sediments deposit under anoxic conditions to reconstruct oceanic anoxia should also be corrected.

Although this dissertation systematically examined the limitations $\delta^{238}U$ in marine carbonate sediments as a robust paleoredox proxy, there are questions that remain unknown: (1) what controls the variability of the U isotope fractionation of 0–0.68 ‰ in carbonate sediments from the Bahamas? (2) what causes the variation in the U isotope fractionation factors during U(VI) reduction in biotic and abiotic experiments, and modern environments.

6.2 Future Directions

To further test the fidelity of $\delta^{238}U$ in sedimentary rocks as a proxy to reconstruct oceanic anoxia and understand U isotope geochemistry in nature, future work should be done to: (1) develop an optimal leaching protocol to extract carbonate fraction U from carbonate sediments with varying non-carbonate fractions; (2) study U isotope fractionation in carbonate sediments from different depositional and diagenetic environments; (3) examine the mechanisms of U isotope fractionation during U reductions by laboratory experiments and field studies.

First, it is urgent to develop a robust leaching protocol to extract U from the carbonate fraction, minimizing the effects of U from non-carbonate fractions (e.g., phosphates, Fe-Mn oxides, clay minerals, organic matter). Current studies examined the effects of different molarities of hydrochloric acid, nitric acid, and acetic acid on the sequential leaching of U from carbonate sediments (Lau et al., 2016; Zhang et al., 2018a; Tissot et al., 2015; Dahl et al., 2017). Lau et al. (2016) and Zhang et al. (2018a) found that $\delta^{238}U$ values in bulk carbonate sediments did not depend on the molarities of different acids. Step-leaching of sedimentary carbonates and modern fossil corals using acetic acid showed that $\delta^{238}U$ values in the initial (<30 % of carbonate dissolution) and last (>70 % of carbonate dissolution) leachates were different by up to 0.50 ‰ relative to the central cut (Zhang et al., 2018a; Tissot et al., 2018). The central cut of $\delta^{238}U$ was suggested to represent carbonate fraction $\delta^{238}U$, which was similar to $\delta^{238}U$ of the bulk carbonate sediments (Tissot et al., 2018). All these sequential leaching experiments examined carbonate sediments (e. g., fossil corals, limestone, dolomite) of almost pure calcium carbonates (>95 wt%) with a relatively high U concentration of ~3 ppm. This suggests that the non-carbonate fractions in these carbonate samples only hold a very tiny fraction of U, which would not be able to

significantly change $\delta^{238}U$ values of the bulk carbonates even if all the U in these fractions were released during acid leaching.

However, in sedimentary carbonate rocks that have lower fractions of calcium carbonate, the non-carbonate fraction (e.g., clay minerals, organic matter, phosphates, Fe-Mn oxides) can affect $\delta^{238}U$ values in the extracted carbonate fraction during acid leaching. For example, deep-sea carbonate sediments are composed of calcium carbonate precipitates (e.g., foraminiferal calcite) with a very low U concentration of ~0.025 ppm, and detrital components with significantly higher U concentration of ~1.1 ppm (Delaney and Boyle, 1983; Russell et al., 1994; McLennan, 2001). Another example is the anoxic organic-rich carbonate sediments formed in the permanently redox-stratified Fayetteville Green Lake, New York. These carbonate sediments consist of 80 wt % of calcium carbonates by weight percentage and 4 wt % of organic matter. The non-carbonate fraction accounted for more than 90 % of the total U in the bulk sediments with significantly higher $\delta^{238}U$ values than the carbonate fraction U. Obviously, acidic leaching of these carbonate sediments under oxic conditions could easily oxidize the isotopically heavy U(IV) in the non-carbonate fractions and shift $\delta^{238}U$ values in the leachates to be more positive than that in the carbonate fraction. Seafloor phosphorites have varying $\delta^{238}U$ vales ranging from –0.42 to –0.85 ‰ and very high U concentrations (65–328 ppm; Kolodny et al., 2017). Leaching of phosphate-rich black shales using dilute HCl and pH-buffered 10 % acetic acid could release significant amount of phosphate-associated U (70 and 30 %; Dahl et al., 2017). Thus, current leaching methods would not work for phosphate-rich carbonate sediments. The presence of Mn-oxides, which preferentially adsorbed ^{235}U, in carbonate sediments was suggested to shift $\delta^{238}U$ values to be lighter than seawater (Herrmann et al., 2018; Brennecka et al., 2011b). In summary,

further leaching experiments should be conducted to examine the effects of these different non-carbonate fractions on the extraction and $\delta^{238}U$ values of the carbonate fraction U from bulk carbonate sediments.

Second, to better calibrate $^{238}U/^{235}U$ in sedimentary carbonate rocks as a robust paleoredox proxy, further work should examine what controls the variability of $\delta^{238}U$ in carbonate sediments during diagenesis, and explore the U isotope fractionation in carbonate sediments under different depositional and diagenetic environmental settings. Diagenetic effects result in a significant and variable U isotopic offset of 0.27±0.14 ‰ (1 SD) in modern shallow-water carbonate sediments from the Bahamas relative to seawater (Chen et al., 2018; Tissot et al., 2018). This isotopic offset was hypothesized to result from authigenic reduction of U(VI) to U(IV), which preferentially enriches ^{238}U (Chen et al., 2018; Tissot et al., 2018; Andersen et al., 2017). To test this hypothesis, synchrotron-based X-ray spectroscopic and diffraction techniques could be used to characterize the speciation (e.g., oxidation states of U, the presence of U(IV) as insoluble UO_2(s), non-crystalline U(IV), or U(IV) substituted for Ca in calcium carbonate crystal lattice) of U in carbonate sediments, and quantify the fractions of U(VI) and U(IV). Because U(IV) is isotopically heavier than U(VI), a positive correlation of larger fractions of U(IV) with higher $\delta^{238}U$ values in carbonates would be expected. If U(IV) exists as dispersed U(IV) in carbonate sediments, oxidative leaching of powdered carbonate sediments under alkaline conditions would separate U(IV) from the lattice-bound U(VI) for their mass quantifications and isotopic measurements to further interpret the variability of $\delta^{238}U$ values in carbonate sediments during diagenesis. The proposed study might provide insights into understanding of the

significantly larger U isotope fractionation during meteoric diagenesis relative to marine phreatic diagenesis.

U isotope fractionation in carbonate sediments from different depositional and diagenetic environments needs to be determined to provide robust calibrations to $\delta^{238}U$ in ancient carbonates as a paleoredox proxy. Different depositional environments (shallow-marine tropical, shallow-marine non-tropical warm-temperature and cool-temperature, and deep-sea) form carbonates sediments with varying carbonate mineralogical composition and U concentrations, which might lead to different characteristics of U isotope fractionation during carbonate diagenesis. For example, shallow-marine tropical carbonates are mainly composed of metastable aragonite and high-Mg calcite, which are easily and intensively dissolved/transformed. In contrast, deep-sea carbonates mainly consist of the more stable low-Mg calcite and have a lower diagenetic potential (Schlanger and Douglas, 1974; Flügel, 2010). Additionally, U concentration in shallow-marine primary carbonates (~1.5 ppm) are significantly higher than the deep-sea primary calcium carbonates (~0.025 ppm; Romaniello et al., 2013; Delaney and Boyle, 1983; Russell et al., 1994). These differences in depositional environments could possibly lead to different U isotope fractionation during carbonate diagenesis.

The shallow-marine carbonate sediments from the Bahamas showed that vadose meteoric diagenesis caused significantly larger U isotope fractionation than phreatic meteoric and marine diagenesis, suggesting that different diagenetic environments (meteoric vadose, meteoric phreatic, marine phreatic, and burial) might also affect U isotope fractionation during carbonate diagenesis (Chen et al., 2018; Tissot et al., 2018). These different diagenetic environments have their own specific characteristics of diagenesis. For example, meteoric diagenetic zones are filled

with freshwater and/or air while marine phreatic and burial diagenetic zones are filled with seawater and brines of varying salinity, respectively (Flügel, 2010). Current studies only focus on the vadose meteoric, phreatic meteoric and marine diagenesis in the shallow-marine tropical carbonate sediments from the Bahamas. To provide better correction to the U isotope fractionation during carbonate diagenesis, U isotope fractionation in carbonate sediments of other types of depositional and diagenetic environments should be explored in the future.

Third, U isotope fractionation during biotic and abiotic U reduction reactions in laboratory experiments and natural environments should be further explored to better constrain the U isotope fractionation between U in seawater and various marine sinks. Laboratory experiments biotic and abiotic U redox reactions fractionate U isotopes in opposite directions with varying isotope fractionation factors (Basu et al., 2014; Stirling et al., 2015; Stylo et al., 2015; Rademacher et al., 2006; Brown et al., 2018). Currently, all biotic U reduction experiments preferentially reduced ^{238}U with a pretty consistent isotope fractionation factor of 0.86±0.12 ‰ (Basu et al., 2014; Stirling et al., 2015; Stylo et al., 2015). In contrast, abiotic U(VI) reductions fractionated U isotopes in opposite directions at various magnitudes. Specifically, U(VI) reduction by zero-valent Fe and Zn, chemogenic FeS, biogenic FeS, and peat did not show measurable U isotope fractionation (Rademacher et al., 2006; Stirling et al., 2007; Stylo et al., 2015). In contrast, magnetite, green rust, HS^-, and aqueous Fe(II) preferentially reduced ^{235}U (Stylo et al., 2015). Surprisingly, synthetic mackinawite preferentially reduced ^{238}U with an isotope fractionation of 0.23–0.83 ‰, depending on the U(VI) reduction kinetics and aqueous U speciation (Brown et al., 2018). U isotope fractionation during U removal by suboxic and anoxic sediments are also variable, ranging from 0.15 to 1.1 ‰ (Bopp et al., 2010; Noordmann et al.,

2016; Andersen et al., 2017; Jemison et al., 2018). To better understand U isotope fractionation in natural environments and characterize $\delta^{238}U$ values in different marine U sinks, the mechanisms of U isotope fractionation needs to be elucidated via experimental and field studies.

REFERENCES

Abe M., Suzuki T., Fujii Y., Hada M. and Hirao K. (2008) An *ab initio* molecular orbital study of the nuclear volume effects in uranium isotope fractionations. *J. Chem. Phys*. **129**, 164309.

Adey W. H. and Loveland K. (2007) Biomineralization and Calcification: A Key to Biosphere and Ecosystem Function. In *Dynamic Aquaria: Building and Restoring Living Ecosystems*. Third Edition, Academic Press, London. pp. 145–147.

Algeo T. J. and Maynard J. B. (2004) Trace-element behavior and redox facies in core shales of Upper Pennsylvanian Kansas-type Cyclothems. *Chem. Geol.* **206**, 289–318.

Algeo T. J. and Rowe H. (2011) Paleoceanographic applications of trace-metal concentration data. *Chem. Geol.* **324–325**, 6–18.

Algeo T. J., Luo G. M., Song H. Y., Lyons T. W. and Canfield D. E. (2015) Reconstruction of secular variation in seawater sulfate concentrations. *Biogeosciences* **12**, 2131–2151.

Al-Horani F. A., Al-Moghrabi S. M. and de Beer D. (2003) The mechanism of calcification and its relation to photosynthesis and respiration in the scleractinian coral *Galazea fascicularis*. *Mar. Biol*. **142**, 419–426.

Anagnostou E., Sherrell R. M., Gagnon A., LaVigne M., Field M. P. and McDonough W. F. (2011) Seawater nutrient and carbonate ion concentrations recorded as P/Ca, Ba/Ca, and U/Ca in the deep-sea coral *Desmophyllum dianthus*. *Geochim. Cosmochim. Acta* **75**, 2529–2543.

Anbar A. D. and Rouxel O. (2007) Metal stable isotopes in paleoceanography. *Annu. Rev. Earth Planet. Sci*. **35**, 717–46.

Andersen M. B., Erel Y. and Bourdon B. (2009) Experimental evidence for ^{234}U-^{238}U fractionation during granite weathering with implications for $^{234}U/^{238}U$ in natural waters. *Geochim. Cosmochim. Acta* **73**, 4124–4141.

Andersen M. B., Romaniello S., Vance D., Little S. H., Herdman R. and Lyons T. W. (2014) A modern framework for the interpretation of $^{238}U/^{235}U$ in studies of ancient ocean redox. *Earth. Planet. Sci. Lett*. **400**, 184–194.

Andersen M. B., Vance D., Morford J. L., Bura-Nakić E., Breitenbach S. F. M. and Och L. (2016) Closing in on the marine $^{238}U/^{235}U$ budget. *Chem. Geol.* **420**, 11–22.

Andersen M. B., Stirling C. H., Zimmermann B. and Halliday A. N. (2010) Precision determination of the open ocean $^{234}U/^{238}U$ composition. *Geochem. Geophys. Geosyst*. **11**, Q12003, doi:10.1029/2010GC003318.

Andersen M. B., Stirling C. H. and Weyer S. (2017) Uranium isotope fractionation. *Rev. Mineral. Geochem*. **82**, 799–850.

Andersen M. B., Stirling C. H., Potter E., Halliday A. N., Blake S. G., McCulloch M. T., Ayling B. F., O'Leary M. (2008) High-precision U-series measurements of more than 500, 000 year old fossil corals. *Earth Planet. Sci. Lett*. **265**, 229–245.

Anderson R. F. (1982) Concentration, vertical flux, and remineralization of particulate uranium in seawater. *Geochim. Cosmochim. Acta* **46**, 1293–1299.

Anderson R. F. (1984) A method for determining the oxidation state of uranium in natural waters. *Nucl. Instrum. Methods Phys. Res*. **233**, 213–217.

Anderson R. F., Fleisher M. Q. and LeHuray A. P. (1989a) Concentration, oxidation-state and particulate flux of uranium in the Black Sea. *Geochim. Cosmochim. Acta* **53**, 2215–2224.

Anderson R. F., LeHuray A. P., Fleisher M. Q. and Murray J. W. (1989b) Uranium deposition in Saanich Inlet sediments, Vancuver Island. *Geochim. Cosmochim. Acta* **53**, 2205–2213.

Armid A., Asami R., Fahmitati T., Sheikh M. A., Fujimura H., Higuchi T., Taria E., Shinjo R. and Oomori T. (2011) Seawater temperature proxies based on D_{Sr}, D_{Mg}, and D_U from culture experiments using the branching coral *Porites cylindrical*. *Geochim. Cosmochim. Acta* **75**, 4273–4285.

Arnold G. L., Anbar A. D., Barling J. and Lyons T. W. (2004) Molybdenum isotope evidence for widespread anoxia in Mid-Proterozoic ocean. *Science* **304**, 87–90.

Asael D., Tissot F. L. H., Reinhard C. T., Rouxel O., Dauphas N., Lyons T. W., Ponzevera E., Liorzou C. and Chéron S. (2013) Coupled molybdenum, iron and uranium stable isotope as oceanic paleoredox proxies during the Paleoproterozic Shunga Event. *Chem. Geol*. **362**, 193–210.

Azmy K., Kendall B., Brand U., Stouge S. and Gordon G. W. (2015) Redox conditions across the Cambrian-Ordovician boundary: Elemental and isotopic signatures retained in the GSSP carbonates. Palaeogeogr. *Paleoclimatol. Paleoecol*. **440**, 440–454.

Banner J. L. and Hanson G. N. (1990) Calculation of simultaneous isotopic and trace element variations during water-rock interaction with applications to carbonate diagenesis. *Geochim. Cosmochim. Acta* **54**, 3123–3137.

Barnes C. E. and Cochran J. K. (1991) Geochemistry of uranium in Black Sea sediments. Deep-Sea Res., A, *Oceanogr. Res. Pap*. 38, S1237–S1254.

Barnes C. E. and Cochran J. K. (1990) Uranium removal in oceanic sediments and the oceanic U balance. *Earth Planet. Sci. Lett*. **97**, 94–101.

Bartlett R., Elrick M., Wheeley J. R., Polyak V., Desrochers A. and Asmerom Y. (2018) Abrupt global-ocean anoxia during the Late Ordovician-early Silurian detected using uranium isotopes of marine carbonates. Proc. *Natl. Acad. Sci*. **115**, 5896–5901.

Basu A., Sanford R. A., Johnson T. M., Lundstrom C. C. and Löffler F. E. (2014) Uranium isotopic fractionation factors during U(VI) reduction by bacterial isolates. *Geochim. Cosmochim. Acta* **136**, 100–113.

Bates N. R., Samuels L. and Merlivat L. (2001) Biogeochemical and physical factors influencing seawater fCO_2 and air-sea CO_2 exchange on the Bermuda coral reef. *Limnol. Oceanogr*. **46**, 833–846.

Beerling D. J., McElwain J. C. and OsborneC. P. (1998) Stomatal responses of the 'living fossil' Ginkgo biloba L. to changes in atmospheric CO_2 concentrations. *J. Exp. Bot*. **49**, 1603–1607.

Berner R. A. and Kothavala Z. (2001) GEOCARB III: A revised model of atmospheric CO_2 over Phanerozoic time. *Am. J. Sci*. **301**, 182–204.

Berner R. A., VandenBrooks J. M. and Ward P. D. (2007) Oxygen and evolution. *Science* **316**, 557–558.

Bernhard G., Geipel G., Brendler V. and Nitsche. (1998) Uranium speciation in waters of different uranium mining areas. *J. Alloys Compd*. **271–3**, 201–205.

Bernhard G., Geipel G., Reich T., Brendler V., Amayri, S. and Nitsche H. (2001) Uranyl(VI) carbonate complex formation: Validation of the $Ca_2UO_2(CO_3)_3(aq)$ species. *Radiochim. Acta*. **89**, 511–518.

Bopp C. J., Lundstron C. C., Johnson T. M. and Glessner J. J. G. (2009) Variations in $^{238}U/^{235}U$ in the uranium ore deposits: Isotopic signatures of the U reduction process? *Geology* **37**, 611–614.

Bopp C. J., Lundstrom C. C., Johnson T. M., Sanfor R. A., Long P. E. and Wiliams K. H. (2010) Uranium $^{238}U/^{235}U$ isotope ratio as indicators of reduction: result from an in situ biostim- ulation experiment at Rile, Colorado, U. S. A. *Environ. Sci. Technol*. **44**, 5927–5933.

Borowitzka M. A. (1982) Mechanisms in algal calcification. *Progress in Phycological Research, 1* (Eds. Round F. E. and Chapman D. J.). Elsevier Biomedical Press B. V. pp. 138–177.

Bowen G. J. and Revenaugh J. (2003) Interpolating the isotopic composition of modern meteoric precipitation. *Water Resour. Res*. **39**, 1299.

Brennecka G. A., Borg L. E., Hutcheon I. D., Sharp M. A. and Anbar A. D. (2010) Natural variations in uranium isotope ratios of uranium ore concentrate: understanding the $^{238}U/^{235}U$ fractionation mechanism. *Earth Planet. Sci. Lett*. **291**, 228–233.

Brennecka G. A., Wasylenki L. E., Bargar J. R., Weyer S. and Anbar A. D. (2011a) Uranium isotope fractionation during adsorption to Mn-oxyhydroxides. *Environ. Sci. Technol*. **45**, 1370–1375.

Brennecka G. A., Herrmannn A. D., Algeo T. J. and Anbar A.D. (2011b) Rapid expansion of oceanic anoxia immediately before the end-Permian mass extinction. *Proc. Natl. Acad. Sci.* **108**, 17631–17634.

Brocker W. S. (1970) A boundary condition on the evolution of atmospheric oxygen. *J. Geophy. Res*. **75**, 3553–3557.

Broecker W. S. and Thurber D. L. (1965) Uranium-series dating of corals and oolites from Bahaman and Florida Key Limestones. *Science*, **148**, 58–60.

Brown S. T., Basu A., Christensen J. N., Reimus P., Heikoop J., Simmons A., Woldegabriel G., Maher K., Weaver K., Clay J. and DePaolo D. J. (2016) Isotopic evidence for reductive immobilization of uranium across a roll-front mineral deposition. *Environ. Sci. Technol.* **50**, 6189–6198.

Brown J. M. (2015) Cyanobacteria-associated bacteriophage communities across scales of spatial, temporal and environmental change. Ph. D. thesis, Cornell Univ.

Buick R. (2008) When did oxygenic photosynthesis evolve? *Phil. Trans. R. Soc. B* **363**, 2731–2745.

Burdige D. J., Hu X. and Zimmerman R. C. (2010) The widespread occurrence of coupled carbonate dissolution/reprecipitation in surface sediments on the Bahamas Bank. *Am. J. Sci*. **310**, 492–521.

Brunskill G. J. and Ludlam S. D. (1969) Fayetteville Green Lake, New York. I. Physical and chemical limnology. *Limnol. Oceanogr*. **14**, 817–829.

Brunskill G. J. (1969) Fayetteville Green Lake, New York II. Precipitation and sedimentation of calcite in a meromictic lake with laminated sediments. *Limnol. Oceanogr*. **14**, 830–847.

Bura-Nakić E., Andersen M. B., Archer C., de Souza G. F., Marguš M., Vance D. (2018) Coupled Mo-U abundances and isotopes in a small marine euxinic basin: Constraints on processes in euxinic basins. *Geochim. Cosmochim. Acta* **222**, 212–229.

Canfield D. E. (2005) The early history of atmospheric oxygen: homage to Robert M. Garrels. *Annu. Rev. Earth and Planet. Sci*. **33**, 1–36.

Canfield D. E., Poulton S. W. and Narbonne G. W. (2007) Late-Neoproterozoic deep-ocean oxygenation and the rise of animal life. *Science* **315**, 92–95.

Chabaux F., Riotte J. and Dequincey R. O. (2003) U-Th-Ra fractionation during weathering and river transport. *Rev. Mineral. Geochem*. **52**, 533–576.

Chen J. H., Edwards R. J. and Wasserburg G. C. (1986) ^{238}U, ^{234}U and ^{232}Th in seawater. *Earth Planet. Sci. Lett.* **80**, 241–251.

Chen X. (2015) Uranium isotope fractionation during coprecipitation with aragonite and calcite. Master Thesis, Arizona State Univ.

Chen X., Romaniello S. J., Herrmann A. D., Wasylenki L. E. and Anbar A. D. (2016) Uranium isotope fractionation during coprecipitation with aragonite and calcite. *Geochim. Cosmochim. Acta* **188**, 189–208.

Chen X., Romaniello S. J., Anbar A. D. (2017) Uranium isotope fractionation induced by aqueous speciation: Implications for U isotopes in marine $CaCO_3$ as a paleoredox proxy. *Geochim. Cosmochim. Acta* **215**, 162–172.

Chen X., Romaniello S. J., Herrmann A. D., Samankassou E. and Anbar A. D. (2018a) Biological effects on uranium isotope ($^{238}U/^{235}U$) in primary biogenic carbonates. *Geochimica et Cosmochimica Acta*, **240**, 1–10.

Chen X., Romaniello S. J., Herrmann A. D., Hardisty D., Gill B. C. and Anbar A. D. (2018b) Diagenetic effects on uranium isotope fractionation in carbonate sediments from the Bahamas. *Geochimica et Cosmochimica Acta*, **237**, 294–311.

Cheng H., Edwards R. L., Sehe C. C., Polyak V. J., Asmerom Y., Woodhead J., Hellstrom J., Wang Y., Kong X., Spoetl C., Wang X. and Alexander Jr. E. C. (2013) Improvements in ^{230}Th dating, ^{230}Th and 234U half-life values, and U-Th isotopic measurements by multi-collector inductively coupled plasma mass spectrometry. *Earth Planet. Sci. Lett*. **371-372**, 82–911.

Chun C. O. J., Delaney M. L. and Zachos J. C. (2010) Paleoredox changes across the Paleocene-Eocene thermal maximum, Walvis Ridge (ODP Sites 1262, 1263, and 1266): Evidence from Mn and U enrichment factors. *Paleoceanography*, **25**, PA4204, *doi:10.1029/2009PA001861*.

Chung G. S. and Swart P. K. (1990) The concentration of uranium in freshwater vadose and phreatic cements in a Holocene ooid cay: A method of identifying ancient water tables. *J. Sediment. Petrol.* **60**, 735–746.

Clarkson, M.O., Kasemann, S.A., Wood, R.A., Lenton, T.M., Daines, S.J., Richoz, S., Ohnemueller, F., Meixner, A., Poulton, S.W. and Tipper, E.T. (2015) Ocean acidification and the Permo-Triassic mass extinction. *Science* **348**, 229–232.

Cohen A. L. and McConnaughey T. A. (2003) Geochemical perspectives on coral mineralization. *Rev. Mineral. Geochem.* **54**, 151–187.

Condie K. C., Des Marais D. J. and Abbott D. (2001) Precambrian superplumes and supertercontinents: a record in black shales, carbon isotopes, and paleocalimate? *Precambr. Res*. **106**, 239–260.

Culver D. A. and Brunskill G. J. (1969) Fayetteville Green Lake, New York: V. Studies of primary production and zooplankton in a meromictic marl lake. *Limnol. Oceanogr*. **14**, 862–873.

Curti E. (1999) Coprecipitation of radionuclides with calcite: Estimation of partition coefficients based on a review of laboratory investigations and geochemical data. *Appl. Geochem.* **14**, 433–445.

Czaja A. D., Johnson C. M., Roden E. E., Beard B. L., Voegelin A. R., Nägler T. F., Beukes N. J. and Wille M. (2012) Evidence for free oxygen in the Neoarchean ocean based on coupled iron-molybdenum isotope fractionation. *Geochim. Cosmochim. Acta* **86**, 118–137.

Dahl T. W., Canfield D. E., Rosing M. T., Frei R. E., Gordon G. W., Knoll A. H. and Anbar A. D. (2011) Molybdenum evidence for expansive sulfidic water masses in ~750 Ma oceans. *Earth. Planet. Sci. Lett*. **311**, 264–274.

Dahl T. W., Boyle R. A., Canfield D. E., Connelly J. N., Gill B. C., Lenton T. M. and Bizzaro M. (2014) Uranium isotopes distinguish two geochemically distinct stages during the later Cambrian SPICE event. *Earth. Planet. Sci. Lett*. **401**, 313–326.

Dahl T. W., Connelly J. N., Kouchinsky A., Gill B. C., Mansson S. F., Bizzarro M. (2017) Reorganisation of Earth's biogeochemical cycles briefly oxygenated the oceans 520 Myr ago. *Geochem. Perspect. Lett.* **3**, 210–220.

Dang D. H., Novotnik B., Wang W., Georg R. B. and Evans R. D. (2016) Uranium isotope fractionation during adsorption, (co)precipitation, and biotic reduction. *Environ. Sci. Technol*. **50**, 12695–12704.

D'Arcy J., Gilleaudeau G. J., Peralta S., Gaucher C. and Frei R. (2017) Redox fluctuations in the Early Ordovician oceans: An insight from chromium stable isotopes. *Chem. Geol*. **448**, 1–12.

DeCarlo T. M., Gaetani G. A., Holcomb M. and Cohen Anne. (2015) Experimental determination of factors controlling U/Ca of aragonite precipitated from seawater: Implications for interpreting coral skeleton. *Geochim. Cosmochim. Acta* **162**, 151–165.

Delaney M. L. and Boyle E. A. (1983) Uranium and thorium isotope concentrations in foraminiferal calcite. *Earth. Planet. Sci. Lett.* **62**, 258–262.

Diaz M. R., Eberli G. P., Blackwelder P., Phillips B. and Swart P. K. (2017) Microbially mediated organomineralization in the formation of ooids. *Geology* **45**, 771–774.

Diaz M. R., Van Norstrand J. D., Eberli G. P., Piggot A. M., Zhou J. and Klaus J. S. (2014) Functional gene diversity of oolitic sands from Great Bahama Bank. *Geobiology* **12**, 231–249.

Diaz M. R., Swart P. K., Eberli G. P., Oehlert A. M., Devlin Q., Saeid A. and Altabet M. A. (2015) Geochemical evidence of microbial activity within ooids. *Sedimentology* **62**, 2090–2112.

Dickson A. J. and Cohen A. S. (2012) A molybdenum isotope record of Eocene Thermal Maximum 2: Implications for global ocean redox during the early Eocene. *Paleoceanography* **27**, PA3230.

Dickson A. J., Cohen A. S. and Coe A. L. (2012) Seawater oxygenation during the Peleocene-Eocene Thermal Maximum. *Geology* **40**, 639–642.

Dickson A. J., Jenkyns H. C., Porcelli D., van den Boorn S. and Idiz E. (2016) Basin-scale controls on the molybdenum isotope composition of seawater during Oceanic Anoxic Event 2 (Late Cretaceous). *Geochim. Cosmochim. Acta* **178**, 291–306.

Docrat T., Mosselmans J., Charnock J., Whiteley M., Collision D., Livens F., Jones C. and Edmiston M. (1999) X-Ray absorption spectroscopy of tricarbonatodioxouranate(V), $[UO_2(CO_3)_3]^{5-}$, in aqueous solution. *Inorg. Chem*. **38**, 1879–1882.

Dong W. and Brooks S. C. (2006) Determination of the formation constants of ternary complexes of uranyl and carbonate with alkaline earth metals (Mg^{2+}, Ca^{2+}, Sr^{2+}, and Ba^{2+}) using anion exchange method. *Environ. Sci. Technol.***40**, 4689–4695.

Duan Y., Anbar A. D., Arnold G. L., Lyons T. W., Gordon G. W. and Kendall B. (2010) Molybdenum isotope evidence for mild environmental oxygenation before the Great Oxygenation Event. *Geochim. Cosmochim. Acta* **74**, 6655–6668.

Duguid S. M. A., Kyser T. K., James N. P. and Rankey E. C. (2010) Microbes and ooids. *J. Sediment. Res.* 80 236–251.

Dunk R. M., Mills R. A. and Jenkins W. J. (2002) A reevaluation of the oceanic uranium budget for the Holocence. *Chem. Geol.***190**, 45–67.

Eberli G. P., Swart P. K., McNeill D. F., Kenter J. A. M., Anselmetti F. S., Melim L. A. and Ginsburg R. N. (1997) A synopsis of the Bahamas Drilling Project: Results from two deep core borings drilled on the Great Bahama Bank, *in* Eberli, G. P., Swart P. K., Malone M. J. et al., ed., Proceedings of the Ocean Drilling Program: College Station, Texas, Ocean Drilling Program, Initial reports, v. 166, p. 23–41.

Eggleton F. E. (1956) Limnology of a meromictic, interglacial, plunge-basin lake. Trans. *Am. Microsc. Soc*. **75**, 334–378.

Elrick M., Polyak V., Algeo T. J., Romaniello S. J., Asmerom Y., Herrmann A. D., Anbar A. D., Zhao L. and Chen Z. (2016) Global ocean redox variation during the middle-late Permian through Early Triassic based on uranium isotope and Th/U trends of marine carbonates. *Geology* G38585.1

Endrizzi F. and Rao L. (2014) Chemical speciation of Uranium(VI) in marine environments: Complexation of calcium and magnesium ions with $[(UO_2)(CO_3)_3]^{4-}$ and the effect on the extraction of Uranium from seawater. *Chem. Eur. J.* **20**, 14499–14506.

Endrizzi F., Leggett C. J. and Rao L. (2016) Scientific basis for efficient extraction of uranium from seawater. I: Understanding the chemical speciation of uranium under seawater conditions. *Ind. Eng. Chem. Res*. **55**, 4249–4256.

Fairbanks R. G. (1989) A 17000-year glacio-eustatic sea level record: influence of glacial melting rates on the Younger Dryas event and deep-ocean circulation. *Nature* **342**, 637–642.

Farquhar J., Bao H. and Thiemens M. (2000) Atmospheric influence of Earth's earliest sulfur cycle. Science **289**, 756–758.

Farquhar J., Zerkel A. L. and Bekker A. (2011) Geological constraints on the origin of oxygenic photosynthesis. *Photosynth. Res*. **107**, 11–36.

Felis T., Suzuki A., Kuhnert H., Dima M., Lohmann G. and Kawahata H. (2009) Subtropical coral reveals abrupt early twentieth-century freshening in the western North Pacific Ocean. *Geology* **37**, 527–530.

Fenchel T. and Finlay B. J. (1994) The evolution of life without oxygen. *Am. Sci*. **82**, 22–29.

Fletcher B. J., Brentnall S. J., Anderson C. W., Berner R. A. and Beerling D. J. (2008) Atmospheric carbon dioxide linked with Mesozoic and early Cenozoic climate change. *Nat. Geosci*. **1**, 43–48.

Florence T., Batley G., Ekstrom A., Fardy J. and Farrar Y. (1975) Separation of uranium isotopes by uranium(IV)-uranium(VI) chemical exchange. *J. Inorg. Nucl. Chem*. **37**, 1961–1966.

Flügel E. (2010) Microfacies of Carbonate Rocks: Analysis, Interpretation and Application. Springer-Verlag Berlin Heidelberg. pp. 267–278.

Frank T. D. and Bernet K. (2000) Isotopic signature of burial diagenesis and primary lithological contrasts in periplatform carbonates (Miocene, Great Bahama Bank). *Sedimentology* **47**, 1119–1134.

Frei R., Gaucher C., Døssing L. N. and Sial A. N. (2011) Chromium isotopes in carbonates—A tracer for climate change and for reconstructing the redox state of ancient seawater. *Earth. Planet. Sci. Lett.* **312**, 114–125.

Frei R., Gaucher C., Stolper D. and Canfield D. E. (2013) Fluctuations in late Neoproterozoic atmospheric oxidation—Cr isotope chemostratigraphy and iron speciation of the late Ediacaran lower Arroyo del Soldado Group (Uruguay). *Gondwana Res*. **23**, 797–811.

Fujii Y.., Higuchi N., Haruno Y., Nomura M. and Suzuki T. (2006) Temperature dependence of isotope effects in uranium chemical exchange reactions. *J. Nucl. Sci. Technol*. **43**, 400–406.

Fulton J. M., Arthur M. A., Thomas B. and Freeman K. H. (2018) Pigment carbon and nitrogen isotopic signatures in euxinic basins. *Geobiology* **16**, 429–445.

Gabitov R. I., Gaetani G. A., Watson E. B., Cohen A. L. and Ehrlich H. L. (2008) Experimental determination of growth rate effect on U^{6+} and Mg^{2+} partitioning between aragonite and fluid at elevated U^{6+} concentration. *Geochim. Cosmochim. Acta* **72**, 4058–4068.

Gaetani A. A., Cohen A. L., Wang Z. and Crusius J. (2011) Rayleigh-based, multi-element coral thermometry: A biomineralization approach to developing climate proxies. *Geochim. Cosmochim. Acta* **75**, 1920–1932.

Gagnon A. C., Adkins J. F., Fernandez D. P. and Robinson L. F. (2007) Sr/Ca and Mg/Ca vital effects correlated with skeletal architecture in a scleractinian deep-sea coral and the role of Rayleigh fractionation. *Earth Planet. Sci. Lett*. **261**, 280–295.

Gagnon A. C., Adkins J. F. and Erez J. (2012) Seawater transport during coral biomineralization. *Earth Planet. Sci. Lett*. **329–330**, 150–161.

Galloway S. B.., Work T. M., Bochsler V. S., Harley R. A., Kramarsky-Winter E., McLaughlin S. M. (2007) *Coral Disease and Health Workshop: Coral Histopathology II.* NOAA Technical Memorandum NOSNCCOS 56 and NOAA Technical Memorandum CRCP 4. National Oceanic and Atmospheric Administration, Silver Spring, MD. pp 10–11.

Gattuso J. P., Pichon M., Delesalle B. and Frankignoulle M. (1993) Community metabolism and air-sea CO_2 fluxes in a coral reef ecosystem (Moorea, French Polynesia). *Mar. Ecol. Prog. Ser.* **96**, 259–267.

Gattuso J. P., Pichon M., Delesalle B., Canon C. and Frankignoulle M. (1996) Carbon fluxes in coral reefs: I. Lagrangian measurement of community metabolism and resulting air-sea CO_2 disequilibrium. *Mar. Ecol. Prog. Ser.* **145**, 109–121.

Georgiou L., Falter J., Trotter J., Kline D. L., Holcomb M., Dove S. G., Hoegh-Guldberg O. and McCulloch M. (2015) pH homeostatis during coral calcification in a free ocean CO_2 enrichment (FOCE) experiment, Heron Island reef flat, Great Barrier Reef. *Proc. Natl. Acad. Sci.* **112**, 13219–13224.

German, C. R. and Elderfield, H. (1990) Application of the Ce anomaly as a paleoredox indicator: the ground rules. *Paleoceanography* **5**, 823–833.

Gibbs M. T., Bluth G. J. S., Fawcett P. J. and Kump L. (1999) Global chemical erosion over the last 250 My: Variations due to changes in paleogeography, paleoclimate, and paleogeology. *Am. J. Sci*. **299**, 611–651.

Gilbert P. U. P. A., Wilt F. H. (2011) Molecular aspects of biominieralization of the Echindoderm Endoskeleton. In: Müller W. *Molecular Biomineralization*. Springer, Berlin-Heidelberg, 199–223.

Gill B. C., Lyons T. W. and Frank T. D. (2008) Behavior of carbonate–associated sulfate during meteoric diagenesis and implications for the sulfur isotope paleoproxy. *Geochim. Cosmochim. Acta* **72**, 4669–4711.

Gilleaudeau G. J., Frei R., Kaufman A. J., Kah L. C., Azmy K., Bartley J. K., Chernyavskiy P. and Knoll A. H. (2016) Oxygenation of the mid-Proterozoic atmosphere: Clues from chromium isotopes in carbonates. *Geochem. Persp. Let*. **2**, 178–187.

Gillikin D. P. and Dehairs F. (2012) Uranium in aragonitic marine bivalve shells. *Palaeogeogr. Palaeoclim. Palaeocol*. **373**, 60–65.

Ginsburg R.N. (2001) Subsurface geology of a prograding carbonate platform margin, Great Bahama Bank: Results of the Bahamas Drilling Project. Society of Economic Paleontologists and Mineralogists, Tulsa, OK.

Gipel G., Amayri S. and Bernhard G. (2008) Mixed complexes of alkaline earth uranyl carbonates: A laser-induced time-resolved fluorescence spectroscopic study. *Spectrochim. Acta Mol. Biomol. Spectrosc*. **71**, 53–58.

Glock N., Liebetrau V. and Eisenhauer A. (2014) I/Ca ratios in benthic foraminifera from the Peruvian oxygen minimum zone: Analytical methodology and evaluation as a proxy for redox conditions. *Biogeosciences* **11**, 7077–7095.

Goto K. T., Anbar A. D., Gordon G. W., Romaniello S. J., Shimoda G., Takaya Y., Tokumaru A., Nozaki T., Suzuki K., Machida S., Hanyu T. and Usui A. (2014) Uranium isotope systematics of ferromanganese crusts in the Pacific Ocean: Implications for the marine $^{238}U/^{235}U$ isotope system. *Geochim. Cosmochim. Acta* **146**, 43–58.

Grenthe I., Fuger J., Konings R. J. M., Lemire R. J., Muller A. B., Gregu C. N. T. and Wanner H. (1992) Chemical Thermodynamics 1: Chemical Thermodynamics of Uranium. North-Holland Elsevier Science, New York.

Grotzinger J. P., and James N. P. (2000) *Carbonate Sedimentation and Diagenesis in the Evolving Precambrian World*. SEPM (Society for Sedimentary Geology), Special Publication no. 67.

Grotzinger J. P. and Knoll A. H. (1995) Anomalous carbonate precipitates: Is the Precambrian the key to the Permian? *Palaios* **10**, 587–596.

Guillaumont R., Fanghanel T., Fuger J., Grenthe I., Neck V., Palmer D. and Rand M. H. (2003) Update on the Chemical Thermodynamics of Uranium, Neptonium, Plutonium, Americium and Technetium. Elsevier, Amsterdam.

Gulin S. B. (2000) Recent changes of biogenic carbonate deposition in anoxic sediments of the Black Sea: Sedimentary record and climatic implication. *Mar. Environ. Res.* **49**, 319–328.

Hardie L. A. (1996) Secular variation in seawater chemistry: An explanation for the coupled variation in the mineralogies of marine limestones and potash evaporatesover the past 600 m.y. *Geology*, **24**, 279–283.

Hardisty D. S., Lu Z., Bekker A., Diamond C. W., Gill B. C., Jiang G., Kah L., Knoll A. H., Loyd S. J., Osburn M. R., Planavsky N. J., Wang C., Zhou X. and Lyons T. W. (2017) Perspectives on Proterozoic surface ocean redox from iodine contents in ancient and recent carbonate. *Earth. Planet. Sci. Lett.* **463**, 159–170.

Harris P. M. (2010) Delineating and quantifying depositional facies patterns in carbonate reservoirs: Insights from modern analogs. *AAPG Bulletin* **94**, 61–68.

Havig J. R., McCormick M. L., Hamilton T. L. and Kump L. R. (2015) The behavior of biologically important trace elements across the oxic/euxinic transition of meromictic Fayetteville Green Lake, New York, USA. *Geochim. Cosmochim. Acta* **165**, 389–406.

Havig J. R., Hamilton T. L., McCormick M., McClure B., Sowers T., Wegter B. and Kump L. R. (2017) Water column and sediment stable carbon isotope biogeochemistry of permanently redox-stratified Fayetteville Green Lake, New York, U. S. A. *Limnol. Oceanogr*. **63**, 570–587.

Henderson G. M., Slowey N. C. and Haddad G. A. (1999) Fluid flow through carbonate platforms: Constraints from $^{234}U/^{238}U$ and Cl^- in Bahamas pore-waters. *Earth. Planet. Sci. Lett.* **169**, 99–111.

Henderson G. M. (2002) Seawater ($^{234}U/^{238}U$) during the last 800 thousand years. *Earth. Planet. Sci. Lett.* **199**, 97–110.

Henehan W. J., Foster G. L., Bostock H., Greenop R., Marshall B. J., Wilson P. A. (2016) A new boron isotope-pH calibration for *Orbulina universa*, with implications for understanding and accounting for 'vital effects'. *Earth Planet. Sci. Lett*. **454**, 282–292.

Herrmann A. D., Kendall B., Algeo T. J., Gordon G. W., Wasylenki L. E. and Anbar A. D. (2012) Anomalous molybdenum isotope trends in Upper Pennsylvanian euxinic facies: Significance for use of $\delta^{98}Mo$ as a global marine redox proxy. *Chem. Geol*. **324–325**, 87–89.

Herrmann A., Gordon G. W. and Anbar A. D. (2018) Uranium isotope variations in a dolomitized Jurassic carbonate platform (Tithonian; Franconian Alb, Southern Germany). *Chem. Geol*. **497**, 41–53.

Herndon E. M., Havig J. R., Singer D. M., McCormick M. L. and Kump L. R. (2018) Mangnese and iron geochemistry in sediments underlying the redox-stratified Fayetteville Green Lake. *Geochim. Cosmochim. Acta* **231**, 50–63.

Hiess J., Condon D. J., McLean N. and Noble S. R. (2012) $^{238}U/^{235}U$ systematics in terrestrial uranium-bearing minerals. *Science* **335**, 1610–1614.

Higgins J. A., Blattler C. L., Lundstrom E. A., Santiago-Ramos D. P., Akhtar A. A., Cruger Ahm A. S., Bialik O., Holmden C., Bradbury H., Murray S. T. and Swart P. K. (2018) Mineralogy, early marine diagenesis, and the chemistry of shallow-water carbonate sediments. *Geochim. Cosmochim. Acta* **220**, 512–534.

Hilfinger, IV, M. F., Mullins H. T., Burnett A. and Kirby M. E. (2001) A 2500 year sediment record from Fayetteville Green Lake, New York: Evidence for anthropogenic impacts and historic isotope shift. *J. Paleolimnol*. **26**, 293–305.

Hinojosa J. L., Stirling C. H., Reid M. R., Moy C. M. and Wilson G. S. (2016) Trace metal cycling and $^{238}U/^{235}U$ in New Zealand's fjords: Implications for reconstructing global paleoredox conditions in organic-rich sediments. *Geochim. Cosmochim. Acta* **179**, 89–109.

Hoffmeister J. E. and Multer H. G. (1968) Geology and origin of the Florida Keys. *Geological Society of American Bulletin*, **79**, 1487–1502.

Holland H. D. (2006) The oxygenation of the atmosphere and oceans. *Phil. Trans. R. Soc. B* **361**, 903–915.

Holmden C., Jacobson A. D., Sageman B. B. and Hurtgen M. T. (2016) Response of the Cr isotope proxy to Cretaceous Ocean Anoxic Event 2 in a pelagic carbonate succession from the Western Interior Seaway. *Geochim. Cosmochim. Acta* **186**, 277–295.

Hood A., Planavsky N. J., Wallace M. W., Wang X., Bellefroid E. J., Gueguen B. and Cole D. B. (2016) Integrated geochemical-petrographic insights from component-selective $\delta^{238}U$ of Cryogenian marine carbonates. Geology 44, 935–938.

Hortia J., Zimmermann H. and Holland H. D. (2002) Chemical evolution of seawater during the Phanerozoic: Implications from the record of marine evaporites. *Geochim. Cosmochim. Acta* **66**, 3733–3756.

Hu X. and Burdige D. J. (2007) Enriched stable carbon isotopes in the pore waters of carbonate sediments dominated by seagrasses: Evidence for coupled carbonate dissolution and reprecipitation. *Geochim. Cosmochim. Acta* **71**, 129–144.

Huang J., Chu X., Chang H. and Feng L. (2009) Trace element and rare earth element of cap carbonate in Edicaran Doushantuo Formation in Yangtze Gorges. *Chinese. Sci. Bull*. **54**, 3295–3302.

Inoue M., Suwa R., Suzuki A., Sakai K. and Kawahata H. (2011) Effects of seawater pH on growth and skeletal U/Ca ratios of *Acroporadigitifera* coral polyps. *Geophys. Res. Lett*. **38**, L12809.

Jacobsen S. B. and Kaufman A. J. (1999) The Sr, C and O isotopic evolution of Neoproterozoic seawater. *Chem. Geol*. **161**, 37–57.

Jaffey A., Flynn K., Glendenin L., Bentley W. and Essling A. (1971) Precision measurement of half-lifes and specific activities of ^{238}5U and ^{238}U. *Phys. Rev. C* **4**, 1889–1906.

Jemison N. E., Johnson T. M., Shiel A. E. and Lundstrom C. C. (2016) Uranium isotopic fractionation induced by U(VI) adsorption onto common aquifer minerals. *Environ. Sci. Technol*. **50**, 12232–12240.

Jemison N., Brown S. and Druhan J. (2018) Large ^{238}U/^{235}U fractionation in an alkaline, euxinic lake: Implications for the marine sedimentary record. *Goldschmidt conference*, Boston, MA, (abstr.).

Jenkins W. (2003) Tracer of Ocean Mixing. *In The Oceans and Marine Geochemistry: Treatise on Geochemistry* (eds. H. D. Holland and K. K. Turekian). Elseiver-Pergammon, Oxford, U. K. pp. 223–246.

Jodrey L. H. (1953) Studies on shell formation. 3. Measurement of calcium deposition in shell and calcium turnover in mantle tissue using the mantle-shell preparation and Ca^{45}. *Biol. Bull*. **104**, 398–407.

John S. G. and Adkins J. F. (2010) Analysis of dissolved iron isotopes in seawater. *Mari. Chem*. **119**, 65–76.

Jost A. B., Bachan A., Schootbrugge B. v. d., Lau K. V., Weaver K. L., Maher K. and Payne J. L. (2017) Uranium isotope evidence for an expansion of marine anoxia during the end-Triassic extinction. *Geochem. Geophys. Geosyst*. **18**, 3093–3108.

Kalmykov S. N. and Choppin G. R. (2000) Mixed $Ca^{2+}/UO_2^{2+}/CO_3^{2-}$ complex formation at different ionic strengths. *Radiochim. Acta* **88**, 603–606.

Karhu J. A. and Holland H. D. (1996) Carbon isotopes and the rise of atmosphere oxygen. *Geology* **24**, 867–870.

Kasting J. F. and Siefert J. L. (2002) Life and the evolution of Earth's atmosphere. *Science* **296**, 1066–1068.

Kasting J. F. (1993) Earth's early atmosphere. *Science* **259**, 920–925.

Kendall B., Gordon G. W., Poulton S. W. and Anbar A. D. (2011) Molybdenum isotope constraints on the extent of late Paleoproterozoic ocean euxinia. *Earth. Planet. Sci. Lett.* **307**, 450–460.

Kendall B., Brennecka G. A., Weyer S. and Anbar A. D. (2013) Uranium isotope fractionation suggests oxidative uranium mobilization at 2.50 Ga. *Chem. Geol.* **362**, 105–114.

Kendall B., Komiya T., Lyons T. W., Bates S. M., Gordon G. W., Romaniello S. J., Jiang G., Creaser R. A., Xiao S., McFadden K., Sawaki Y., Tahata M., Shu G., Han J., Li Y., Chu X. and Anbar. D. A. (2015) Uranium and molybdenum isotope evidence for an episode of widespread ocean oxygenation during the late Ediacaran Period. *Geochim. Cosmochim. Acta* **156**, 173–193.

Kenter J. A. M., Ginsburg R. N. and Troelstra S. R. (2001) Sea-level-driven sedimentation patterns on the slope and margin in: Ginsburg, R.N. (Ed.), Subsurface Geology of a progragding carbonate platform margin, Great Bahama Bank: Results of the Bahamas Drilling Project. Society of Economic Paleontologists and Mineralogists, Tulsa, OK, pp. 61–100.

Kerisit S. and Liu C. (2010) Molecular simulation of the diffusion of uranyl carbonate species in aqueous solution. *Geochim. Cosmochim. Acta* **74**, 4937–4952.

Klinkhammer G. P., Palmer M. R. (1991) Uranium in the oceans: Where it goes and why. *Geochim. Cosmochim*. Acta **55**, 1799–1806.

Knauth L. P. and Kennedy M. J. (2009) The late Precambrian greening of the Earth. *Nature*, **460**, 728–732.

Kolodny Y., Torfstein A., Weiss-Sarusi K., Zakon Y. and Halicz L. (2017) ^{238}U-^{235}U-^{234}U fractionation between tetravalent and hexavalent uranium in seafloor phosphorites. *Chem. Geol*. **451**, 1–8.

Ku T. L., Knauss K. G. and Mathieu G. G. (1977) Uranium in open ocean—concentration and isotopic composition. *Deep-Sea Res*. **24**, 1005–1017.

Ku T. L. (1965) An evaluation of ^{234}U-^{238}U method as a tool for dating pelagic sediments. *J. Geophys. Res*. **70**, 3457–3474.

Kump L. R. and Arthur M. A. (1999) Interpreting carbon-isotope excursions: Carbonates and organic matter. *Chem. Geol*. **161**, 181–198.

Kump L. R. (2012) Sulfur isotopes and the stepwise oxygenation of the biosphere. *Elements* **8**, 189–198.

Kurzweil F., Drost K., Pašava J., Wille M., Taubald H., Schoeckle D. and Schoenberg. (2015) Coupled sulfur, iron and molybdenum isotope data from black shales of the Tepla -Barrandian unit argue against deep ocean oxygenation during the Ediacaran. *Geochim. Cosmochim. Acta* **171**, 121–142.

Kerisit S. and Liu C. (2010) Molecular simulation of the diffusion of uranyl carbonate species in aqueous solution. *Geochim. Cosmochim. Acta* **74**, 4937–4952.

Keul N., Langer G., Nooijer L. J. de., Nehrke G., Reichart G. and Bijma, J. (2013) Incorporation of uranium in benthic foraminiferal calcite reflects seawater carbonate ion concentration. *Geochem.Geophys*. **14**, 102–111.

Krumbein W. E. (1979) Calcification by bacteria and algae. In *Biogeochemical Cycling of Mineral-Forming Elements* (eds. P. A. Trudinger and D. J. Swaine). Elsevier, Amsterdam. Pp. 47–68.

Land L. S. (1985) The origin of massive dolomite. *J. Geol. Educ*. **33**, 112–125.

Langmuir D. (1978) Uranium solution-mineral equilibria at low temperatures with applications to sedimentary ore deposits. *Geochim. Cosmochim. Acta* **42**, 542–569.

Lau K. V., Maher K., Altiner D., Kelley B. M., Kump L. R., Lehrmann D. J., Silva-Tamayo J. C., Weaver K. L., Yu M. and Payne J. L. (2016) Marine anoxia and delayed Earth system recovery after the end-Permian extinction. *Proc. Natl. Acad. Sci.* **113**, 2360–2365.

Lau K. V., Macdonald F. A., Maher K., Payne J. L. (2017) Uranium isotope evidence for temporary ocean oxygenation in the aftermath of the Sturtian Snowball Earth. *Earth Planet. Sci. Lett*. **458**, 282–292.

Le Heron D. P., Craig J. and Etienne J. L. (2009) Ancient glaciations and hydrocarbon accumulations in North Africa and the Middle East. *Earth-Sci. Rev*. **93**, 47–76.

Lee J. and Yun J. (2013) Formaion of ternary $CaUO_2(CO_3)_3^{2-}$ and $Ca_2UO_2(CO_3)_3$(aq) complexes under neutral to weakly alkaline conditions. *Dalton Trans*. **42**, 9862–9869.

LeGrande A. N. and Schmidt G. A. (2006) Global gridded data set of the oxygen isotopic composition in seawater. *Geophy. Res. Lett*. **33**, 10.1029/2006GL026011.

Lenton T. M., Boyle R. A., Poulton S. W., Shields-Zhou G. A. and Butterfield N. J. (2014) Co-evolution of eukaryotes and ocean oxygenation in the Neoproterozoic era. *Nat. Geosci*. **7**, 257–265.

Liu X., Hardisty D., Lyons T. W. and Swart P. K. (2015) Evaluating the integrity of the Ce anomaly as a paleoredox tracer using modern marine carbonates. In *AGU Fall Meeting, San Francisco, CA. #2253* (abstr.).

Lowenstein T. K., Kendall B. and Anbar A. D. (2013) The Geologic History of Seawater. In *Treatise on Geochemistry: Second Edition.* Vol. 8, pp. 569–622.

Lowenstein T. K., Hardie L. A., Timofeeff M. N. and Demicco R. V. (2003) Secular variation in seawater chemistry and the origin of calcium chloride basinal brines. *Geology* **31**, 857–860.

Lowenstein T. K., Timofeeff M. N. Kovalevych V. M. and Hortia J. (2005) The major-ion composition of Permian seawater. *Geochim. Cosmochim. Acta* **69**, 1701–1719.

Lowenstein T. K. and Demicco R. V. (2006) Elevated Eocene atmospheric CO_2 and its subsequent decline. *Science* **313**, 1928.

Lu Z., Jenkyns H. C. and Rickaby R. E. M. (2010) Iodine to calcium ratios in marine carbonate as a paleo-redox proxy during oceanic anoxic Events. *Geology* **38**, 1107–1110.

Lyons T. W., Reinhard C. T. and Planavsky N. J. (2014) The rise of oxygen in Earth's early ocean and atmosphere. *Nature* **506**, 307–315.

Lyons T. W., Anbar A. D., Severmann S., Scott C. and Gill B. C. (2009) Tracking euxinia in the ancient ocean: A multiproxy perspective and Proterozoic case study. *Annu. Rev. Earth Planet. Sci*. **37**, 507–34.

Mackenzie F. T., Morse J. W. (1992) Sedimentary carbonates through Phanerozoic time. *Geochim. Cosmochim. Acta* **56**, 3281–3295.

Malone M. (2000) Data report: Geochemistry and mineralogy of periplatform carbonate sediments: Sites 1006, 1008, and 1009, *in* Swart P. K., Eberli, G. P., Malone M. J. et al., ed., Proceedings of the Ocean Drilling Program: College Station, Texas, Ocean Drilling Program, Initial reports, v. 166, p. 145–152.

Martin G. D., Wilkinson B. H. and Lohmann K. C. (1986) The role of skeletal porosity in aragonite neomorphism-Strombus and Montastrea from the Pleistocene Key Largo Limestone, Florida. J. *Sediment. Petrol*. **56**, 194–203.

Martin P., Goodkin N. F., Stewart J. A., Foster G. L., Sikes E. L., White H. K., Hennige S. and Roberts J. M. (2016) Deep-sea coral $\delta^{13}C$: A tool to reconstruct the difference between seawater pH and $\delta^{11}B$-derived calcifying fluid pH. *Geophys. Res. Lett*. **43**, 299–308.

McConnaughey T., Burdett J., Whelan J. and Paull C. (1997) Carbon isotopes in biological carbonates: respiration and photosynthesis. *Geochim. Cosmochim. Acta* **61**, 611–622.

McCormick M. L., Banishki N., Powell S., Rumack A. and Garrett J. M. (2014) A low cost multi-level sampling device for synchronous aseptic collection of environmental water samples. *J. Microbiol. Methods* **105**, 51–53.

McMaus J., Berelson W. M., Klinkhammer G. P., Hammond D. E. and Holm C. (2005) Authigenic uranium: relationship to oxygen penetration depth and organic carbon rain. *Geochim. Cosmochim*. Acta **69**, 95–108.

Meece D. E. and Benninger L. K. (1993) The coprecipitation of Pu and other radionuclides with $CaCO_3$. *Geochim. Cosmochim. Acta* **57**, 1447–1458.

Melim L. A., Swart P. K. and Maliva R. G. (1995) Meteoric-like fabrics forming in marine waters: Implications for the use of petrography to identify diagenetic environments. *Geology*, **23**, 755–758.

Melim L. A., Westphal H., Swart P. K., Eberli G. P. and Munnecke A. (2002) Questioning carbonate diagenesis paradigms: Evidence from the Neogene of the Bahamas. *Mar. Geol*. **185**,

27–54.

Melim L. A., Swart P. K. and Eberli G. P. (2004) Mixing-zone diagenesis in subsurface of Florida and the Bahamas. *J. Sediment. Res.* **74**, 904–913.

Melim L. A., Swart P. K. and Maliva R. G. (2001) Meteoric and marine-burial diagenesis in the subsurface of Great Bahama Bank, subsurface geology of a prograding carbonate platform margin, Great Bahama Bank: results of the Bahamas Drilling Project. *Society for Sedimentary Geology*, 137–161.

Meyer K. M. and Kump L. R. (2008) Oceanic euxinia in Earth history: cause and consequences. *Annu. Rev. Earth and Planet. Sci*. **36**, 251–288.

Mills D. B., Ward L. M., Jones C., Sweeten B., Forth M., Treusch A. H. and Canfield D. E. (2014) Oxygen requirements of the earliest animals. *Proc. Natl. Acad. Sci.* **111**, 4168–4172.

Min G. R., Edwards R. L., Taylor F. W., Recy J., Gallup C. D. and Beck J. W. (1995) Annual cycles of U/Ca in coral skeletons and U/Ca thermometry. *Geochim. Cosmochim. Acta* **59**, 2025–2042.

Miner N. A. (1933) The origin and history of Green and Round Lakes in Green Lake State Park at Fayetteville, N. Y. MS. Thesis, Syracuse Univ.

Montoya-Pino C., Weyer S., Anbar A. D., Pross J., Oschmann W., Schootbrugge B. V. and Arz H. W. (2010) Global enhancement of ocean anoxia during Oceanic Anoxic Event 2: A quantitative approach using U isotopes. *Geology* **38**, 315–318.

Morin G., Mangeret A., Othmane G., Stetten L., Seder-Colomina M., Brest J., Ona-Nguema G., Bassot S., Courbet C., Guillevic J., Thouvenot A., Mathon O., Proux O. and Bargar J. R. (2016) Mononuclear U(IV) complexes and ningyoite as major uranium species in lake sediments. *Geochem. Persp. Let*. **2**, 95–105.

Morse, J. W., and Mackenzie, F. T., 1990, Geochemistry of sedimentary carbonates, Elsevier, New York.

Muramatsu Y., Tagami K. and Uchida S. (1994) Levels of artificial radionuclides and uranium in rain water collected from Ibaraki (Japan) following the Tomsk-7 accident in Russia. *J. Radioanal. Nucl. Chem*. **188**, 305–311.

Nakano E., Okazaki K. and Iwamatsu T. (1963) Accumulatio of radioactive calcium in larvae of the sea urchin *pseudocentrotus depressus*. *Biol. Bull*. **125**, 125–132.

Neumann A. C. and Land L. S. (1975) Lime mud deposition and calcareous algae in the bight of Abaco, Bahamas: A budget. *J. Sediment. Petrol*. **45**, 763–786.

Nielsen S. G., Mar-Gerrison S., Gannoun A., LaRowe D., Klemm V., Halliday A. N., Burton K. W. and Hein J. R. (2009) Thallium isotope evidence for a permanent increase in marine organic carbon export in the early Eocene. *Earth Planet. Sci*. **278**, 297–307.

Nooijer L. J. D., Toyofuku T. and Kitazato H. (2009) Foraminifera promote calcification by elevating their intracellular pH. *Proc. Natl. Acad. Sci.* **106**, 15374–15378.

Noordmann J., Weyer S., Montoya-Pino C., Dellwig O., Neubert N., Eckert S., Paetzel M. and Böttcher M. E. Uranium and molybdenum isotope systematics in modern euxinic basins: case studies from the central Baltic Sea and the Kyllaren fjord (Norway). *Chem. Geol*. **396**, 182–195.

Oehlert A. M. and Swart P. K. (2014) Interpreting carbonate and organic carbon isotope covariance in the sedimentary record. *Nat. Commun*. **5**, 4762. doi:10.0138/ncomms5672.

Ohde S. and van Woesik R. (1999) Carbon dioxide flux and metabolic processes of a coral reef, Okinawa. *Bull. of Mar. Sci.* **65**, 559–576.

Ortegón-Aznar I., Chuc-Contreras A. and Collado-Vides L. (2017) Calcareous green algae standing stock in a tropical sedimentary coast. *J. of Appl. Phycol.* **29**, 2685–2693.

Owens J. D., Nielsen S. G., Horner T. J., Ostrander C. M. and Peterson L. C. (2017) Thallium-isotopic compositions of euxinic sediments as a proxy for global manganese-oxide burial. *Geochim. Cosmochim. Acta* **213**, 291–307.

Parkhurst D. L. and Appelo C. A. (2004) User's Guide to PHREEQC (Version 2)—A Computer Program for Speciation, Batch-Reaction, One-Dimension Transport, and Inverse Geochemical Calculations. U. S. Geological Survey: Reston, VA.

Partin C. A., Bekker A., Planavsky N. J., Scott C. T., Gill B. C., Li C., Podkovyrov V., Maslov A., Konhauser K. O., Lalonde S. V., Love G. D., Poulto S. W. and Lyons T. W. (2013) Large-scale fluctuations in Precambrian atmospheric and oceanic oxygen levels from the record of U in shales. *Earth Planet. Sci. Lett*. **369-370**, 284–293.

Payne, J.L., Turchyn, A.V., Paytan, A., DePaolo, D.J., Lehrmann, D.J., Yu, M. and Wei, J. (2010) Calcium isotope constraints on the end-Permian mass extinction. *Proc. Natl. Acad. Sci.* **107**, 8543–8548.

Pearson P. N., Foster G. L. and Wade B. S. (2009) Atmospheric carbon dioxide through the Eocene-Oligocene climate transition. *Nature* **461**, 1110–1113.

Pingitore N. E., Iglesias A., Lytle F. and Wellington G. M. (2002) X-Ray absorption spectroscopy of uranium at low ppm levels in coral skeletal aragonite. *Microchem. J*. **71**, 261–266.

Planavsky N. J., Asael D., Hofmann A., Reinhard C. T., Lalonde S. V., Knudsen A., Wang X., Ossa F. O., Pecoits E., Smith A. J. B., Beukes N. J., Bekker A., Johnson T. M., Konhauser K. O.,

Lyons T. W. and Rouxel O. J. (2014) Evidence for oxygenic photosynthesis half a billion years before the Great Oxidation Event. *Nat. Geosci*. **7**, 283–286.

Planavsky N. J., Bekker A., Hofmann A., Owens J. D. and Lyons T. W. (2012) Sulfur record of rising and falling marine oxygen and sulfate levels during the Lomagundi event. Proc. *Natl. Acad. Sci. U. S. A*. **109**, 18300–18305.

Pretet C., Samankassou E., Felis T., Reynaud S., Böhm F., Eisenhauer A., Ferrier-Pagès C., Gattuso J. P. and Camoin G. (2013) Constraining calcium isotope fractionation ($\delta^{44/40}$Ca) in modern and fossil scleractinian coral skeleton. *Chem. Geol*. **340**, 49–58.

Proemse B. C., Grasby S. E., Wieser M. E., Mayer B. and Beauchamp B. (2013) Molybdenum isotopic evidence for oxic marine conditions during the latest Permian extinction. *Geology* **41**, 967–970.

Prokoph A., Shields G. A. and Veizer J. (2008) Compilation and time-series analysis of a marine carbonate δ^{18}O, δ^{13}C, ^{87}Sr/^{86}Sr and δ^{34}S database through Earth history. *Earth Sci. Rev*. **87**, 113–133.

Pufahl P. K. and Hiatt E. E. (2012) Oxygenation of the Earth's atmosphere-ocean system: A review of physical and chemical sedimentologic responses. *Mar. Petrol. Geol*. **32**, 1–20.

Raddatz J., Rüggeberg A., Flögel S., Hathorne E. C., Liebetrau V., Eisenhauer A. and Dullo W. Chr. (2014) The influence of seawater pH on U/Ca ratios in the scleractinian cold-water coral *Lopheliapertusa*. *Biogeosciences* **11**, 1863–1871.

Rademacher L. K., Lundstrom C. C., Johnson T. M., Sanford R. A., Zhao J. and Zhang Z. (2006) Isotope fractionation during reduction of hexavalent U by bacteria and zero valent by iron. *Environ. Sci. Technol*. **40**, 6943–6948.

Reeder R. J., Nugent M., Lamble G. M., Tait C. D. and Morris D. E. (2000) Uranyl incorporation into calcite and aragonite: XAFS and luminescence studies. *Environ. Sci. Technol.* **34**, 638–644.

Reeder R. J., Nugent M., Tait C. D., Morris D. E., Heald S. M., Beck K. M., Hess W. P. and Lanzirotti A. (2001) Coprecipitation of uranium(VI) with calcite: XAFS, micro-XAS, and luminescence characterization. *Geochim. Cosmochim. Acta* **65**, 3491–3503.

Reinhard C. T., Planavsky N. J., Olson S. L., Lyons T. W. and Erwin D. H. (2016) Earth's oxygen cycle and the evolution of animal life. *Proc. Natl. Acad. Sci.* **113**, 8933–8938.

Ridgwell A. (2005) A mid Mesozoic revolution in the regulation of ocean chemistry. *Mar. Geol*. **217**, 339–357.

Rolison J. M., Stirling C. H., Middag R. and Rijkenberg M. J. A. (2017) Uranium stable isotope fractionation in the Black Sea: Modern calibration of the ^{238}U/^{235}U paleo-redox proxy. *Geochim. Cosmochim. Acta* **203**, 69–88.

Rollion-Bard C. and Erez J. (2010) Intra-shell boron isotope ratios in the symbiont-bearing benthic foraminiferan *Amphisteginalobifera*: Implications for $\delta^{11}B$ vital effects and paleo-pH reconstructions. *Geochim. Cosmochim. Acta* **74**, 1530–1536.

Romaniello S. J., Brennecka G., Anbar A. D. and Colman A. S. (2009) Natural isotopic fractionation of $^{238}U/^{235}U$ in the water column of the Black Sea. In *AGU Fall Meeting*. San Francisco, CA. #V54C-06 (abstr.).

Romaniello S. J., Herrmann A. D. and Anbar A. D. (2013) Uranium concentrations and $^{238}U/^{235}U$ isotope ratios in modern carbonates from the Bahamas: Assessing a novel paleoredox proxy. *Chem. Geol*. **362**, 305–316.

Rosenheim B. E., Swart P. K. and Thorrold S. R. (2005) Minor and trace elements in sclerosponge Ceratoporella nicholsoni: biogenic aragonite near the inorganic endmember? *Palaeogeogr. Palaeoclim. Palaeocol*. **228**, 109–129.

Royer T. K. (2013) Atmospheric CO_2 and O_2 during the Phanerozoic: Tools, Patterns, and Impacts. In *Treatise on Geochemistry: Second Edition*. Vol. 6, pp.251–267.

Royer D. L., Berner R. A., Montanez I. P. and Beerling D. J. (2004) CO_2 as a primary driver of Phanerozoic climate. *GSA Today* **14**, 4–10.

Russell A. D., Hönisch B., Spero H. J. and Lea D. W. (2004) Effects of seawater carbonate ion concentration and temperature on shell U, Mg, and Sr in cultured planktonic foraminifera. *Geochim. Cosmochim. Acta* **68**, 4347–4361.

Russell A. D., Emerson S., Nelson B. K., Erez J. and Lea D. W. (1994) Uranium in forminiferal calcite as a recorder of seawater uranium concentrations. *Geochim. Cosmochim. Acta* **58**, 671–681.

Schaller M. F., Wright J. D. and Kent D. V. (2011) Atmospheric pCO_2 perturbations associated with the Central Atlantic Magmatic Province. *Science* **331**, 1404–1409.

Schidlowski M. (1988) A 3,800-million-year isotopic record of life from carbon in sedimentary rocks. *Nature* **333**, 313–318.

Schlanger S. O. and Douglas R. G. (1974) The pelagic ooze-chalk—limestone transition and its implication for marine stratigraphy. *Spec. Publ. Int. Assoc. Sedimentol*. 1, 117–148.

Seki O., Foster G. L., Schmidt D. N., Mackensen A., Kawamura K. and Pancost R. D. (2010) Alkenone and boron-based Pliocene pCO_2 records. *Earth. Planet. Sci. Lett*. **292**, 201–211.

Shen G. T. and Dunbar R. B. (1995) Environmental controls on uranium in reef corals. *Geochim. Cosmochim. Acta* **59**, 2009–2024.

Shiel A. E., Laubach P. G., Johnson T. M., Lundstrom C. C., Long P. E. and Williams K. H.

(2013) No measurable changes in $^{238}U/^{235}U$ due to desorption-adsorption of U(VI) from ground-water at the Rifle, Colorado, integrated field sesearch challenge site. *Environ. Sci. Technol*. **47**, 2535–2541.

Shields G. and Veizer J. (2002) Precambrian marine carbonate isotope database: Version 1.1. *Geochem. Geophys. Geosyst*. **3**, 1–12.

Siebert C., Nägler T. F., von Blanckenburg F. and Kramers J. D. (2003) Molybdenum isotope records as a potential new proxy for paleoceanography. *Earth. Planet. Sci. Lett.* **211**, 159–171.

Song H., Song H., Algeo T. J., Tong J., Romaniello S. J., Zhu Y., Chu D., Gong Y. and Anbar A. D. (2017) Uranium and carbon isotopes document global-ocean redox productivity relationships linked to cooling during the Frasnian-Famennian mass extinction. *Geology* **45**, 887–890.

Stanley, S. M. (2007) An analysis of the history of marine animal diversity. *Paleobiology*, **33**, 1–55.

Stewart J. A., Gutjahr M., Pearce F., Swart P. K. and Foster G. L. (2015) Boron during meteoric diagenesis and its potential implications for Marinoal snowball Earth δ^{11}B-pH excursions. *Geology*, **43**, 627–630.

Stirling C. H., Andersen M. B., Potter E. K. and Halliday A. N. (2007) Low-temperature isotopic fractionation of uranium. *Earth. Planet. Sci. Lett*. **264**, 208–225.

Stirling C. H., Anderson M. B., Warthmann R. and Halliday A. N. (2015) Isotope fractionation of ^{238}U and ^{235}U during biologically-mediated uranium reduction. *Geochim. Cosmochim. Acta* **163**, 200–218.

Stüeken E. E., and Buick R. and Schauer A. J. (2015) Nitrogen isotope evidence for alkaline lakes on late Archean contients. *Earth. Planet. Sci. Lett.* **411**, 1–10.

Sturchio N. C., Antonio M. R., Soderholm L., Sutton S. R. and Brannon J. C. (1998) Tetravalent uranium in calcite. *Science*, **281**, 971–973.

Stylo M., Neubert N., Wang Y., Monga N., Romaniello S. J., Weyer S. and Bernier-Latmani R. (2015) Uranium isotopes fingerprint biotic reduction. *Proc. Natl. Acad. Sci.* **112**, 5619–5624.

Swart P. K. and Hubbard J. A. E. B. (1982) Uranium in coral skeletons. *Coral Reefs* **1**, 13–19.

Swart P. K. (2015) The geochemistry of carbonate diagenesis: the past, present and future. *Sedimentology*, **62**, 1233–1304.

Swart P. K. and Oehlert A. M. (2018) Revised interpretations of stable C and O patterns in carbonate rocks resulting from meteoric diagenesis. *Sediment. Geol*. **364**, 14–23.

Swart P. K. (2000) The oxygen isotopic composition of interstitial waters: Evidence for fluid flow and recrystallization in the margin of the Great Bahama Bank. *Proceedings of the Ocean Drilling Program: Scientific Results* **166**, 91–98.

Swart P. K., Elderfield H. and Ostlund G. (2001) The geochemistry of pore fluids from bore holes in the Great Bahama Bank, subsurface geology of a prograding carbonate platform margin, Great Bahama Bank: results of the Bahamas Drilling Project. *Society for Sedimentary Geology*, 163–173.

Swart P. K. and Melim L. A. (2000) The origin of dolomites in Tertiary sediments from the margin of Great Bahama Bank. *J. Sediment. Res*. **70**, 738–748.

Swart P. K., Reijmer J. J. G. and Otto R. (2009) A re-evaluation of facies on Great Bahama Bank II: variations in the $\delta^{13}C$, and $\delta^{18}O$ and mineralogy of surface sediments. *Int. Assoc. Sedimentol. Spec. Publ.* **41**, 47–59.

Takahashi T., Broecker W. S., Li Y. H. and Thurber D. L. (1968) Chemical and isotopic balances for a meromictic lake. *Limnol. Oceanogr*. **13**, 272–292.

Tambutté T., Tambutté S., Segonds N., Zoccola D., Venn A., Erez J. and Allemand D. (2012) Calcein labelling and electrophysiology: Insights on coral tissue permeability and calcification. *Proc.R. Soc. London, Ser. B* **219**, 19–27.

Tanaka K., Holcomb M., Takahashi A., Kurihara H., Asami R., Shinjo R., Sowa K., Rankenburg K., Watanabe T. and McCulloch M. (2015) Response of *Acroporadigitifera* to ocean acidification: constrains from $\delta^{11}B$, Sr, Mg, and Ba compositions of aragonitic skeletons cultured under variable seawater pH. *Coral Reefs*, **34**, 1139–1149.

Taylor S. R. and McLennan S. M. (1995) The geochemical evolution of the continental crust. *Rev. Geophys*. **33**, 241–265.

Thannickal V. J. (2009) Oxygen in the evolution of complex life and the price we pay. *Am. J. Respir. Cell Molec. Biol*. **40**, 507–510.

Thompson J. B., Ferris F. G. and Smith D. A. (1990) Geomicrobiology and sedimentology of the mixolimnion and chemocline in Fayetteville Green Lake, New York. *Palaios.* 52–75.

Thompson J. B. and Ferris F. G. (1990) Cyanobacterial precipitation of gypsum, calcite, and magnesite from natural alkaline lake water. *Geology* **18**, 995–998.

Thompson J. B., Schultze-Lam S., Beveridge T. J. and Des Marais D. J. (1997) Whiting events: Biogenic origin due to the photosynthetic activity of cyanobacterial picoplankton. *Limnol. Oceanogr*. **42**, 133–141.

Thurber D. L. (1962) Anomalous ^{234}U-^{238}U in nature. *J. Geophys. Res*. **67**, 4518–4520.

Timofeeff M. N., Lowenstein T. K., da Silva A. M. and Harris N. B. (2006) Secular variation in the major-ion chemistry of seawater: Evidence from fluid inclusions in Cretaceous halites. *Geochim. Cosmochim. Acta* **70**, 1977–1994.

Tissot F. L. H. and Dauphas N. (2015) Uranium isotopic compositions of the crust and ocean: Age corrections, U budget and global extent of modern anoxia. *Geochim. Cosmochim. Acta* **167**, 113–143.

Tissot F. L. H., Chen C., Go. B. M., Naziemiec M., Healy G., Bekker A., Swart P. K. and Dauphas N. (2018) Controls of eustasy and diagenesis on the $^{238}U/^{235}U$ of carbonates and evolution of the seawater ($^{234}U/^{238}U$) during the last 1.4 Myr. *Geochim. Cosmochim. Acta in press*.

Torgersen T., Hammond D. E., Clarke W. B. and Peng T. H. (1981) Fayetteville Green Lake, New York: ^{3}H-^{3}He water mass ages and secondary chemical structure. *Limnol. Oceanogr*. **26**, 110–122.

Tourtelot H. A. (1979) Black shales—its deposition and diagenesis. *Clays Clay Miner*. **27**, 313–321.

Tribovillard N., Algeo, T. J., Lyons T. and Riboulleau A. (2006) Trace metals as paleoredox and paleoproductivity proxies: An update. *Chem. Geol.* **232**, 12–32.

Tripati A. K., Roberts C. D. and Eagle R. A. (2009) Coupling of CO_2 and ice sheet stability over major climate transitions of the last 20 million years. *Science* **326**, 1394–1397.

Trotter J., Montagna P., McCulloch M., Silenzi S., Reynaud S., Mortimer G., Martin S., Ferrier-Pages C., Gattuso J. P. and Rodolfo-Metalpa R. (2011) Quantifying the pH 'vital effect' in the temperature zooxanthellate coral *Cladocoracaespitosa*: Validation of the boron seawater pH proxy. *Earth. Planet. Sci. Lett.* **303**, 163–173.

Veizer J., Ala D., Azmy K., Bruckschen P., Buhl D., Bruhn F., Carden G. A. F., Diener A., Ebneth S., Godderis Y., Jasper T., Korte C., Pawellek F., Podlaha O. G. and Strauss H. (1999) $^{87}Sr/^{86}Sr$, $\delta^{13}C$ and $\delta^{18}O$ evolution of Phanerozoic seawater. *Chem. Geol*. **161**, 59–88.

Verbruggen A., Alonso-Munoz A., Eykens R., Kehoe F., Kuhen H., Richter S. and Arbegbe Y. (2008) Preparation and certification of IRMM-3636, IRMM-3636a and IRMM-3636b. OPOCE*, 24pp*.

Voegelin A. R., Nägler T. F., Beukes N. J. and Lacassie J. P. (2010) Molybdenum isotopes in late Archean carbonate rocks: Implications for early Earth oxygenation. *Precambrian Res*. **182**, 70–82.

Vollstaedt H., Eisenhauer A., Wallmann Klaus., Böhm F., Fietzke J., Liebetrau V., Krabbenhöft A., Farkaš J., Tomaš ovych A., Raddatz Jacek. and Veizer J. (2014) The Phanerozoic $\delta^{88/86}Sr$

record of seawater: New constrains on past changes in oceanic carbonate fluxes. *Geochim. Cosmochim. Acta*, **128**, 249–265.

Wang X. L, Planavsky N. J., Hull P. M., Tripati A. E., Zou H. J., Heneha M. (2017) Chromium isotopic composition of core-top planktonic foraminifera. *Geobiology* doi: 10.1111/gbi.12198.

Wang X., Johnson T. M. and Lundstrom C. C. (2015a) Isotope fractionation during oxidation of tetravalent uranium by dissolved oxygen. *Geochim. Cosmochim. Acta* **150**, 160–170.

Wang X., Planavsky N. J., Reinhard C. T., Hein J. R. and Johnson T. M. (2016) A Cenozoic seawater record derived from $^{238}U/^{235}U$ in ferromanganese crusts. *Am. J. Sci*. **316**, 64–83.

Wang X., Johnson T. M. and Lundstrom C. C. (2015b) Low temperature equilibrium isotope fractionation and isotope exchange kinetics between U(IV) and U(VI). *Geochim. Cosmochim. Acta* **158**, 262–275.

Wedepohl K. H. (1971) Environmental influences on the chemical composition of shales and clays. In: Ahrens L. H., Press F., Runcorn S. K. and Urey H. C. (Eds.), *Physics and Chemistry of the Earth*. Pergamon, Oxford, pp. 305–333.

Wedepohl K. H. (1991) The composition of the upper Earth's crust and the natural cycles of selected metals. In: Merian E. (Ed.), *Metals and their Compounds in the Environment*. VCH-Verlagsgesellscraft, Weinheim, pp. 3–17.

Weiner S. and Dove P. M. (2003) An overview of biomineralization processes and the problem of the vital effect. *Rem. Mineral. Geochem.* **54**, 1–29.

Wen H., Fan H., Zhang Y., Cloquet C. and Carignan J. (2015) Reconstruction of early Cambrian ocean chemistry from Mo isotopes. *Geochim. Cosmochim. Acta* **164**, 1–16.

Weyer S., Anbar A. D., Gerdes A., Gordon G. W., Algeo T. J. and Bolye E. A. (2008) Natural fractionation of $^{238}U/^{235}U$. *Geochim. Cosmochim. Acta* **72**, 345–359.

Wilhelm M. B. and Hewson I. (2012) Characterization of thrombolytic bioherm cyanobacterial assemblages in a meromictic marl lake (Fayetteville Green Lake, New York). *Geomicrobiol. J.* **29**, 727–732.

Wille M., Kramers J. D., Nägler T. F., Beukes N. J., Schröder S., Meisel Th., Lacassie J. P. and Voegelin. (2007) Evidence for a gradual rise of oxygen between 2.6 and 2.5 Ga from Mo isotopes and Re-PGE signatures in shales. *Geochim. Cosmochim. Acta* **71**, 2417–2435.

Wille M., Nebel O., Kranendonk M. J. K., Schoenberg R., Kleinhanns I. C. and Ellwood M. J. (2013) Mo-Cr isotope evidence for a reducing Archean atmosphere in 3.46–2.76 Ga black shales from the Pilbara, Western Australia. *Chem. Geol.* **340**, 68–76.

Wizemann A., Meyer F. W. and Westphal H. (2014) A new model for the calcification of the green macro-alga *Halimeda opuntia* (Lamouroux). *Croal Reefs* **22**, 951–964.

Wray J. L. (1977) Calcareous Algae Developments in Paleontology and Stratigraphy, Volume 4. Elsevier, Amsterdam.

Wunder S. J. (1974) Diagenetic Features and Inferred Diagenetic Processes in Partially Altered Corals from the Key Largo Limestone (Pleistocene) South Florida. Masters Thesis, University of Illinois-Urbana.

Xu L., Lehmann B., Mao J., Nägler T. F., Neubert N., Böttcher M. E. and Escher P. (2012) Mo isotope and trace element patterns of Lower Cambrian black shales in South China: Multi-proxy constraints on the paleoenvironment. *Chem. Geol.* **318–319**, 45–49.

Yang S., Kendall B., Lu X., Zhang F. and Zheng W. (2017) Uranium isotope compositions of mid-Proterozoic black shales: Evidence for an episode of increased ocean oxygenation at 1.36 Ga and evaluation of the effect of post-depositional hydrothermal fluid flow. *Precambrian. Res*. **298**, 187–201.

Zerkel A. L., Kamyshny Jr A., Kump L. R., Farquhar J., Oduro H. and Arthur M. A. (2010) Sulfur cycling in a stratified euxinic lake with moderately high sulfate: Constraints from quadruple S isotopes. *Geochim. Cosmochim. Acta* **74**, 4953–4970.

Zhang F., Algeo T. J., Romaniello S. J., Cui Y., Zhao L., Chen Z. and Anbar A. D. (2018a) Congruent Permian-Triassic $\delta^{238}U$ records at Panthalassic and Tethyan sites: Confirmation of global-oceanic anoxia and validation of the U-isotope paleoredox proxy. *Geology* **46**, 327–330.

Zhang F., Romaniello S. J., Algeo T. J., Lau K. V., Clapham M. E., Richoz S., Herrmann A. D., Smith H., Horacek M. and Anbar A. D. (2018b) Multiple episodes of extensive marine anoxia linked to global warming and continental weathering following the latest Permian mass extinction. *Sci. Adv*. **4**, 61602921.

Zhou X., Thomas E., Rickaby R. E. M., Winguth A. M. E. and Lu Z. (2014) I/Ca evidence for upper ocean deoxygenation during the PETM. *Paleoceanography* **29**, 964–975.

Zhou X., Jenkyns H. C., Owens J. D., Junium C. K., Zheng X., Sageman B. B., Hardisty D. S., Lyons T. W., Ridgwell A. and Lu Z. (2015) Upper ocean oxygenation dynamics from I/Ca ratios during the Cenomanian-Turonian OAE 2. *Oceanography* **30**, 510–526.

Zoccola D., Tambutte E., Kulhanek E., Puverel S., Scimeca J., Allemand D., Tambutte S. (2004) Molecular cloning and localization of a PMCA P-type calcium ATPase from the coral *Stylophorapistillata*. *BBA-biomembranes* **1663**, 117–126.

APPENDIX A

SUPPLEMENTARY INFORMATION FOR CHAPTER 3

Text A.1 Statistical analyses

In Table A.1, I present the average and standard deviation for $\delta^{238}U$ in corals, algae and all primary biogenic carbonates and modern seawater. Student's t test in Table A.2 demonstrates that $\delta^{238}U$ in corals, algae and all primary biogenic carbonates are statistically different from modern seawater with *p* values <0.05.

Table A.1 $\delta^{238}U$ in corals, algae and all primary biogenic carbonates vs. modern seawater

Terms	Coral	Calcareous algae	Biogenic	Seawater
$\delta^{238}U_{mean}$	–0.372	–0.354	–0.357	–0.392
2 SD	0.008	0.036	0.052	0.046
N	6	8	17	22

Note: Biogenic represents all the primary biogenic carbonates. Algae includes green and red algae. $\delta^{238}U$ in modern seawater is from Tissot and Dauphas (2015).

Table A.2 Student's t-test of $\delta^{238}U$ in corals, algae and all primary biogenic carbonates vs. modern seawater

Student's t-test groups	d*f*	*t*	*p*	$\Delta^{238}U$
Coral-Seawater	27	2.151	0.04	0.020
Calcareous algae-Seawater	29	4.317	<0.01	0.038
Biogenic-Seawater	38	4.529	<0.01	0.035

Note: d*f* is the degree of freedom. *p* values are 95 % confidence level. Calcareous algae include green and red algae. Biogenic means all the primary biogenic carbonate samples in this study.

Text A.2 U partition coefficients in abiotic aragonite coprecipitation experiments

To explore the correlation of U isotope fractionation during U incorporation into $CaCO_3$ with U partition coefficients (K_d) and carbonate growth rate (R), I revisit the experimental data from my previous abiotic aragonite coprecipitation experiments (Chen et al., 2016). The basic experimental conditions and measured concentrations of U and Ca in the aqueous solution and aragonite are displayed in Table A.3. The U partition coefficient in abiotic aragonite coprecipitation experiments is calculated using equation A.3. Because the pH, carbonate ion concentration, temperature, and aragonite growth rate stayed invariant over the duration of each aragonite coprecipitation experiment, the U partition coefficients estimated at all sampling intervals showed a good linear regression (R^2=0.8483–0.9777). Thus, I used the average ratios of $([U]/[Ca])_{CaCO3}$ to $([U]/[Ca])_{aqueous}$ of all the samples from each experiment.

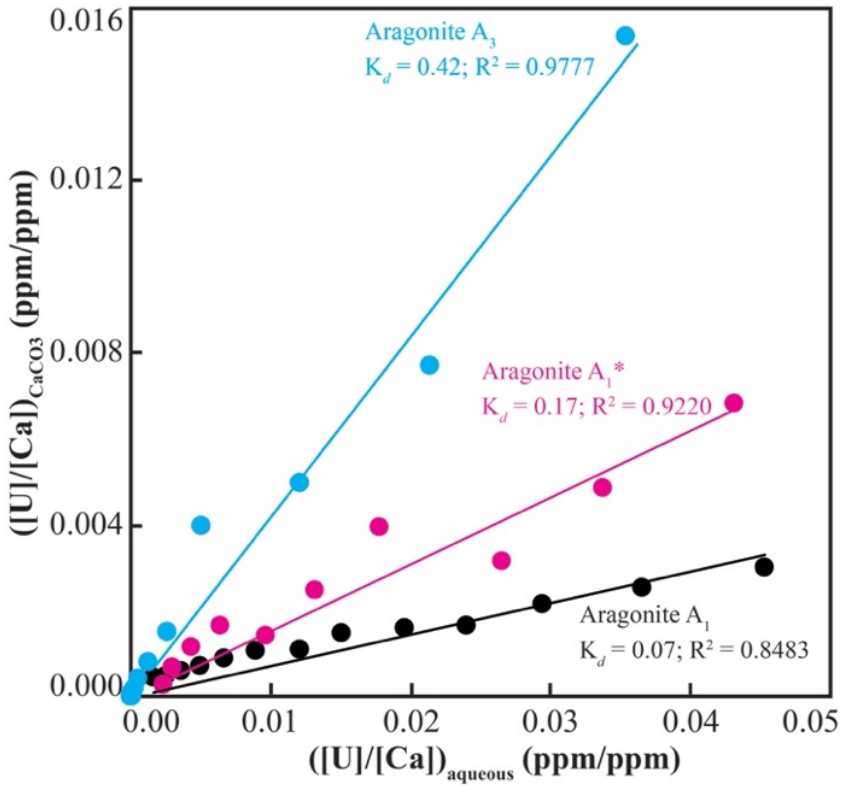

Figure A.1. $([U]/[Ca])_{CaCO3}$ versus $([U]/[Ca])_{aqueous}$ in abiotic aragonite coprecipitation experiments (A_1, A_1* and A_3; Chen et al., 2016). The black, pink, and blue solid circles stand for concentrations of U to Ca in the solid and aqueous solution at different sampling intervals for experiments A_1, A_1* and A_3. The colored lines represent the linear regression of the data points in each experiment.

Text A.3 Estimation of carbonate bulk growth rates in abiotic aragonite coprecipitation experiments

The saturation sate ($\Omega_{aragonite}$) of the fluid relative to aragonite was calculated using the equation:

$$\Omega_{aragonite} = \frac{a_{Ca^{2+}} a_{CO_3^{2-}}}{K_{sp}} \quad \text{Eq. A.1}$$

where a_{Ca2+} and a_{CO32-} are activities of calcium and carbonte ions. K_{sp} is the solubility product of aragonite (=6.24; Mucci, 1983). With the experimental conditions of alkalinity (Table A.3), the calculation of $\Omega_{aragonite}$ was performed using the software PHREEQC (Parkhurst and Appelo, 2004).

The bulk growth rate (R in mmol m^{-2} hr^{-1}) of the abiotic aragonite from 3.5 % salinity at 25 °C was estimated using the equation (Zhong and Mucci, 1989):

$$\log R = 2.36 \log\left(\Omega_{aragonite} - 1\right) + 1.09 \quad \text{Eq. A.2}$$

Text A.4 U in blanks and $\delta^{238}U$ in CRM-145a after UTEVA column chemistry

Blanks and the reference standard pure CRM-145a were processed exactly as those natural biogenic carbonate samples through UTEVA column chemistry and measured on MC-ICP-MS. The U concentration in the blanks and $\delta^{238}U$ in CRM-145a were reported in Table A.3.

Table A.3. U in blanks and $\delta^{238}U$ in the reference standard CRM-145a

Sample	U ng	Mean ng	2 SD ng	N	Sample	$\delta^{238}U$ ‰	Mean ‰	2 SD ‰	N
Blank_01	0.1				CRM1451_01	0.02			
Blank_02	0.12				CRM1451_02	–0.01			
Blank_03	0.11	0.09	0.05	6	CRM1451_03	0.01	0.00	0.03	6
Blank_04	0.07				CRM1451_04	0.00			
Blank_05	0.07				CRM1451_05	–0.02			
Blank_06	0.07				CRM1451_06	0.01			

Note: The reference standard measured here were pure CRM-145a processed through UTEVA column chemistry as those natural biogenic carbonate samples.

APPENDIX B

SUPPLEMENTARY INFORMATION FOR CHAPTER 4

Text B.1. Statistical analysis of $\delta^{238}U$ in different types of diagenetic carbonates

Because some groups of the $\delta^{238}U$ data follow normal distribution, I used the Wilcoxon-Mann-Whitney (WMW) test to determine whether there is a statistically-significant difference between the average $\delta^{238}U$ value in primary, syndepositional and post-depositional carbonates (Table B.1). I used the same approach to test for statistically-significant differences between average $\delta^{238}U$ values in sediment samples categorized as having undergone meteoric, mixing-zone and phreatic marine diagenesis.

The results showed that $\delta^{238}U$ in primary carbonates are significantly lighter than those in syndepositional and post-depositional carbonates (p<0.01), while syndepositional and post-depositional carbonates have indistinguishable $\delta^{238}U$ values (p=0.75). U isotope fractionation induced by phreatic meteoric diagenesis is likewise indistinguishable from phreatic marine diagenesis (p=0.66), while $\delta^{238}U$ altered by vadose meteoric diagenesis is statistically heavier than phreatic meteoric and marine diagenesis (p<0.01).

Table B.1. Mean and standard deviation of $\delta^{238}U$ in different types of carbonate samples

Groups of carbonates	Number	$\delta^{238}U_{\_mean}$ (‰)	1 SD (‰)
Primary	22	–0.37	0.06
Syndepositional	23	–0.13	0.10
Post-depositional	96	–0.12	0.14
Vadose meteoric	11	0.03	0.22
Phreatic meteoric	17	–0.17	0.12
Marine phreatic	68	–0.14	0.11

Table B.2. WMW test of $\delta^{238}U$ for different types of carbonate diagenesis

Groups of carbonates	z-value	P
Primary-Syndepositional	–5.42	< 0.01
Primary-Post-depositional	–6.19	< 0.01
Syndepositional-Post-depositional	–0.30	0.75
Vadose meteoric-Phreatic meteoric	2.17	< 0.01
Vadose meteoric-Marine phreatic	3.30	< 0.01
Phreatic meteoric-Marine phreatic	–0.44	0.66

Text B.2. Spearman's rank correlation analyses of $\delta^{238}U$ and U concentration versus diagenetic indicators

In order to evaluate correlations between diagenetically-induced U isotope fractionation and several common proxies for carbonate diagenesis, I conducted Spearman's rank correlation analysis of sediment U concentrations and $\delta^{238}U$ with geochemical indicators of diagenetic alteration ($\delta^{13}C$, $\delta^{18}O$ and Mn/Sr), recrystallization from aragonite to calcite (Sr/Ca) or to dolomite (Mg/Ca), detrital input (Al and Th concentrations, and U/Al and Th/U), abundances of redox-sensitive elements (V, Fe, Mo, Re and U), Iodine (I) to (Mg + Ca) ratio, carbonate

mineralogy, and rare earth elements (REEs) anomaly (Ce/Ce* and Eu/Eu*) for meteoric, mixing-zone, and phreatic marine diagenesis.

Neither $\delta^{238}U$ nor U concentration in meteoric, mixing-zone, and phreatic marine diagenesis are statistically correlated with these geochemical parameters, except that U concentration showed moderate correlation with carbonate mineralogy. Specifically, U concentration increases with the fraction of calcite (r=0.61; p=0.04) but decreases with aragonite (r=- 0.61; p=0.04), inconsistent with the preferentially incorporation of U(VI) into aragonite relative to calcite (Reeder et al., 2000).

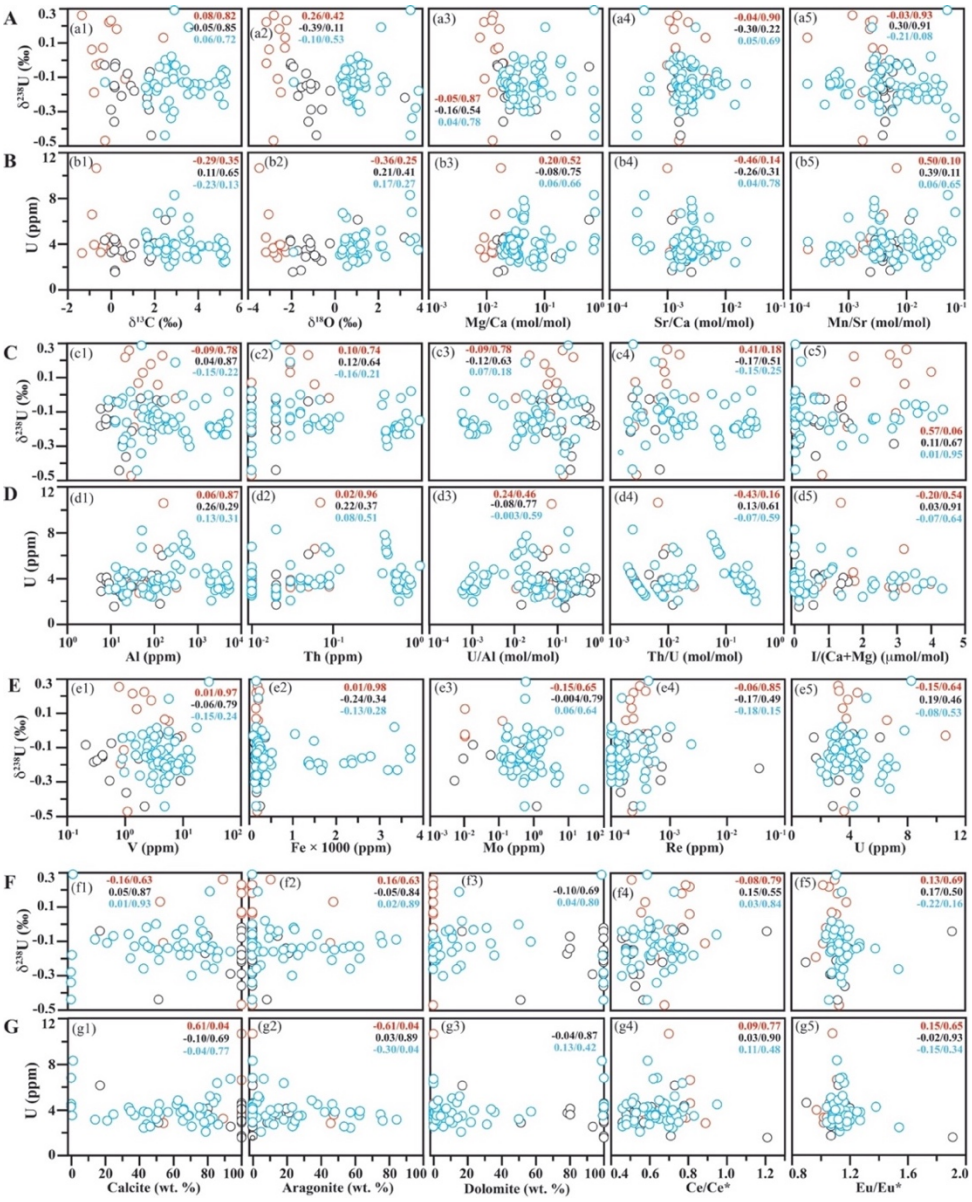

Figure B.1. Comparison of $\delta^{238}U$ (A, C, E and F) and U concentration (B, D, G) to geochemical indicators of carbonate diagenesis ($\delta^{13}C$, $\delta^{18}O$, Mg/Ca, Sr/Ca, Mn/Sr, carbonate mineralogy), detrital input (Al and Th concentrations, and U/Al and Th/U), concentrations of redox-sensitive elements (V, Fe, Mo, Re and U), I/(Ca+Mg), and rare earth elements anomaly (Ce/Ce* and Eu/Eu*) for vadose meteoric (red), phreatic meteoric (black), and phreatic marine diagenesis (blue) in drill cores Clino, Unda and Site 1006. Spearman's rank coefficients (e. g., 0.16/0.63 represents Spearman's rank coefficient *r*/*p*-value) are listed in the same color scheme as data points for different types of carbonate diagenesis (red for vadose meteoric, black for phreatic meteoric, and blue for phreatic marine).

Text B.3. Fluid-rock interaction model

To quantitatively evaluate carbonate diagenesis on alteration of U isotopic compositions in primary carbonates, I applied the open-system fluid-rock interaction model (Banner and Hanson, 1990; Jacobsen and Kaufman, 1999) to track the simultaneous evolution of the concentrations of Mn, Sr and U, and isotopic ratios of $^{13}C/^{12}C$, $^{18}O/^{16}O$, and $^{238}U/^{235}U$ during primary carbonate precipitates alteration by meteoric and marine fluids. In this model, I assume the primary carbonate mineralogy is aragonite and is altered to calcite. All the parameters for the fluid-rock interaction model (e.g., distribution coefficients, and isotope fractionation factors between the rock and the fluid) are displayed in Table B.3.

The parameters for the fluid-rock interaction model here were chosen according to the published data of the Bahamas or the typical values from previous studies in other locations. The elemental concentration of Ca, Mn, and Sr were chosen from previous published data from the Bahamas (Hu and Burdige, 2007; Swart et al., 2009; Whitaker and Smart, 2007). Under oxic conditions, U concentration in meteoric and marine fluids is 3 ppb, respectively (Henderson et al., 1999). Under anoxic conditions, the soluble U(IV) concentrations in meteoric and marine fluids are assigned as 0.5 ppb (Henderson et al., 1999). The partition coefficients (K_d) of C, O, Ca, Mn, Sr and U in calcite were taken from Curti (1999) and Sturchio et al (1998).

The initial $\delta^{13}C$ and $\delta^{18}O$ in the meteoric and marine fluids were the measured values of the Bahamas (Bowen and Revenaugh, 2003; Swart et al., 2009). U isotopic compositions in the meteoric and marine fluids were -0.30 (similar to continental crust) and –0.39 ‰ (modern seawater value), respectively. The initial $\delta^{13}C$, $\delta^{18}O$, and $\delta^{238}U$ in the carbonate rock from the Bahamas were 4.8, 0.5, and –0.37 ‰ (Swart et al., 2009; Romaniello et al., 2013).

The isotope fractionation factors between the rock and diagenetic fluids for C and O were 1.001 and 1.0032, respectively (Tucker and Wright, 2000; Land, 1985). Under oxic conditions, the U isotope fractionation factors during alteration by meteoric and marine fluids were 1.00003 and 1.0001. These U isotope fractionation factors were calculated according to Chen et al. (2016). Under anoxic conditions, the U isotope fractionation were assigned to the typical value (1.0 ‰) during U(VI) reduction to U(IV) in natural environments (Andersen et al., 2017).

Table B.3. Parameters for the open-system fluid-rock interaction model

Symbol	Definition	C	O	Ca	Mn	Sr	U(VI)	U(IV)
C_i^{f0} (ppm)	Initial concentration in initial marine fluid	29[1]	889000[1]	400[1]	0.001[2]	8[1]	0.003[3]	0.0005[4]
	Initial concentration in meteoric fluid	29[1]	889000[1]	100[5]	0.0015[2]	4[5]	0.003[3]	0.0005[4]
C_i^{r0} (ppm)	Initial concentration in primary carbonates	120000[1]	480000[1]	400000[1]	3[6]	4500[6]	3[6]	3[6]
D_i	Element distribution coefficient in marine fluid	4138	0.54	1000	20000	100	200	200000
	Element distribution coefficient in meteoric fluid	4138	0.54	1000	12000	200	160	200000
K_{di}	Distribution coefficient in marine fluid	1[1]	1[1]	1[1]	20[7]	0.30[7]	0.20[7]	200[7-8]
	Distribution coefficient in meteoric fluid	1[1]	1[1]	1[1]	3[7]	0.09[7]	0.04[7]	50[7-8]
δ_i^{f0} (‰)	Initial isotopic ratio in marine fluid	2[9]	–29.3[10]	NA	NA	NA	–0.39[11]	–0.39[11]
	Initial isotopic composition in meteoric fluid	–1.2[12]	–34.2[13]	NA	NA	NA	–0.34[11]	–0.34[11]
δ_i^{r0} (‰)	Initial isotopic composition in the rock	4.8[14]	0.5[14]	NA	NA	NA	-0.37[6]	-0.37[6]
$\alpha_{r\text{-}f}$	Isotope fractionation factor between the rock and marine fluid	1.001[12]	1.032[15]	NA	NA	NA	1.0001[16]	1.001[17]
	Isotope fractionation factor between the rock and meteoric fluid	1.001[12]	1.032[15]	NA	NA	NA	1.00003[16]	1.001[17]

Note: (1) $\delta^{18}O$ of the marine and meteoric fluids is reported relative to the VPDB (Vienna Pee Dee Belemnite) using the equation: $\delta^{18}O_{VPDB}=0.97001\times\delta^{18}O_{VSMOW}-29.29$ (‰). Here, VSMOW (Vienna Standard Mean Ocean Water) is the oxygen isotope standard for water.
(2) K_{di} is the distribution coefficient of element i. It is defined as: $K_{di}= [C_i^r/C_{Ca}]_{rock}/[C_i^f/C_{Ca}]_{fluid}$, where $[C_i^r/Ca]_{rock}$ and $[C_i^f/Ca]_{fluid}$ are molar ratio of element i to Ca in the rock and fluid, respectively.
(3) The distribution coefficient and concentration of U in meteoric and marine fluids were for U(IV) because of the reducing diagenetic environments indicated by authigenic enrichments of redox-sensitive elements (e.g., U and Mo) and presence of H_2S (Romaniello et al., 2013).
(4) The O isotope between carbonates and the fluids is set as 32 ‰, because the carbonate sediments in the phreatic marine diagenetic section have experienced varying degrees of dolomitization, which generally elevates $\delta^{18}O$ by 3–4 ‰ in dolomite relative to the coexisting calcite[16]. Since the O isotope fractionation between calcite and water is 29.46 ‰ at 20 °C. Thus, I set an isotope fractionation factor between carbonate sediments and the fluid as 1.0032.

[1]Banner and Hanson, 1990
[2]Swart et al., 2000
[3]Chen et al., 1986
[4]Henderson et al., 1999

[5]Whitaker and Smart, 2007
[6]Romaniello et al., 2013
[7]Curti, 1999
[8]Sturchio et al., 1998
[9]Hu and Burdige, 2007
[10]LeGrande and Schmidt, 2006
[11]Tissot and Dauphas, 2015
[12]Tucker and Wright, 1990 (isotope fractionation factor at 20 °C)
[13]Bowen and Revenaugh, 2003
[14]Swart et al., 2009
[15]Land, 1985
[16]Chen et al., 2017
[17]Andersen et al., 2014

Text B.4. Long-term external reproducibility of $\delta^{238}U$ for an in-house coral standard PB-0010

The external reproducibility of a matrix-matched standard (an in-house coral standard PB-0010) was assessed via 11 times measurements in the laboratory over the past 6 years. The data in Table B.4 represents independent digestion and processing of a separate aliquots of the PB-0010 coral powder and shows that a long-term external reproducibility is ±0.05 ‰. In addition, the accuracy of these data shows excellent agreement with other published data for modern corals and the isotopic composition of modern seawater (–0.39 ‰, Tissot and Dauphas, 2015; Andersen et al., 2016).

Table B.4. Long-term analyses of $\delta^{238}U$ of an in-house coral standard PB-0010

Time	$\delta^{238}U$ (‰)	2 SD (‰)	N
2013	–0.46	0.10	3
2013	–0.40	0.11	3
2015	–0.41	0.10	6
2016	–0.45	0.01	3
2017	–0.40	0.03	3
2017	–0.42	0.08	3
2017	–0.40	0.05	3
2018	–0.39	0.10	4
2018	–0.39	0.07	4
2018	–0.40	0.03	3
2018	–0.42	0.08	3
Average	**–0.41**	**0.05**	

Text B.5. Summary of published data of $\delta^{238}U$ of CRM-129a

The CRM-129a standard has been independently measured and reported by other workers in other laboratories who found comparable results. Almost all these measurements of $\delta^{238}U$ for CRM-129a gave indistinguishable values of about –1.70 ‰ within analytical uncertainty (Table B.5; Brennecka et al., 2011; Kendall et al., 2013; Wang et al., 2015; Amzy et al., 2015; Lau et al., 2016; Chen et al., 2016; Shiel et al., 2016). Given the excellent interlaboratory agreement, I assert my measurements are correct and accurate and that the certified value of CRM-129a is incorrect or at least that the isotope fractionation is inaccurate relative to CRM-145a.

The CRM-129a was certified at NBL in 2008 using an older generation of TIMS methods which had to be themselves calibrated using a variety of other standard reference materials. The certified precision (0.53 ‰) is quite low compared to typical precision obtainable with MC-ICP-MS (0.05–0.10 ‰). Lau et al. (2016) working with a separate aliquot of CRM-129a at Stanford University initially determined a $\delta^{238}U$ of –1.52±0.13 ‰. I subsequently provided an aliquot of the CRM-129a from the laboratory in ASU which Lau et al. (2016) measured and reported as 1.71±0.10 ‰ in agreement with

other laboratories. Thus, one or more batches of CRM-129a are heterogeneous or may have been contaminated in isolated incidents, but argue that the consensus of analyses by multiple independent laboratories support my results.

Table B.5. Summary of published data for $\delta^{238}U$ of CRM-129a.

$\delta^{238}U_{CRM\text{-}129a}$ ‰	2 SD ‰	N	References
–1.79	0.13	33	Brennecka et al., 2011
–1.75	0.07	38	Kendall et al., 2013
–1.71	0.06	10	Wang et al., 2015
–1.71	0.08	16	Azmy et al., 2015
–1.52	0.13	40	Lau et al., 2016
–1.71	0.10	28	Lau et al., 2016*
–1.70	0.10	20	Chen et al., 2016
–1.70	0.08	33	Shiel et al., 2016
–1.70	0.08	23	This study
–0.90	0.53	–	Certified value of CRM-129a (NBL)

Note: Lau et al., 2016* is the measurement of $\delta^{238}U$ from an aliquot of CRM-129a from Arizona State University. NBL represents New Brunswick Laboratory.

Text B.6. Supplementary data of element concentrations and $\delta^{238}U$

Table B. 6 Concentrations of elements in carbonate sediments from the Bahamas.

Diagenesis	Samples	Depth	Mg	Al	Ca	Mn	Sr	Ce	Pr	Nd	Sm	Eu	Gd	Th	U
		mbsl	ppm	ppm	wt %	ppm	ppm	ppm	ppm	ppm	ppm	ppm	ppm	ppm	ppm
Meteoric vadose	clino70	21	1811	56	38	1	3809	0.45	0.10	0.42	0.12	0.03	0.17	0.03	3.5
	clino100	30	2190	45	38	3	4140	0.09	0.01	0.05	0.01	0.00	0.02	0.01	2.7
	clino130	40	3357	123	39	6	1162	0.53	0.08	0.31	0.08	0.02	0.10	0.06	6.5
	clino140	43	2963	27	37	2	1225	0.35	0.09	0.39	0.11	0.03	0.16	0.03	3.2
	clino171	52	2155	22	39	7	1932	0.04	0.01	0.03	0.01	0.00	0.01	0.01	4.5
	clino201	61	3869	85	38	4	1128	0.26	0.04	0.16	0.04	0.01	0.05	0.03	3.8
	clino217	66	2965	30	38	3	1285	0.14	0.03	0.11	0.03	0.01	0.05	0.01	3.6
	clino240	73	2905	158	38	3	893	0.47	0.07	0.26	0.07	0.01	0.07	0.05	3.2
	clino277	85	3834	44	39	4	1171	0.23	0.05	0.23	0.06	0.02	0.09	0.02	3.7
	clino314	96	4112	163	38	8	830	0.82	0.14	0.56	0.14	0.03	0.17	0.08	10.6
	clino322	98	3072	35	38	3	1087	0.06	0.01	0.04	0.01	0.00	0.02	0.01	3.9
	clino340	104	4531	322	38	7	1179	0.73	0.11	0.41	0.10	0.02	0.12	0.10	3.2
	clino352	107	3410	117	36	5	1177	0.30	0.05	0.20	0.05	0.01	0.07	0.02	4.3
	clino366	112	4772	86	37	9	1438	0.01	0.00	0.00	0.00	0.00	0.00	0.02	4.2
	clino387	118	4465	50	38	14	1510	0.18	0.04	0.19	0.05	0.01	0.07	0.01	4.1
	clino406	124	5261	31	37	18	1784	0.16	0.04	0.18	0.04	0.01	0.06	0.02	3.3
Phreatic meteoric	clino424	129	84958	152	24	10	623	0.10	0.03	0.12	0.03	0.01	0.04	0.05	6.0
	clino440	134	15433	19	35	9	1608	0.17	0.05	0.20	0.05	0.01	0.07	0.01	2.4
	clino446	136	31238	16	33	7	1240	0.09	0.02	0.09	0.02	0.01	0.03	0.02	2.8
	clino455	139	4424	136	38	5	1035	0.08	0.02	0.08	0.02	0.01	0.03	0.03	1.8
	clino462	141	3655	12	37	4	2126	0.14	0.04	0.15	0.04	0.01	0.05	0.01	1.5
	clino468	143	4393	23	37	6	1307	0.25	0.07	0.29	0.07	0.02	0.10	0.01	4.4
	clino475	145	5631	20	36	8	1332	0.28	0.08	0.32	0.08	0.02	0.11	0.01	3.2
	unda296	90	6237	9	37	6	1326	0.31	0.05	0.19	0.05	0.01	0.06	0.00	3.5
	unda321	98	6076	6	36	3	1193	0.19	0.03	0.14	0.04	0.01	0.04	0.00	2.9

	unda343	105	6056	12	37	4	1379	0.45	0.09	0.39	0.10	0.02	0.14	0.00	3.0
	unda350	107	6870	6	37	5	1340	0.53	0.11	0.46	0.12	0.03	0.15	0.00	4.1
	unda359	109	7220	8	37	5	1246	0.62	0.11	0.43	0.11	0.03	0.15	0.00	3.7
	unda369	112	7740	8	36	7	1261	0.31	0.07	0.29	0.08	0.02	0.10	0.01	4.1
	unda380	116	6087	9	31	7	1037	0.58	0.14	0.58	0.16	0.04	0.24	0.01	3.6
	unda396	121	37029	19	32	6	1534	0.41	0.10	0.44	0.12	0.03	0.15	0.02	2.7
	unda411	125	38367	75	32	7	914	0.28	0.08	0.35	0.09	0.02	0.12	0.04	3.1
	unda428	131	18434	18	34	8	1128	0.37	0.10	0.44	0.11	0.03	0.14	0.03	3.6
	unda442	135	14925	23	35	10	983	0.18	0.05	0.19	0.05	0.01	0.06	0.04	2.0
	unda458	140	16803	59	35	7	1343	0.29	0.08	0.32	0.09	0.02	0.11	0.03	2.7
	unda476	145	18745	29	34	5	1123	0.61	0.16	0.68	0.18	0.05	0.22	0.01	3.3
	unda493	150	18596	54	35	5	1059	0.32	0.09	0.36	0.09	0.02	0.12	0.02	3.2
	unda904	276	52278	105	30	11	328	0.06	0.01	0.06	0.02	0.00	0.02	0.05	3.7
	unda920	280	53251	100	30	10	334	0.22	0.04	0.16	0.04	0.01	0.05	0.04	3.7
	unda936	286	99904	131	23	12	211	0.20	0.03	0.13	0.03	0.01	0.04	0.07	3.4
	unda965	294	100349	52	23	14	189	0.32	0.07	0.31	0.09	0.02	0.10	0.02	8.2
	unda981	299	104336	51	23	17	175	0.23	0.04	0.16	0.04	0.01	0.05	0.01	6.7
	unda992	303	104598	30	23	12	172	0.20	0.04	0.15	0.04	0.01	0.04	0.00	4.4
	unda1005	307	101712	41	23	14	170	0.26	0.05	0.18	0.05	0.01	0.06	0.01	4.2
	clino483	147	7405	13	36	8	2265	0.25	0.04	0.16	0.04	0.01	0.05	0.01	5.0
	clino493	150	7863	15	36	9	2192	0.29	0.05	0.20	0.05	0.01	0.06	0.01	4.1
	clino510	156	11978	19	35	9	1281	0.28	0.04	0.18	0.04	0.01	0.05	0.01	2.5
	clino532	162	10272	9	25	4	590	0.34	0.06	0.22	0.05	0.01	0.06	0.01	3.0
	clino567	173	14315	13	35	7	1130	0.43	0.07	0.28	0.07	0.02	0.08	0.01	3.1
	clino600	183	13678	24	35	10	1237	0.49	0.08	0.29	0.07	0.02	0.08	0.02	2.7
	clino630	192	26284	57	33	17	1079	0.69	0.11	0.41	0.10	0.02	0.11	0.01	4.5
	clino657	200	5639	20	36	1	1522	0.60	0.09	0.35	0.09	0.02	0.09	0.00	4.6
	clino720	220	7754	90	36	5	11654	0.63	0.09	0.35	0.08	0.02	0.09	0.02	2.4
	clino764	233	5663	77	36	2	3424	2.14	0.26	0.94	0.22	0.05	0.23	0.02	2.5
	clino828	252	14739	35	34	8	978	0.88	0.16	0.61	0.15	0.04	0.17	0.01	4.2
Phreatic marine	clino981	299	4289	89	35	3	5543	1.01	0.21	0.86	0.21	0.05	0.27	0.01	3.6
	clino988	301	4228	100	36	2	5303	0.36	0.07	0.26	0.07	0.02	0.08	0.02	3.0
	clino1018	310	3905	107	35	3	5322	0.61	0.10	0.40	0.10	0.02	0.12	0.02	3.5
	clino1039	317	4618	109	36	2	5561	0.30	0.05	0.21	0.05	0.01	0.07	0.02	3.1
	clino1062	324	4598	97	36	3	5916	0.18	0.03	0.12	0.03	0.01	0.04	0.03	3.7
	clino1087	332	5002	98	35	3	6915	0.44	0.10	0.42	0.12	0.03	0.18	0.03	3.8
	clino1109	338	5469	122	37	4	8270	0.58	0.11	0.46	0.12	0.03	0.16	0.04	3.8
	clino1130	345	6085	162	35	4	4325	0.74	0.18	0.74	0.20	0.05	0.26	0.05	3.9
	clino1147	350	5113	199	36	5	3782	0.79	0.19	0.80	0.20	0.05	0.28	0.06	3.5
	clino1153	351	9016	219	36	4	4063	0.79	0.19	0.80	0.20	0.05	0.25	0.09	6.3
	clino1163	354	5456	238	34	4	16803	0.32	0.07	0.29	0.07	0.02	0.10	0.09	4.2
	clino1171	357	6533	306	36	6	2795	0.45	0.09	0.36	0.09	0.02	0.12	0.09	3.4
	clino1188	362	5399	858	35	15	3210	1.29	0.27	1.13	0.30	0.08	0.38	0.41	4.4
	clino1192	364	9519	401	37	14	2101	1.02	0.22	0.90	0.23	0.06	0.31	0.12	4.8
	clino1202	366	6155	278	36	22	1353	1.46	0.30	1.25	0.32	0.08	0.41	0.08	6.7
	clino1214	370	18966	127	35	6	2017	0.35	0.07	0.31	0.07	0.02	0.09	0.04	4.0
	clino1233	376	17567	175	34	6	2210	0.36	0.07	0.29	0.07	0.02	0.09	0.08	4.0
	clino1248	381	21700	313	34	6	2325	0.05	0.01	0.04	0.01	0.00	0.01	0.04	5.2
	clino1262	385	20039	185	34	5	2034	0.31	0.07	0.26	0.06	0.02	0.08	0.02	2.9
	1006A 1H-1 109-110	1.1	5874	1947	36	48	2712							0.59	3.6
	1006A 1H-1 120-121	1.2	5591	1958	36	42	2832							0.60	3.8
	1006A 1H-4 70-71	5.2	5776	2086	37	29	2559							0.59	4.4
	1006A 1H-4 80-81	5.3	5822	2484	36	37	2559							0.61	4.4
	1006B 2H-4 49-50	10.5	19466	2054	36	39	1284							0.65	2.0
	1006B 2H-4 60-61	10.6	10004	1616	37	35	2427							0.69	4.9

	1006A 2H-4 70-71	12.3	10152	472	37	8	2214			0.45	6.6
	1006A 2H-4 80-81	12.4	10398	534	37	9	2196			0.45	7.2
	1006A 2H-4 134-135	12.94	10212	459	38	9	2209			0.44	7.8
	1006B 2H-6 65-66	13.65	10030	667	38	11	2276			0.48	6.1
	1006B 2H-6 74-75	13.75	9940	607	37	10	2170			0.46	6.3
	1006A 2H-6 20-21	14.8	7606	3332	35	62	1518			0.77	3.1
	1006A 2H-6 30-31	14.9	7949	4320	36	47	1430			0.84	2.7
	1006A 2H-6 133-134	15.93	7655	2517	37	40	1920			0.62	3.0
	1006A 3H-1 70-71	17.3	6624	4756	34	92	1573			1.18	5.1
	1006A 3H-1 80-81	17.4	7439	4257	35	58	1790			0.79	4.2
	1006A 3H-4 69-70	21.8	6901	3397	35	47	2065			0.71	3.0
	1006A 3H-4 80-81	21.9	6075	2980	35	47	2125			0.65	3.1
	1006A 3H-6 50-51	24.6	6369	5264	33	56	1240			0.81	3.0
	1006A 3H-6 59-60	24.7	6157	5021	36	50	1745			0.86	3.4
	1006A 4H-1 90-91	27	6324	5225	35	48	1305			0.92	3.5
	1006A 4H-1 100-101	27.1	6164	4667	35	66	1425			0.89	3.9

Table B.7. Carbonate mineralogy, I/Ca+Mg, and C, O and U isotopic compositions in carbonate sediments from the Bahamas.

Diagenesis	Samples	I/(Ca+Mg)	Arag	HMC	LMC	Dolo	Cal	$\delta^{13}C_{carb}$	$\delta^{18}O_{carb}$	$\delta^{238}U_{carb}$	2SD
		µmol/mol	wt. %	wt. %	wt. %	wt. %	wt. %	‰	‰	‰	‰
Meteoric vadose	clino70	3.99	47.68	0.00	52.32	0.00	52.32	2.41	-2.31	0.13	0.08
	clino100	2.95	45.84	0.00	54.16	0.00	54.16	0.65	-2.65	-0.11	0.09
	clino130	3.21	0.00	0.00	100.00	0.00	100.00	-0.88	-3.05	0.06	0.12
	clino140	3.26	10.85	0.00	89.15	0.00	89.15	-1.34	-2.82	0.26	0.08
	clino171	1.72	0.00	0.00	100.00	0.00	100.00	-0.09	-3.17	0.22	0.09
	clino201	2.99	0.00	0.00	100.00	0.00	100.00	0.26	-2.58	0.18	0.10
	clino217	0.79	0.00	0.00	100.00	0.00	100.00	-0.27	-2.84	-0.47	0.09
	clino240	2.78	0.00	0.00	100.00	0.00	100.00	0.00	-2.25	0.23	0.08
	clino277	1.76	0.00	0.00	100.00	0.00	100.00	-0.37	-2.32	0.07	0.10
	clino314	1.36	0.00	0.00	100.00	0.00	100.00	-0.68	-3.48	-0.03	0.09
	clino322	1.53	0.00	0.00	100.00	0.00	100.00	-0.78	-2.51	-0.19	0.13
	clino340	0.68	0.00	0.00	100.00	0.00	100.00	-0.48	-3.17	-0.02	0.12
	clino352	0.55	0.00	0.00	100.00	0.00	100.00	0.17	-1.56	-0.16	0.08
	clino366	0.13	0.00	0.00	100.00	0.00	100.00	0.18	-1.93	-0.04	0.08
	clino387	0.60	0.00	0.00	100.00	0.00	100.00	0.15	-1.24	-0.36	0.08
	clino406	2.89	0.00	0.00	100.00	0.00	100.00	0.00	-1.12	-0.29	0.08
	clino424	0.00	0.00	0.00	100.00	0.00	100.00	0.15	-1.32	-0.15	0.08
	clino440	1.28	0.00	0.00	100.00	0.00	100.00	0.76	-1.34	-0.08	0.08
	clino446	0.55	0.00	0.00	100.00	0.00	100.00	0.91	-0.93	-0.15	0.09
	clino455	0.71	0.00	0.00	100.00	0.00	100.00	1.07	-0.23	-0.18	0.08
Phreatic meteoric	clino462	1.57	21.34	0.00	78.66	0.00	78.66	1.74	-1.12	-0.17	0.09
	clino468	1.43	19.78	0.00	80.22	0.00	80.22	2.00	-1.13	-0.14	0.09
	clino475	1.37	14.96	0.00	80.21	4.82	80.21	1.79	1.17	-0.07	0.08
	unda296	0.87	0.00	0.00	100.00	0.00	100.00	-0.29	-2.05	-0.03	0.08
	unda321	0.00	0.00	0.00	100.00	0.00	100.00	1.66	3.20	-0.22	0.09
	unda343	0.15	0.00	0.00	100.00	0.00	100.00	0.20	-2.04	-0.02	0.10
	unda350	0.00	0.00	0.00	100.00	0.00	100.00	0.48	-1.71	-0.21	0.10
	unda359	0.00	0.00	0.00	16.94	83.06	16.94	2.50	1.05	-0.04	0.09
	unda369	0.13	0.00	0.00	93.52	6.48	93.52	1.75	-0.62	-0.29	0.08
	unda380	0.00	8.62	0.00	51.31	40.07	51.31	1.85	-0.87	-0.44	0.09

	unda396	0.56	24.34	0.00	44.32	31.33	44.32	2.51	1.29	-0.02	0.17
	unda411	0.00	0.00	0.00	49.88	50.12	49.88	2.50	0.70	0.00	0.08
	unda428	0.00	12.99	0.00	76.25	10.76	76.25	2.53	0.46	-0.05	0.08
	unda442	0.13	4.92	0.00	78.94	16.14	78.94	2.67	0.58	-0.24	0.08
	unda458	0.00	9.78	0.00	79.04	11.19	79.04	2.85	0.81	-0.08	0.08
	unda476	0.00	7.62	0.00	75.47	16.91	75.47	2.78	1.04	0.02	0.08
	unda493	0.00	2.70	0.00	83.11	14.19	83.11	-0.27	-1.91	-0.13	0.13
	unda904	0.00	0.00	0.00	64.10	35.90	64.10	1.71	2.08	-0.18	0.08
	unda920	0.00	0.00	0.00	42.76	57.24	42.76	1.73	2.19	-0.10	0.08
	unda936	0.00	0.00	0.00	0.55	99.45	0.55	2.09	3.83	-0.18	0.08
	unda965	0.00	0.00	0.00	1.11	98.89	1.11	2.91	3.46	0.29	0.15
	unda981	0.00	0.00	0.00	0.00	100.00	0.00	2.76	3.54	-0.34	0.08
	unda992	0.00	0.00	0.00	0.00	100.00	0.00	2.46	3.70	-0.28	0.08
	unda1005	0.00	0.00	0.00	0.00	100.00	0.00	2.48	3.46	-0.44	0.12
	clino483	1.12	3.97	0.00	85.15	10.89	85.15	1.60	1.40	-0.16	0.08
	clino493	0.18	15.28	0.00	77.24	7.48	77.24	2.23	0.92	-0.04	0.09
	clino510	1.37	23.46	0.00	70.74	5.80	70.74	2.89	1.15	-0.30	0.08
	clino532	0.57	24.87	0.00	65.64	9.50	65.64	2.95	1.48	-0.03	0.09
	clino567	2.28	18.35	0.00	81.65	0.00	81.65	3.83	1.28	-0.15	0.10
	clino600	0.30	12.45	0.00	86.31	1.24	86.31	3.93	1.39	-0.16	0.09
	clino630	0.99	46.80	0.00	51.65	1.55	51.65	4.96	0.70	-0.21	0.08
	clino657	0.17	2.55	0.00	83.65	13.80	83.65	1.66	0.99	-0.26	0.08
	clino720	2.00	57.40	0.00	42.60	0.00	42.60	5.18	1.06	-0.26	0.09
	clino764	2.91	53.65	0.00	46.35	0.00	46.35	5.25	0.84	-0.14	0.08
	clino828	3.22	0.00	0.00	33.82	0.00	33.82	5.16	0.67	-0.06	0.09
	clino981	3.79	75.14	0.00	24.86	0.00	24.86	5.27	1.18	-0.07	0.10
	clino988	3.59	76.41	0.00	21.19	2.40	21.19	5.14	0.24	-0.11	0.09
	clino1018	0.39	62.65	0.00	37.35	0.00	37.35	2.54	0.82	-0.13	0.10
Phreatic marine	clino1039	4.33	84.50	0.00	14.08	1.42	14.08	5.04	0.33	-0.09	0.08
	clino1062	4.03	57.32	44.96	0.00	0.00	44.96	4.80	0.50	-0.13	0.08
	clino1087	3.06	48.31	0.00	51.08	0.61	51.08	4.50	1.11	-0.15	0.09
	clino1109	2.29	42.45	0.00	56.81	0.74	56.81	4.15	1.09	-0.14	0.08
	clino1130	2.84	62.99	0.00	34.91	2.10	34.91	4.11	0.65	-0.20	0.09
	clino1147	2.36	28.82	3.73	65.54	1.90	69.27	3.85	0.35	-0.14	0.10
	clino1153	1.68	18.35	85.70	0.00	0.00	85.70	3.55	0.53	-0.20	0.12
	clino1163	2.91	23.24	0.00	75.09	1.67	75.09	3.60	0.46	-0.14	0.08
	clino1171	0.00	26.93	0.00	68.85	4.21	68.85	3.84	0.81	-0.18	0.08
	clino1188	3.54	38.10	0.00	61.90	0.00	61.90	3.39	0.48	-0.06	0.09
	clino1192	1.10	34.69	0.00	62.64	2.67	62.64	3.30	1.35	-0.13	0.08
	clino1202	0.78	6.54	0.00	93.46	0.00	93.46	2.15	0.36	-0.16	0.09
	clino1214	0.00	0.00	0.00	66.13	33.87	66.13	2.88	1.35	-0.11	0.10
	clino1233	0.72	10.49	0.00	65.80	23.71	65.80	2.97	1.20	-0.03	0.08
	clino1248	0.17	3.30	0.00	81.46	15.24	81.46	3.58	2.11	0.19	0.08
	clino1262	0.14	0.00	0.00	78.03	21.97	78.03	3.49	2.33	-0.13	0.09
	1006A 1H-1 109-110							2.00	-0.12	-0.19	0.03
	1006A 1H-1 120-121							2.40	-0.20	-0.18	0.17
	1006A 1H-4 70-71							2.48	-0.24	-0.20	0.10
	1006A 1H-4 80-81							2.80	1.21	-0.20	0.07
	1006B 2H-4 49-50							2.95	1.12	-0.20	0.18
	1006B 2H-4 60-61							3.93	-0.14	-0.02	0.04
	1006A 2H-4 70-71							2.88	0.12	-0.22	0.11
	1006A 2H-4 80-81							2.58	0.18	-0.21	0.08
	1006A 2H-4 134-135							2.78	0.98	0.00	0.03
	1006B 2H-6 65-66							1.89	1.78	-0.30	0.08
	1006B 2H-6 74-75							1.63	1.88	-0.26	0.12
	1006A 2H-6 20-21							1.53	1.88	-0.19	0.06
	1006A 2H-6 30-31							1.43	1.99	-0.17	0.10

1006A 2H-6 133-134	1.44	1.83	-0.23	0.02
1006A 3H-1 70-71	1.54	0.78	-0.15	0.09
1006A 3H-1 80-81	1.37	0.75	-0.23	0.11
1006A 3H-4 69-70			-0.17	0.04
1006A 3H-4 80-81			-0.20	0.19
1006A 3H-6 50-51			-0.12	0.02
1006A 3H-6 59-60			-0.17	0.08
1006A 4H-1 90-91			0.00	0.06
1006A 4H-1 100-101	2.26	1.3	-0.23	0.09

Note: I/(Ca+Mg) and carbonate mineralogy data came from Hardisty et al. (2017).

APPENDIX C

SUPPLEMENTARY INFORMATION FOR CHAPTER 5

Text C.1. Estimation of the fraction of detrital Ca

The fraction of detrital Ca ($f_{\text{detrital\_Ca}}$) in the sinking particles and anoxic sediments of FGL was estimated using the equation:

$$f_{\text{detrital\_Ca}} = \frac{\left({}^{\text{Ca}}/_{\text{Al}}\right)_{\text{AS}}}{\left({}^{\text{Ca}}/_{\text{Al}}\right)_{\text{sample}}} \qquad \text{Eq. C.1}$$

where the subscript 'AS' stands for average shale. The concentration ratio of Ca/Al in the average shale is ~ 0.18 ppm/ppm (Wedepohl, 1971, 1991). The estimated fraction of detrital Ca in the sinking particles and anoxic sediments were less than 0.5 %. Thus, I ignored the contribution of the detrital Ca to the estimate of the calcium carbonates in sediments.

Text C.2. Summary of U isotopic data for Fayetteville Green Lake

Table C.1. U concentration, $\delta^{234}U$ and $\delta^{238}U$ in water samples of FGL.

Sample	Depth M	U nM	$\delta^{234}U$ ‰	2 SD ‰	$\delta^{238}U$ ‰	2 SD ‰
TM00	0	2.21	683	6	–0.54	0.10
TM01	0	2.23	679	6	–0.50	0.10
TM02	2	2.21	684	6	–0.56	0.10
TM03	4	2.51	677	6	–0.62	0.10
TM04	6	2.62	663	6	–0.56	0.10
TM05	8	2.66	665	6	–0.53	0.10
TM06	10	2.68	669	6	–0.50	0.10
TM07	12	2.69	670	6	–0.48	0.10
TM08	16	2.80	680	6	–0.52	0.10
TM09	16.5	2.76	683	6	–0.57	0.10
TM10	17	2.77	691	6	–0.57	0.10
TM11	17.5	2.78	694	6	–0.54	0.10
TM12	18	2.92	705	6	–0.53	0.10
TM13	18.5	2.73	699	6	–0.52	0.10
TM14	19.5	2.81	690	6	–0.59	0.10
TM15	20.5	2.68	696	6	–0.61	0.10
TM16	21.5	2.42	701	6	–0.62	0.10
TM17	22	2.33	709	6	–0.68	0.10
TM18	22.5	2.18	708	6	–0.71	0.10
TM19	23	2.10	721	6	–0.67	0.10
TM20	23.5	1.91	714	6	–0.72	0.10
TM21	24	1.70	713	6	–0.69	0.10
TM22	31	1.54	714	6	–0.70	0.10
TM23	33	1.51	717	6	–0.75	0.10
TM24	41	1.04	720	6	–0.83	0.10
TM25	43	0.96	721	6	–0.88	0.10
TM26	46	0.91	722	6	–0.94	0.10
TM27	48	0.85	722	6	–0.96	0.10
Inlet	0	1.81	775	6	–0.55	0.10
Outlet	0	2.28	642	6	–0.57	0.10

Table C.2. Summary of U concentration, $\delta^{234}U$ and $\delta^{238}U$ in solid samples from FGL.

Sample Types	Sample No.	Depth cm	U ppm	$\delta^{234}U$ ‰	2 SD ‰	$\delta^{238}U$ ‰	2 SD ‰
Anoxic carbonate sediments	LS01	0.25	1.75	571	7	–0.32	0.10
	LS03	2.25	1.83	579	8	–0.38	0.10
	LS05	4.25	1.91	637	9	–0.30	0.11
	LS07	6.25	1.69	529	6	–0.43	0.10
	LS09	8.25	2.74	591	7	–0.31	0.10
	LS11	10.5	2.25	521	5	–0.23	0.10
	LS13	14.5	2.11	495	8	–0.32	0.12
	LS15	18.5	2.03	539	9	–0.38	0.17
	LS17	22.5	3.22	640	5	–0.64	0.10
	LS19	26.5	1.92	680	8	–0.43	0.16
	LS21	32	4.66	683	7	–0.33	0.10
	LS23	40	2.61	705	6	–0.28	0.10
Soil	FGLS01	0–5	2.18	–164	4	-0.48	0.10
	FGLS02	0–5	2.37	–103	4	–0.42	0.10
	FGLS03	0–5	2.62	–152	4	–0.40	0.10
	FGLS04	0–5	2.41	–181	4	–0.30	0.10
Bedrock	GVSHC	–	1.29	–69	4	–0.28	0.14
	RVSHC	–	0.57	–92	4	–0.24	0.10
	Dolomite	–	0.26	–148	4	–0.31	0.10
Bioherm carbonates	BC01	–	0.22	738	3	–0.53	0.10
	BC02	–	0.29	720	2	–0.51	0.10
	BC03	–	0.22	711	5	–0.50	0.10
	BC04	–	0.37	716	2	–0.50	0.10
	BC05	–	0.21	731	8	–0.53	0.10

Table C.3. Summary of sediment trap data.

Depth M	Calcite %	R g m^{-2} day^{-1}	Fe ppm	Mn ppm	$\delta^{234}U$ ‰
13.5	78	1.99	1885	342	558.89
21.5	76	2.57	1785	63	557.87
27.5	68	2.14	1953	60	563.96
45.5	60	1.96	1791	54	575.88

Note: R is the sedimentation rate of sinking particles during the sampling period in July 2017.

APPENDIX D

APPENDIX REFERENCES

Andersen M. B., Stirling C. H., Weyer S. (2017) Uranium isotope fractionation. *Rev. Mineral. Geochem*. **82**, 799–850.

Andersen M. B., Romaniello S., Vance D., Little S. H., Herdman R. and Lyons T. W. (2014) A modern framework for the interpretation of $^{238}U/^{235}U$ in studies of ancient ocean redox. *Earth Planet. Sci. Lett.* **400**, 184–194.

Andersen M. B., Vance D., Morford J. L., Bura-Nakic E., Breitenbach S. F. M. and Och L. (2016) Closing in on the marine $^{238}U/^{235}U$ budget. *Chem. Geol*. **420**, 11–22.

Anderson R. F., Fleisher M. Q. and LeHuray A. P. (1989) Concentration, oxidation-state and particulate flux of uranium in the Black Sea. *Geochim. Cosmochim. Acta* **53**, 2215–2224.

Azmy K., Kendall B., Brand U., Stough S. and Gordon G. W. (2015) Redox conditions across the Cambrian-Ordovician Boundary: Elemental and isotopic signatures retained in the GSSP carbonates. *Paleogeogr. Paleoclimatol. Paleoecol*. **440**, 440–454.

Banner J. L. and Hanson G. N. (1990) Calculation of simultaneous isotopic and trace element variations during water-rock interaction with applications to carbonate diagenesis. *Geochim. Cosmochim. Acta* **54**, 3123–3137.

Bowen G. J. and Revenaugh J. (2003) Interpolating the isotopic composition of modern meteoric precipitation. *Water Resour. Res*. **39**, 1299.

Brennecka G. A., Herrmann A. D., Algeo T. J. and Anbar A. D. (2011) Rapid expansion of oceanic anoxia immediately before the end-Permian mass extinction. Proc. *Natl. Acad. Sci. U. S. A*. **108**, 17631–17634.

Brunskill G. J. (1969) Fayetteville Green Lake, New York II. Precipitation and sedimentation of calcite in a meromictic lake with laminated sediments. *Limnol. Oceanogr*. **14**, 830–847.

Chen J. H., Edwards R. J. and Wasserburg G. C. (1986) ^{238}U, ^{234}U and ^{232}Th in seawater. *Earth Planet. Sci. Lett.* **80**, 241–251.

Chen X., Romaniello S. J., Herrmann A. D., Wasylenki L. E., Anbar A. D. (2016) Uranium isotope fractionation during coprecipitation with aragonite and calcite. *Geochim. Cosmochim. Acta* **188**, 189–207.

Chen X., Romaniello S. J. and Anbar A. D. (2017) Uranium isotope fractionation induced by aqueous speciation: Implications for U isotopes in marine $CaCO_3$ as a paleoredox proxy. *Geochim. Cosmochim. Acta* **215**, 162–172.

Curti E. (1999) Coprecipitation of radionuclides with calcite: estimation of partition coefficients based on a review of laboratory investigations and geochemical data. *Appl. Geochem*. **14**, 433–445.

Henderson G. M., Slowey N. C. and Haddad G. A. (1999) Fluid flow through carbonate platforms: Constraints from $^{234}U/^{238}U$ and Cl^- in Bahamas pore-waters. *Earth. Planet. Sci. Lett.* **169**, 99–111.

Hilfinger, IV, M. F., Mullins H. T., Burnett A. and Kirby M. E. (2001) A 2500 year sediment record from Fayetteville Green Lake, New York: Evidence for anthropogenic impacts and historic isotope shift. *J. Paleolimnol*. **26**, 293–305.

Hu X. and Burdige D. J. (2007) Enriched stable carbon isotopes in the pore waters of carbonate sediments dominated by seagrasses: Evidence for coupled carbonate dissolution and reprecipitation. *Geochim. Cosmochim. Acta* **71**, 129–144.

Jacobsen S. B. and Kaufman A. J. (1999) The Sr, C and O isotopic evolution of Neoproterozoic seawater. *Chem. Geol.* **161**, 37–57.

Kendall B., Brennecka G. A., Weyer S. and Anbar A. D. (2013) Uranium isotope fractionation suggests oxidative uranium mobilization at 2.50 Ga. *Chem. Geol*. **362**, 105–114.

Land L. S. (1985) The origin of massive dolomite. *J. Geol. Educ*. **33**, 112–125.

Langmuir D. (1978) Uranium solution-mineral equilibria at low temperatures with applications to sedimentary ore deposits. *Geochim. Cosmochim. Acta* **42**, 547–569.

Lau K. V., Maher K., Altiner D., Kelley B. M., Kump L. R., Lehrmann D. J., Silver-Tamayo J. C., Weaver K. L., Yu M. and Payne J. L. (2016) Marine anoxia and delayed Earth system recovery after the end-Permian extinction. *Proc. Natl. Acad. Sci.* **113**, 2360–2365.

Lawrence M, G., Greig A., Collerson K. D. and Kamber B. S. (2006) Rare earth element and yttrium variability in South Earth Queensland waterways. *Aquat. Geochem*. **12**, 39–72.

LeGrande A. N. and Schmidt G. A. (2006) Global gridded data set of the oxygen isotopic composition in seawater. *Geophy. Res. Lett*. **33**, 10.1029/2006GL026011.

McLennan S. M. (1989) Rare-earth elements in sedimentary-rocks—influence of provenance and sedimentary processes. *Rev. Mineral. Geochem*. **21**, 169–200.

Mucci A. (1983) The solubility of calcite and aragonite in seawater at various salinities, temperatures, and one atmosphere total pressure. *Am. J. of Sci.* **283**, 780–799.

Parkhurst D. L. and Appelo C. A. (2004) *User's Guide to PHREEQC (Version 2)—A Computer Program for Speciation, Batch-Reaction, One-Dimension Transport, and Inverse Geochemical Calculations.* U. S. Geological Survey, Reston, VA.

Romaniello S. J., Herrmann A. D. and Anbar A. D. (2013) Uranium concentrations and $^{238}U/^{235}U$ isotope ratios in modern carbonates from the Bahamas: Assessing a novel paleoredox proxy. *Chem. Geol.* **362**, 305-316.

Shiel A. E., Johnson T. M., Lundstrom C. C., Laubach P. G., Long P. E. and Williams K. H. (2016) Reactive transport of uranium in a groundwater bioreduction study: Insights from high-temporal resolution $^{238}U/^{235}U$ data. *Geochim. Cosmochim. Acta* **187**, 218–236.

Sturchio N. C., Antonio M. R., Soderholm L., Sutton S. R. and Brannon J. C. (1998) Tetravalent uranium in calcite. *Science*, **281**, 971–973.

Swart P. K. (2000) The oxygen isotopic composition of interstitial waters: Evidence for fluid flow and recrystallization in the margin of the Great Bahama Bank. *Proceedings of the Ocean Drilling Program: Scientific Results* **166**, 91–98.

Swart P. K., Reijmer J. J. G. and Otto R. (2009) A re-evaluation of facies on Great Bahama Bank II: variations in the $\delta^{13}C$, and $\delta^{18}O$ and mineralogy of surface sediments. *Int. Assoc. Sedimentol. Spec. Publ.* **41**, 47–59.

Tissot F. L. H. and Dauphas N. (2015) Uranium isotopic compositions of the crust and ocean: Age corrections, U budget and global extent of modern anoxia. *Geochim. Cosmochim. Acta* **167**, 113–143.

Tucker M. E. and Wright V. P. (1990) Carbonate Sedimentology. Blackwell Science Ltd., United Kingdom.

Wedepohl K. H. (1971) Environmental influences on the chemical composition of shales and clays. In: Ahrens L. H., Press F., Runcorn S. K. and Urey H. C. (Eds.), *Physics and Chemistry of the Earth*. Pergamon, Oxford, pp. 305–333.

Wedepohl K. H. (1991) The composition of the upper Earth's crust and the natural cycles of selected metals. In: Merian E. (Ed.), *Metals and their Compounds in the Environment*. VCH-Verlagsgesellscraft, Weinheim, pp. 3–17.

Wang X., Johnson T. M. and Lundstrom C. C. (2015) Isotope fractionation during oxidation of tetravalent uranium by dissolved oxygen. *Geochim. Cosmochim. Acta* **150**, 160–170.

Whitaker F. F. and Smart P. L. Geochemistry of meteoric diagenesis in carbonate islands of the northern Bahamas: 1. Evidence from field studies. *Hydrol. Process*. **21**, 949–966.

Zhong S. and Mucci A. (1989) Calcite and aragonite precipitation from seawater solutions of various salinities: Precipitation rates and overgrowth compositions. *Chem. Geol*. **78**, 283–299.